# Papers presented to the

# SIXTEENTH SYMPOSIUM

# ON ANTARCTIC METEORITES



## June 5-7, 1991

**NATIONAL INSTITUTE OF POLAR RESEARCH,** 国立極地研究所

**TOKYO**

# Papers presented to the

# SIXTEENTH SYMPOSIUM

# ON ANTARCTIC METEORITES



## June 5–7, 1991

## Wednesday, June 5, 1991

0900 - 1200    Registration          Auditorium (6th Floor)

0930 - 0935    Opening Address    **Takao Hoshiai**
                                    Director-General
                                    National Institute of
                                    Polar Research

\* Speaker

**Chairmen:  Akira Shimoyama and Makoto Kimura**

1    0935 - 0950    **Yanai K.**
                          Asuka-87 meteorites collection; preliminary report of the initial processing

2    0950 - 1005    **Kojima H.\* and Yanai K.**
                          Subclassification of unequilibrated ordinary chondrites

3    1005 - 1020    **Yanai K.\* and Kojima H.**
                          Yamato-793592: The first enstatite achondrite (aubrite) in the Yamato meteorites

4    1020 - 1050    **Hutchison R. (Invited Speaker, Dr., Curator of Meteorites, British Museum Natural History)**

                          Title: Euromet: A European project to recover meteorites for study by the International Scientific Community

5    1050 -       **Miura Y.\*, Kato T., Imai M. and Okamoto M.**
                          Possible meteoritic impact craters in Japan

6         -         **Miura Y.\*, Kato T., Imai M. and Ashida T.**
                          Shock metamorphism of silica minerals in meteoritic and artificial impact craters

7       - 1120    **Miura Y.\* and Kato T.**
                          Shock metamorphism of achondrites.  Lunar samples and lunar meteorites

8    1120 - 1135    **Kojima H.\*, Nagata T., Carleton B. J. and Kaito C.**
                          Tetrataenite fine grains in Y-791717 (CO3) chondrite.

9    1135 - 1150    **Tazawa Y.\* and Sasaki T.**
Alteration of fusion crusts of chondrites
- Results of melting experiments -

10    1150 - 1205    **Nayak V. K.**
Pseudobrookite from the Lonar impact crater,
India

       1205 - 1300    Lunch Time

**Chairmen: Yukio Ikeda and Takaaki Fukuoka**

11    1300 - 1330    **Bevan A. W. R. (Invited Speaker, Dr., Curator of Meteorites, Western Australian Museum)**

Title: Meteorites from the Nullarbor region,
Western Australia and comparisons with Ant-
arctic meteorites

12    1330 - 1345    **Yamaguchi A.\* and Takeda H.**
Mineralogical study of three brecciated Ant-
arctic eucrites, Y-82210, Y-793548, and Y-
82202

13    1345 - 1400    **Saito J.\* and Takeda H.**
Mineralogical study of metals at grain bound-
aries of magnesian ureilites

14    1400 - 1415    **Fujita T.\* and Kitamura M.**
Troilite-rich clast in the Moorabie (L3)
chondrite

15    1415 - 1430    **Tomeoka K.\*, Hatakeyama K., Nakamura T. and Takeda H.**
Evidence for Pre-accretionary aqueous alter-
ation in the Yamato-793321 CM carbonaceous
chondrite

16    1430 - 1445    **Nakamura T.\*, Tomeoka K. and Takeda H.**
Mineralogy of chondrule rims in the Yamato-
791198 CM chondrite: Comparison to Murchison

17    1445 - 1500    **Miono S.\* and Nakanishi A.**
Possible evidence of accretion by inter-
stellar medium estimated from historical
records of aurora and meteor in China

| 18 | 1500 - 1515 | Sanchez-Rubio G.*, Rcycs-Salas A. M. and Nieto-Samaniego A. |
| | | Meteorite Allende III: A SEM study of its glass phase |

| | 1515 - 1530 | Tea Time |

| 19 | 1530 - 1545 | Komiya M.*, Shimoyama, A. and Harada K. |
| | | Thermal release of insoluble organic matter isolated from some Antarctic CI and CM chondirtes |

| 20 | 1545 - 1600 | Kitajima F.* and Masuda A. |
| | | On insoluble organic matter in carbonaceous chondrites |

| 21 | 1600 - 1615 | Kagi H.*, Takahashi K. and Masuda A. |
| | | Raman scattering and laser-induced luminescence from micro diamonds in ureilites |

--------------------------------------------------------------------------------

Chairman: Nobuo Takaoka

-- Special Lecture (I) --

| 22 | 1615 - 1730 | Paul Pellas (Invited Speaker, Dr., de Mineralogie du Museum, Paris) |
| | | Title: Early chronology, thermal history, internal structure and dimensions of the H-chondrite parent asteroid |

| | 1730 - | Discussion |

# Thursday, June 6, 1991

**Chairmen:** Noboru Nakamura and Mitsuru Ebihara

23  0900 - 0915  **Shimaoka T.* and Nakamura N.**
The effect of total pressure on vaporization of alkalimetals from a partially molten chondritic material

24  0915 - 0930  **Yurimoto H.*, Oishi K., Nagasawa H., Yuasa H. and Sueno S.**
Sector-zoned pyroxene in Allende CAI and the implications for oxygen isotope distribution

25  0930 - 0945  **Fujimaki H.*, Aoki K., Kojima H. and Yanai K.**
Rb-Sr features of the shock-melted LL-chondrites from Antarctica: Y-790723 and -790528

26  0945 - 1000  **Fujiwara T.* and Nakamura N.**
Rb-Sr isotopic systematics and trace element features of the impact-melted L-chondrite, Chico

27  1000 - 1015  **Takahashi K.* and Masuda A.**
REE abundances and cosmochronology of ureilites

28  1015 - 1030  **Inoue M.* and Nakamura N.**
REE abundances in chondrules from the Murchison (CM) chondrite

29  1030 - 1045  **Amari S.*, Zinner E. and Lewis R. S.**
Isotopic analyses of size-separated SiC from the Murchison meteorite

30  1045 - 1100  **Shimamura T.*, Takahashi T., Honda M. and Nagai H.**
Elemental and isotopic analysis of Y-791694 iron meteorite by glow discharge mass spectrometer

31  1100 - 1115  **Ebihara M.*, Ozaki H. and Hirano K.**
On the possibility of new subclassification of UOC's

**Special Session:**

32  1115 - 1130  **Kimura M.\* and Ikeda Y.**
Mineralogical and petrological study of anomalous Belgica-7904 carbonaceous chondrite

33  1130 - 1145  **Ikeda Y.\*, Mayeda T., Clayton R. N. and Prinz M.**
Petrography and oxygen isotopic compositions of chondrules, clasts, and matrix separated from Belgica-7904 and Yamato-86720 carbonaceous chondrites

34  1145 - 1200  **Kimura M.\*, Tsuchiyama A., Fukuoka T. and Iimura Y.**
Mineralogy and chemistry of Antarctic winonaites: Y-74025, Y-75300 and Y-75305

1200 - 1300  **Lunch Time**

**Chairmen:  Hiroshi Takeda and Hirokazu Fujimaki**

35  1300 - 1315  **Yamamoto K., Nakamura N.\*, Misawa K., Kojima H. and Yanai K.**
Lithophile trace elements and Sr isotopes in unique meteorites, Y-74063, ALH-78230, Y-74357, Y-8002 and Y-75300

36  1315 - 1330  **Kaneoka I.\*, Takaoka N. and Yanai K.**
$^{40}$Ar-$^{39}$Ar analyses of Antarctic meteorites Y-74063 and ALH-78230: Consortium study on unique chondrites from Antarctica

37  1330 - 1345  **Takaoka N.\*, Nagao K. and Miura Y.**
Noble gas study of unique meteorite Yamato-74063 by laser extraction

38  1345 - 1400  **Takeda H.\*, Mori H. and Saito J.**
Crystallization and brecciation histories of lunar mare meteorites, Yamato-793274 and EET87521

39  1400 - 1415  **McKay D. S.**
Lunar meteorites and lunar regolith breccias: Some similarities and differences

40  1415 - 1430  **Misawa K., Tatsumoto M. and Yanai K.\***
U-Th-Pb chronology of Asuka-31 gabbro

| 41 | 1430 - 1500 | Lindstrom M. M. (Invited Speaker, Dr., Curator of U.S. Antarctic Meteorites, NASA-JSC), Mittlefehldt D. W. and Martinez R. R. |
|----|-------------|---|

Title: Geochemistry of Asuka-31: Comparison to basaltic lunar meteorites and mare basalts

| 42 | 1500 - 1515 | Zbik M.*, Jackiewicz E. and Kopcewicz M. |
|----|-------------|---|

Impact markers in basaltic regolithes

| 43 | 1515 - 1530 | Marakushev A. A. |
|----|-------------|---|

Origin of the Moon and "lunar" meteorites

**Chairmen:  Nobuo Takaoka and Hiroshi Takeda**

-- Special Lecture (II and III) --

| 44 | 1530 - 1620 | Eugster O. (Invited Speaker, Professor, University of Bern) |
|----|-------------|---|

Title: From how many ejection sites on the Moon do the lunar meteorites originate?

| | 1620 - 1630 | Discussion |
|--|-------------|-----------|

| 45 | 1630 - 1720 | McKay D. S. (Invited Speaker, Dr., NASA-JSC) |
|----|-------------|---|

Title: Utilization of lunar and Martian resources

| | 1720 - 1730 | Discussion |
|--|-------------|-----------|

------------------------------------------------------------------------

| | 1745 - 2000 | Reception | Lecture Room (2F) |
|--|-------------|-----------|-------------------|

## Friday, June 7, 1991

Chairmen:  Nobuo Takaoka and Jun-ichi Matsuda

46  0900 - 0915  **Tsuchiyama A.\*, Kitamura M., Ohbori K., Shibata H. and Hosokawa Y.**
Multielement EDX mapping of meteorites

47  0915 - 0930  **Uyeda C.\* and Tsuchiyama A.**
Isotopic behaviors of Mg and Si during gas-condensation process

48  0930 - 0945  **Tsuchiyama A.\* and Uyeda C.**
Isotopic and chemical fractionations of refractory elements during condensation and vaporization in the solar nebula

49  0945 - 1000  **Sugiura N.\* and Hashizume K.**
Nitrogen isotopic composition of a primitive achondrite Y-74063

50  1000 - 1015  **Sugiura N.\*, Kiyota K. and Hashizume K.**
Nitrogen isotopic composition of a gas rich chondrite ALH-77216

51  1015 - 1030  **Hashizume K.\* and Sugiura N.**
The origin and the trapping sites of the primordial argon in the UOCs; the correlation with the anomalous nitrogen

52  1030 - 1045  **Miura Y.\*, Nagao K. and Fujitani T.**
$^{81}$Kr terrestrial ages and grouping of Yamato eucrites

53  1045 - 1100  **Nagai H.\*, Honda M., Asano M., Imamura M. and Kobayashi K.**
$^{10}$Be in meteoritic carbons

54  1100 - 1115  **Nagao K.\*, Ogata A. and Miura Y.**
Study on noble gas distribution in carbonaceous chondrites using laser microprobe

55  1115 - 1130  **Fukunaga K.\* and Matsuda J.**
Noble gases in amorphous carbon and the origin of carbon material in ureilites

**56** 1130 - 1145 **Matsuda J.\* and Maekawa T.**
Trapping mechanism of noble gases in Vapor-growth diamonds

**57** 1145 - 1200 **Matsubara K.\* , Matsuda J. and Koeberl C.**
Noble gases in impact glasses

1200 - 1300 Lunch Time

**Chairmen: Naoji Sugiura and Akira Tsuchiyama**

**58** 1300 - 1315 **Futagami T.\*, Ozima M., Nagai S. and Aoki Y.**
Behavior of noble gases implanted into minerals

**59** 1315 - 1330 **Naraoka H.\*, Shimoyama A. and Harada K.**
Organic compounds in Asuka carbonaceous chondrites -II

**60** 1330 - 1345 **Kaito C.\* and Nagata T.**
Iron-sulfide grains in carbonaceous chondrite and experimental demonstration of formation of iron-sulfide grains with Fe-S coalescence technique

**61** 1345 - 1400 **Ninagawa K.\*, Nishimura S., Kubono N., Yamamoto I., Kohata M., Wada T., Yamashita Y. Matsunami S. and Nishimura H.**
Thermoluminescence characteristics and chemical compositions of mesostases in primitive ordinary chondrites -I

**62** 1400 - 1415 **Matsunami S.\*, Ninagawa K., Nishimura S., Kubono N., Yamamoto I., Kohata M., Wada T., Yamashita Y. and Nishimura H.**
Thermoluminescence characteristics and chemical compositions of mesostases in primitive ordinary chondrites - II: A type IA chondrule with high TL in Semarkona (LL3.0) chondrite

**63** 1415 - 1430 **Nagai H.\*, Moriyama A., Funaki M. and Momose K.**
The magnetic properties of Antarctic iron meteorites

| 64 | 1430 - 1445 | Funaki M.* and Sakai H.<br>Identification of the fine magnetic structures in some ordinary chondrites using magnetic fluid and magnetotactic bacteria |
| 65 | 1445 - 1500 | Miyamoto M.* and Takeda H.<br>Cooling history of Antarctic primitive achondrite Yamato-74357 |
| 66 | 1500 - 1515 | Scorzelli R. B.* and Azevedo I.<br>Mössbauer spectroscopy studies in Antarctic carbonaceous chondrites Y-86720 and Y-82162 |

---------------------------------------------------------------------------

**Chairman: Akira Shimoyama**

-- Special Lecture (IV) --

| 67 | 1515 - 1615 | Ponnamperuma C. A. (Invited Speaker, Professor, The University of Maryland)<br><br>Title: Origin of life |

Poster Session, Friday, June 7, 1991

68    0900 - 1500    Kaito C. and Saito Y.
                     Experimental demonstration of formation of
                     magnetite and wustite fine grains


Abstract only

69    Wang D., Xie X., Li Z. and Chen Y.
      A new fallen Yanzhuang chondrite from China

70    Gorbatchev N. S. and Krot A.
      Features of chromite chemism of the upper mantle and
      meteorites: Oxygen fugasity and composition of chromite-
      bearing asociations

71    Karpenko S. F., Smoliar M. I., Petaev M. I. and
      Shukolykov Y. A.
      Rb-Sr and Sm-Nd systematics in pomozdino meteorite

72    Krot A., Mitrejkina O. B., Zinov'eva N.G., Stroganov I. A.,
      Ivanova M. A. and Petaev M. I.
      Chromite-rich inclusions in ordinary chondrites

73    Marakushev A. A.
      The genetic types of meteorites

74    Mardon A. A.
      Aeolian transport of Antarctic meteorites immediately after
      impact: Implications for current transportation models

75    Nishiizumi K., Arnold J. R., Klein J., Fink D., Middleton R.,
      Sharma P. and Kubik P. W.
      Cosmic ray exposure history of lunar meteorite Yamato-
      793274

76    Lin W.
      Infrared studies on shock-loading Jilin meteorite

77    Zbik M. and Czechowski L.
      Does Venus expand?

78    Zolensky M., Prinz M. and Lipschutz M.
      Mineralogy and thermal history of Y-82162, Y-86720 and
      B-7904

*Wednesday, June 5, 1991*

*0900-1200    Registration, 6th Floor*

*0930-0935    Opening address, Auditorium*

*0935-1615    Symposium, Auditorium*

*1615-1730    Special Lecture (I)*

*Dr. Paul Pellas (Invited Speaker)*

*de Mineralogie de Museum,*

*Paris,*

*France*

ASUKA-87 METEORITES COLLECTION; PRELIMINARY REPORT OF THE INITIAL PROCESSING;
Keizo Yanai, Department of Meteorites, National Institute of Polar Research
9-10, Kaga 1-chome, Itabashi-ku, Tokyo 173, Japan

Asuka-87 meteorites have been collected in the bare ice field around the Sör Rondane Mountains by the Asuka wintering party (1987-89). The meteorites search carried out on the bare ice area around **Mt. Balchen**, (January - February, 1988), **Mt. Nils Larsen** and **Nansenisen** (February - March, 1988), and **Mt. Balchen** (April, 1988). Table shows the preliminary data of meteorite specimens collected each area including total number and weight with some types of meteorite.

**Mt. Balchen** area was fairly concentrated meteorites which include only one ureilite (contains much carbon matter) and mesosiderite, but most of all meteorites are fragmental and weathered chondritic specimens, excepting the largest one is almost complete L type chondrite. However this field is one of area where is expected large number of meteorites. Much more search in the area will be needed in future.

**Nansenisen** is recognized as an one of the most excellent area on meteorite concentration by the result of the reconnaissance search at February to March, 1988. Over 200 specimens are relatively large mass (average: -300g) and most of them are individual with less fragmental specimens. This collection includes 46kg chondrite (the largest one, almost complete stone) and 5.7kg eucrite (complete-angular stone). This collection also include some unique specimens of unbrecciated eucrites, brecciated diogenites (similar to Johnstown diogenite), carbonaceous chondrites with many irregular-rounded white inclusions, ureilites and others. However any lunar meteorite and martin meteorite had not been discovered in this expedition.

Table 1  Asuka-87 meteorites collection

|  | Mt. Balchen | Mt. Nils Larsen | Nansenisen |
|---|---|---|---|
| Total | 113 | 3 | 246 |
| The largest sp. | 19kg(L) | - | 46kg(L-LL) |
| Iron | - | - | 1 |
| Mesosiderite | 1 | - | - |
| Ureilite | 1 | - | 1 |
| Euc-Diog | - | - | 1 |
| Eucrite | - | - | 3(2 mono.) |
| Diogenite | - | - | 3 |
| C. chondrite | - | - | 7 |
| Chondritic | 106 | 3 | 225 |
| Doubtful | 5 | 0 | 5 |
| Total weight | -30kg | < kg | >89kg |

Fig.1 Field view of **Asuka-87251** chondrite: the largest specimen in the Asuka-87 meteorites collection is about 46kg in weight and measured 42 x 27 x 27 cm, almost complete stone with brownish dull black fusion crust which is partly ablated.



Fig.2 Field view of **Asuka-87272** eucrite: the largest achondrite in the Asuka-87 meteorites collection. This fresh stone weighed 5.7kg and measured 20 x 16 x 11 cm, showing angular and complete stone with shiny-black fusion crust.

Subclassification of unequilibrated ordinary chondrites

Hideyasu Kojima and Keizo Yanai
Department of Meteorites, National Institute of Polar Research
9-10, Kaga 1-chome, Itabashi-ku, Tokyo 173, Japan

Sears et al(1982) devided type 3 ordinary (hereafter UOC) chondrites into 10 stages, from type 3.0 to 3.9 by the thermoluminescence sensitibity. However, this classification is not well examined by petrographycally and petrochemically. This study focuses on this view point.

One of the criteria of type 3 ordinary chondrite is high dispersion of olivine and pyroxene compositions. For exsample, Percent mean diviation (%MD) of Fe of olivines and pyroxenes of type 3 chondrites is larger than 5%. However, the range of the %MD of Fe varies very wide. It indicates posibility of subclassification of UOC.

Thirty of UOC were studied. UOC studied divided into 3 groups on histograms of Fe of olivine and pyroxene as following .

I. The chondrites which belong to group I show the largest %MD and histograms of both olivines and pyroxenes lack modes.

II. Histograms for group II chondrites show distinct mode in the olivine distribution but histograms lack mode in the low-Ca pyroxene distribution.

III. Histgrams for group III chondrites which show smaller %MD show distinct modes in the olivine and low-Ca pyroxene distributions.

On the other hand, Kojima et al(1985) presented that UOC was divided into 4 groups on $Cr_2O_3$ contents. Olivines in group 1 UOC contain 0.2-0.3% $Cr_2O_3$ and the co-existing low-Ca pyroxenes contain 0.6-0.7% $Cr_2O_3$. In group 2, $Cr_2O_3$ is olivines is lower (0.05-0.1%) but $Cr_2O_3$ in low-Ca pyroxenes is the same as in group 1. In group 3, the low-Ca pyroxene has significantly lower $Cr_2O_3$ content than group 2. in group 4, $Cr_2O_3$ in olivines is about 0.02%, and $Cr_2O_3$ in low-Ca pyroxenes ranges 0.15 to 0.33%. However, criterion that divide group 3 and 4 is not clear.

We present a new subclassification of UOC in connection with histgrams of Fe and $Cr_2O_3$ contents in olvines and pyroxenes ( table 1).

1. Histograms of Fe contents of both olivines and low-Ca pyroxene lack modes.
   Olivines contain $Cr_2O_3$ larger than 0.2%.

2. Histograms of Fe content of both olivines and low-Ca pyroxene lack modes as same as group 1.
   olivines contain less amount of $Cr_2O_3$ than group 1. However $Cr_2O_3$ of low-Ca pyroxene is the same as that of group 1.

3. Histograms show distinct mode in the olivine distribution but histgrams lack modes in the low-Ca pyroxene distribution.

4. Histgrams show distinct modes in the olivine and low-Ca pyroxene distributions.

References:
Kojima H., Yanai K. and Ikadai S.(1985): Papers presented to the 10th Symposium on Antarctic Meteorites, 43-44.
Sears D.W., Grossman J.N. and Melcher C.L.(1982):Geochim. Cosmochim. Acta 46, 2471-2481.

| Name | Type | ol | | | | px | | | | TL |
|------|------|------|------|---|------|------|------|---|------|----|
| | | mean | M.D. | P | Cr2O3 | mean | M.D. | P | Cr2O3 | |
| Y-74660 | LL3 | 10.20 | 6.50 | | 0.31 | 8.30 | 6.38 | | 0.61 | |
| ALH-77176 | L3 | 12.40 | 6.77 | | 0.25 | 9.20 | 6.27 | | 0.61 | 3.2 |
| Y-793408 | | 11.40 | 4.53 | | 0.19 | 10.70 | 7.18 | | 0.69 | |
| Y-791835 | | 13.50 | 9.27 | | 0.22 | 11.90 | 7.21 | | 0.67 | |
| ALH-77011 | L3 | 14.70 | 7.57 | | 0.06 | 8.10 | 5.13 | | 0.60 | 3.5 |
| Y-74417 | L3 | 14.80 | 6.75 | | 0.09 | 11.10 | 6.56 | | 0.61 | |
| ALH-764 | LL3 | 19.00 | 9.73 | | 0.09 | 11.40 | 7.58 | | 0.67 | 3.3 |
| ALH-77167 | L3 | 17.60 | 9.09 | | 0.06 | 8.80 | 5.79 | | 0.64 | 3.4 |
| Y-791052 | | 15.00 | 5.01 | | 0.09 | 11.70 | 6.43 | | 0.59 | |
| Y-82038 | LL3 | 11.18 | 5.57 | | 0.11 | 8.28 | 2.20 | | 0.67 | |
| Y-793567 | L3 | 18.00 | 5.88 | | 0.09 | 10.00 | 4.46 | | 0.49 | |
| ALH-78237 | | 17.70 | 11.31 | | 0.04 | 9.40 | 6.01 | | 0.65 | |
| ALH-77278 | LL3 | 22.50 | 7.93 | P | 0.09 | 13.90 | 5.86 | | 0.42 | 3.6 |
| Y-791428 | H3 | 17.40 | 0.35 | P | 0.03 | 14.40 | 5.30 | | 0.33 | |
| Y-791429 | L3 | 22.10 | 1.48 | P | 0.08 | 15.70 | 3.76 | | 0.38 | |
| Y-791014 | L3 | 20.90 | 2.38 | P | 0.04 | 14.40 | 5.24 | | 0.63 | |
| ALH-77299 | H3 | 16.50 | 3.05 | P | 0.07 | 12.40 | 6.29 | | 0.51 | 3.7 |
| Y-791338 | H3 | 18.30 | 1.20 | P | 0.02 | 12.60 | 5.04 | | 0.38 | |
| Y-791325 | H3 | 17.60 | 0.33 | P | 0.02 | 14.60 | 3.57 | | 0.37 | |
| Y-791057 | H3 | 18.20 | 0.29 | P | 0.02 | 13.60 | 3.11 | | 0.38 | |
| Y-791038 | H3 | 18.00 | 3.04 | P | 0.03 | 11.60 | 4.63 | | 0.42 | |
| Y-791961 | L3 | 21.00 | 1.10 | P | 0.02 | 14.60 | 4.87 | | 0.29 | |
| Y-793375 | L3 | 24.50 | 1.40 | P | 0.03 | 12.80 | 4.79 | | 0.39 | |
| Y-793396 | L3 | 21.30 | 0.32 | P | 0.04 | 13.30 | 4.59 | | 0.35 | |
| Y-791340 | H3 | 16.80 | 1.45 | P | 0.04 | 14.30 | 1.40 | P | 0.19 | |
| Y-791354 | H3 | 18.20 | 1.07 | P | 0.02 | 13.50 | 3.42 | P | 0.23 | |
| Y-791370 | H3 | 16.90 | 1.83 | P | 0.03 | 13.90 | 4.28 | P | 0.37 | |
| Y-791377 | H3 | 17.30 | 1.02 | P | 0.03 | 15.00 | 0.95 | P | 0.30 | |
| Y-791387 | H3 | 17.90 | 0.76 | P | 0.02 | 15.60 | 0.86 | P | 0.20 | |
| Y-791828 | L3 | 21.70 | 3.52 | P | 0.05 | 16.00 | 4.35 | P | 0.36 | |

Table 1.

YAMATO-793592: THE FIRST ENSTATITE ACHONDRITE (AUBRITE) IN THE YAMATO METEORITES; Keizo Yanai and Hideyasu Kojima, Department of Meteorites, National Institute of Polar Research, 9-10, Kaga 1-chome, Itabashi-ku, Tokyo 173, Japan

Introduction: Yamato-793592 (Y-793592) has been classified as the first enstatite achondrite (aubrite) in about 4000 specimens of the Yamato meteorites collections. Y-793592 is a friable stone (Fig.1) weighing only 31g. This stone is conspicuous by its white interior and retains only a minor amount of black fusion crust. It consists most of coarse-grained angular white pyroxene with minor plagioclase, and less abundant smaller black mineral and lithic fragments. Some metal is present and oxidation (brown color) occurs around the metal grains.

Texture and mineral compositions: Under the microscope, Y-793592 shows typical brecciated texture (Fig.2) and angular enstatites (1-6mm across) enclosed in a breccia of much smaller enstatite crystals (under 1mm across) with minor plagioclase, metal, opaques and traced olivine (under 0.1mm across). Composition of the silicates and opaque phases are given (Table 1). The iron content of the silicate sphases is remarkably low and it is similar to those of known aubrites. Most of Mg-rich pyroxene and Mg-olivine are pure enstatite and pure forsterite respectively. Ca-rich pyroxene is also nearly iron free-diopsidic pyroxene. The feldspar is albite (Table 1) and is present up to 0.1mm across.

Opaque phases are not abundant in Y-793592. Metal is grains with remarkably lower content of Ni(average 3.10%, range 2.91-3.47%). Most common sulfides are daubreelite and troilite. Daubreelite is Fe-Cr sulfide and is one of common opaque in Y-793592. Troilite is also common opaque, but there are abundant in compositional varieties of each troilite grains, especially iron content(42-62%), Mn(0-1.5%), Cr(0.2-9.3%), Ti(0.4-10%), Zn(0-4.4%), Ni(0-2.5%). Common kamacite, taenite, perryite, alabandite, oldhamite and schreibersite were looked for but not found in Y-793592 aubrite so far.

Bulk chemistry: The major-element composition of Y-793592 was determined by standard wet chemical analysis by H. Haramura. The results are presented in Table 2 with data for Allan Hills(ALH)-78113 aubrite and Y-691 enstatite chondrite for comparison. The similarity in bulk composition of the two aubrites; Yamato and Allan Hills, is obvious. Some elements; $Al_2O_3$ CaO, and
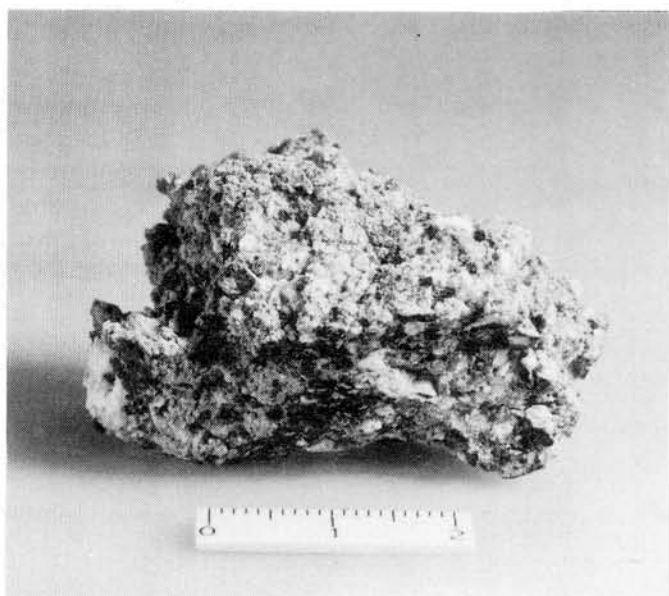


Fig.1 Yamato-793592 is newly classified as an aubrite showing friable stone with less fusion crust, weighing 31g.

$Na_2O$ of Y-793592 are slightly higher than those of ALH-78113, and FeO and MgO are slightly lower. But two aubrites differs markedly from Y-691 enstatite chondrite, in particular poor $SiO_2$ and MgO, but enrich metal and sulfide in Y-691.

Table 1    Microprobe analyses of silicates and opaque phases in the Yamato-793592, in weight percent. Numbers in parentheses are those of analyses averaged.

| Silicates | Pyroxene (Mg-rich) (31) | Pyroxene (Ca-rich) (15) | Olivine (9) | Plagioclase (9) |
|---|---|---|---|---|
| $SiO_2$ | 58.97 | 54.94 | 41.42 | 67.66 |
| $TiO_2$ | 0.02 | 0.47 | 0.01 | 0.01 |
| $Al_2O_3$ | 0.10 | 0.29 | 0.02 | 19.23 |
| FeO | 0.04 | 0.04 | 0.03 | 0.02 |
| MnO | 0.07 | 0.01 | 0.04 | 0.02 |
| MgO | 39.87 | 20.11 | 57.62 | 0.01 |
| CaO | 0.44 | 23.37 | 0.06 | 0.47 |
| $Na_2O$ | 0.02 | 0.28 | 0.02 | 10.95 |
| $K_2O$ | 0.01 | 0.01 | 0.00 | 0.55 |
| $Cr_2O_3$ | 0.02 | 0.01 | 0.00 | 0.01 |
| Totals | 99.55 | 99.55 | 99.23 | 98.92 |
| En | 99.16 | 54.44 | Fo 99.98 | Ab 94.66 |
| Fs | 0.06 | 0.06 | Fa 0.02 | An 2.26 |
| Wo | 0.78 | 45.50 | | Or 3.11 |

| Opaque phases | Ni-poor metal (7) | Daubreelite (17) | Troilite average (22) | Troilite range |
|---|---|---|---|---|
| Ca | 0.01 | 0.01 | 0.01 | 0.00- 0.03 |
| Fe | 96.85 | 17.33 | 57.35 | 42.52-62.11 |
| Mn | 0.02 | 0.45 | 0.13 | 0.00- 1.48 |
| Cr | 0.02 | 36.57 | 0.83 | 0.18- 9.26 |
| Ti | 0.01 | 0.13 | 3.79 | 0.36- 9.96 |
| Zn | 0.06 | 0.21 | 0.43 | 0.00- 4.42 |
| Mg | 0.01 | 0.03 | 0.02 | 0.00- 0.06 |
| S | 0.01 | 43.87 | 37.08 | 35.89-38.41 |
| Ni | 3.10 | 0.14 | 0.22 | 0.00- 2.48 |
| Si | 0.00 | 0.01 | 0.02 | 0.00- 0.11 |
| P | 0.10 | 0.02 | 0.02 | 0.00- 0.08 |
| Co | 0.24 | 0.24 | 0.09 | 0.00- 0.55 |
| Total | 100.42 | 99.01 | 99.99 | |
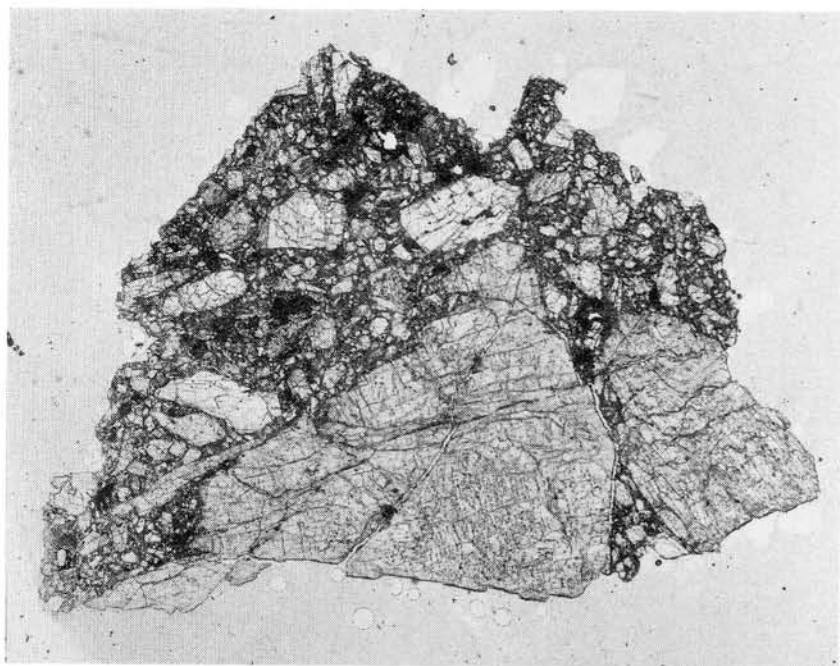
Fig.2 Textural relationship in the new found Antarctic aubrite in Yamato collections. Typical brecciated texture of enstatite with plagioclase and traced olivine and opaques. Open nicol, field view 8 mm wide.

Table 2 Bulk composition of enstatite achondrite Y-793592, compared with ALH-78113(aubrite) and Y-691(EH), in weight percent

|  | Y-793591 (aubrite) | ALH-78113 (aubrite) | Y-691 (EH3) |
|---|---|---|---|
| $SiO_2$ | 56.41 | 57.16 | 36.31 |
| $TiO_2$ | Trace | 0.02 | 0.08 |
| $Al_2O_3$ | 2.20 | 0.18 | 2.93 |
| $Fe_2O_3$ | <0.05 | 0.0 | 0 |
| FeO | <0.1 | 0.97 | 0.96 |
| MnO | 0.18 | 0.17 | 0.24 |
| MgO | 35.53 | 39.25 | 19.59 |
| CaO | 1.72 | 0.62 | 1.29 |
| $Na_2O$ | 0.96 | 0.15 | 0.83 |
| $K_2O$ | 0.11 | 0.02 | 0.07 |
| $H_2O(-)$ | 0.25 | 0.69 | 0.50 |
| $H_2O(+)$ | 1.41 | 0.0 | 0.5 |
| $P_2O_5$ | 0.07 | tr. | 0.46 |
| $Cr_2O_3$ | 0.025 | 0.06 | 0.45 |
| FeS | 0.97 | 0.77 | 16.31 |
| Fe } | 0.0 | 0.0 | 17.8 |
| Ni | 0.32 | 0.055 | 1.71 |
| Co | 0.23 | 0.003 | 0.077 |
| Total | 100.32 | 100.11 | 100.10 |

EUROMET: A EUROPEAN PROJECT TO RECOVER METEORITES FOR STUDY BY THE INTERNATIONAL SCIENTIFIC COMMUNITY.
Robert Hutchison,

Mineralogy Department, The Natural History Museum, London SW7 5BD.

Introduction  Following the success of the Japanese and American programmes for meteorite recovery in Antarctica, meetings were held among European scientists interested in undertaking similar work.  Forty research groups from eleven European nations offered support.  An application for funds was made to the European Commission, which subsequently agreed to provide support for 32 months.  Funding will cover part of the cost of re- covery, curation and classification of meteorites and cosmic dust from Antarctica.

Collection of material  Some 230 meteorites already collected by two German expeditions to Victoria Land have generously been donated to Euromet.  In 1990-91, the first Euromet field party of four, operating from the Italian base at Terra Nova, collected 260 meteorites in the Frontier Mountains.  These meteorites have now arrived at The Open University in the UK, where processing has begun.  In all, some 500 meteorites are assigned to Euromet, of which only 60 have been classified to date.

Recovery of micrometeorites from Antarctic ice is largely supported by France.  Following earlier successful operations, in 1990-91 Dr M Maurette used a steam generator to melt 256 tonnes of ice near Cap Prudhomme.  Sieving was used to recover over 10,000 micrometeorites, from 50μm to 400μm, from the water.  The samples are held in the Université de Paris, Campus Orsay.

Euromet organisation  On April 4 1991, a Council of four was con- stituted under the Chairmanship of Professor C T Pillinger.  The Council is supported by a Working Group on Meteorites:

METEORITES WORKING GROUP
Chairman, Dr R Hutchison, London.
Dr A Bischoff, Munster.
Dr O Eugster, Bern.
Dr C Koeberl, Vienna.
Dr M Maurette, Orsay.
Dr G-T Sighinolfi, Modena.
Dr I P Wright, Milton Keynes.

After classification, and notification of a meteorite in The Meteoritical Bulletin, applications for research material may be made to the Chairman of the Working Group at any time.  A decision will normally be made by the Chairman in consultation with one member of the Working Group approp- riate for the area of research to be pursued.  This should only take a few weeks, unless difficulty arises, when the application may come before the whole Working Group and Council.  Applications are invited from all nations.

Micrometeorites will be dealt with in a similar way, except that it is not practicable to classify or describe individual particles prior to their being issued for research. Applicants should contact Dr Maurette, direct. In general, aliquots of particular size-fractions collected at particular times will be issued.

Conclusion We aim to make Euromet meteorites and micrometeorites available to competent members of the international scientific community. It is an exciting prospect to be able to work on new and interesting samples. For example, among the first 60 Allan Hills 88--- meteorites classified, 5 are unequilibrated ordinary chondrites and one is EH3. In addition, there are several carbonaceous chondrites. New data on Euromet meteorites will be presented.

POSSIBLE METEORITIC IMPACT CRATERS IN JAPAN

Yasunori MIURA, Toshio KATO, Masashi IMAI and Makoto OKAMOTO

Department of Min. Sci. & Geology, Fac. of Sci., Yamaguchi University Yoshida, Yamaguchi 753, Japan.

## 1. Introduction

Meteoritic impact craters can be discussed by the following evidences:

1) Projectile: meteorites exist.
2) Structure: circular or semi-circular basin structure can be found by field research or satellite image.
3) Shock metamorphism: materials of shocked minerals, tektites or brecciated rocks are found near craters [1-3].

From complicated characteristics of Japanese island, possible meteoritic impact craters in Japan are considered as follows.

1) Iron meteorites are found as projectiles of small impact craters,
2) Almost all circular impact structures are destroyed by progressive plate tectonic movements and volcanic activities except small craters, and
3) Shocked minerals and rocks can be found as impact indicators. Tektites and diaplectic glasses could not found in Japan.

Main purpose of this study is to discuss possible impact craters in Japan mainly by applying the shock metamorphic data.

## 2. Impact indicators

From the above three evidences of impact craters, possible impact craters in Japan are considered in this study.

1) Iron meteorite as projectile: Among 18 iron meteorites reported in Japan, 14 iron meteorites are described in details. Among 14 iron meteorites 7 iron meteorites (Tanokami, Shirahagi, Okano, Sakauchi, Kuga, Saotome, and Tendo) are exceeded the weight by 1kg to make impact craters which evidences are applied from data of Australian impact craters.

2) Circular structures in Japan which are easily formed by local volcanic and tectonic activities should be checked also by shocked minerals if there exist possible impact craters.

3) Impact indicators of shocked metamorphism are summarized as follows:
   a) High-pressure silica minerals: metastable stishovite and coesite are difficult to find in Japanese destroyed large structure except drilled samples, if there.
   b) Anomalous quartz: this type of quartz can be easily checked by opical and X-ray density and found in all types of impact craters.
   c) Anomalous secondary cristobalite: this type of cristobalite can be found at the rim of craters if there is circular structure.
   d) Anomalous feldspar: this type of diaplectic glassy plagioclase can be found in impact craters of plagioclase-bearing target rocks.
   e) Increased ratio of anomalous quartz to feldspar (Q/F): the ratio Q/F can be checked only in feldspar-bearing target rocks.

## 3. Candidates for Japanese impact craters:

The following results are summarized in this study [2,3].

1) The largest Japanese iron meteorites of Tanokami (ca. 170kg) might form Henbury-size impact craters, but the exact place is still unknown.

2) The second and third largest Japanese iron meteorites of Shirahagi (ca. 23kg) and Saotome (ca. 11kg) found in the rivers indicate possible impact craters (but exact location is unknown) or similar meteorite collection type transported by glacier movement of the Japanese Alps with the Antarctic meteorites.

3) Anomalous quartz grains are obtained in Kuga iron meteorite (ca. 6kg) with probable semi-circular impact crater (cf. Table 1).

4) Hoshinoko-Zan impact crater [4,5] without iron meteorites shows circular structure. But few shocked data have been obtained so far.

5) Ohtaki circular impact structure with anomalous shocked data and cristobalite have no meteorite. But before concluding the meteoritic impact crater of Ohtaki structure, it should be checked by the possibility of impacted structure formed by ejected big rock from errupted Mt. Ontake or by finding the meteorite.

6) Very small impact crater (ca. 30 cm in diameter) formed by Kokubunji L6 chondrite (Total ca. 11 kg) has no distinct shocked data of target rock.

7) From shocked mineral data, Kuga and Ohtaki target rocks are possible impacted target rocks in Japan.

Table 1. Shocked mineral data of target rocks in Japanese possible impact craters, compared with artificial and natural impact craters.

| Sample | $\Delta \rho$ (%), anomalous quartz | Anomalous cristobalite (vol.%) | Ratio, Q/F | Stishovite and Coesite (vol.%) | Meteorite, Crater structure |
|---|---|---|---|---|---|
| Kuga | +0.52(rim) | 7 | >100 | 0, 0 | Iron, small |
| Ohtaki | +0.32(rim) | 5 | 5.6 | 0, 0 | Non, circular |
| Hoshinoko-Zan | +0.16(rim) | 6.5 | 2.5 | 0, 0 | Non, circular |
| Tanokami(?) | +0.21 | 0 | 0 | 0, 0 | Iron(?), Non |
| Artificial (ACG) | +0.30(r,c) | 3 | 3.6(rim) | 0, 0 | Fe metal |
| Barringer(B-3) | +0.64(rim) | 5 | >100 | 2,20 | Iron |
| Dalgaranga(4) | +0.35(rim) | 0 | >100 | 0, 0 | Stony-iron |

**References:**

[1] French B. (1968): <u>Shock metamorphism of natural materials,</u> 1-17.
[2] Miura Y. et al.(1990): Intern. Workshop on Meteoritic Impact on the Early Earth (Perth), <u>LPI Contribution</u>, No. 746, 30-35.
[3] Miura Y. (1991): <u>Shock Waves, an International Journal</u>, 1, 35-41.
[4] Graham A., Bevan A. and Hutchison R. (1985): Catalogue of Meteorites (British Museum), 423-454.
[5] Classen J. (1977): Meteoritics, 12. 61.

SHOCK METAMORPHISM OF SILICA MINERALS IN METEORITIC AND ARTIFICIAL
IMPACT CRATRES.

Yasunori MIURA, Toshio KATO, Masashi IMAI and Takako ASHIDA.
Department of Min. Sci. & Geology, Fac. of Sci., Yamaguchi University
Yoshida, Yamaguchi 753, Japan.

## 1. Introduction

Shock (or impact) metamorphism (i.e. high pressure shock wave effect
within a few microseconds [1-7]) of natural materials is mainly discussed
by physical, mineralogical and morphological changes of rocks and minerals.

However, there are few detailed data of constituent minerals and density
variation by shock metamorphism.
   The purposes of the present study are
1) characterization of silica minerals formed by shock metamorphism in
   in natural and artificial impact craters, and
2) application of these indicators and formation processes to natural
   impact craters and Cretaceous-Tertiary (K/T) boundary samples.

## 2. Characterization of silica minerals

Impact metamorphism of silica minerals can be analyzed by the
followingexperimental procedure:
1) optical change at cross nicols,
2) constituent minerals,
3) volume change of vein-type lamellae in shocked quartz [4], and
4) change of cell-dimensions and calculated densities.

From the characterization of shocked silica minerals, the following
minerals are formed by various formation processes [7,3].
1) Compression stage of shock impact.
   a) At low pressure:
      Low pressure type quartz with anomalous density (<1%) and
      optical properties (i.e. "anomalous quartz") is formed.
   b) At high pressure:
      High pressure silicas, stishovite and coesite, are formed.
      Low pressure type quartz by transformation from higher
      pressure (i.e. "anomalous quartz") is formed.

2) The initial release stage.
  a) At low pressure: **anomalous quartz** with wavy extinction is formed.
  b) From high pressure: **Shocked quartz grains** (i.e. **anomalous quartz**) **with shock lamellae** are formed. The difference in volume between stishovite (or coesite) and quartz is the mechanism for generating the vein formation which indicates shock lamellae after expanding in volume with relict of higher density.
  c) **'Secondary cristobalite'** as by-product of shock metamorphism is formed after decreasing the pressure.
  d) **'Secondary shocked quartz'** as by-product of shock metamorphism is formed.
3) The later release of contamination stage.
  Shocked quartz with lamellar veins with a decorated planar texture (with glass, tridymite, cristobalite, relict coesite etc.) is formed.

## 3. Artificial impact crater

Experiments that generated artificial impact craters have been carried out with rail-gun at the National Institute of Space and Astronautical Science (ISAS), Japan by using two kinds of target rocks (i.e. Khoyama gabbroic anorthosite ACB and Tokuyama granite ACG) and projectiles (i.e. steel and plastic projectiles) performed at higher velocity from 2.8 to 7.9 km/sec. The following results are obtained in this study [7,8]:

1) Optical data: **Irregularly wavy extinction** of quartz (and feldspar) grains can be often observed at the center(C), medium(M) and rim(R) walls and ejecta(E) samples of both craters. However, clear shock lamellae could not observed in quartz minerals.
2) Density data: Density variation ($\Delta \rho$) maxima of anomalous quartz are obtained at the **rim** walls of both target craters. Density of quartz at the center wall of granite target is the same of original granite before bombardment (i.e. center wall is up-lift rock). Density of anomalous quartz of **the ejecta** shows the largest value. Density of anomalous quartz is **larger in gabbroic anorthosite target** rock with smaller regular grains, than the granitic target with larger irregular garins. The impact energy was used to break the grain boundary of irregular larger grains, resulted in irregular crater shape of granitic target.
3) Mineral abundances: High-pressure type silica could not observed. By-products by decreaing pressure are 'cristobalite' which obtained at the middle and rim walls. Ratio of anomalous quartz to feldspar is increased at the **rim walls** and the ejecta samples of two target craters.

Electron probe data indicate that **K, Na, Ca and Al ions of feldspar** minerals in the original rocks are moved partly to form silica phase (i.e. anomalous quartz or cristobalite).

The content of quartz between original rock and the center wall of the crater is almost the same after removing largely shocked materials.

4) Type of projectile: **Steel projectile** shows similar ratio (of quartz to feldspar) in the natural impact craters, compared with the plastic projectile. Density of the anomalous quartz is larger **in gabbroic anorthosite** target by the steel projectile due to textural difference of target rock.

## 4. Application of shocked quartz to natural impact craters and K/T boundary

Mineralogical, petrological and morphological evidences of shock metamorphism are discussed by the following indicators [8]:

1) Stishovite (S1) and coesite (C1) exist at the rim and ejecta of craters.
2) Anomalous quartz (types Q1, Q2 and/or Q3) ca be found in all types of impact craters.
3) Shocked quartz with lamellar vein (type Q1 + glassy vein G1) can be found in larger impact craters.
4) Cristobalite (CR1) formed in almost all types of imapct craters.
5) Ratio of quartz to feldspar (Q/F) is increased in almost all types of impact craters.

Three indicators of shock metamorphism (i.e. quartz and cristobalite contents and density variation) are checked at impact samples of various impact craters [7-10].

1) Anomalous contents of cristobalite up to 20 volume percents are found in larger impact craters of the Manicouagan and Charlevoix. Stishovite and coesite are found only in Barringer crater.
2) Density variations of anomalous quartz are obtained in these impact craters up to +0.7 %, compared with standard rock crystal.
3) Possible impact craters in Japan (e.g. Kuga, Ohtaki and Hoshinoko) will be checked by these indicators of shock metamorphism.

Relation between crack-lamellar vein percentage (i.e. **x** vol.%) and shock pressure (i.e. **y** kbar) is expressed by the following equation.

$$y = 9.41 \cdot x - 33.77 \ (r=0.98)$$

Relation between density deviation $\Delta \rho$ (%) obtained from unit cell-parameters of quartz grains (i.e. **x** %) and shock pressure obtained from shock lamellae of Charlevoix Impact structure [9] (i.e. **y** kbar).

$$\mathbf{y} = 494.3 \cdot \mathbf{x} + 14.8 \quad (r=0.89)$$

Table 1. Maximum mineral contents of quartz, cristobalite, stishovite and coesite, the ratio Q/F and density variation of quartz.

| Sample | Cristobalite (vol.%) | Quartz/ Feldspar | Stishovite (vol.%) | Coesite (vol.%) | $\Delta \rho$ of quartz(%) |
|---|---|---|---|---|---|
| Artificial ACG | 3 | 3.6 (rim) | 0 | 0 | +0.30 (r,c) |
| ACAG | 0 | 0.5 (rim) | 0 | 0 | +0.04 (rim) |
| Barringer (B-3) | 5 | – | 2 | 20 | +0.64 (rim) |
| Charlevoix (7,11) | 20 | 7.4 (rim CP) | 0 | 0 | +0.30 (rim) |
| Manicouagan | 30 | 6.7 (CP) | 0 | 0 | +0.08 (rim) |
| Clearwater Lakes | 2 | – | 0 | 0 | +0.42 (Hole) |
| Lake Mistastin | 0 | – | 0 | 0 | +0.42 (melt) |
| Dalgaranga (4) | 0 | >100 | 0 | 0 | +0.35 (rim) |
| Gosses Bluff (3) | 0 | >100 | 0 | 0 | +0.38 (shat) |
| Japanese K/T (HB) | – | – | 0 | 0 | +0.15 |
| American K/T (CCN) | – | – | 0 | 0 | +0.83 |

**References:**
[1] Dietz R.S. (1960): Science, 131, 1781-1784.
[2] Chao E.T.C. (1967): Science, 156, 192-202.
[3] French B. (1968): Shock metamorphism of natural materials, 1-17.
[4] Bohor B. F. et al. (1986): Science, 224, 867-869.
[5] Miura Y. and Imai M. (1990): Intern. Workshop on Meteoritic Impact on the Early Earth (Perth), LPI Contribution, No. 746, 30-31.
[6] Miura Y., Ashida, T. and Okamoto M. (1990): Intern. Workshop on Meteoritic Impact on the Early Earth, LPI Contribution, 746, 34-35.
[7] Miura Y. (1991): Shock Waves, an International Journal, 1, 35-41.
[8] Miura Y. (1991): LPSC XXII (NASA, LPI), 905-908.
[9] Robertson P.B. (1975): Geol. Soc. America Bull., 86, 1630-1638.
[10] Grieve, R.A.F. and Floran, R. (1883): J. G. R., 88, A807-A818.

SHOCK METAMORPHISM OF ACHONDRITES, LUNAR SAMPLES AND LUNAR METEORITES

Yasunori MIURA, and Toshio KATO

Department of Min. Sci. & Geology, Fac. of Sci., Yamaguchi University
Yoshida, Yamaguchi 753.

## 1. Introduction

There are no detailed data on shock metamorphism of achondrites and lunar meteorites. It is found that shock metamorphism of silica and feldspar minerals can be discussed by using five impact indicators of high pressure silica (HPS), shocked quartz with lamellae (SQL), anomalous quartz (AQ), anomalous cristobalite (AC), and increased ratio of anomalous quartz to feldspar (AQ/F) [1,2].

The purposes of the present study are
1) characterization of silica and feldspar minerals in achondrites and lunar meteorites (lunar samples) formed by shock metamorphism, and
2) estimation of shocked conditions at the meteoroid and lunar surface by using these impact indicators.

## 2. Meteorites

Achondrite meteorites contain shocked minerals of silica and feldspar (cf. Table 1 [3-7]).
1) Plagioclase phases show anomalous composition (with minor Fe·Mg contents etc.) and diaplectic structure (called as maskelynite). Anomalous plagioclase grains are found Yamato-691(EH3) chondrite, and Stannern, Camel-Donga and Juvinas eucrites.
2) Anomalous quartz with high density are found.

## 3. SNC meteorites

Zagamic SNC achondrite contains of anomalous quartz and feldspar grains with the largest deviated density as follows (cf. Table 1 [3,4]):
1) Anomalous plagiocalse grain is obtained with diaplectic diffuse structure with high density (i.e. +2.4 % of density deviation).
2) Anomalous quartz grains of diaplectic diffuse structure is obtained as high density data (i.e. +1.7% of density deviation).
3) Estimated shocked pressure of anomalous quartz is calculated as about 835 (kbar) from regression equation of Charlevoix impact crater [5,6].

Such anomalous data could not obtained in terrestrial impact craters. It is considered to be partly recrystallized phase of ejected glassy materials from the Martian surface.

## 4. Lunar Regolith

Lunar samples collected are almost all regolith meterials ejected from the lunar impact craters. Thus silica and feldspar of lunar samples are brecciated or recrystallized phases formed by lunar shock metamorphism as follows (cf. Table 1 [3]).

1) Lunar plagioclases show anomalous compositions which are considered to be impact indicators of the lunar surface, compared with stoichiometric plagioclases formed at terrestrial plutonic conditions.
  Anomalous plagioclase compositions (normalized by Si) consist of
   a) Ca-excess (11 vol.%),
   b) Ca(Al)-excess and Na(Al)-deficient (37 vol.%),
   c) Fe·Mg(Ca)-excess and Al·Na-decient (21 vol.%), and
   d) Ca·Fe·Mg(Al)-excess and Na(Al)-deficient (31 vol.%)
  These lunar plagioclases of the regolith materials show similar smaller density to the diaplectic phases obtained in the terrestrial impact craters.
2) Lunar quartz of silica minerals is anomalous quartz with high density. Anomalous quartz in lunar basaltic compositions is considered to be formed by impact-induced high temperature (not from magma).
  No high pressure type silica minerals of stishovite and coesite can find at lunar samples due to rapid decreasing the pressure at impact event if silica minerals exist in lunar target rocks.
3) Anomalous cristobalite and tridymite found in lunar mare basaltic compositions contain minor elements of Al, Ca, Fe, Ti, K and Na, resulted in smaller density than terrestrial low cristobalite and tridymite (i.e. -0.7% and -0.4% density deviations, respectively).

## 5. Lunar meteorites

Anomalous silica and feldspar minerals formed by shock metamorphism of lunar meteorites are found from the lunar meteorites of the Antarctica (Yamato-86032) and from Non-Antarctica. Detailed dat will be discussed at the 1991 NIPR symposium.

Table 1. Preliminary shocked mineral data of achondrite and lunar samples.

| Sample | $\rho/\rho_0$(%), anomalous quartz | $\rho/\rho_0$(%), anomalous cristobalite | $\rho/\rho_0$(%), anomalous tridymite | $\rho/\rho_0$(%), anomalous plagioclase |
|---|---|---|---|---|
| Meteorites | | | | |
| Y-691 | - | - | - | +0.5± |
| Juvinas | - | - | - | +0.1~+0.7 |
| Stannern | - | - | - | +0.1~+1.0 |
| Camel Donga | - | - | - | +0.8 |
| | | | | |
| SNC achondrite | | | | |
| Zagami | +1.66 | - | - | +2.44 |
| | | | | |
| Lunar samples | | | | |
| | +1.0± | -0.7(min) | -0.4(min) | 0.0~-0.7 |
| Lunar Meteorites | | | | |
| | | - | - | |

The present research is partly supported by the Grant-in-Aid for Scientific Research on Priority Areas (Shock Wave Research) of the Japanese Ministry of Education, Science and Culture of the senior author.

## References:

[1] Miura Y. et al. (1991): 16th NIPR Sympo. on Antarctic Meteorites (in press).
[2] Miura Y. et al. (1991): 16th NIPR Sympo. on Antarctic Meteorites (in this volume).
[3] Miura Y. (1988): LPSC XIX, 792-793.
[4] Miura Y. et al. (1988): EOS, 69, 1292.
[5] Miura Y. and Hanaura Y. (1990): LPSC XXI, 793-794.
[6] Miura Y. et al. (1990): Intern. Workshop on Meteoritic Impact on the Early Earth, LPI Contribution, No. 746, 30-35.
[7] Miura Y. (1991): Shock Waves (Springer-Verlag), 1, 35-41.

Tetrataenite fine grains in Y-791717(CO3) chondrite.

Hideyasu Kojima, Takesi Nagata, Barbara J. Carleton and Chihiro Kaito*

National Institute of Polar Research, 9-10, Kaga 1-chome, Itabashi-ku, Tokyo 173, Japan
*Department of Electronics and Information Science, Kyoto Institute of Technology, Matsugasaki, Kyoto 606, Japan

A matrix of Yamato(Y)-791717 CO3 carbonaceous chondrite consists mainly of Fe-rich olivine with minor troilite, Fe-Ni metal and probably magnetite. The mineral assemblage indicates that the matrix was formed under the highly unequilibrated condition. Ninty of isolated fine grains of metal in the matrix of Y-791717 have been analyzed. They are approximately 10um in diameter. Five grains of tetrataenite were newly confirmed. Tetrataenite occures as isolate grains and accompanied grains with kamacite and taenite. The proportion of tetrataenite in metal grains is 5.5%.

Nagata and Carleton(1990) estimated with the aid of a magnetic granulometry analysis that Y-791717 chondrite contained tetrataenite grains of about 0.5%, and the smallest grains less than 6.5 nm in diameter occuppied 20% of all tetrataenite grains. Tetrataenite occupies 20% of fine metal grains less than 1um in Y-791717 (Nagata personal communication).

These results indicate that fine grains of tetrataenite less than 1um in diameter are more richer than lager grains.

On the other hand tetrataenite fine grains of 10-40nm in diameter were experimentally formed by combining a Ni smoke stream with a Fe smoke stream at a temperature around 200 C. The experimental results provided the evidence that tetrataenite can be produced at low temperature by the coalescence of Fe and Ni grains. (Kaito and Saito, 1989).

These facts read the authers to following conclusion. It seems likely that these fine tetrataenite in Y-791717 CO3 chondrite were formed by the coalescence process of Fe and Ni smoke ultra-fine particles rather than the generally proposed hypothesis that extremely slow cooling of Ni-rich disordered taenite formed tetrataenite.

References:
Nagata T. and Carleton B. J. (1990): Proc. Japan Acad., 66B, 183-188.
Kaito C. and Saito Y. (1989): Proc. Japan Acad., 65B, 125-128.

ALTERATION OF FUSION CRUSTS OF CHONDRITES -Results of Melting Experiments-

Yuji Tazawa: Department of Physics, Kyoto University, Kyoto 606, Japan
Takashi Sasaki: Sakuranomiya Osaka City High School, Osaka 534, Japan

Introduction   A large number of "Cosmic Spherules" have been recovered from a wide variety of the terrestrial environment. Because of the spherical shape and the composition similar to meteorites, the spherules have been supposed to be droplets of meteoritic bodies ( or fragments ) ablated during the atmospheric entry [e.g., 1]. As for irons and carbonaceous chondrites, genesic relation between fusion crusts, artificially ablated debris and "cosmic spherules" had been explained [e.g., 2, 3, 4]. While as for ordinary chondrites, though they are the most common type of meteorites, yet the relation has been uncertain.
    As reported previously [5, 6, 7], by means of INAA and SEM/EDX, we have been studying chemical and mineralogical alterations in the fusion crusts and the next interiors of several types of ordinary chondrites: e.g., Y-7304(L6), Y-74155(H3), Y-790448(LL3), ALH-77272(L6), Aomori(L6). INAA results could not clearly discriminate the abundances of trace elements between the crusts and the interiors because of the inhomogeneous local constituents and the incomplete sample separation. SEM/EDX results for thin-sections of L6 types showed the abundances of major and minor elements in Olivines (Ol), Pyroxenes (Px) and Plagioclases (Pl) altered systematically in order of depth from the surface.
    In this report, we have made fusion experiments on fragments of chondrites listed above, and Jilin(H6), Calliham(L6) and Allende(CV3) as well, by an electric furnace and a CO2-laser, to compare the previous results.

General Features of Fusion Crusts and Next Interiors   (1) The fusion crust (FC) of Aomori consists of two vitreous sub-layers; the outermost layer (FO) in which um-sized magnetite grains are prevalent and the inner layer (FI) in which the grains are rare, whose thickness are about 50-100 um and 100-200 um, respectively. While those of Antarctic chondrites fully (or considerably) lack FO, which seems to be due to a weathering. (2) Chemical compositions of FC are mostly homogenized in small scale ( 10 um) exept for the um-sized magnetite grains, but they vary in large scale ( 10 um). This seems to reflect the chemical composition of original constituents. FC of ordinary chondrites do not deplete volatile elements so much as those of carbonaceous chondrites. On the contrary, S and Na are not always depleted in FC but enriched, in some cases, into micro-spots. (3) A partially melted zone exists between FC and unmelted interiors (UMI), whose thickness is about 200-500 um and the chemical compositions vary transitionally from UMI toword FC. Grain bounderies of Ol and Px are more or less deformed and chemically influenced by surrounding constituents. Pl are mostly vitrified. We call this zone Transition Zone (TZ). Many chinks develop into Ol and Px, most of which are filled with Fe-rich materials. The fillings occur in the Antarctic (find) samples and the Aomori (fall) sample, which seem to be formed not by a terrestrial weathering but by the heating during atmosheric entry.

Melting Experiments   Melting experiments were made in vacuo by using a CO2 laser and an electric furnace. A few mg each of fragments taken from unmelted interiors of respective chondrites were heated in a boron nitride crucible. Sample temperatures and ambient pressures were measured by a thermospot sensor and a Pirani gauge. The samples were weighed and photomicrographed again after

heating. The samples thin-sectioned were studied by SEM/EDX.

All the samples except Calliham, which were heated by the furnace, became unglazed foamy spheres and/or partially broken balloons. On the surface of which, in some cases, tiny metal nuggets were seen. In the case of Calliham, several metal spheres and a transparent residue glazed on the bottom of crucible were only seen. The samples eradiated by the laser mostly preserved original forms: a vitrification developed well on the eradiated (top) side, vesicules and micrograins of opaque minerals (probably of magnetite or metal) were seen on the other (bottom) side. These features are somewhat different from those of FC mentioned before, which may be due to difference of thermal history, aerodynamic effect, and size of the matter.

References   [1] Murray J. and Renard A.F. (1883), Proc. Roy. Soc. Edinburgh, 12, 474. [2] Blanchard M.B. (1972), J. G. R., 77, 2442. [3] Fruland R.M. (1974), Meteoritics, 9, 339. [4] Brownlee D.E. et al. (1975), J. G. R., 80, 4917. [5,6,7] Tazawa Y. and Sasaki T. (1987,88,90), Abst. 12,13,15th Symp. Antarctic Meteor., NIPR.

# PSEUDOBROOKITE FROM THE LONAR IMPACT CRATER, INDIA

V. K. NAYAK

Department of Applied Geology, Indian School of Mines, Dhanbad, India

The polished thin sections of monomict breccia from the Indian Impact Crater at Lonar ($19^\circ 58'$N : $76^\circ 31'$E), consists of coarse grained shocked basalt fragments, fine to medium grained unshocked basalt fragments, impactite glasses of various shapes and sizes and all these are embedded in powdery clayey-calcareous matrix.

The examination of shocked basalt fragments revealed that it is coarse grained, exhibits porphyritic texture and contains maskelynite (Nayak, 1988), pyroxene and the opaques are magnetite, ilmenite, titanomagnetite and the later sometimes with exsolved ilmenite and/or ulvospinel. Pseudobrookite ($Fe_2TiO_5$) identified on the margins of ilmenite is characterized by optical characters that are: shades of grey to dark grey colours, weak bireflectance, weak anisotropism, low reflectivity (13% to 15%) and red to deep red internal reflections in oil. Generally, it occurs on the margins of ilmenite but in one case is pseudomorph after ilmenite. Although, pseudobrookite is a minor constituent among the opaque minerals in shocked basalt fragment but is considered significant because the behaviour of Fe-Ti oxide minerals in shock metamorphic environment has been found to be useful in the interpretation of impact structures.

Two possible mechanisms conjectured for the formation of pseudobrookite in shock environment at Lonar Crater are:
(a) conversion of naturally occurring ilmenite into pseudobrookite as a result of shock-induced high temperature oxidation.
(b) exsolution of ilmenite from titanomagnetite due to shock-induced transient heating followed by partial and/or complete conversion or transformation of this ilmenite component into pseudobrookite.

These aspects are discussed by a phase diagram in a system $FeO-Fe_2O_3-TiO_2$

METEORITES FROM THE NULLARBOR REGION, WESTERN AUSTRALIA AND COMPARISONS
WITH ANTARCTIC METEORITES

A.W.R. Bevan
Department of Earth and Planetary Sciences, Western Australian Museum,
Francis Street, Perth, Western Australia 6000

The Nullarbor is a region of generally treeless limestone plains in the
south of the Australian Continent straddling the border between Western
Australia and South Australia. The region is coincident with a geological
structure, the Eucla Basin, consisting of flat-lying limestones of Early
Miocene age that outcrop over a total area of approximately 239,108 sq. km.
The semi-arid to arid climate of the region, combined with a lack of
vegetation and pale country rock makes the Nullarbor ideal for the
preservation and recognition of meteorites. To date, several thousand
specimens from more than 107 possibly distinct meteorites have been recovered
from the Western Australian Nullarbor and >500 specimens of potentially new
meteorites remain to be described. Excluding Antarctica, The Nullarbor
Region has proved to be one of the world's most prolific sources of meteorite
finds. In the Nullarbor, the concentration of meteorites appears to be a
function of prolonged aridity and may not have involved additional
concentration processes as in Roosevelt County and Antarctica [1,2,3].

Comparisons between the populations of meteorites recovered from the
Nullarbor and those from Antarctica show some remarkable similarities. The
percentage of iron meteorite finds from the Nullarbor [2.8%] is close to that
in Antarctica and approximately half that predicted from the modern flux of
meteorites [5%]. Additionally, in the Nullarbor population there is a
relatively high proportion of rare, or anomalous types of chondrites. For
example, two crystalline carbonaceous chondrites, Mulga (west) (C5/6) and an
as yet unnamed CK4, and another anomalous chondrite (Carlisle Lakes), have
been recovered from the Nullarbor. Two additional crystalline CK4 chondrites,
Karoonda and Maralinga have also been recovered from Australia adjacent to
the Nullarbor. Karoonda (CK4) is the only observed fall of this type of
meteorite. A number of meteorites similar to Karoonda and Mulga (west) have
been recovered from Antarctica. Two other meteorites from Antarctica, ALH
85151 and Yamato75302, are similar to Carlisle Lakes and Rubin and Kallemeyn
[4] have suggested that these three meteorites belong to an entirely new
group of chondrites. Interestingly, only one C4 chondrite, Coolidge, is known
from the northern hemisphere. However, Scott and Taylor [5] have shown that
Coolidge has different affinities to the CK chondrites. The remaining non-
Antarctic examples of CK4-6, or Carlisle Lakes-like chondrites are all from
southern Australia. This apparent concentration of rare meteorite types in
the southern hemisphere may be related to the terrestrial time-span of the
populations of meteorites sampled in both Antarctica and the Nullarbor, their
ease of recognition in those environments compared with the rest of the world,
or is possibly the product of meteor streams [6].

Similar to Antarctica, many stony meteorites recovered from the Nullarbor
weigh 100 grams or less, with most in the range 10-50 grams. However, there
are also large masses such as Mundrabilla of which more than 22 tonnes of
material have been collected. Moreover, the two irons Mundrabilla and Haig
account for more than 99% of the total mass of meteorites so far collected
from the Nullarbor.

The sample of probably distinct meteorites from the Nullarbor [107] for
which classification data are currently available is an order of magnitude
smaller than that from Antarctica [>1000] and may not be statistically
significant. However, a major problem with the Antarctic meteorite population

is determining the actual number of falls that are represented [7]. While the number of different falls represented in Antarctica is uncertain, in the case of the Nullarbor the general lack of transportation processes in the region and the documentation of the distribution of finds has allowed pairing of meteorites to at least 90% level of confidence, and most paired meteorites have been deleted [2]. In addition, strewnfields of showers are relatively undisturbed and can be easily recognised and mapped.

Terrestrial ages of meteorites from the Nullarbor are not yet available and the age range of the population of meteorites is unknown. Geological evidence indicates that the onset of severe aridity in southern Australia dates from 18,000-16,000 years ago [8]. Recent data on the thermoluminescence -C14 correlation of two chondritic meteorites (Moorabie and Starvation Lake) found on similarly arid land near the South Australian/New South Wales border [9] indicate terrestrial ages of 10,000-20,000 years. Significantly, these ages are within the range of the majority of Antarctic meteorites

Ultimately, terrestrial ages of Nullarbor meteorites may help to constrain the age range of the surfaces on which they are found and the onset of dry conditions in the Nullarbor. In addition to providing important information on the flux of meteorites with time, these data may also have implications for palaeoclimatic research in Australia. Furthermore, data from the Nullarbor may serve as a cross-ckeck against the population of meteorites from Antarctica particularly in terms of the mass distribution and frequency of meteorite showers.

References: [1] Bevan, A.W.R. and Binns, R. A.(1989) Meteoritics, 24, 127-133.
[2] Bevan, A. W. R. and Binns, R. A. (1989) Meteoritics, 24, 134-141.
[3] Bevan, A.W.R. and Binns, R.A. (1989) Meteoritics, abs.,24, 251.
[4] Rubin, A.E. and Kallemeyn, G.W. (1989) Geochim. Cosmochim. Acta., 53, 3035-3044.
[5] Scott, E.R.D. and Taylor, G.J. (1985) Proc. 15th Lunar and Planetary Sci. Conf., Journ. Geophys. Res., 90, Supple, C699-C709.
[6] Kallemeyn, G.W., Rubin, A.E. and Wasson, J.T. (1991) Geochim. Cosmochim. Acta, 55, 881-892.
[7] Cassidy, W.A. and Harvey, R.P. (1991) Geochim. Cosmochim. Acta, 55, 99-104.
[8] Bowler, J.M. (1976) Earth Sci. Reviews, 12, 279-310.
[9] Sears, D.W.G., Batchelor, J.D., Mason, B., Scott, E.R.D., Clayton, R.N. and Mayeda, T.K. (1990) Meteoritcs abs., 25, 407-408.

# MINERALOGICAL STUDY OF THREE BRECCIATED ANTARCTIC EUCRITES, Y-82210, Y-793548, AND Y-82202

Akira Yamaguchi and Hirosh Takeda
Mineralogical Inst., Faculty of Science, Univ. of Tokyo, Hongo, Tokyo 113

Eucrites have been proposed to be shallow lavas of the HED (Howardite-Eucrite-Diogenite) parent body [1]. Many eucrites are breccias formed by impacts and suffered from subsequent thermal metamorphism [2]. Many polymict breccias are considered to be members of a componental and compositional continuum with several lithic components mixed in varying proportions. It is very important to deduce the origin of the lithic clasts to deduce the impact cratering history on the HED parent body. We investigated the polished thin sections (PTS) of three specimens by optical microscope, scanning electron microscope (SEM) equipped with energy dispersive spectrometer (EDS), and electron microprobe analyzer (EPMA) to identify the rock fragments in clastic breccias of eucrites, Y-82210, Y-793548, and Y-82202.

Y-82210 is mainly composed of chemically zoned pigeonite (Fig. 1) and plagioclase, and minor minerals are ilmenite, chromite, troilite, silica minerals, and fayalite. Clasts in Y-82210 consist of subophitic large fine-grained clasts with phenocrysts of pigeonites (< 3×0.3mm) and clasts with the matrix of comminuted mineral fragments. Minor components are glassy clasts and clasts with dendritic crystals of plagioclases and pyroxenes. These clasts are irregular to subrounded in shape. Shock features, such as wavy extinction in plagioclases are common.

Preliminary description of textures of Y-82202 and Y-793548 is given in Yamaguchi and Takeda [3]. Y-82202 and Y-793548 are mainly composed of the lava-like eucrite.

Y-793548 contains various types of unequilibrated mafic clasts. This eucrite is mainly composed of 5 types of lithic clasts: (a) fine-grained variolitic clasts. (b) Coarse-grained clast. (c) Dendritic clasts. (d) Glassy clasts. (e) Mineral clasts of pigeonites and plagioclases. Pyroxene compositions of individual clasts are summarized in pyroxene quadrilaterals (Fig. 1A to D). The chemical zoning trend and variations of pyroxene compositions are slightly different among individual clasts. The chemical compositions of the glassy clasts are also slightly different and can be classified three types.

Y-82202 are characterized by impact melt veins [3]. The host rock of Y-82202 is clastic breccia which is mainly composed of the fine-grained subophitic clasts and glassy clasts. Variation of the clasts are smaller than Y-82210 and Y-793548.

These three eucrites are unique types in that they are breccias of surface materials, and have several similarities. These are mostly composed of various types of unequilibrated clasts. A small xenolith (< 30μm) is found in the Y-793548 and Y-82210. This xenolith is a finely exsolved pyroxene (width of augite lamella is less than 1μm) which is probably fragment of ordinary eucrite. Such xenolith has been found in unequilibrated monomict eucrite Pasamonte [4]. There are fayalites as a minor mineral within the cracks of pyroxenes or mesostasis in these eucrites. The chemical zoning trend of coarse-grained clast of Y-793548 (Fig. 2B) is similar to that of Y-75011 [2].

The textures of clasts in Y-793548 vary widely from large clasts of coarse-grained (<1×1.5 mm) to very fine-grained (< 50μm). Y-793548 is different from Y-82202 and Y-82210 in the range of the textures of the clasts. The Y-793548 is rather closer to the typical polymict eucrites [5].

In summary, these eucrites are the polymict eucrites which composed only the surface materials. These three eucrites are intermediate between monomict eucrite and the typical polymict eucrite as described by Delaney et al.[5]. These meteorite are experienced low-grade thermal annealing. According to the degree of thermal metamorphism [6], these eucrites are from type-1 to type-2. These eucrites may be locate at the ejecta blanket of the HED parent body [7], and lithified by shock events without influence of thermal annealing. We suggest that these eucrites represent portions of the continuum from unequilibrated monomict eucrite (Pasamonte) to typical clastic matrix polymict eucrite on the surface of ejecta blanket judging from the mixing ratio of clasts and degree of equilibration.

We thank the National Institute of Polar Research for the meteorite specimens, and Mr. O. Tachikawa and Mr.H.Yoshida for technical assistance for the SEM-EDS and EPMA studies.

REFERENCE

[1] Takeda, H. (1979) *Icarus*, 40, 455-470.
[2] Takeda, H., J. L. Wooden, H. Mori, J. S. Delaney, M. Prinz, and L. E. Nyquist (1983) *Proc. Lunar Planet. Sci. Conf.* 14th, in *J. Geophys. Res.*, 88, *suppl.*, B245-B246.
[3] Yamaguchi, A. and H. Takeda (1990) *Syp. Ant. Meteor.* 15th, 13-16, (abstract).
[4] Takeda, H., M. Miyamoto, T. Ishii, and A. M. Reid (1976) *Proc. Lunar Sci. Conf.* 7th, 3535-3548.
[5] Delaney, J. S., M. Prinz, and H. Takeda (1984) *Proc. Lunar Planet. Sci. Conf.* 15th, in *J. Geophys. Res.*,89, *suppl.*, C251-C288.
[6] Takeda, H. and A. L. Graham (1991) *Meteoritics*, in press.
[7] Stöffler, D., H. -D. Knöll, and U. Maez (1979) *Proc. Lunar Planet. Sci. Conf.* 10th, 639-675.
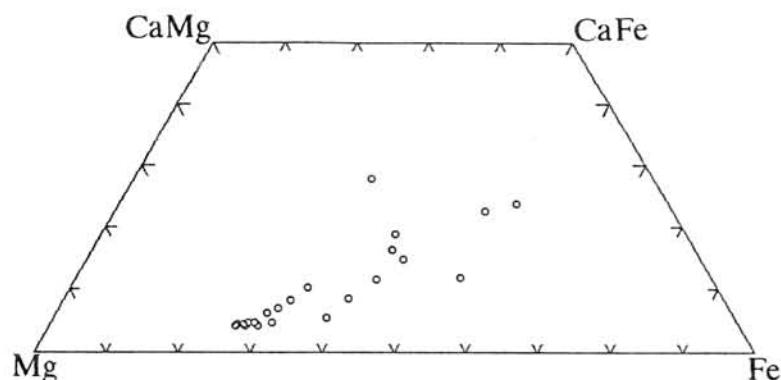
Fig. 1. Pyroxene quadrilateral of Y-82210.
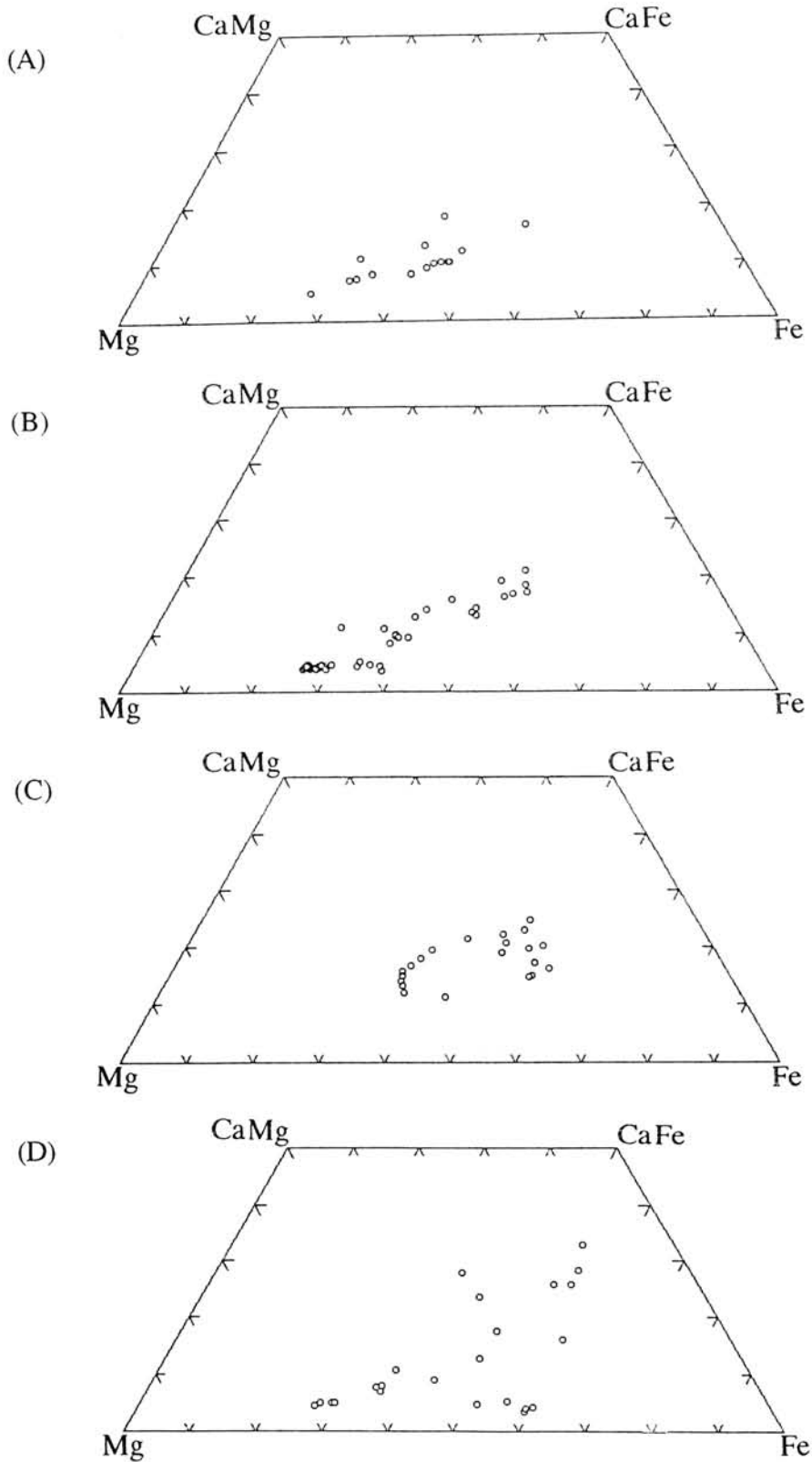
Fig. 2. Pyroxene quadrilaterals for individual clasts from Y-793548. (A) variolitic clast. (B) Coarse-grained clast. (C) Dendritic clast. (D) Matrix.

MINERALOGICAL STUDY OF METALS AT GRAIN BOUNDARIES OF MAGNESIAN UREILITES

Jun Saito and Hiroshi Takeda
Mineralogical Institute, Faculty of Science, University of Tokyo, Hongo, Tokyo
113, Japan

Ureilite is a unique type of achondrite composed predominantly of coarse-grained olivine, pyroxene and carbonaceous materials. The textures are similar to those of some terrestrial ultramafic rocks. Their oxygen isotope anomalies (Clayton and Mayeda, 1988) similar to those of CV, CO mixing-line strongly suggest the close link between ureilites and carbonaceous chondrites, and indicate that no ureilites have experienced heavy fractionation processes.

Magnesian ureilites are found only in Antarctica (Takeda, 1989), and well-known for having larger oxygen isotope anomalies than other types of ureilites (Clayton and Mayeda, 1988). Saito and Takeda (1990) reported that two Antarctic ureilites, Y-791538 and LEW85440 have grain boundaries almost totally filled with Fe-rich metals and those with small amounts of S and Ni. Such texture have been also found in other magnesian ureilites, but scarcely in other types of ureilites.

We studied the occurrence, texture and chemical compositions of metals in four magnesian ureilites (Y-74659, Y-791538, LEW85440, ALH82106), and compared with those of other types of ureilite.

The polished thin sections (PTS) of Y-791538 and Y-74659 supplied by National Institute of Polar Research (NIPR), LEW85440 and ALH82106 by Antarctic Meteorite Working Group (AMWG) were investigated by an optical microscope, scanning electron microscope (SEM) equipped with EDS (Energy Dispersive Spectroscopy) detector, and chemical map analysis (CMA) utilities of Kevex Super 8000 to correlate textures and variations of chemical compositions in these ureilites.

Backscattered electron images (BEI) of ALH82106 and Y-74659 show that most of grain boundaries between mafic silicates filled with Fe-rich metals and Fe-rich metal with small amounts of Ni, S and Si being too heavily weathered to be precisely analysed by EPMA (Fig. 1). These metallic materials exists at most of grain boundaries, that is, olivine-olivine, pyroxene-pyroxene and olivine-pyroxene ones. The elemental maps of the metallic materials at grain boundaries of magnesian ureilites show that these consist of mainly Fe-rich metals, but some metallic materials consist of Fe plus small amounts of Ni and S.

Such grain boundary texture filled with metallic materials is also seen in Y-791538 and LEW85440. In these four magnesian ureilites (Y-74659, ALH82106, LEW85440, Y-791538), a mode of occurrence of the Fe-rich metals and metals with small amounts of Ni, S shows that they are distributed at most of grain boundaries between mafic silicates.

The chemical compositions of unweathered metals (vein metals and inclusions) of magnesian ureilite (Y-74659 and ALH82106) shows slightly Ni-poorer compositions than other unshocked ureilite, for example, ALH78019.

In other types of ureilites except magnesian ones, metallic materials (mainly Fe-rich metals) exist at olivine-olivine and olivine-pyroxene grain boundaries, but scarcely at pyroxene-pyroxene boundaries.

Since magnesian ureilites have been thought to be annealed under reducing condition *before* the parent-body breakup (Takeda, 1989), the Fe-rich metals of the magnesian ureilites filled in grain boundaries might have been derived from reduced metals produced by such annealing process. The CMA data showing that most of metallic materials at grain boundaries consist of Fe-rich metals also supports that these Fe-rich metals had been produced by reduced metals, and migrated at grain boundaries.

Fe-rich metals which occurred at olivine-olivine and olivine-pyroxene grain boundaries in the intermediate and Fe,Ca-rich ureilites are thought to be

produced mainly by reduction during rapid cooling at the time of the parent body breakup, because these metals contact the small metal spherules at olivine reduced rims. These metals may have been solidified too rapidly to migrate to almost all grain boundaries, especially those between pyroxenes
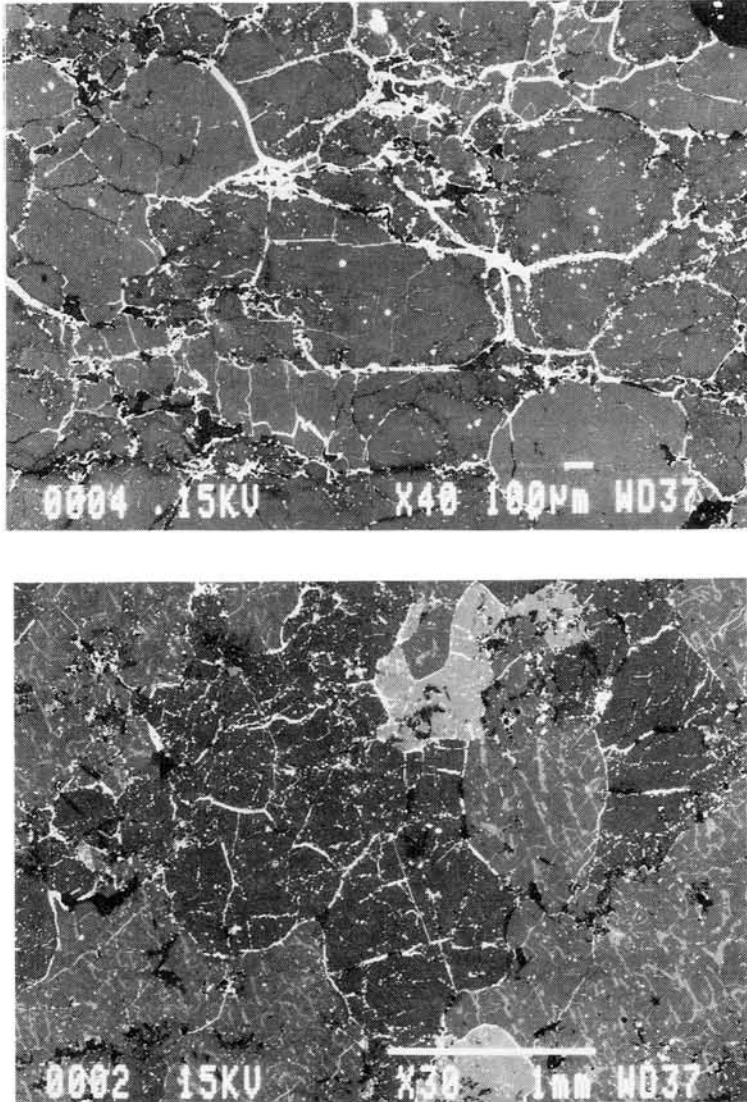


Fig. 1. *Backscattered electron image of magnesian ureilites:*
*Y-74659 (upper); ALH82106 (lower)*

Although many Fe-rich metals were produced by reduction process during annealing on their parent body, the metals of magnesian ureilites show only slightly Ni-poorer contents than those of unshocked ones. In many cases, vein

metals contact Fe-sulfides, indicating that they are produced from Fe-Ni-S melt. These surrounding Fe-sulfides around vein metals may protect vein metals against dilution by Fe-rich reduced metals migrating at grain boundaries. Some metals occurs are embedded in carbonaceous vein materials, and may have been protected by surrounding silicates from reduced metals at grain boundaries.

In both cases, Fe-rich reduced metals migrated at grain boundaries had diluted these pre-existing metals only minimal so that the metals (inclusion and vein) have only slightly Ni poorer content than those of unshocked ureilites (eg. ALH78019).

In summary, the magnesian ureilites must have been heavily reduced during annealing on the parent body before the breakup, and the degrees of reduction and migration of reduced metals to grain boundaries are different from those of other types of ureilites. Further study is required to compare the chemical compositions, occurrences, texture, and trace element distribution of ureilitic metals between three types (magnesian, intermediate and Fe,Ca-rich) of ureilites to confirm our proposal.

References:

Clayton, R.N. and Mayeda, T. (1988): GCA 52, 1313-1318.

Takeda, H. (1989): Earth Planet. Sci. Lett. 93, 181-194.

Saito, J. and Takeda, H. (1990): Meteoritics 25, 404.

TROILITE-RICH CLAST IN THE MOORABIE (L3) CHONDRITE

Takashi Fujita and Masao Kitamura

Department of Geology and Mineralogy, Kyoto University,
Sakyo Kyoto 606, Japan.

A troilite-rich clast was found in the Moorabie (L3) chondrite (Figure 1). The shock-melting after the accretion of the chondrite was suggested as the origin of the clast.

Chondrules of the Moorabie chondrite have elongated shapes whose longest axes are roughly aligned to the same orientation. Olivine often shows wavy extinction. Chondrule olivines larger than several tens microns have normal Fe-Mg zoning and Fe-rich rims of all the olivines have nearly the same composition ($\sim$Fo86) (Figure 2). Ca-poor pyroxenes show striated Fe-Mg heterogeneity. Some chondrules include metals, chromites and less amount of troilites. The mineral assemblages and compositions of chondrules are essentially the same as those in typical L3 chondrites.

The troilite-rich clast (8 x 6 x few mm) (Figure 1) consists of troilites and small amount of Fe-Ni metal (Figure 3). The clast also include several chondrules and fragments of olivine and pyroxene (Figures 4). Troilite grains (max. 630$\mu$m in diameter) in the clast are larger than troilite grains (max. 300$\mu$m in diameter) among chondrules in the chondrite. Relative ratio of troilite to metal in the clast is 90 : 16 in a thin section. The chondrules and fragments in the clast have almost similar textures and compositions to those in the host rock. For example, compositions of olivines of the chondrules in two regions are similar with each other(Figure 2).

Resemblance in texture and composition between the chondrules and mineral fragments in the clast and those in the host suggests that the clast must be formed after the chondrule formation. The large size of the troilite grains in the clast indicates that the clast is not a simple aggregate of the metal-troilite grains among chondrules in the host. A ratio in weight percent of Fe-Ni metal to troilite in the clast was roughly estimated to be 68 : 32. This value is different from typical Fe/S ratio of L chondrites (Fe:S 3:1, e.g. Dodd,1981), but close to the eutectic composition (S:$\sim$31 wt per cent) of the Fe-FeS system. Then, the large grain size of troilite and the composition of the clast suggest a possible formation process of the clast where the melt with eutectic composition of the Fe-S system was formed and then cooled.

The heating condition for the eutectic melt is restricted by the fact that chondrules in the clast show no evidence of reheating and remelting after the chondrule formation. This fact implies that the melting occurred at the temperature no so much higher than the eutectic temperature of the Fe-S system (988°C). Growth zoning of olivine grains several tens micron size would be

erased at 1000°C within a year (Freer, 1981). Therefore, it is likely that the melting event must have occurred around the eutectic temperature and finished within a year. The heating event must have occurred locally, because of the large difference in grain sizes of troilite in the clast from those in the host. This local heating event suggests the shock-impact origin of the clast after the chondrite formation.

The elongated shapes of chondrules with the preferred orientation resemble those observed in the Leoville (CV3) chondrite. The texture in Leoville has been interpreted to be formed by compaction of gravity (Cain et al.,1986) or shock impact (Wasson, 1985). Recently, the shock origin has been confirmed based on the micro-textures of constituent minerals (wavy and mosaic extinction of olivines, high dislocation density of matrix olivines etc.) by Nakamura et al. (1990). Therefore, the elongated shapes of chondrules and wavy extinction of olivines in the present chondrite indicate the shock impact after the accretion, and then support the shock-origin of the clast.

Wasson (1985) estimated the shock heating temperature to be 1000-1200°C in order to explain the elongated shape of chondrules by plastic deformation of silicates in the Leoville chondrite. This estimated temperature range is near the eutectic temperature of the Fe-FeS system. This also supports the shock-origin of the clast.

## References

Cain, P.M., McSween,Jr.H.Y. and Woodward, N.B. (1986): Earth Planet Sci. Lett.,77,165-175.
Dodd, R.T. (1981): Meteorite.,Cambridge University Press.
Freer, R. (1981): Contrib. Mineral. Petrol., 76, 440-454.
Nakamura,T., Tomeoka,K. and Takeda,H. (1990): Proc. 23th ISAS Lunar Planet. Symposium., 188-193.
Wasson, J.T. (1985): Meteorites. Their Record of Early Solar-system History.,Freeman.

Figure 1. Photograph of the Moorabie chondrite. tr: troilite rich clast.
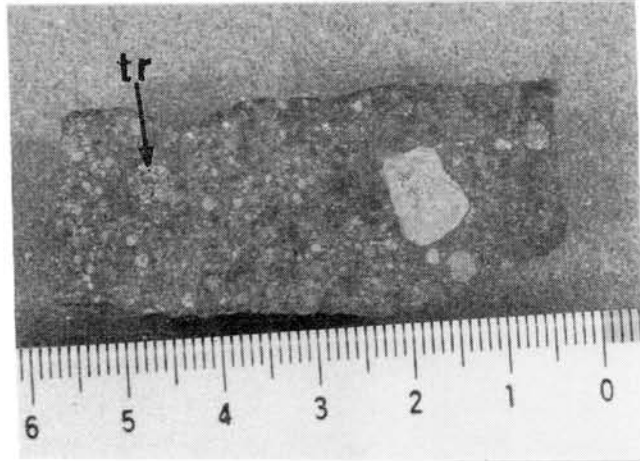


Figure 2. Mg# of olivines within and outside the troilite rich clast.



olivins outside the clust

olivins enclosed in the troilite-rich clust

MgO/(MgO+FeO)*100
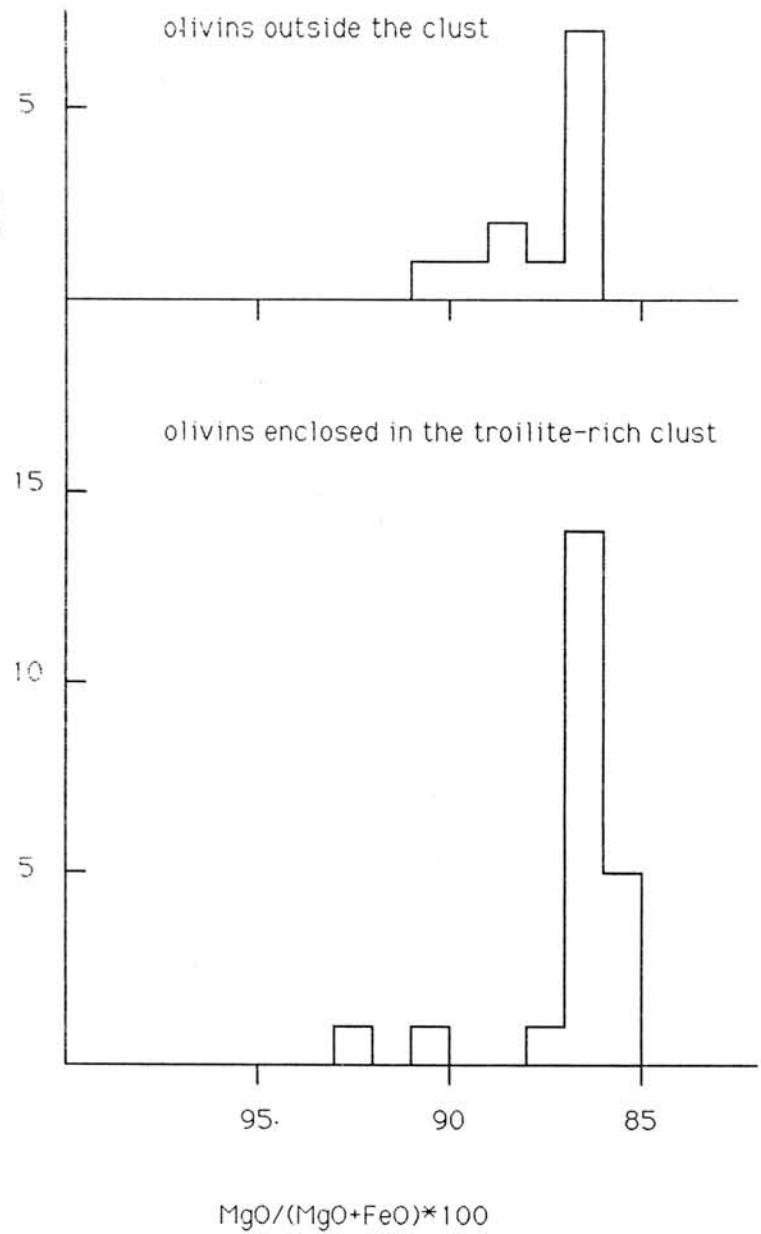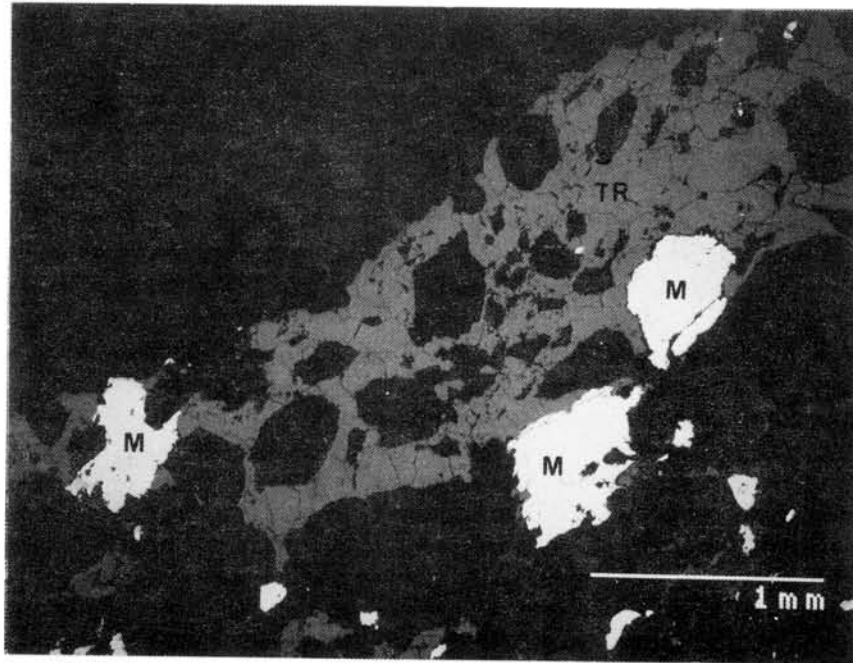
Figure 3. Back scattered electron image of the troilite rich clast. M: metal.  TR: troilite
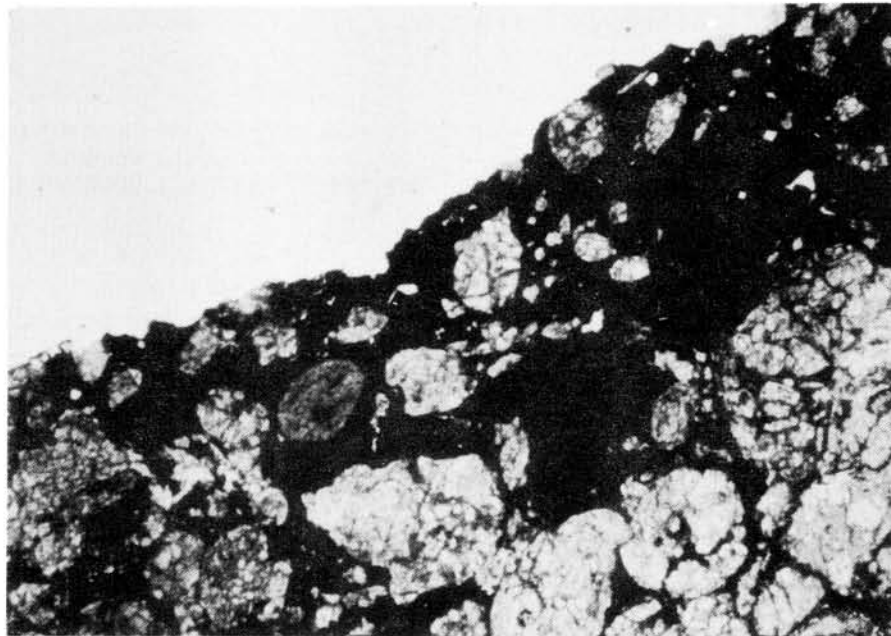


Figure 4. Optical micrograph of the troilite rich clast. Transparent regions are chondrules and silicate fragments. Black parts are Fe-Ni metals and troilites. Vertical scale of the figure is 2mm.

EVIDENCE FOR PRE-ACCRETIONARY AQUEOUS ALTERATION IN THE YAMATO-793321 CM CARBONACEOUS CHONDRITE

Kazushige Tomeoka, Kiichiro Hatakeyama, Tomoki Nakamura and Hiroshi Takeda

Mineralogical Institute, Faculty of Science, University of Tokyo, Hongo, Tokyo 113, Japan

INTRODUCTION

The carbonaceous chondrites, CI and CM types in particular, are now believed to be not the pristine, unmodified samples of the early solar system materials, but they have experienced various degrees of aqueous alteration process (e.g., refs. 1-3). Most of these chondrites probably have experienced the aqueous alteration after accretion, on the meteorite parent bodies by the activity of liquid water (e.g., refs. 1-5). Thus, it appears to be difficult to derive information about the processes that occurred prior to the alteration from these meteorites. However, it has been recently recognized by several workers that Yamato-791198 may be an exceptional CM chondrite that has not been much affected by aqueous alteration and brecciation on its parent body [6-8]; thus it may provide insights into the primary, accretionary processes experienced by these meteorites.

Yamato-793321 (Y793321) is another unusual CM chondrite from Antarctica, which has mineralogical and textural characteristics indicating much milder aqueous alteration and brecciation on its parent body than most CM chondrites previously studied. Thus, this meteorite also may preserve primitive nature since accretion to the parent body. We present here the results of detailed petrographic and scanning electron microscope studies of chondrules and chondrule rims in Y793321. We will compare the mineralogy and texture of this meteorite with those of Y791198 and other CM chondrites, and infer the processes that occurred prior to consolidation of the meteorites.

TEXTURE AND MINERALOGY

Y793321 contains clastic fragments; thus, it was probably affected by brecciation on the meteorite parent body. However, the boundaries between clasts and surrounding matrix are commonly sharp, unlike most of the CM chondrites studied, and show no indications of significant reactions between them, suggesting that this meteorite was little affected by aqueous alteration after brecciation. One of the distinguished characteristics of this meteorite is that most of the chondrules are surrounded by well-developed rims, although some chondrules are free of rims. Chondrules are only objects enclosed by the rims, which is in contrast to Y791198, in which almost all of the large objects including chondrules. mineral fragments, and PCP are enclosed by the rims.

Chondrules

Chondrules consist mainly of forsterite, enstatite, Ca-rich clinopyroxenes (mostly diopside and fassaite), and phyllosilicates. Lesser amounts of PCP, kamacite, and Fe sulfides (troilite and pentlandite) occur. The predominent phyllosilicate is magnesian cronstedtite. A very minor amount of Fe-rich serpentine also occurs. There are no essential differences in mineralogy and mineral composition between chondrules with rims and without rims. The phyllosilicate mineralogy within chondrules is distinctly different from that in Y791198 chondrules, in which Fe-bearing serpentine is the most common phyllosilicate. PCP occurs as rounded or oval grains and mainly consists of tochilinite, corresponding to Type-I PCP [2] It is evident from texture that cronstedtite was produced by replacing mainly mesostasis glass and Ca-rich clinopyroxenes. Most

forsterite and enstatite remain unaltered, but Fe-rich olivine was replaced by Fe-rich serpentine. The tochilinite-rich PCP grains were probably formed by replacing kamacite and/or troilite. In general, the extent of aqueous alteration in the chondrules is very minor compared to most of the CM chondrites.

Chondrule rims

The chondrule rims have characteristic rounded or oval external shapes regardless of how irregular the chondrule shapes are. They have a wide range of thickness (10 to 100 $\mu$m); it varies within and between chondrules. The rims contain small particles (1 to 10 $\mu$m in diameter) of a variety of minerals including forsterite, kamacite, troilite and tochilinite, similar to the rims in Y791198. Of paricular interest is that some chondrules have double rims. The boundaries between the inner rims and the outer rims are commonly sharp in back-scattered SEM images. These characteristics contrast with those in Y791198, where all of the chondrules have single, homogeneous rims with relatively consistent thicknesses.

We performed defocused-electron beam analysis of the chondrule rims. When the results are plotted in the Fe-Mg-(Si+Al) ternary diagram, most analyses cluster near the serpentine (ideal) solid solution line. Most single rims have relatively consistent compositions close to Fe-bearing serpentine, resembling the rims in Y791198 and Murchison [8]. The inner rims of the double rims are almost identical in composition to the single rims, whereas the outer rims are distinctly richer in Fe. The cronstedtites in the chondrules have compositions clearly different from any of the rims.

PCP in matrix

PCP is widely distributed in the matrix. It occurs both as massive (20 to 100 $\mu$m in diameter) and smaller fragmental grains. No PCP grains are surrounded by the rims unlike those in Y791198. PCP in the matrix is predominently composed of tochilinite. Tomeoka and Buseck [2] found that PCP in the matrices of Mighei, Murchison and Murray consists of various proportions of tochilinite and cronstedtite, and suggested that PCP was increasingly replaced by cronstedtite, as the alteration proceeded. Therefore, the mineralogy of the PCP in Y793321 suggests that the degree of aqueous alteration in this meteorite was very low compared to those in Mighei, Murchison, and Murray.

DISCUSSION

Our observations revealed that most chondrules in Y793321 have experienced aqueous alteration. The alteration product in the chondrules is mostly cronstedtite, whereas the chondrule rims are composed mainly of Fe-bearing serpentine. The cronstedtite replaces chondrules over the areas $\sim$50 $\mu$m x$\sim$100 $\mu$m. The rims in the Y793321 chondrules contain submicron-to-micron-size particles of olivine and Fe sulfide. Considering the extent of aqueous alteration suffered by the chondrules, if the alteration should have occurred after the rims were formed, it would be difficult for the olivine and sulfide particles to survive without being replaced; these minerals should have been transformed to serpentine and tochilinite during alteration. Based on these observations and evidence, we suggest that the aqueous alteration that produced the phyllosilicates and tochilinite in the Y793321 chondrules occurred before the rims accreted on the chondrules. We believe that the alteration in the chondrules occurred by reaction with the solar nebula.

Some of the chondrules in Y793321 are enclosed by double rims which are clearly different in composition from each other. The compositions of the single rims and the inner rims are almost identical to those of the rims in Y791198. The results suggest that there were at least two different reservoirs of the dust which formed the rims; one is rich in Fe-bearing serpentine (reservoir A), and the

other is rich in more Fe-rich serpentine (reservoir B). Most of the chondrules as well as mineral fragments and PCP grains in Y791198 appeared to have developed their rims in reservoir A. However, there are three kinds of chondrules in Y793321; the first went through only reservoir A, the second went through both reservoirs A and B, and the third went through neither of them.

Based on the studies of Y793321 and Y791198, we suggest that CM chondrites have experienced aqueous alteration even before consolidation into its present configuration and, perhaps, to accretion. However, most CM chondrites studied have been also affected by aqueous alteration after accretion.

REFERENCES
[1] Bunch, T.E. and Chang, S. (1980) Carbonaceous chondrites--II. Carbonaceous chondrite phyllosilicates and light element geochemistry as indicators of parent body processes and surface conditions. Geochim. Cosmochim. Acta 44, 1543-1577.
[2] Tomeoka, K. and Buseck, P.R. (1985) Indicators of aqueous alteration in CM carbonaceous chondrites: Microtextures of a layered mineral containing Fe, S, O and Ni. Geochim. Cosmochim. Acta 49, 2149-2163.
[3] McSween, H.Y. (1987) Aqueous alteration in carbonaceous chondrites: Mass balance constraints on matrix mineralogy. Geochim. Cosmochim. Acta 51, 2469-2477.
[4] Richardson, S.M. (1978) Vein formation in the CI carbonaceous chondrites. Meteoritics 13, 141-159.
[5] Tomeoka, K. (1990) Phyllosilicate veins in a CI meteorite: evidence for aqueous alteration on the parent body, Nature 345, 138-140.
[6] Kojima, H. and Yanai, K. (1990) Alteration of matrices in CM chondrites, Meteoritics 25 (Abstr.), 376.
[7] Metzler, K. and Bischoff, A. (1990) Petrography and chemistry of accretionary dust mantles in the CM chondrites Y-791198, Y-793321, Y-74662 and ALHA83100 - Indications for nebula processes, Papers presented to the 15th Symposium on Antarctic meteorites (Abstr.), 198-200.
[8] Nakamura, T., Tomeoka, K. and Takeda, H. (1991) Papers presented to the 16th Symposium on Antarctic meteorites (Abstr.)(in this volume).

# MINERALOGY OF CHONDRULE RIMS IN THE YAMATO-791198 CM CHONDRITE: COMPARISON TO MURCHISON

Tomoki Nakamura, Kazushige Tomeoka and Hiroshi Takeda
Mineralogical Institute, Faculty of Science, University of Tokyo, Hongo, Tokyo 113.

## INTRODUCTION

The CI and CM carbonaceous chondrites are commonly regarded as primitive solar system material that formed directly from the solar nebula. However, these meteorites show abundant evidence of aqueous alteration [e. g., 1, 2]. Whether such alteration occurred before or after accretion to the parent bodies has long been a subject of controversy. Most previous studies have suggested that the alteration probably occurred by the activity of liquid water on the parent bodies [1-3]. Recently, several workers [4, 5] have studied the Yamato-791198 (Y791198) CM chondrite and suggested that this meteorite may not have been much affected by aqueous alteration and brecciation on the parent body and may preserve primary, accretionary features.

We present here the results of petrographic, scanning electron microscope (SEM) and transmission electron microscope (TEM) studies of the Y791198 and Murchison CM carbonaceous chondrites. The purposes of this study are to compare the mineralogy and texture of Y791198 and Murchison as well as other CM chondrites, and thus to understand the early processes of aqueous alteration experienced by the CM chondrites.

## RESULTS

### Y791198

Y791198 shows almost brecciation-free texture, which differs from most of other CM chondrites previously studied. Another distinguished characteristic is that almost all the chondrules, olivine and pyroxene fragments and metal, sulfide and PCP grains are surrounded by well-developed rims.

Chondrules consist mostly of forsterite, enstatite, and Fe-bearing serpentine and minor amounts of kamacite, troilite and PCP. Forsterite and enstatite are partly replaced by Fe-bearing serpentine, and the degree of alteration varies between the chondrules. PCP occurs as rounded or oval grains ranging in diameter from 2 to 10 μm, corresponding to Type-I PCP described in [2].

PCP is abundant in the matrix; it occurs as massive and fragmental grains ranging in diameter from 20 to 100 μm. Most PCP grains are intimate mixtures of tochilinite and cronstedtite, corresponding to Type-II PCP in [2]. They commonly coexist with calcite, pentlandite, and troilite.

The rims surrounding chondrules, mineral fragments and PCP grains range in thickness from 20 to 50 μm. The total of 40 rims were analyzed by using a defocused-electron beam. When the results are plotted in the Fe-Mg-(Si+Al) ternary diagram, most analyses cluster near the point Fe/Mg = 1 on the serpentine tie line, indicating that most of the rims have relatively homogeneous compositions. The rims contain numerous particles of a variety of minerals ranging in diameter from 2 to 10 μm; they are forsterite, pentlandite, troilite, PCP, enstatite and kamacite.

### Murchison

Murchison is clearly a breccia composed of submillimeter to millimeter clasts, indicating that it suffered from regolith gardening in its parent body.

Chondrules consist of forsterite, enstatite, serpentine having a wide range of Fe/Mg ratios, PCP, and minor amounts of kamacite and troilite. There are chondrules enclosed by rims and free of rims. There is an apparent tendency that large chondrules (>300 μm) have rims and small chondrules (<100 μm) do not have rims. PCP grains in the matrix do not have rims.

Most of the rims have relatively consistent compositions close to Fe-rich serpentine;

compared with the compositions of the rims in Y791198, those in Murchison are ~4% higher in Mg content. Particles ranging from 1 to 10 μm in diameter also occur in most of the rims. Most abundant are the particles of serpentine having much lower Fe contents than the rim matrix, and PCP. There are also particles of troilite, pentlandite and forsterite in much lesser amounts.

DISCUSSION

Chondrules in both Y791198 and Murchison have experienced aqueous alteration, resulting in serpentines having various Fe/Mg ratios; the alteration occurred over the areas of 50 μm x 50 μm. On the other hand, most of the rims in both Y791198 and Murchison contain numerous particles of anhydrous minerals such as forsterite and Fe-Ni sulfides. If the alteration in the chondrules should have occurred after the rims were formed, it would be difficult for those anhydrous mineral particles to survive without being replaced. Based on these observations, we support the view that the chondrules experienced aqueous alteration before the rims accreted on the chondrules.

The rims in both Y791198 and Murchison have similar compositions corresponding to serpentine having a Fe/Mg ratio close to 1. However, there are distinct differences in relative abundances of mineral particles between the rims in those two meteorites. In the rims in Y791198, forsterite, pentlandite, troilite and PCP particles are most abundant, and enstatite and kamacite particles also occur. However, in Murchison, Mg-rich serpentine and PCP particles are most abundant, but forsterite, pentlandite and troilite particles are rare, and enstatite and kamacite particles are absent. It is known that forsterite is more resistant to aqueous alteration than enstatite, and pentlandite and troilite are more resistant than kamacite. Assuming that the rims in Y791198 and Murchison were formed from common material, the differences in the mineralogy of the particles may be explained by that Murchison has been affected by mild aqueous alteration after the rim formation, probably after accretion to the parent body. The serpentine particles in the rims in Murchison may have resulted from alteration of enstatite and forsterite, and the PCP particles may have resulted from alteration of kamacite, pentlandite and troilite. Our TEM observation of the rims in Murchison showed evidence that forsterite particles are partly replaced by serpentine.

In summary, chondrules in Y791198 and Murchison probably have experienced aqueous alteration before the rim formation. Although Y791198 appears to have not been affected by any significant secondary process after accretion, Murchison probably experienced additional aqueous alteration in the parent body.

REFERENCES; [1] Bunch, T. E. and Chang, S. (1980) Carbonaceous chondrites-II. Carbonaceous chondrite phyllosilicates and light element geochemistry as indicators of parent body processes and surface conditions. Geochim. Cosmochim. Acta 44, 1543-1577. [2] Tomeoka, K. and Buseck, P. R. (1985) Indicators of aqueous alteration in CM carbonaceous chondrites; Microtextures of a layered mineral containing Fe, S, O and Ni. Geochim. Cosmochim. Acta 49, 2149-2163. [3] McSween, H. Y. (1987) Aqueous alteration in carbonaceous chondrites: Mass balance constraints on matrix mineralogy. Geochim. Cosmochim. Acta 51, 2469-2477. [4] Kojima, H. and Yanai, K. (1990) Alteration of matrices in CM chondrites, Meteoritics 25 (Abstr.), 376. [5] Metzler, K. and Bischoff, A. (1990) Petrography and chemistry of accretionary dust mantles in the CM chondrites Y-791198, Y-793321, Y-74662 and ALHA83100-indications for nebula processes, Papers presented to the 15th Symposium on Antarctic meteorites (Abstr.), 198-200.

# POSSIBLE EVIDENCE OF ACCRETION BY INTERSTELLAR MEDIUM ESTIMATED FROM HISTORICAL RECORDS OF AURORA AND METEOR IN CHINA.

*S.Miono, Osaka City University,Sumiyoshi-ku,Sugimoto,Osaka,Japan.*
*A.Nakanishi, Shiga University of Medical Science,Seta,Otsu,Japan.*

Recently one of the authors suggested that the Solar System encountered with a interstellar molecular cloud in the past Jurassic-Triassic boundary[1]. On the other hand such possible evidence is found in the historical record of astronomical phenomena in China. A decade distribution of meteor records show an anomalous increase around A.D. 11-12 centuries as shown in Fig.1 [2]. In 1968, M.Keimatsu et al. reported the study of historical aurorae and sunspots[3]. According to their results, it was suggested that the geomagnetic dipole axis might have been inclined toward China around A.D. 11-12 centuries. It neverthless seems more consistent to infer Solar System encountered with a small molecular cloud, although F.R.Stephenson[4] concerning this increase pointed out changing in attitude to celestial portents and varying degrees of preservation of observer's reports.
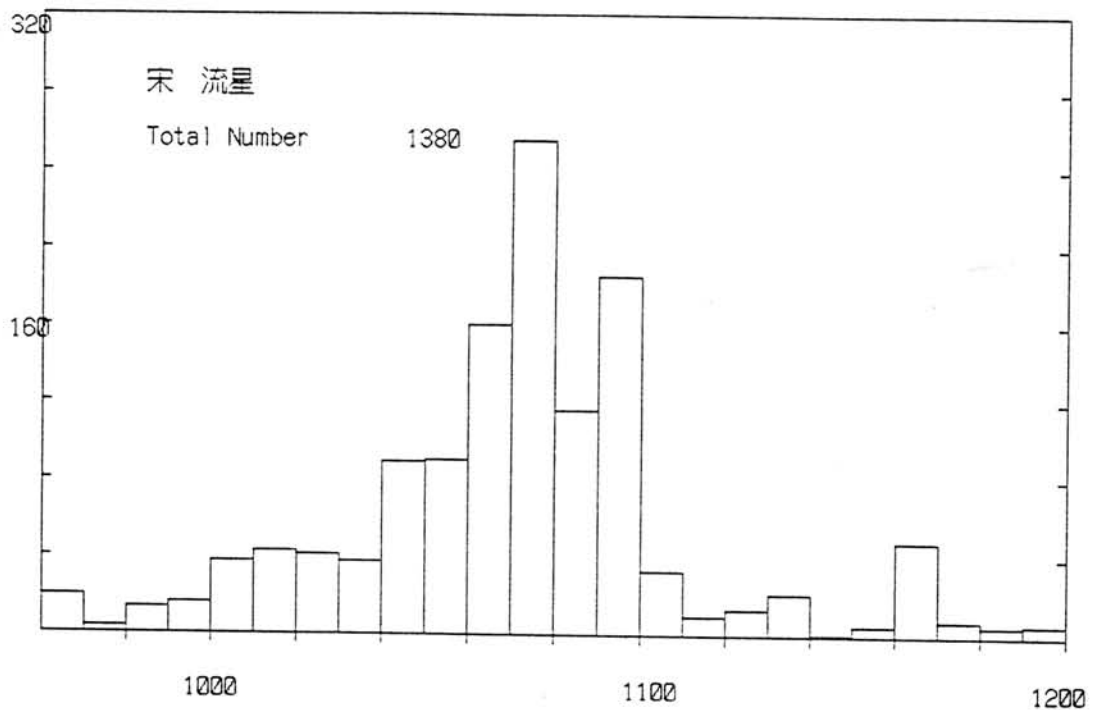


Fig. 1 Decade distribution of meteor
during the Sung dynasty in China

References (1) S.Miono, Proc. 2nd Int. Symp. Geology in Sri Lanka (1991), In press   (2) 中國古代天象記録総集　　江蘇科学技術出版社
(3) M. Keimatsu et al., J. Geomg. Geoelectr.20(1968) 45
(4) F.R.Stephenson, Phil. Trans. R. Soc. Lond. A330(1990) 499

# METEORITE ALLENDE III: A SEM STUDY OF ITS GLASS PHASE

G. Sànchez-Rubio, A. M. Rcycs-Salas and A. Nieto-Samaniego, Instituto de Geología (UNAM), Ciudad Universitaria, 04510 México, D. F., Mexico

**Introduction** Volcanism (i.e. magmatism or igneous phenomena) is among the main geologic processes that shaped the planets and satellitics of the solar system. Some features like microporphyritic clasts and chondrules with phenocrysts of euhedral shape suggest that chondrites were not totally divorced from such processes. It is therefore probably wise to have a closer look into these objects and compare them with analogs from our planet.

Allende III is an ordinary chondrite with features like those described above. It is an olivine-hypersthene chondrite, petrologic type 4; chondrules show readily delineated shapes in a cryptocrystalline or fine granular groundmass; glass in chondrules and clasts appears somewhat devitrified.

Using the scanning electron microscope that exists in the Institute of Geology (UNAM), as many as 180 chemical analyses (major elements) were done upon the glass phase in clasts and chondrules of Allende III, and the results were compared with similar data from terrestrial volcanic rocks.

**Results** Table 1 lists a few representative chemical analyses and corresponding CIPW norms. I and C are clasts with euhedral olivine phenocrysts and interstitial glass; F is a chondrule with euhedral olivine and interstitial glass; and A is a clast with anhedral olivine phenocrysts and interstitial glass.

The study was carried out with a JEOL JSM35c with an EDS detector (Tracer). Accelerating voltage, 20 kv; acquisition time, 100 seconds, with a narrow beam.

The results obtained were compared with a garnet of known composition and also with some results obtained formerly in the National Institute of Polar Research, in Tokyo.

**Discussion** The glass phase of Allende III shows some interesting resemblance to terrestrial andesitic rocks. Silica, as well as most other components, appears in similar amounts in both rock types, although CaO is much higher and $Al_2O_3$ a bit lower in the meteorite. Silica oversaturation is also conspicuous through the presence of quartz in the CIPW norm. Plotted on diagram AFM (alkalis, total iron, magnesium) the glass overlaps much of the calc-alkaline areas in the triangle.

Widespread evidence in subduction related volcanic rocks indicates that assimilation of crustal material may be one of the main causes of variation of calc-alkaline magmas. The occurrence of "calc-alkaline magmas" so closely associated to rocks of ultrabasic composition, as illustrated by Allende III, suggests that some of the peculiarities shown by rocks of the calc-alkaline series could be explained by such an association, i.e., that some calc-alkaline magmas actually may form closely associated to rocks of ultrabasic composition.

Table 1. Major element composition and CIPW norm of some glasses in meteorite Allende III.

| | I | C | F | A |
|---|---|---|---|---|
| $SiO_2$ | 58.7 | 62.0 | 62.9 | 65.7 |
| $Al_2O$ | 23.2 | 12.2 | 19.9 | 14.0 |
| $FeO$ | 2.9 | 2.8 | 7.0 | 2.8 |
| $CaO$ | 5.5 | 13.3 | 3.3 | 6.9 |
| $MgO$ | 0.1 | 4.7 | 1.3 | 4.1 |
| $Na_2O$ | 4.4 | 4.1 | 5.0 | 4.6 |
| $K_2O$ | 0.2 | 0.2 | 0.4 | 1.4 |
| $TiO_2$ | 0.8 | 0.2 | 0.1 | 0.2 |
| $Cr_2O_3$ | 4.3 | 0.5 | 0.3 | 0.3 |
| Total | 95.8 | 99.3 | 99.9 | 99.7 |
| | | | | |
| il | 1.5 | | 0.2 | 0.4 |
| or | 1.1 | 1.2 | 2.5 | 8.4 |
| ab | 36.0 | 33.8 | 44.0 | 39.6 |
| an | 26.4 | 13.9 | 17.0 | 13.8 |
| di | | 36.5 | | 18.2 |
| hy | 1.6 | | 7.2 | 4.0 |
| qz | 18.0 | 10.5 | 18.2 | 15.5 |
| c | 11.1 | | 10.9 | |
| wo | | 3.4 | | |
| Total | 95.8 | 99.3 | 100.0 | 99.7 |

THERMAL RELEASE OF INSOLUBLE ORGANIC MATTER ISOLATED FROM SOME ANTARCTIC CI AND CM CHONDRITES.

Komiya, M., Shimoyama, A., and Harada, K.

Department of Chemistry, University of Tsukuba, Tsukuba, 305

Organic compounds in carbonaceous chondrites are mostly present as insoluble macromolecular organic matter. We have examined bulk samples of some CI and CM chondrites without any treatment by a DTA/TG-GC/MS method[1]. In the present study, we examined particularly the insoluble organic matter isolated from those CI and CM chondrites by the same method.

Samples used are five Antarctic carbonaceous chondrites. Two of them are CI chondrites, Yamato-86720 and Belgica-7904, and three are CM chondrites, Yamato-74662, Yamato-791198 and Yamato-793321. Among these chondrites, we have found various kinds of soluble organic compounds, such as amino acids, carboxylic acids, hydrocarbons, and purines from Yamato-74662 and Yamato-791198[2]-[7]. On the other hand, we could not find these compounds from Yamato-793321 and Belgica-7904[3][8].

For analyses pulverized each chondrite sample was treated with HF/HCl in order to demineralize and concentrate the insoluble organic matter. Then it was washed with carbon disulfide, methanol, etc, to remove inorganic sulfur compounds.

The sample of insoluble organic matter was placed in the DTA/TG instrument and heated under a helium flow from room temperature to 800°C at the rate of 10°C/min. The released compounds were directly introduced into a mass spectrometer(direct-MS method), and continuous temperature profiles of compounds released was obtained. For identification of compounds released, those released from the bulk Yamato-791198 sample without any treatment were once stored in a cold trap and introduced into GC/MS(trap-GC/MS method).

The bulk Yamato-791198 sample released various organic compounds as identified by the trap-GC/MS method. Those compounds consists of aliphatic and aromatic hydrocarbons, nitriles, thiophene, and furan. Among these organic compounds, benzene was the largest in amount.

The insoluble organic matter from Yamato-74662 released hydrocarbons as shown in Fig.1. Each hydrocarbons shows a similar release pattern, starting at 300-400°C, and ending at 500-600°C with maximum at 400-500°C. There was no remarkable difference in release pattern among each compounds. However, benzene was released at relatively low temperature. This release probably comes from remaining benzene used in the wash. Fig.2 shows the release of hydrocarbon from the insoluble

organic matter from Yamato-791198. These release patterns resemble those of Yamato-74662. However, the insoluble organic matter from Yamato-793321, Belgica-7904, and Yamato-86720 released almost no organic compounds. Only a small amount of benzene was released. These data suggest that the insoluble organic matter in these chondrites are more graphitic than those in Yamato-74662 or Yamato-791198.

The results of thermal analyses of all samples did not show any prominent peak related with decomposition of the insoluble organic matter on the DTA curve. The TG curves of all samples show continuous decrease in weight. But between 200 to 500°C, the slope of TG curves of Yamato-74662 and Yamato-791198 is slightly steeper in comparison with those of other temperature range. So, these parts probably correspond to the release of organic compounds such as hydrocarbons. Total weight loss of these samples are about in the range of 12 to 30%. In addition, the weight losses of samples, Yamato-74662 and Yamato-791198 which released relatively large quantity of organic compounds, are larger than those of other samples.

Elemental analyses of H, C, and N in the isolated insoluble organic matter were also carried out before and after the heating. The H/C ratio of insoluble organic matter in Yamato-74662 and Yamato-791198 are 0.57 and 0.67, respectively. However, the H/C ratios of other samples are relatively lower. These results suggest that the insoluble organic matter in Yamato-793321, Yamato-86720, and Belgica-7904 are more graphitic than those in Yamato-74662 and Yamato-791198, and likely reflect their thermal history on the parent bodies.

References
[1] Shimoyama, A., Komiya, M., and Harada, K. (1991)
    Proc. NIPR Symp. Antarctic Meteorites, in press
[2] Shimoyama, A., Ponnamperuma, C., and Yanai, K. (1979)
    Nature, 282, 394
[3] Shimoyama, A., Naraoka, H., Komiya, M., and Harada, K.
    (1989) Geochem. J., 23, 181
[4] Shimoyama, A., Harada, K., and Yanai, K. (1985)
    Chem. Lett., 1985, 1183
[5] Shimoyama, A., Naraoka, H., Yamamoto, H., and Harada, K.
    (1986) Chem. Lett., 1986, 1561
[6] Naraoka, H., Shimoyama, A., Komiya, M., Yamamoto, H., and
    Harada, K. (1988) Chem. Lett., 1988, 831
[7] Shimoyama, A., Hagishita, S., and Harada, K. (1990)
    Geochem. J., 24, 343
[8] Shimoyama, A., and Harada, K. (1984) Geochem. J., 18, 281

m/z                                         Scale

58 $C_4H_{10}$                                100

56 $C_4H_8$                                300

78                                 200

92    CH₃                      200

128                               100

 100    200    300    400    500    600    700    800

Temp. (°C)
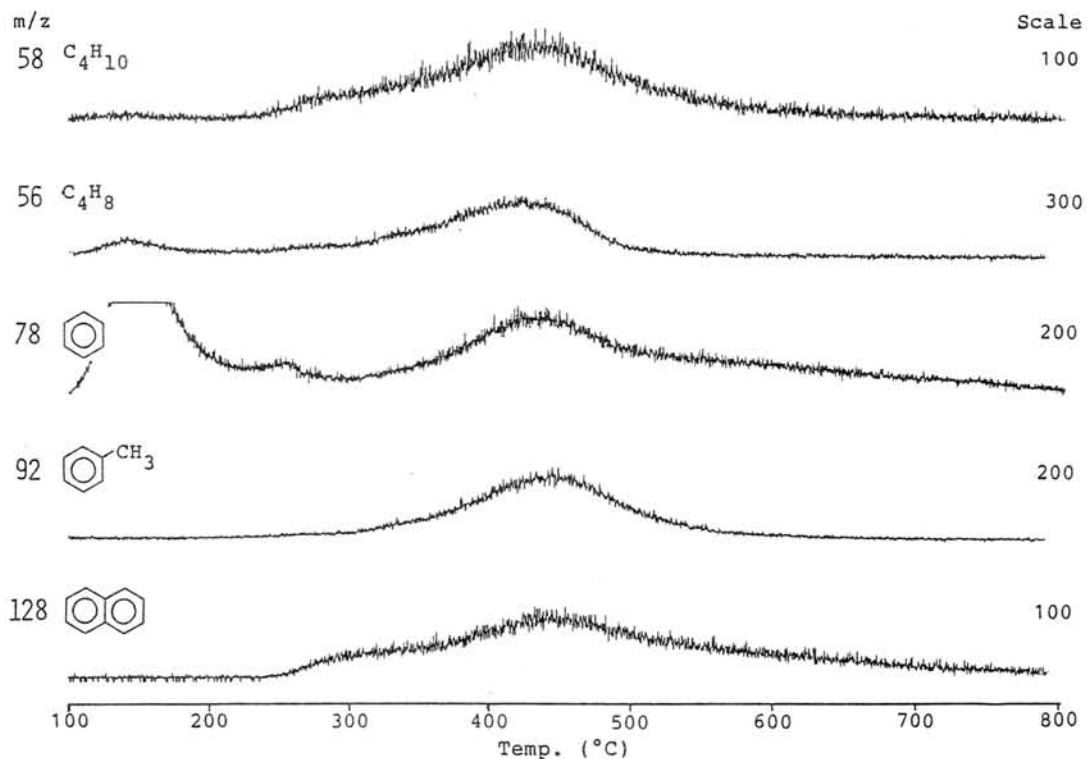
Fig.1   Thermal release patterns of ions for compounds released
from Yamato-74662 sample treated with HF/HCl

m/z                                        Scale
                                         200

58 $C_4H_{10}$

56 $C_4H_8$                                200

78                                 100

92    CH₃                      200

128                               200

 100    200    300    400    500    600    700    800

Temp. (°C)
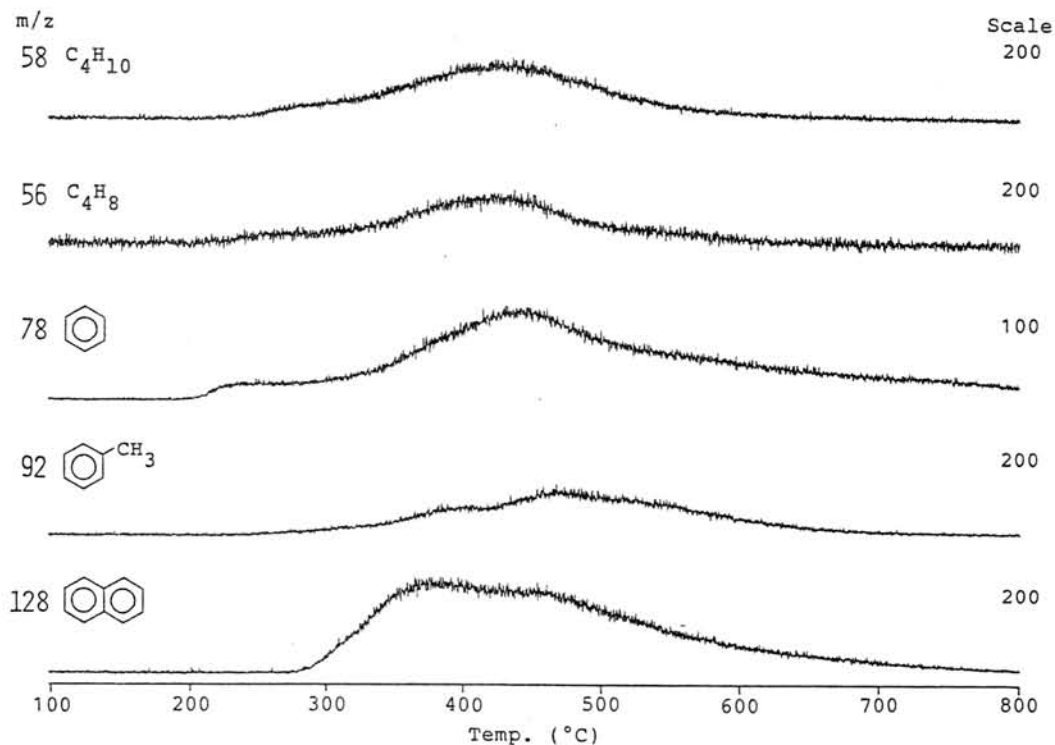
Fig.2   Thermal release patterns of ions for compounds released
from Yamato-791198 sample treated with HF/HCl

ON INSOLUBLE ORGANIC MATTER IN CARBONACEOUS CHONDRITES.

Fumio Kitajima and Akimasa Masuda

Department of Chemistry, Faculty of Science, The University of Tokyo, Hongo, Bunkyo-ku, Tokyo 113

Carbonaceous chondrites are a group of primitive meteorites and one of those characteristics is relatively high carbon contents. Certain fractions of the carbon exhibit enrichments in $^{12}C$, $^{13}C$ or D, and are considered as the host phases for isotopically anomalous noble gases. The isotopic heterogeneity indicates the various origins of the carbonaceous materials in the carbonaceous chondrites. The major component of the carbon is insoluble macromolecular materials. The fine-structure of those materials is considered to reflect those formation histories. But the structure has not yet been understood well because of the difficulty of chemical separation and the lack of satisfactory method of characterization.

In this investigation, we have examined the structure of carbonaceous materials in carbonaceous chondrites with pyrolysis GC-MS technique. And we compared the pyrolysis products from the meteorites with those of several synthetic polymers to estimate the structure which can give the pyrolysis products from the meteorites.

Figure 1 shows the pyrograms (the gas chromatograms of the pyrolysis products) of the Murchison (CM2) and the Allende (CV3) carbonaceous chondrites, at $740^{\circ}C$ (without HCl-HF treatment). The principal pyrolysis products are aromatic hydrocarbons (including heterocyclic compounds), alkanes and alkenes. These pyrolysis products are considered to be derived from edge defects of the carbonaceous macromolecular materials because complete graphite does not yield any pyrolysis products except low-molecular compounds such as $CO_2$ under the pyrolysis condition.

In addition, to examine structural heteogeneity of the macromolecular materials, we carried out size-separation of the samples using freeze-thaw method and analysed each size fraction with pyrolysis GC-MS technique, but have not yet found notable difference between the pyrograms of each size fraction because of imperfection of the separation.

Because the macromolecular materials have various structural units instead of "monomer", we must list possible candidates for each structural unit to estimate the whole structure. For the synthetic mechanism of the aromatic hydrocarbons (except heterocyclic compounds), at least two mechanisms exist. 1)The cleavage of C-C bonds which link the aromatic rings (Figure 2-A). 2)The aromatization of polyene generated in the course of pyrolysis reaction (Figure 2-B). For the alkanes and alkenes, the random cleavage of methylene C-C bonds (Figure 2-C) is a candidate.

Figure 3 shows the pyrograms of polyvinylchloride and polyethylene under the same pyrolysis condition as that of the meteorites. The pyrolysis products from the polyvinylchloride

are similar to the aromatic hydrocarbons from the meteorites. The polyethylene gave n-alkanes, 1-alkenes and $\alpha,\omega$-alkenes as the pyrolysis products. These facts suggest that the reactions described above can proceed under the condition of pyrolysis concerned.
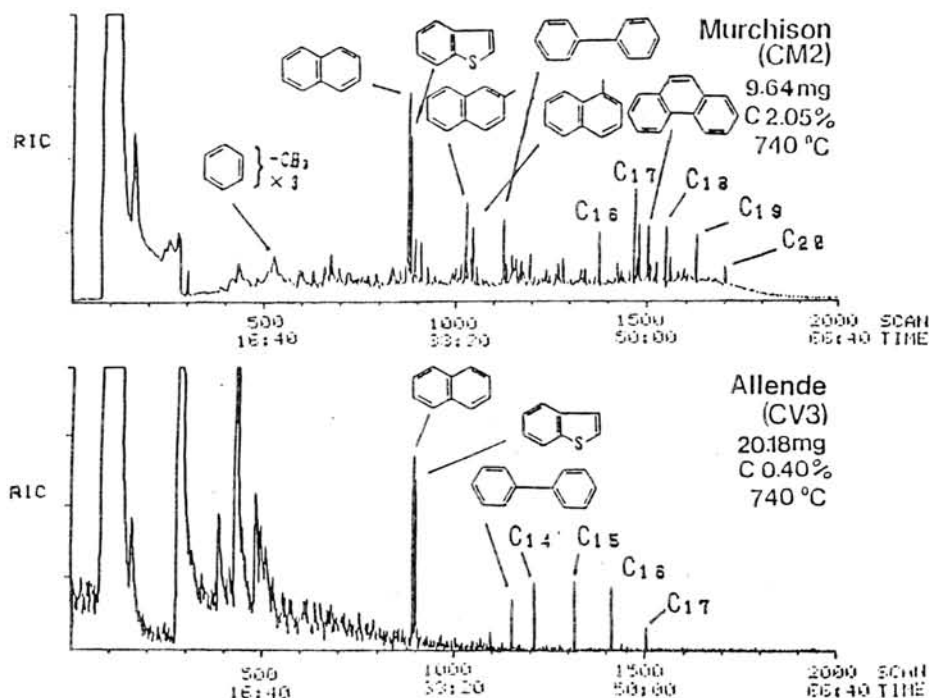


Figure 1. Pyrograms of the carbonaceous chondrites.
          Column : OV-1 50m 0.25mm i.d.
          Temperature : 4°C/min from 60 to 260°C
                        after 16 min at 60°C
          Pyrolysis condition : 740°C for 3s



X,Y,Z : Substituent groups.
        Aromatic hydrocarbons.
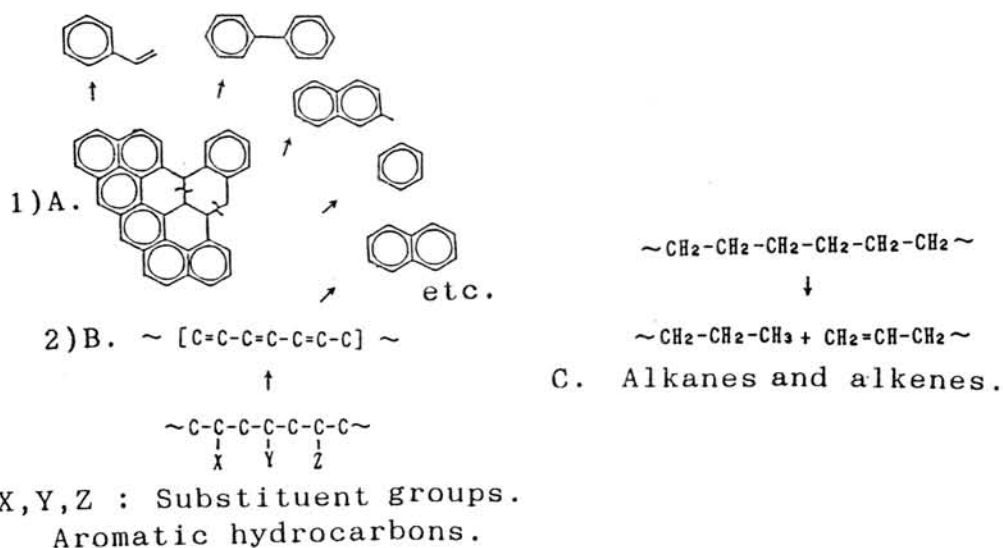
Figure 2. Synthetic mechanisms of the pyrolysis products.
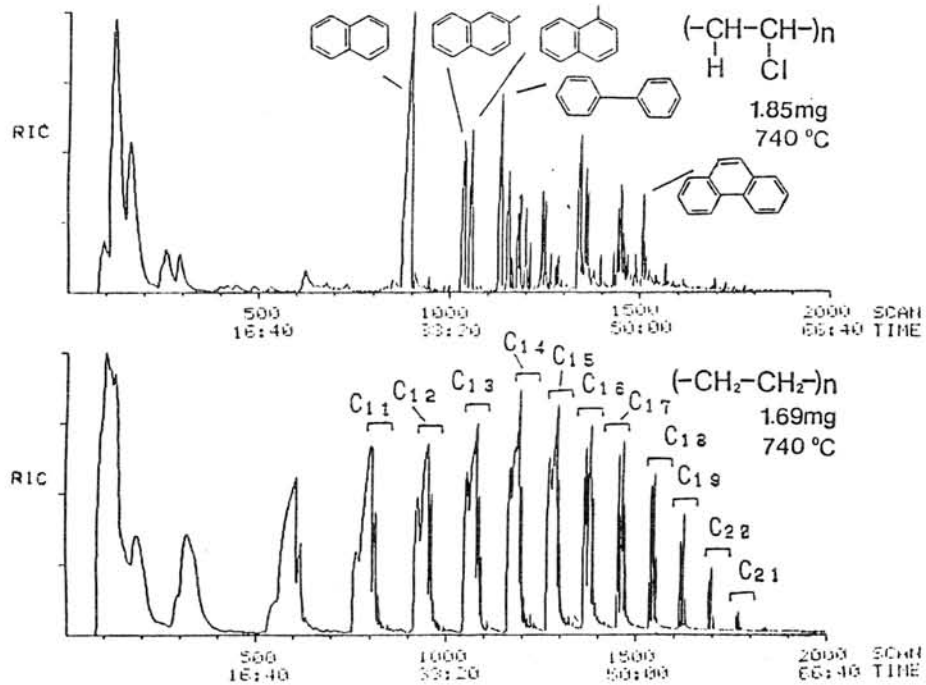
Figure 3. Pyrograms of the synthetic polymers.
Column : OV-1 50m 0.25mm i.d.
Temperature : 4°C/min from 60 to 260°C
after 16 min at 60°C
Pyrolysis condition : 740°C for 3s

# Raman scattering and laser-induced luminescence from micro diamonds in ureilites

Hiroyuki Kagi[1], Kazuya Takahashi[2] and Akimasa Masuda[1],[2]

1) Department of Chemistry, Faculty of Science, University of
   Tokyo, Hongo, Bunkyo-ku, Tokyo 113, Japan.
2) Earth Science Laboratory, Institute of Physical and Chemical
   Research (RIKEN), Hirosawa, Wako-shi, Saitama 351-01, Japan.

## 1. Introduction

The genetic history of diamonds found in ureilites has been a crux of controversy, and there have been various opinions on their origin. The most persuasive theory is a shock origin, while CVD origin is also considered as a convincing story of the diamond genesis. In this study, optical property of the diamonds was investigated by means of Raman and laser-induced luminescence spectroscopy on the micro region for making their optical characterization.

## 2. Experimental procedure

The ureilites studied here were Allan Hills (ALH)-77257, Yamato (Y)-791538 and Novo Urei. Y-791538 was chemically decomposed with HCl and HF at room temperature for two weeks for the purpose of collecting the diamond particulates. ALH-77257 and Novo Urei were transferred to RAMANOR U-1000 as PTS (polished thin section) and diamond particulates were observed in-situ. Furthermore, a natural irradiated diamond aggregate, carbonado, was investigated for evaluating temperature dependence of the luminescence bands.

## 3. Results and Discussion
### (1) Wide variation in genetic conditions for individual diamond particulates

Raman spectra and incidental photoluminescence spectra of the diamonds collected from Y-791538 are shown in Fig. 1. The sharp lines at 552 nm, which derive from Raman active lattice vibration excited by incident 514.5 nm green laser light, were observed in all spectra. In the spectrum in Fig. 1a only one Raman band at 552 nm is observed, while in the two spectra in Fig. 1b and c very broad bands, whose fine structures differ slightly from each other, are observed in addition to the sharp line at 552 nm. Similarly, in case of the polished thin section of Novo Urei, Raman and photoluminescence bands at 585 nm, whose intensity ratio between the three varied significantly, have been observed. This phenomenon implies that diamond particulates collected from a small portion of ureilite reflect the wide range of their formation condition, whose chemical and physical environments differ greatly from each other. Thus, if the diamonds had been formed in the parent body by shock events, they would have traveled a long distance in the parent body, resulting in their present location in the ureilites. Otherwise, if the diamonds had been formed by CVD, our results suggest that the diamond would have been deposited in various states within a nebula or in nebulae with varying chemical composition or physi-

cal condition, and accreted to the parent body of ureilites.

## (2) The cause of the characteristic photoluminescence spectra

In order to identify the origin of the photoluminescence observed in the diamonds in ureilites, heating experiment on the terrestrial natural irradiated diamond, Carbonado, was carried out. Carbonado emits very strong luminescence at 504 nm derived from radiation damages. In Fig.2 are shown photoluminescence spectra of five small chips of Carbonado which were heated up to 300, 400, 500 and 600 ℃ for half an hour. A remarkable spectral change takes place between 400 ℃ and 500 ℃, and the luminescence feature of resulting spectra above 500 ℃ has a strong resemblance to that of the micro diamonds in ureilites. From the above experimental results, it is assumed that the lattice vacancies, which were formed by radiation damage and emit the 504 nm luminescence, were moved, by heating, to sites of nitrogen atoms and trapped by these atoms, while conjugated vacancies emitting 575 nm luminescence were formed. From the similarity between the heated Carbonado and the meteoritic diamonds found in ureilites, it is evident that the meteoritic diamond crystal is damaged to form color centers.

The origin of color centers observed in the meteoritic diamonds may be open to two possibilities. First, highly accelerated particles, i.e. cosmic ray, had brought radiation damages on the meteoritic diamond crystals. Second, the color center was formed in the growing process of diamond crystal. However, we cannot tell which is the true origin at present. Anyway, the meteoritic diamonds are proved to have been exposed to considerable high temperature after the forming event of diamonds. On the analogy of the heating experiment, the maximum temperature which the diamonds have suffered can be estimated to be not lower than 500 ℃. The optical property can give a new clue to the thermal history of diamonds in ureilites independently of the surrounding silicate minerals.

## 4. Conclusion

Raman spectra and photoluminescence spectra were observed on micro diamonds found in several ureilites. Their band shapes varied widely within a small chip of ureilite sample, which shows the heterogeneity in the conditions of development of the parent body of ureilite. Furthermore, a junction of spectral information from carbonado with those of the meteoritic diamonds suggests a possibility that the luminescence profile can be expected to serve as a new thermal indicator for the meteoritical diamonds.

Reference:
Kagi, H., Takahashi, K. and Masuda, A.: Naturwissenschaften, **77**, 531-532, 1990
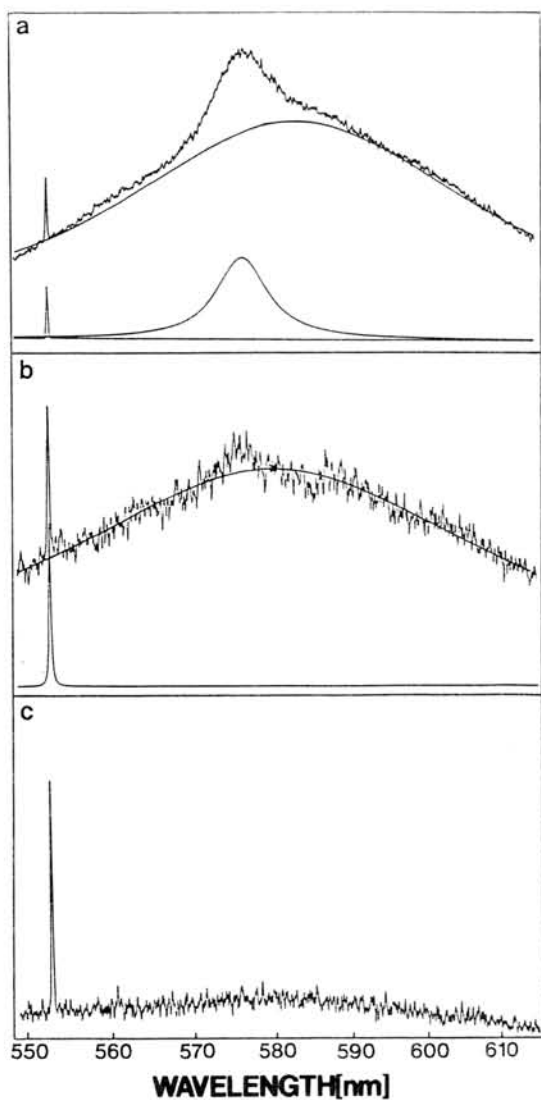
Fig. 1. Raman and photoluminescence spectra of diamonds in Antarctic ureilite; Y-791538. Smooth curves are decovoluted Lorentzian components.
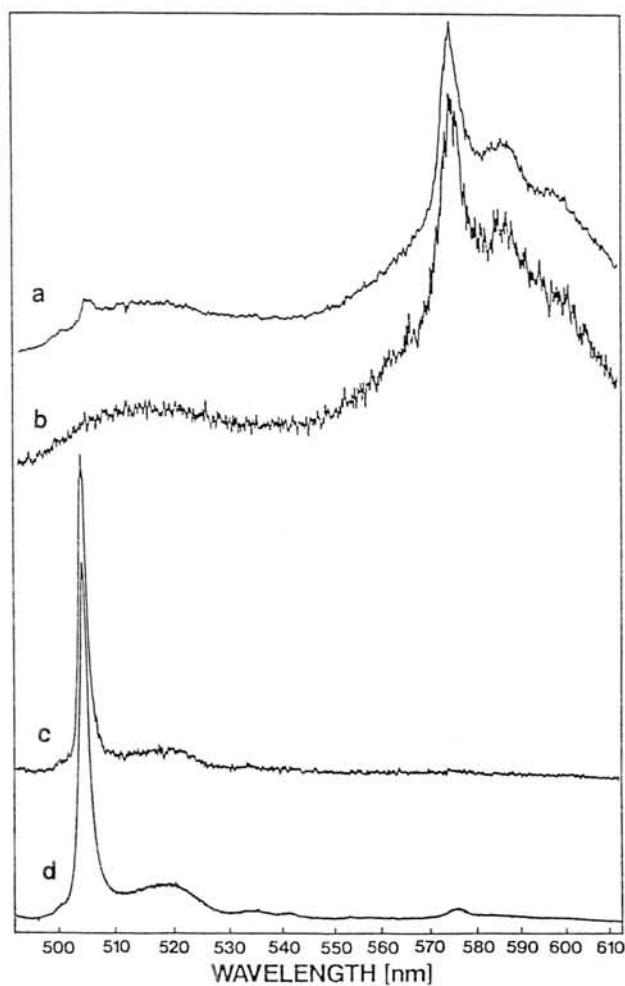


Fig. 2. Photoluminescence spectra of the heated carbonado. (a)sample heated to 600℃ (b)sample heated to 500℃ (c)sample heated to 400℃ (d) sample heated to 300℃

# Special Lecture (I)

## Dr. Paul Pellas

# EARLY CHRONOLOGY, THERMAL HISTORY, INTERNAL STRUCTURE AND DIMENSIONS OF THE H-CHONDRITE PARENT ASTEROID

## Paul Pellas

Equipe Météorites, Lab. de Minéralogie du Muséum, 61 rue Buffon, 75005 Paris, France.

The search for coherence between age data for ordinary chondrites (OCs) using absolute and relative chronologies has been a major challenge in meteoritics since 1962 (when J. Reynolds discovered the short-lived $^{129}$I-$^{129}$Xe radiogenic system), with very little success until recently.

The Multiple Fission Track Detector method (MFTD)

In 1974 we started to use a specific method able to retrace the early thermal history of chondritic asteroids in the low temperature regime (ca 600 - ca 350 K) by means of the MFTD method (1, 2). The method is based on analyses of the $^{244}$Pu fission track record in phosphates (merrillite, apatite) and _adjacent_ mineral track-detectors (ortho- and clinopyroxenes, olivine, feldspar). In chondritic phosphates the fossil track densities represent 4 components : 1) cosmic ray tracks from the Fe group of the galactic cosmic radiation; 2) $^{238}$U spontaneous fission tracks; 3) spallation recoil tracks; 4) $^{244}$Pu spontaneous fission tracks. The three first components can be corrected for by various experimental procedures. All tracks in excess of the above contributions are then attributed to the spontaneous fission of $^{244}$Pu ($^{244}$Pu has a high fission probability and a half-life of 82 Ma). To avoid shock-induced dislocations, only chondrites showing the lowest degree of shock were studied. An extension of the method to a higher temperature regime was obtained by measuring the $^{244}$Pu fission xenon contents of phosphates, which can also be converted into equivalent fission track densities. A linear extrapolation of the fission track densities of the various (adjacent) detectors of a given chondrite to its phosphate fission xenon data allows us to estimate fission xenon retention temperatures in phosphates of roughly 900($\pm$100 K) (3). Thus, after appropriate corrections to convert the $2\pi$ registration geometry of mineral phases adjacent to phosphates into a $4\pi$ geometry, it becomes possible a) to deduce the time elapsed in the temperature range (ca 900-ca 350 K) and b) to trace sequentially the early thermal histories of chondritic materials over the time interval 4.6-4.3 Ga, when $^{244}$Pu was still alive as an easily observable fission track source (3).

Applications to OCs.

It was soon found that among OCs, the H chondrites of various petrologic types (6 to 4; samples of type 3 cannot be used because of the smallness of their phosphate grain-sizes) and of homogeneous textures were the best samples, due in many cases to their low level of shock. In this respect, regolith and most fragmental breccias have been discarded. Samples on which the MFTD method was used have also been given to various groups using diverse chronometric systems ($^{129}$I-$^{129}$Xe, $^{87}$Rb-$^{87}$Sr, $^{87}$Sr/$^{86}$Sr initial, $^{39}$Ar-$^{40}$Ar, Pb-Pb/U-Pb) in order to look for coherence between chronometers. The preliminary results of the MFTD method have indeed shown that there was an inverse correlation between the Pu fission track cooling rates and the petrologic types (3). In this case, it could be expected that the

results of the $^{129}I$-$^{129}Xe$ system should have shown some concordance. The best H chondrite samples used for Pu studies were consequently given to the Heidelberg group, and it became soon evident to the present author, from the results of Jordan et al. (4), that there was no coherence between the petrologic degree and the I-Xe systematics. The cause of such a disagreement seems to be due to isotopic heterogeneities of the $^{129}I/^{127}I$ ratio

Similarly selected materials were distributed to G. Turner, and the $^{39}Ar$-$^{40}Ar$ plateau ages of ten H chondrites showed no clear-cut difference between metamorphic types (5). This result is still valid to-day, with five more Ar-Ar results for H chondrites. It took 10 years to understand that the sensitivity of the Ar-Ar method ($\pm 30$ Ma) was not precise enough to distinguish between different layers of a relatively small ($R_o \lesssim 80$ km) asteroid (6). On the other hand, the Ar-Ar plateau method when applied to the most equilibrated LL chondrites shows that there is agreement between the long metamorphism intervals detected by the MFTD method (150-250 Ma) and the rather young ages (ca 4.37 Ga) found for five LL6-7 samples (7, 8). Such a result was in some way predicted by Kaneoka (9), although at that time the data were based on only two chondrites. This suggests that the LL parent asteroid was a much larger body than the H asteroid (6).

The definite confirmation of the layered internal structure of the H-body has come recently from Pb-Pb/U-Pb absolute ages of phosphates from several H chondrites (10, 11) which were previously studied with the MFTD method. Göpel et al. (1989, 1990) have indeed found a clear-cut difference in ages between the innermost layers of H6 materials (4.504 - 4.521 Ga) and three H5 samples (4.550 - 4.555 Ga), the age data having a very high precision of less than 1 Ma. As a consequence, the H asteroid appears to be an object having a simple layered internal structure, produced through a thermal spike ($^{26}Al$ being the most probable heating source) which brought in a very short time some of its internal layers to peak metamorphic temperatures of 1000-1100 K (for petrologic type 5) and 1100-1200 K (for type 6), followed by a fast cooling to the closure temperature of the Pb-Pb/U-Pb system (ca 800-700 K ?) in a very few millions of years.

It is worth noting that 14 H samples (all non-Antarctic in origin) of the various petrologic types do fit in such a layered internal structure at their respective petrological location, whatever their exposure ages (which range between 1.5 and 80 Ma). These results put strong doubts on recent suggestions that Antarctic H chondrites would have to come from various parent objects (12).

References. (1) Pellas P. & Storzer, D. (1975), C.R.Acad.Sci. Paris, 280D, 225-228. (2) Pellas P. & Storzer D. (1977), in Comets, Asteroids, Meteorites, ed. A.H. Delsemme, 355-362. (3) Pellas P. & Storzer D. (1981), Proc.R.Soc.Lond. A374, 253-270. (4) Jordan J., Kirsten T. & Richter H. (1980), Z.Naturforsch. 35A, 145-170. (5) Turner G., Enright M.C. & Cadogan P.H. (1978), Proc.Lunar Planet;Sci.Conf. 9th, 989-1025. (6) Pellas P. & Fiéni C. (1988), Lunar Planet.Sci. 19, 915-916. (7) Trieloff M.,Jessberger E.K. & Oehm J. (1989), Meteoritics 24, 332. (8) Pellas P., Fiéni C. Trieloff M. & Jessberger E.K. (1990), Meteoritics 25, 397. (9) Kaneoka I. (1980), Proc.5th Symp.Antarctic Met., 177-188. (10) Göpel C., Manhès G. & Allègre C.J. (1989), Meteoritics 24, 270-271. (11) Göpel C., Manhès G. & Allègre C.J. (1990), Meteoritics 25, 367-368. (12) Lipschutz M.E. & Samuels S.M. (1991), Geochim.Cosmochim. Acta 55, 19-34.

## Thursday, June 6, 1991

0900-1530    Symposium, Auditorium

1115-1530    Special Session; Reports of Consortium
Studies on Carbonaceous Chondrites,
Unique Meteorites and Lunar Meteorites

1530-1730    Special Lectures (II and III)
Professor Otto Eugster (Invited Speaker)
Physikalisches Institut,
University of Bern,
Switzerland

Dr. David S. McKay (Invited Speaker)
Mission Science and Technology,
NASA-JSC, Houston,
USA

1745-2000    Reception, Lecture Room, 2nd Floor

THE EFFECT OF TOTAL PRESSURE ON VAPORIZATION OF ALKALI METALS
FROM A PARTIALLY MOLTEN CHONDRITIC MATERIAL. Taro Shimaoka[1] and Noboru
Nakamura[1,2] [1]Department of Science of Material Differentiation, Graduate School of Science
and Technology, Kobe University, [2]Department of Earth Sciences, Faculty of Science, Kobe
University, Nada, Kobe 657, Japan.

Introduction Alkali metals are moderately volatile at high temperatures and their vaporization
behavior can constrain melting conditions of meteoritic materials [1,2]. Shimaoka and Nakamura
[3] performed a series of vaporization experiments to study vaporization behavior of alkalis from
a partially molten chondritic material and showed the vaporization is controlled mainly by the
loss of elements from the partial melt, which is similar to the case of total melt [1], despite the
differences of absolute values of vaporization rates. The vaporization rate can be influenced by
total pressure, oxygen fugacity, and the chemical composition of charge as well as temperature.
In order to investigate the effect of total pressure on vaporization of alkalis, a heating experiment
of a chondritic material was carried out under various total pressures ($\sim 10^{-5}$-$\sim 10^{-1}$torr) at a
constant temperature (1300°C). Preliminary results for the total pressure effect on vaporization
of alkali metals were presented previously [4].

Experimental A fine grained starting material ($\phi < 10 \mu m$) was newly prepared from the Etter
(L5) chondrite. Sample was heated in a Ta or Mo-crucible at a constant heating rate up to a
1300°C and held at the temperature for 40 min. Total pressure ($\sim 10^{-5}$-$\sim 10^{-1}$torr) was adjusted
using He gas with high purity (99.999%). Quenched run products were analyzed for Na by the
atomic absorption spectroscopy, and for K and Rb by isotope dilution mass spectrometry. The
proportions of holes and melt in the run products were estimated from the SEM back-scattered
electron images of run products [3,4].

Results and Discussion The general procedure used for the calculating of vaporization rates
of alkalis was described previously [3,4]. Fig. 1 shows the vaporization rates of alkalis at
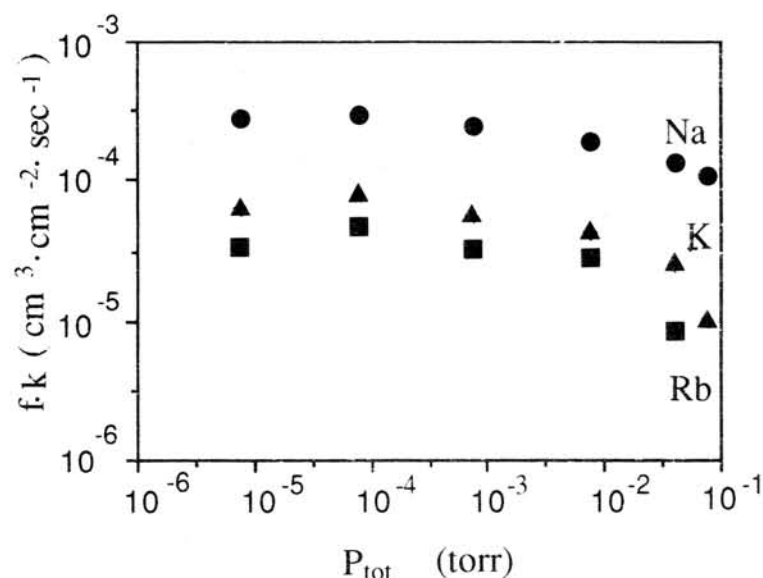


Fig. 1. Plot of the vaporization rate of alkali metals as a function of total
pressure.

various total pressures. In general, the vaporization rates of alkalis decrease with increasing total
pressure. Actually, almost no vaporization loss of Rb was detected for the run product at

~10⁻¹torr. It is interesting to note, that the pressure effect is the greatest for Rb and the smallest for Na. It is possible that at the lower total pressures (~$10^{-5}$ and ~$10^{-4}$torr), relatively high oxygen partial pressure in residual air influenced the vaporization rates of alkalis [1]. Then total pressure effect on vaporization rate of alkali metals may be seen at the relatively higher total pressures as shown in Fig. 2. In this figure, a relatively good linear fitting of data points are
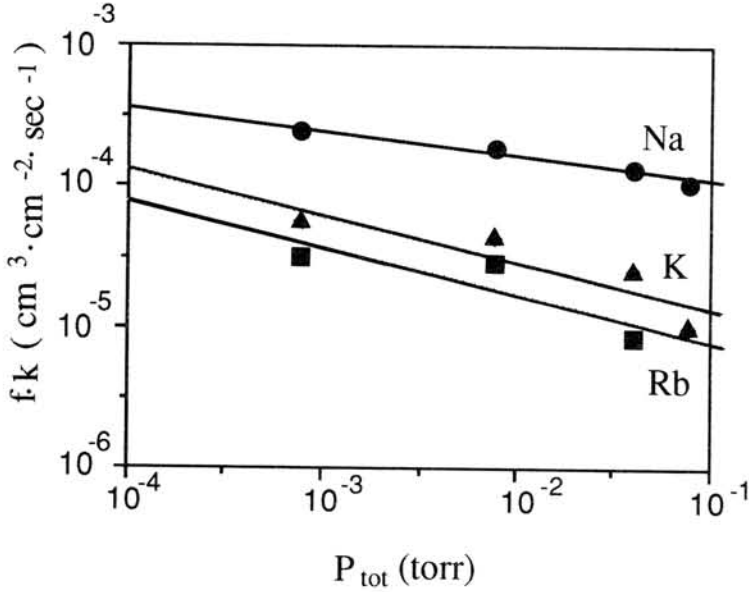


Fig.2. Plot of the vaporization rate of alkali metals as a function of relatively high total pressure.
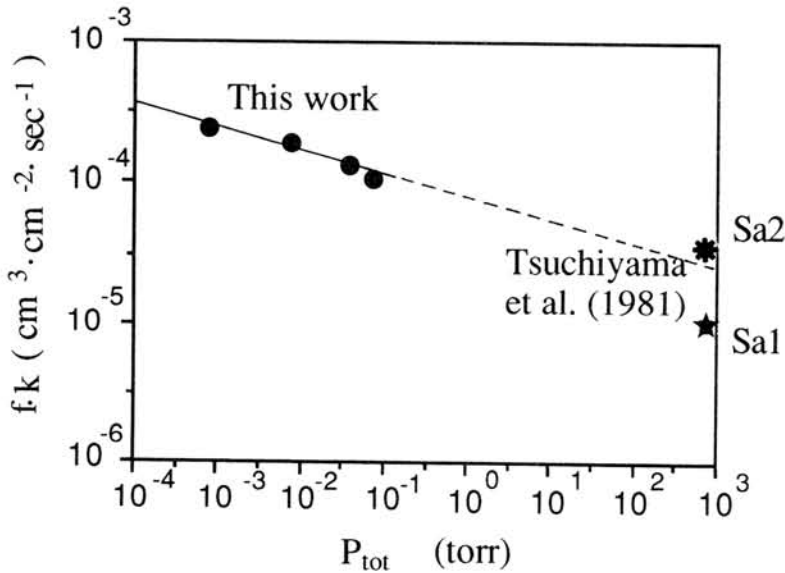


Fig. 3. Plot of the vaporization rate of alkali metals in this work and in [1] as a function of relatively high total pressure.

recognized. These data are compared with those obtained by Tsuchiyama et al. [1] in Fig. 3. The vaporization rate of Na was calculated to be $1.2 \times 10^{-4}$ cm$^3$/min·cm$^2$ at 1300°C (f=0.2) by extrapolating this line to 1 atm. This value seems to be consistent with the value ($0.5-1.7 \times 10^{-4}$ cm$^3$/min.cm$^2$) calculated from Tsuchiyama's experiment at the same temperature and oxygen

partial pressure ($10^{-11.6}$ atm). Further work using Mo crucible is needed to check the effect of oxygen partial pressure on vaporization rate of alkalis and now in progress.

References 1. Tsuchiyama A., Nagahara H. and Kushiro I. (1981) GCA 45, 1357-1367. 2. Matsuda H., Nakamura N. and Noda S. (1990) Meteoritics 25, 137-143. 3. Shimaoka T. and Nakamura N. (1989) Proc. NIPR Symp. Antarct. Meteor. 2, 252-267. 4. Shimaoka T. and Nakamura N. (1991) Proc. IAU Colloq. No.126 Origin and Evolution of Interplanetary Dust, (A. C. Levasseur Regound and H. Hasegawa, eds.), (in press).

SECTOR-ZONED PYROXENE IN ALLENDE CAI AND THE IMPLICATIONS FOR OXYGEN ISOTOPE DISTRIBUTION. Hisayoshi Yurimoto, Kazumasa Oishi, Hiroshi Nagasawa *, Hidemi Yuasa and Shigeho Sueno. Institute of Geoscience, The University of Tsukuba, Tsukuba, Ibaraki 305 and * Department of Chemistry, Gakushuin University, Mejiro, Tokyo 171, Japan.

Introduction Ca, Al-rich inclusion (CAIs) of carbonaceous chondrite show heterogeneous distribution of O isotopes among coexisting minerals, suggesting mixing of $^{16}$O-rich component in spinel and Ti-rich pyroxene [1]. Clayton et al. [2] suggested that whole CAI were formed originally with O isotope ratios similar to those in spinel ($\delta^{17}$O= $\delta^{18}$O= ca. -40‰) and O isotopes in melilite and anorthite were later replaced by those in the surrounding gas with normal O isotope ratios by heating. To evaluate such O isotope exchange after formation of CAI, sector-zoned Ti-rich pyroxene in Allende HN-3 CAI has been observed by concentration mapping technique using electron micro-probe (EPMA) and secondary ion mass spectrometry (SIMS).

HN-3 is a carse-grained CAI in Allende meteorite which has a typical B-1 structure: mantle composed exclusively of melilite and core of Ti-rich pyroxene, anorthite, melilite and spinel. The detail petrographical description is given by Nagahara [3].

Experimental Quantitative concentration map of $SiO_2$, $Al_2O_3$, $TiO_2$, CaO, MgO have been obtained by JEOL JXA-6821 electron micro probe. Quantitative SIMS concentration map of Fe has been obtained by Cameca IMS-3F ion microscope combined with AIM88 cooling-CCD detector [4].
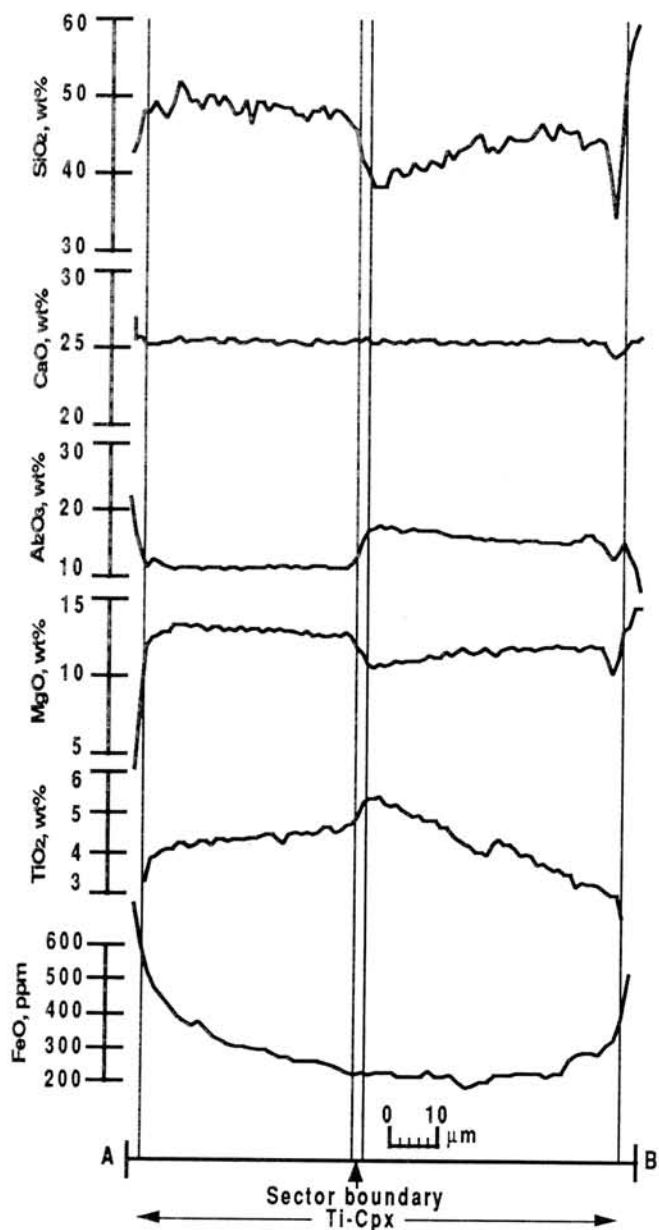


Fig. 1 Analytical data along the traverse crossing sector boundary of Ti-rich pyroxene.

Results and Discussion Analytical results along a traverse of the concentration maps of Ti-rich pyroxene in HN-3 are shown in Fig. 1. A clear sector boundary are recognized from all analyzed elements except for Ca. The width of the boundary is less than 2 μm which is spatial resolution limit of this study.

The sector zoning were grown kinetically with the crystal growth of the pyroxene. If the pyroxene is heated after the crystallization, the sector boundary become disappeared by inter diffusion between both sectors. Therefore, a width of sector boundary corresponds to the period of post-heating event of CAI. The upper limit width of the sector boundary, 2 μm, restrict the heating period.

Fig. 2 Degree of O exchange as a function of heating period. Fe diffusion path is assumed 2 μm.

Using the cation diffusion coefficients in pyroxene the maximum period of post-heating event was calculated as a function of temperature from the width of sector boundary. Since average grain size of CAI minerals can be analyzed under microscope, maximum O exchange degree in CAI minerals were derived from the combination of the heating period and O diffusion coefficient in literature (Fig. 2). The calculation results show that diffusion processes during the heating event cannot establish the heterogeneous O isotope distribution reported. The heterogeneous O distribution must be generated with crystal growth of each minerals.

References 1. Clayton R.N., Onuma N., Grossman L. and Mayeda T.K. (1977) *EPSL* 34, 209-224. 2. Clayton R.N. and Mayeda T.K. (1977) *GRL* 4, 295-298. 3. Nagahara H. (1987) *Rept. Overseas Scientific Resarch Project No. 59042011, 60041064 and 61034059, 65-78.* 4. Yurimoto H., Kosaka K., Kamiya H., Okudera S. and Sueno S. (1989) *Ann. Meet. Mineral. Soc. Jpn.* 63.

## Rb-Sr FEATURES OF THE SHOCK-MELTED LL-CHONDRITES FROM ANTARCTICA: Y-790723 and 790528

Hirokazu Fujimaki[1], Ken-ichiro Aoki[1], Hideyasu Kojima[2], and Keizo Yanai[2]
1) Institute of Mineralogy, Petrology and Economic Geology, Tohoku University, Sendai, Miyagi 980, Japan, 2) National Institute of Polar Research, Kaga, Itabashi, Tokyo 173, Japan

The young ages such as several hundreds Ma for the severely-shocked meteorites (e.g., Heymann, 1967; Bogard et al., 1976; Bogard and Hirsch, 1980) indicate the time of one of the latest impacts on the parent body. The ages also evidence that the parent body could have existed for as long as 4 Ga. Most of those young ages for the shock events were obtained by K-Ar method. In contrast, the shock events dated by Rb-Sr method are very rare (e.g., Minster and Allegre, 1979; Nakamura and Okano, 1985; Nakamura et al. 1990). Since most shock-melted meteorites consist of mixtures of melted and non-melted materials, mineral separation (or any kind of separation) is quite difficult. Therefore, in order to contribute to the chronological studies of this kind of meteorites, we tried to clarify the Rb-Sr features of the partially-melted shocked meteorites.

We crushed two of the LL-chondrites (Y-790723 ad Y-790528) to smaller than 100-mesh size and separated in alcohol with a hand magnet into six portions. A pinch of fine powder floated in acetone when washing makes an additional portion. The Sr isotopic compositions as well as Rb and Sr abundances were analyzed. Since they are similar to the other shock-melted Yamato-79 LL-chondrites (Yanai and Iguchi, 1981; Sato et al., 1982), they may have 1,200 Ma as the age of the shock-melting enent (Nakamura and Okano, 1985; Takigami and Kaneoka, 1987).

Y-790723: The Rb abundances of the seven portions of Y-790723 range from 5.523 ppm to 20.70 ppm, and the Sr concentrations vary from 5.466 ppm to 25.87 ppm. Those values do not differ much from the Yamato-79 chondrite group. The isotopic ratios of $^{87}Sr/^{86}Sr$ of the seven portions are high. The lowest ratio was obtained from the least magnetic portion (0.82483), and the highest ratio (0.93619) from the next portion to the most magnetic one. The $^{87}Rb/^{86}Sr$ of seven portions of Y-790723 are plotted against $^{87}Sr/^{86}Sr$ in Fig. 1. The points are roughly scattered. Line A was obtained by four points, and line B by three points; both indicate about 3,100 Ma. The meaning of the calculated age should be examined carefully.

Y-790528: In contrast to Y-790723, Y-790528 is exceedingly depleted in Rb: the highest concentration of Rb in the magnetically separated portion is only 1.330 ppm, and the lowest is 0.8792 ppm. The Sr abundances of the separated portions of Y-790528 (11.52 - 20.64 ppm) are similar to the other LL-chondrites. Consequently, the $^{87}Sr/^{86}Sr$ ratios are very low (0.71284 - 0.71846), and the variation between the portions is small. The isochron plot of the analytical

results is shown in Fig. 2. The points seem scattered since the scale differs from Fig. 1. The solid line indicates the 4,400 Ma reference isochron obtained by five points. If the impact was so immense, even heavy alkaline elements could have vaporized and the Sr isotopic compositions did not develop much thereafter. We interpreted the low $^{87}Sr/^{86}Sr$ ratios as the result of Rb vaporization in very early period of the solar sytem. If the interpretation is correct, obtained 4,400 Ma may be close to the real age of an impact. The age however should be inspected in some way or other, since the variations of the results are so small.

References

Bogard, Husain, and Wright, (1976) Jour. Geophys. Res., Bogard and Hirsch, (1980) Geochim. Cosmochim. Acta, Heymann, (1967) Icarus, Minster and Allegre, (1979) Nature, Nakamura and Okano, (1985) Nature, Nakamura, Fujiwara and Nhoda, (1990) Nature, Takigami and Kaneoka (1985), Mem. Natl. Inst. Polar Res., Spec. Issue, Sato, Takeda, Yanai and Kojima (1982), Mem. Natl. Inst. Polar Res., Spec. Issue, Yanai and Iguchi (1981) Catalog of Meteorites.
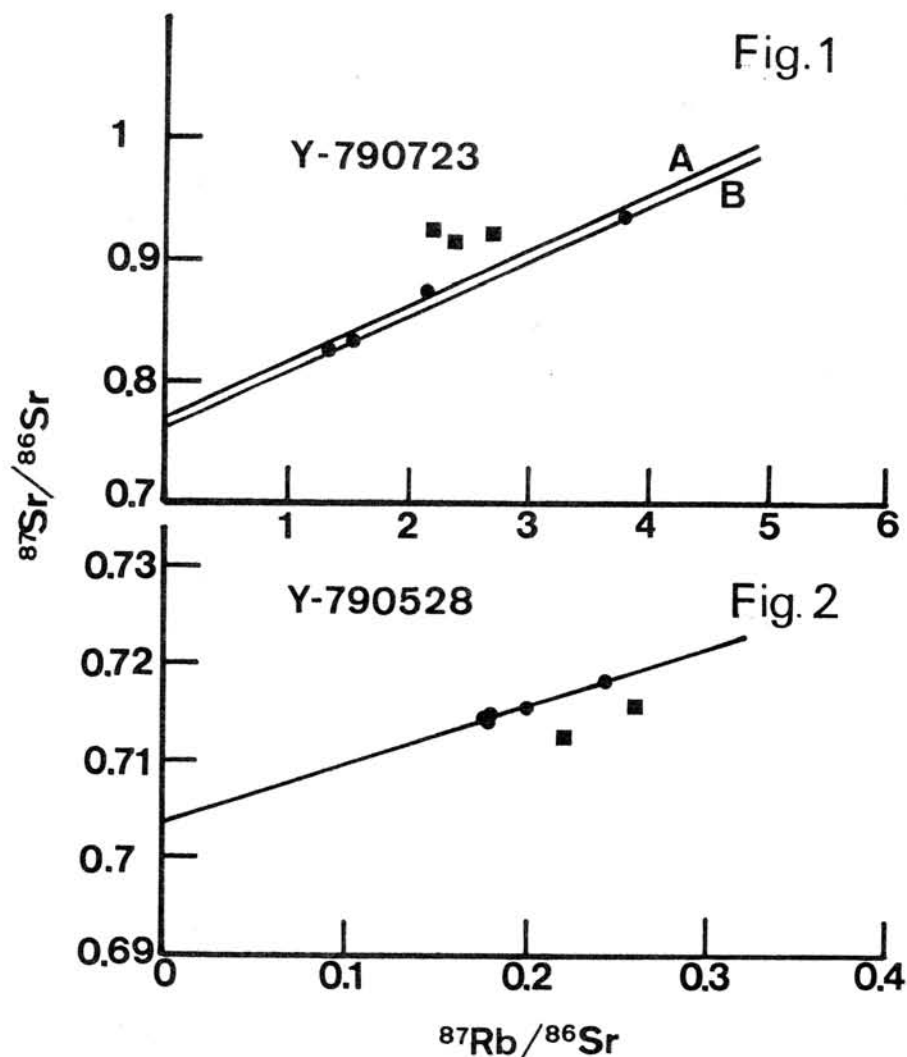
Rb-Sr isotopic systematics and trace element features of the impact-melted L-chondrite, Chico

Toshiki FUJIWARA[1] & Noboru NAKAMURA[1],[2]

1) Depertment of Material Differentiation, Graduate School of Science and Technology, Kobe University, Nada, Kobe 657.

2) Depertment of Earth Science, Faculty of Science, Kobe University, Nada, Kobe 657.

Impact processes recorded in the brecciated meteorites are imporant in understanding the evolutionary history of meteorite parent bodies. Age determination and trace element analysis for shocked meteorites may provides us with the information on the duration and chemical nature of impact processes on meteorite parent bodies. Many K-Ar ages accumlated so far indicate that impact events occured continuously throughout the history of meteorite parent bodies. Except for a few cases[1], however, the meaning of younger ages have not been well-examined so far by much less susceptible radio-nuclides such as $^{87}$Rb-$^{87}$Sr or $^{147}$Sm-$^{144}$Nd.

The Point of Rocks and Chico meteorites, consist of relatively clast free impact-melt regions and heavily shocked chondritic regions, thought to be possibly paired, are suitable samples for investigation of the impact-processes[2,3]. In order to determine the impact age and to clarify some chemical behavior, we have undertaken analyses of Rb-Sr isotopes and trace elements were carried out.

Recently we obtained an age of 460 Ma, well-defined by a Rb-Sr internal isochron for Point of Rocks[4]. This young age is concordant with the K-Ar age data with a peak of 500 Ma for the L-chondrites, suggesting

that the age represents an intense impact event leading to melting on the L-chondrite parent body.

For Chico we obtained so far four Rb-Sr data sets and one set of lithophile trace elements for whole-rock fragments. The absolute and relative abundances of REE in one Chico fragment are typical of L-group chondrite, but alkali metals are somewhat enriched. Compared with well-defined Rb-Sr isochron of Point of Rocks, data points of four whole-rocks from Chico show relatively large scatter in a Rb-Sr diagram, suggesting a perturbation of Rb-Sr system. Three of four data points deviate from the 460 Ma isochron, but an weighted-mean data point of all whole-rock samples of Chico is deviates from the 4,500 Ma line to right side but almost plotted on the 460 Ma isochron. Therefore, the Rb-Sr system of Chico is consistent with the 460 Ma impact event. In order to obtain further information, additional analyses of whole-rock and separeted specimens from the almost completely melted portion of Chico are now in progress.

[1] Okano,O., Nakamura,N. and Nagao,K., Geochim.Cosmochim.Acta 54,3509-3523(1990).
[2] Scott,E.D.R., Maggiore,P., Taylor,G.J., Keil,K., & Szuwalski,D. Lunar planet.Sci.XVII,785-786(1986).
[3] Bogard,D.D., Garisson,D.H., Scott,E.D.R., Keil,K., Taylor,G.J., Vogt,S., Herzog,G.F., &Klein,J., Lunar planet.Sci.XXI,103-104(1990).
[4] Nakamura,N., Fujiwara,T., & Nohda,S., Nature 345,51-52(1990).

# REE ABUNDANCES AND COSMOCHRONOLOGY OF UREILITES

Kazuya TAKAHASHI and Akimasa MASUDA*
The Institute of Physical and Chemical Research,
Wako-shi, Saitama 351-01, Japan.
*The University of Tokyo, Tokyo 113, Japan.

Ureilite is one group of achondritic meteorites, characterized by chemically ultramafic composition, oxygen isotope anomalies (Clayton and Mayeda, 1988), and the existence of carbonaceous material between silicate grains. According to the mineralogical study by Takeda. (1987), ureilites have been roughly classified into 3 groups, calcic, ordinary and magnesian groups and planetesimal collision model has been proposed for the genesis of ureilites. We have performed the Rb-Sr and Sm-Nd datings and measurements of REE abundances on MET-78008, one of the most Ca-rich ureilites. This meteorite consists mainly of olivine and augite. Each mineral was separated by fractional dissolution, heavy liquid separation and hand-picking separation method.

REE patterns of MET-78008 are shown in Fig.1 with the patterns of separated samples and the pattern of ALH-77257 (Shimizu and Masuda, 1981). ALH-77257 belongs to the ordinary group and olivine is dominant in mineral composition. As shown in Fig. 1, the REE patterns of ALH-77257 and MET-78008 are quite different from each other and this difference is considered to reflect the difference in mineral and chemical compositions between these two meteorites.

The results of Rb-Sr and Sm-Nd dating on MET-78008 are shown in Figs. 2 and 3 respectively. In these isochron plots, following three characteristics can be seen.
(1) The ages obtained from Rb-Sr and Sm-Nd isochron are around 4.0 Gyr.
(2) The point of whole rock sample falls on the 4.5 b.y. isochron formed by other meteorites such as
Juvinas eucrite on both of isochron plots.
(3) The $\varepsilon_{Nd}$ (T=4.0 Gyr.) is +4.9 (±0.6). This deviation was calculated from the initial ratio of Sm-Nd isochron plot and the Nd isotopic evolution curve for carbonaceous chondrite such as Allende and Murchison (Jacobsen and Wasserburg, 1980).

The ages obtained by two isochrons, around 4.0 Gyr., can be regarded as the age of last igneous event, shock metamorphism or the accretion of source material. The second characteristic mentioned above suggests that the source material of MET-78008 underwent some differentiation 4.5-4.6 Gyr. ago and the source material of MET-78008 was not mixed with the material producing other type of ureilites at the event, having produced MET-78008 4.0 Gyr. ago. Furthermore, the third characteristics indicates that the source material of MET-78008 would have been already fractionated in REE abundances 4.0 Gyr. ago and the Sm-Nd isotopic data also suggest that the difference of REE patterns between MET-78008 and ALH-77257 shown in Fig 1. had been caused at the stage of differentiation 4.5-4.6 b.y. ago. It has been generally believed that ureilites would have been produced from C-chondrite like materials. From these observation, however, it is considered that MET-78008 could not have been directly formed from C-chondrite like materials and the source material of MET-78008 had been already fractionated in major element composition and REE abundances prior to 4.0 Gyr. ago, compared with carbonaceous chondrites. These results and the oxygen isotope anomalies reported by Clayton and Mayeda (1988) speak against the genesis of ureilites by single planetesimal collision and indicate plural and complicated processes. It is also possible that the parent body of ureilites would have been heterogeneous or there would have existed plural parent bodies for ureilites. We are going to analyze the different type of ureilite. Y-791538 (Mg-rich), to compare with the MET-78008.

References:
Clayton, R. N. and Mayeda, T. K. (1988) Geochim. Cosmochim. Acta, 52, 1313-1318.
Jacobsen, S. B. and Wasserburg, G. J. (1980) Earth and Planetary Sci. Lett., 50, 139-155.
Takeda, H. (1987) Earth Planet. Sci. Lett., 81, 358-370.
Shimizu, H. and Masuda, A. (1981) Mem. Natl. Inst. Polar Res., Spec. Issue, 20, 211-220.
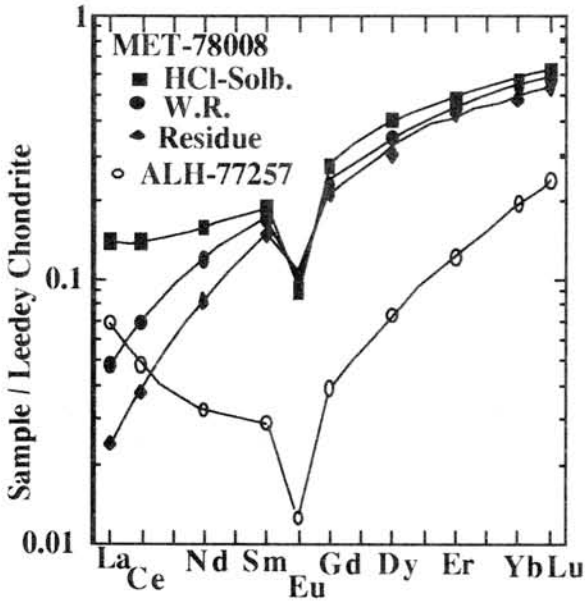
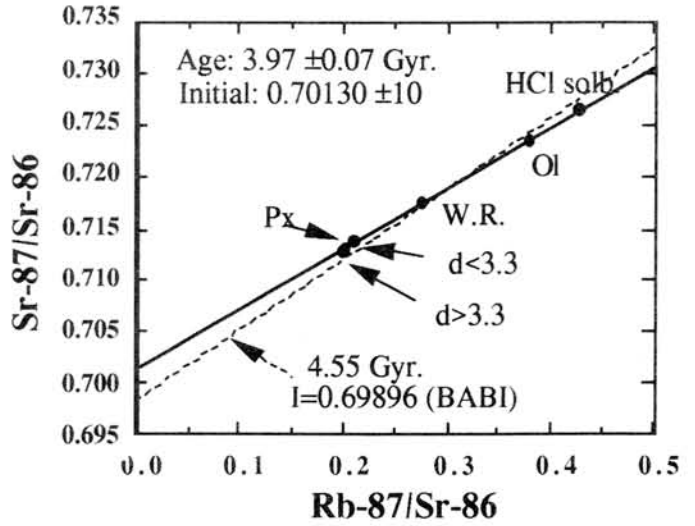Fig. 1 The REE abundance patterns for the samples from ureilites
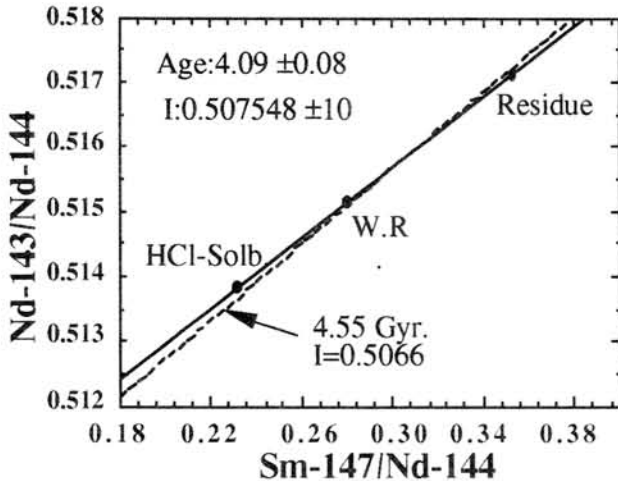


Fig. 2 The Rb-Sr isochron plot of MET-78008



Fig. 3 The Sm-Nd isochron plot of MET-78008

## REE abundances in chondrules from the Murchison (CM) chondrite

Mutsuo Inoue   and   Noboru Nakamura
Department of Earth Science, Faculty of Science, Kobe
university, Nada, Kobe 657, Japan.

Many REE patterns for chondrules from the carbonaceous chondrites have been reported until today. For examples, large REE fractionations and Ce,Eu and Yb anomalies were observed in Allende (CV) and Felix (CO) chondrules, suggesting that these REE fractionations had been established during the high temperture processes in the primitive solar nebla (1,2). Since the REE patterns of CM chondrules have not been obtained, we have undertaken precise analyses of REE in chondrules from the Murchison (CM) chondrite by Isotope Dilution Mass Spectrometry (IDMS). Here we report preliminary results of the trace element analysis for Murchison chondrules which give rise to new REE patterns never reported for chondrules from other groups of chondrites.

The analytical procedures were similar to those previously described (1,3). The 17 chondrules or chondrule-fragments (?) were obtained by hand-picking through freeze-thaw processing. Individual chondrules were broken into two parts; One half was for a thin section preparation and the other half was for REE analysis. The constituent minerals and their chemical compositions were examined by SEM-EDS and EPMA using the thin sections. The 4 samples (total weight of 0.457~2.806 mg) were analyzed so far for trace elements.

The results are shown in Fig.1. Except for Eu, the REE patterns of Murchison chondrules are generally smoothly fractionated from light to heavy REE; MC-2,-5 and -7 indicate light REE depleted patterns but MC-9 shows light REE enriched pattern. The three chondrules (MC-5,-7 and -9) have large negative Eu anomalies. Anomalous REE fractionations and Ce,Yb irregularities, as found in Allende (1,2), are not observed here. It is also pointed out that any UOC chondrule so far reported never shows such REE fractionations. These remarkable REE fractionations observed for Murchison chondrules rather resemble those of basalts from the Moon. The pattern of MC-9 is similar to those of lunar highland basalts while MC-5 and-7 are similar to mare basalts for their REE patterns. The fine structure of REE patterns of both types of planetary materials are, however, substantially different from each other. In any case, we think that these REE fractionations did not reflect the gas/solid (or liquid) distributions process of REE in nebla, like other chondrules, but may have reflected solid/liquid processes. For example, it is supposed that MC-9 represents a residual melt formed after the removal of orthopyroxene and plagioclase from the chondritic melt with initially flat REE pattern through the process of fractional crystallization. And it is also possible that MC-2,-5 and -7 formed from a chondritic material by two stages of fractionation processes; fractional crystallization and partial melting.

Reference
(1) Misawa,K. and Nakamura,N. (1988a):Geochim.Cosmochim.Acta, 52,1699-1710.
(2) Misawa,K. and Nakamura,N. (1988b):Nature,334,47-50.
(3) Nakamura,N. and Yamamoto,K. Noda,S. Nishikawa,Y. Komi,H. Nakagawa,T. and Misawa,K. (1989):Anal.chem,61,755-762.
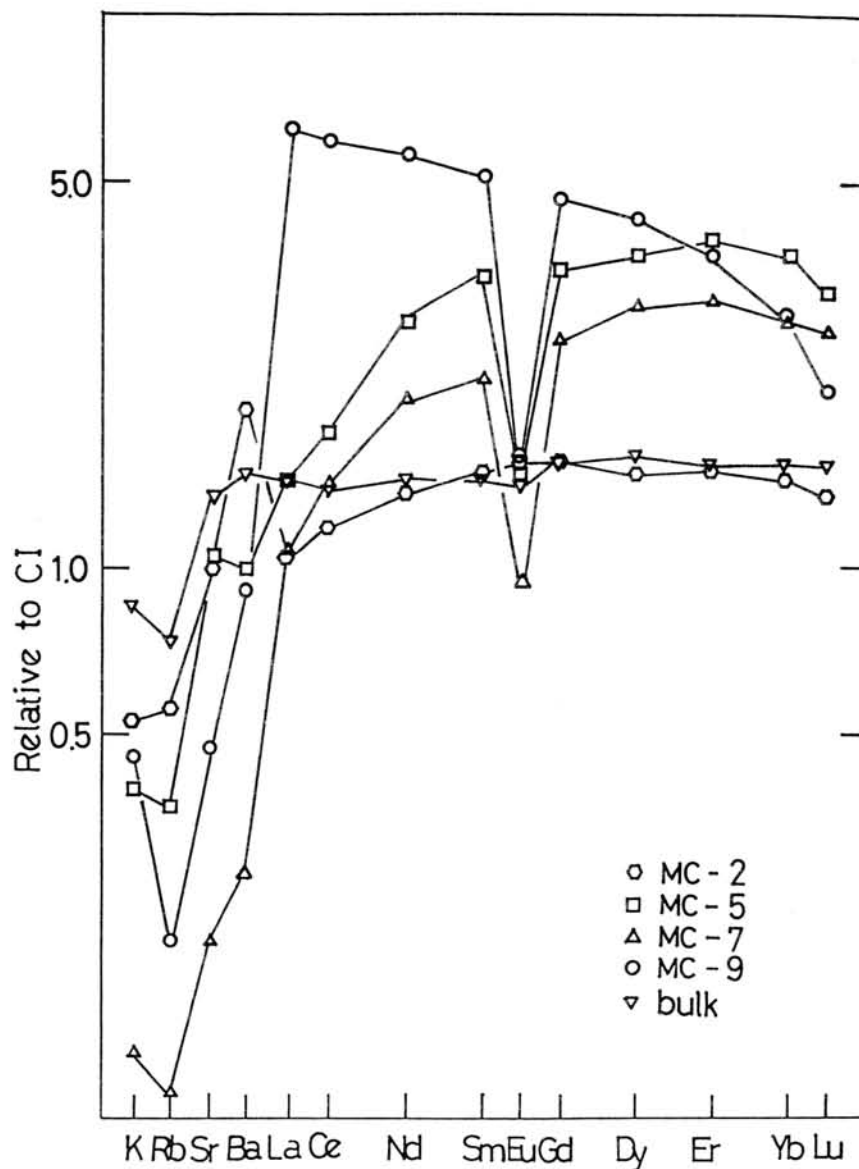


Fig.1.  CI-chondrite normalized  REE patterns of four chondrules and a whole rock sample  from Murchison (CM).

ISOTOPIC ANALYSES OF SIZE-SEPARATED SIC FROM THE MURCHISON METEORITE

Sachiko Amari[1,2], Ernst Zinner[1], and Roy S. Lewis[2]
1 McDonnell Center for the Space Sciences and Physics Department, Washington University, One Brookings Drive, St. Louis, MO 63130-4899, USA.
2 Enrico Fermi Institute, University of Chicago, 5640 S. Ellis Ave., Chicago, IL 60637-1433, USA

Silicon carbide has recently been discovered and isolated from primitive meteorites[1]. It not only carries isotopically anomalous noble gases[1,2] but has anomalies in other elements such as C, N, Si, Mg and Ba[3-7]. Lewis et al.[8] have shown that the Kr isotopic ratios vary systematically with grain size in different fractions from the Murchison meteorite. Gallino et al.[9] have interpreted these variations within the framework of an AGB star origin of SiC as the result of different temperature and/or neutron exposures in the He-burning shell of such stars.

We measured C, N, Si, and Mg isotopic ratios in five size-separated SiC fractions from $0.05-0.8\mu m$ in which Lewis et al.[8] had measured noble gases. Since grain sizes are too small to allow single grain analysis, measurements were made on aggregates (bulk measurements).

The results shown in the Table and the Figures are mass weighted averages of about 10 runs for each fraction. They show two important features. First, the averages for the different size fractions vary only little from one to another. $\delta^{13}C$ values range from 1100 to 1400‰ (12/13=37-42). $\delta^{15}N$ values show larger variations from -480 to -260‰ (14/15=370-520). Silicon is isotopically heavy with $\delta^{29}Si=20-30$‰ and $\delta^{30}Si=30-40$‰. For the isotopic ratios of C, N and Si, we do not observe the systematic trend shown by the Kr-isotopic ratios. However, it should be emphasized that we do not know whether all grains carry noble gas anomalies or not, that is, the C-, N-, and Si-isotopic ratios of grains with Kr isotopic anomalies may not be the same as those for the bulk of the SiC.

Second, as shown in Fig.1, the variations among individual measurement of a given grain size fraction increase with grain size. This suggests that isotopic ratios significantly vary from grain to grain.

For comparison, we show single grain measurements of grain size separate KJG and two calculated means, one for all measured

grains, another without a very anomalous grain. These averages fall in the same range as those of the bulk measurements, while the single grain data show a large scatter. (Fig.2)

The $^{26}Al/^{27}Al$ ratio correlates with the $^{28}Si^+/^{27}Al^+$ ratio (Fig. 3). This can be explained by mixing of Si-rich, high $^{26}Al/^{27}Al$ grains and Al-rich grains with low $^{26}Al/^{27}Al$. The former would be SiC. The latter would be $Al_2O_3$, which is observed in coarser size fractions of SiC bearing separates. However, we cannot exclude the possibility that some of them are contaminants.

References
1. Tang M. and Anders E. Geochim. Cosmoshim. Acta **52**, 1235-1244 (1988).
2. Ott U., Begemann F., Yang J., and Epstein S. Nature **332**, 700-702 (1988).
3. Zinner E., Tang M., and Anders E. Nature **330**, 730-732 (1987).
4. Zinner E., Tang M., and Anders E. Geochim. Cosmochim. Acta **53**, 3273-3290.
5. Zinner E., Amari S. Anders E., and Lewis R.S. Nature **349**, 51-54 (1991).
6. Zinner E., Amari S., and Lewis R. S. Lunar Planet Sci. **22**, 1553-1554. (1991).
7. Ott U. and Begemann F. Astrophys. J. **353**, L57-L60 (1990).
8. Lewis R.S., Amari S., and Anders E., Nature **348**, 293-298 (1990).
9. Gallino R., Busso M., Picchio G., and Raiteri C.M., Natlure **348**, 298-302 (1990).

Table Isotopic ratios of size separated SiC fractions

| Sample | Size | δ13C | δ15N | δ29Si | δ30Si | 26Al/27Al |
|--------|------|------|------|-------|-------|-----------|
| | μm | ‰ | ‰ | ‰ | ‰ | x10-3 |
| KJA | 0.05-0.1 | 1126 | -264 | 21.7 | 34.5 | 4.1 |
| | | ±14 | ±8 | ±1.2 | ±2.2 | ±0.2 |
| KJB | 0.1-0.2 | 1404 | -474 | 24.7 | 37.6 | 2.4 |
| | | ±31 | ±57 | ±0.7 | ±1.5 | ±0.2 |
| KJC | 0.2-0.3 | 1400 | -475 | 29.3 | 29.3 | 2.8 |
| | | ±60 | ±18 | ±1.3 | ±2.7 | ±0.2 |
| KJD | 0.3-0.5 | 1303 | -302 | 27.7 | 35.0 | 3.5 |
| | | ±62 | ±64 | ±1.8 | ±3.7 | ±0.4 |
| KJE | 0.5-0.8 | 1271 | -479 | 31.5 | 42.0 | 1.4 |
| | | ±48 | ±48 | ±2.8 | ±3.4 | ±0.3 |
| KJG 1 | 1.5-3.0 | 1473 | -367 | 41.2 | 35.6 | 4.1 |
| | | ±290 | ±196 | ±8.2 | ±9.7 | ±3.0 |
| KJG 2 | | 1523 | -665 | 50.7 | 49.6 | 1.0 |
| | | ±289 | ±30 | ±5.7 | ±4.0 | ±0.3 |

KJG 1 Average for all measured grains
KJG 2 Average without a very anomalous grain
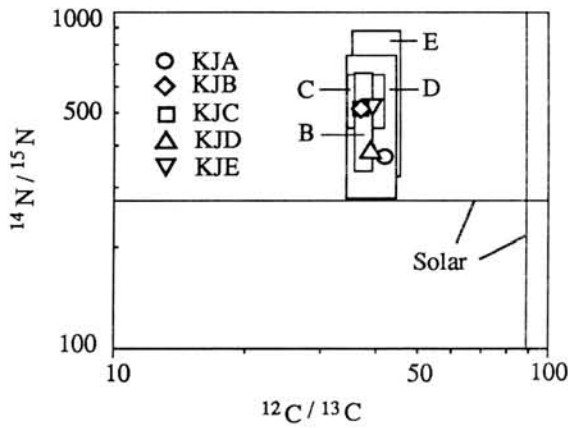


Fig. 1
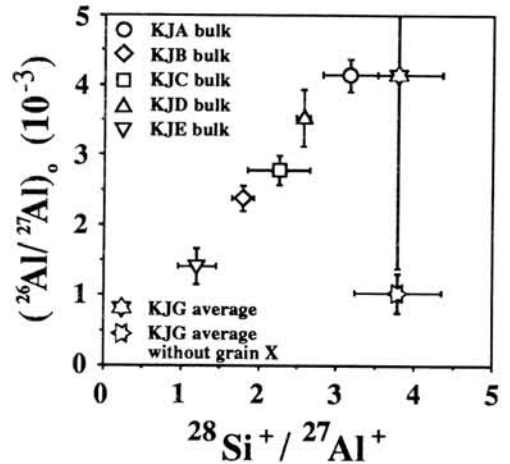


Fig. 3
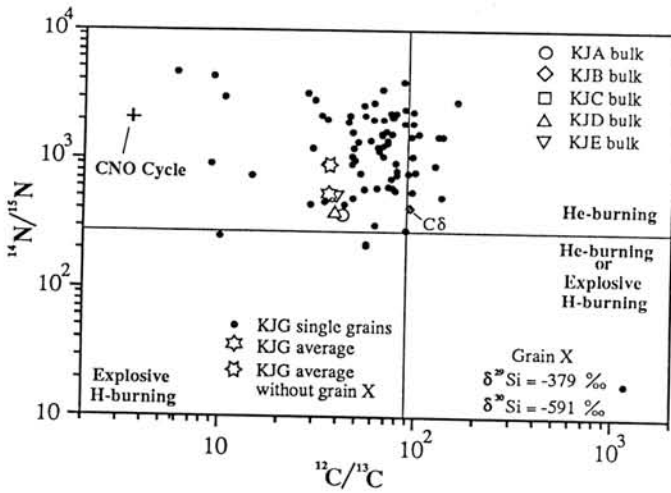


Fig. 2

ELEMENTAL AND ISOTOPIC ANALYSIS OF Y791694 IRON METEORITE BY GLOW
DISCHAREGE MASS SPECTROMETER

Tadashi Shimamura, Takako Takahashi·,Masatake Honda··and Hisao Nagai·· School
of Hygienic Sciences Kitasato University, 1-15-1 Kitasato Sagamihara Kanagawa
228, ·Analytical Research Laboratory, Marubun Corporation, 3-3-4 Minamisuna
Kotoku Tokyo 136,  ··Department of Chemistry, College of Humanities and
Sciences, Nihon University, Sakurajosui 3, Setagayaku, Tokyo, 156, JAPAN

Introduction   Y791694 iron meteorite is quite unique in composition
e.g. high Ni(342 mg/g), Cu(1943 $\mu$g/g) and Sb(4 $\mu$g/g) and low Cr(8 $\mu$g/g) [1]
[2].  We performed wide range of elemental analysis (42 elements) and isotopic
analysis for Pb using Glow Discharge Mass Spectrometer (GDMS).  GDMS is
capable to analyse all the elements on the periodic table excluding noble gas
and hydrogen with good sensitivity down to sub ng/g for the most of elements.
Though iron meteorite is suitable sample for GDMS analysis only a few reports
are available [3][4].

Experimental  (1) Sample  The sample was sawed to be $2\times2\times15$ mm$^3$ pin
shape, etched by $HNO_3$:HCl:$H_2O$ = 1:3:4 for 1 min. and rinsed with $H_2O$ and
acetone.  Because glow discharge can remove surface contamination, no further
cleaning was made.  (2) Instrument  GDMS (VG9000) was used for either
elemental or isotopic analysis.  Sample was inserted into glow discharge cell
which was maintained pressure of 1 mb by high purity Ar flow.  Sample itself
was cathode and cell body was anode.  Applied voltage of glow discharge and
discharge current was 1 kV and 3 mA respectively.  Main components (Fe, Co, Ni
) were detected by Faraday cup and minor and trace components were detected by
Daly detector equipped with ion counting assembly.  With those dual collector
system dynamic range of detector is reached to $10^{11}$.  Major advantages of GDMS
are 1) direct elemental and isotopic analysis of solid conductive samples, 2)
whole coverage of elements on periodic table, 3) uniform sensitivity among
various elements, typically within an order of magnitude.

Results and Discussions   (1) Elemental analysis   Mass resolution of
instrument was set to 5000.  After detection of ions of each element, peak
area integration and isotopic abundance correction,total ion beam intensity of
each element was ratioed to tatal ion beam of major components (Fe+Co+Ni)
(Ion Beam Ratio IBR).  Total ion intensity was $2\times10^{-9}$ A.  To convert IBR to
actual concentration (g/g) we need Relative Sensitivity Factor (RSF).  We
define RSF = IBR/concentration(g/g).  To obtain RSFs we analysed NIST steel
standards SRM 662,663 and 665.  In some cases we obtained RSFs from neutron
activation analysis [4].   In Table1 our results are summerized together with
Canyon Diablo and Odessa results as referenses and RSFs.  We repeated analysis
three times and showed average of these.  Na, Mg, Al, Si, Cl, K, Rb, Sr, Y, Zr
and Br data are omitted because poor reproducibilities and possible surface
contaminations.  In case of Ca, Ti. Mn, Nb, Mo and Cd there were severe
isobaric or poly atomic interferences which were not able to resolve with
resolution of 5000.   Most of the rare earth elements which are not listed
in Table1 are below detection limits (generally less than 0.1 ng/g).  For Li,
Be, N, F, Tb, Hg, Tl, Th and U RSFs are not available, so only IBRs are
presented.  However except N, F and Hg we believe IBRs are reasonably close to
real concentration within factor 3. Judgeing from reproducibilities of IBR and
uncertainties of RSFs we estimated accuracy of the data to be 30 %.  Several

points are evident from Table1, 1) High Ni concentration, 2) Extremely high Cu, In, Sn, Sb, Te, Pb and Bi. In Fig1 we plotted concentration ratios of several calcophile elements to Canyon Diablo. 3) Though calcophile elements seems to be quite anomalous, siderophile elements Ga, Ge and Ir concentration show normal IAB trend. This is also true for Cu even though its extremely high concentration [5][6], 4) Cr concentration is much lower than the data from Wasson et al.[1], We do not find out the reason of this discrepancy yet, but we point out that in INAA low level Cr determination is suffered from severe interference from Ir [7], 5) Pb is paticularly interesting. Comparing Pb concentration of 860 ng/g to that of S 1280 ng/g, we conclude Pb does not reside in FeS phase but most likely in metal phase.

(2) Isotopic Analysis. Knowing high concentrationof Pb, we decided to analyse isotopic composition of Pb. We expected primordial composition of Pb (or even less radiogenic because in metal phase Th and U concentration can be two orders of magnitude less than FeS phase)[8]. Unfortunately GDMS is not suitable for precise isotopic analysis and $^{204}Pb$ concentration will be order of 10 ng/g, isotopic analysis would be quite difficult and cannot obtain sufficient precision. However it is very useful to have preliminary results for further investigations. First, analysis was done with resolution of 5000 to check possible interferences, then resolution was set to 1300 to have enough flat top width. $^{202}Hg$ was monitored for $^{204}Hg$ correction. No significant interferences were observed on masses 206, 207 and 208 and small correction on 204 were made (from 2 % to 0.3 %) from $^{204}Hg$ which seemed to be surface contaminations. Beam variation was monitored by $^{56}Fe$ peak and linear correction was made. Results are shown in Table2. We also analysed NIST steel standard SRM465, which contains about same amount of Pb (400 ng/g),as a reference of "common"Pb. The SRM465 data do not show any significant detector bias. We performed analyses twice. The first run is average of 7 sets of ratios and the second run is average of 22 ratios. Though precisions are still poor, isotopic composition of Pb in Y791694 is indeed very close to primordial [8]. We have not measured isotope standard of Pb yet, consequently we cannot make mass discremination correction, thus no further discussion can be made. But it is certainly worth while to pursue isotopic analysis of Pb in metal phase using thermal ionization mass spectrometry.

Conclusion   1) Y791694 contains very high level of calcophile elements.   2) Ni, Cu, Ga, Ge and Ir concentrations are consistent with IAB classification.   3) Pb may reside in metal phase.   4) GDMS isotopic analysis suggests that Pb in Y791694 has primordial composition.

References   [1] Wasson J.T., Ouyang X., Wang J. and Jerde E. GCA 53 735-744 (1989). [2] Nagata T, Masuda A. Taguchi I and Ono Y., Mem.NIPR Spec. Issue 41 287-296 (1986). [3] Shimamura T., Nagai H. and Honda M. LPS XVII 795-796 (1986). [4] Honda M., Nagai H. Shimamura T. Proceeding of The Institute of Natural Science, Nihon University 26 113-126 (1991) in Japanese. [5] Kracker A., Willis J. and Wasson J.T. GCA 44 773-787 (1980). [6] Malvin D.J., Wang D. and Wasson J.T. GCA 48 785-804 (1984). [7] Willis J. and Wasson J.T., Radiochim. Acta 29 45-51 (1981). [8] Tatsumoto M., Knight R.J. and Allegre C.J. Science 180 1279 (1973)

Table1  Elemental Concentration of Y791694 (Canyon Diablo, Odessa as ref.)

| Element | IBR | Conc. (g/g) | Honda[*] (g/g) | Wasson[**] (g/g) | C.D. (g/g) | Odessa (g/g) | RSF |
|---|---|---|---|---|---|---|---|
| Li | <5.0E-11 | - | - | - | <1.0E-10 | - | - |
| Be | <6.0E-11 | - | - | - | - | - | - |
| B | 2.2E-9 | 2.3E-9 | - | - | 6.0E-10 | - | 0.94 |
| C | 5.0E-5 | 3.2E-4 | - | - | 9.8E-5 | - | 0.16 |
| N | 7.7E-8 | - | - | - | - | - | - |
| O | 4.3E-7 | 3.3E-5 | - | - | 9.2E-5 | - | 0.013 |
| F | 1.4E-8 | - | - | - | - | - | - |
| P | 2.3E-4 | 9.0E-4 | - | - | 1.5E-3 | 3.0E-3 | 0.25 |
| S | 5.3E-7 | 1.3E-6 | - | - | 1.1E-6 | 2.4E-5 | 0.41 |
| Sc | 3.8E-10 | 1.9E-10 | 8.8E-11 | - | 3.0E-10 | 5.0E-10 | 2.0[‡] |
| V | 3.2E-9 | 1.4E-9 | - | - | 1.8E-9 | 6.3E-9 | 2.3 |
| Cr | 2.5E-7 | 4.4E-7 | - | 8.0E-6 | 5.6E-6 | 8.2E-6 | 0.57 |
| Fe | 7.1E-1 | 6.1E-1 | - | 6.5E-1 | 8.9E-1 | 9.2E-1 | 1.0 |
| Co | 5.9E-3 | 5.1E-3 | - | 5.7E-3 | 5.0E-3 | 5.0E-3 | 1.0 |
| Ni | 2.8E-1 | 3.8E-1 | - | 3.4E-1 | 1.1E-1 | 7.9E-2 | 0.63 |
| Cu | 2.8E-4 | 1.6E-3 | 1.4E-3 | 1.9E-3 | 1.8E-4 | 1.1E-4 | 0.17 |
| Zn | 6.1E-6 | 3.8E-5 | - | - | 2.5E-5 | 4.4E-5 | 0.16 |
| Ga | 6.0E-6 | 2.0E-5 | 1.3E-5 | 1.3E-5 | 2.0E-4 | 6.1E-5 | 0.30[‡] |
| Ge | 1.3E-5 | 3.2E-5 | 3.7E-5 | 3.7E-5 | 3.8E-4 | 2.3E-4 | 0.40[‡] |
| As | 1.9E-6 | 9.5E-6 | 2.5E-5 | 3.4E-5 | 4.5E-6 | 8.5E-6 | 0.20 |
| Se | 2.5E-7 | 7.2E-7 | - | - | - | 6.7E-7 | 0.35 |
| Ag | 5.8E-8 | 2.5E-7 | - | - | - | - | 0.23 |
| Ru | 9.6E-7 | 5.3E-7 | - | - | - | 5.0E-6 | 1.8[‡] |
| Rh | 2.0E-7 | 5.0E-7 | 2.1E-7 | - | 3.5E-6 | 2.3E-6 | 0.40[‡] |
| Pd | 4.1E-6 | 1.4E-5 | 1.4E-5 | - | 3.7E-6 | 4.0E-6 | 0.30[‡] |
| In | 2.3E-7 | 1.3E-7 | 1.3E-7 | - | 1.6E-8 | 5.5E-9 | 2.0[‡] |
| Sn | 5.0E-5 | 9.0E-5 | 9.0E-5 | - | 7.9E-6 | 3.6E-6 | 0.56 |
| Sb | 3.6E-7 | 2.4E-6 | - | 4.0E-6 | 2.2E-7 | 3.0E-7 | 0.15 |
| Te | 1.4E-7 | 5.6E-7 | - | - | 6.8E-8 | 6.2E-8 | 0.25 |
| La | <2.0E-10 | <8.0E-11 | - | - | <4.0E-11 | <2.0E-11 | 2.5 |
| Tb | <6.0E-11 | - | - | - | - | - | - |
| W | 8.6E-8 | 1.2E-7 | - | - | 6.3E-7 | 3.4E-7 | 0.70 |
| Re | 2.6E-8 | 4.3E-8 | 5.0E-8 | - | 3.3E-7 | 2.7E-7 | 0.60[‡] |
| Os | 8.9E-8 | 2.2E-7 | 2.0E-7 | - | 2.2E-6 | 2.5E-6 | 0.40[‡] |
| Ir | 1.1E-7 | 2.0E-7 | 3.7E-7 | 2.4E-7 | 2.4E-6 | 2.3E-6 | 0.55[‡] |
| Pt | 1.9E-7 | 5.2E-7 | - | - | 6.4E-6 | 5.0E-6 | 0.36[‡] |
| Au | 5.8E-7 | 1.6E-6 | 1.7E-6 | - | - | - | 0.50 |
| Hg | <3.0E-11 | - | - | - | - | - | - |
| Tl | <8.0E-11 | - | - | - | - | - | - |
| Pb | 3.7E-7 | 8.6E-7 | - | - | 1.8E-8 | 2.3E-8 | 0.43 |
| Bi | 7.1E-9 | 2.8E-8 | - | - | <1.0E-10 | - | 0.25 |
| Th | <4.0E-11 | - | - | - | - | - | - |
| U | <4.0E-11 | - | - | - | - | - | - |

[*] ref.(4)  [**] ref.(1)  [‡] obtained by NAA

Table2 Isotopic Analysis of Pb in Y791694

| | $^{206}Pb/^{204}Pb$ | $^{207}Pb/^{204}Pb$ | $^{208}Pb/^{204}Pb$ | |
|---|---|---|---|---|
| Run1 | 9.20 ± 0.39 | 10.23 ± 0.40 | 29.95 ± 1.0 | $(1\sigma)$ |
| | 0.32 | 0.36 | 0.82 | $(2\sigma_m)$ |
| Run2 | 9.39 ± 0.29 | 10.32 ± 0.27 | 29.82 ± 0.92 | $(1\sigma)$ |
| | 0.14 | 0.14 | 0.40 | $(2\sigma_m)$ |
| SRM 465 | 18.34 ± 0.54 | 15.57 ± 0.41 | 38.57 ± 0.93 | $(1\sigma)$ |
| | 0.54 | 0.41 | 0.93 | $(2\sigma_m)$ |
| Tatsumoto· | 9.304±0.003 | 10.294±0.003 | 29.479±0.009 | |

· ref.[8] Canyon Diablo FeS

Fig.1    Relative Concentrations To Canyon Diablo
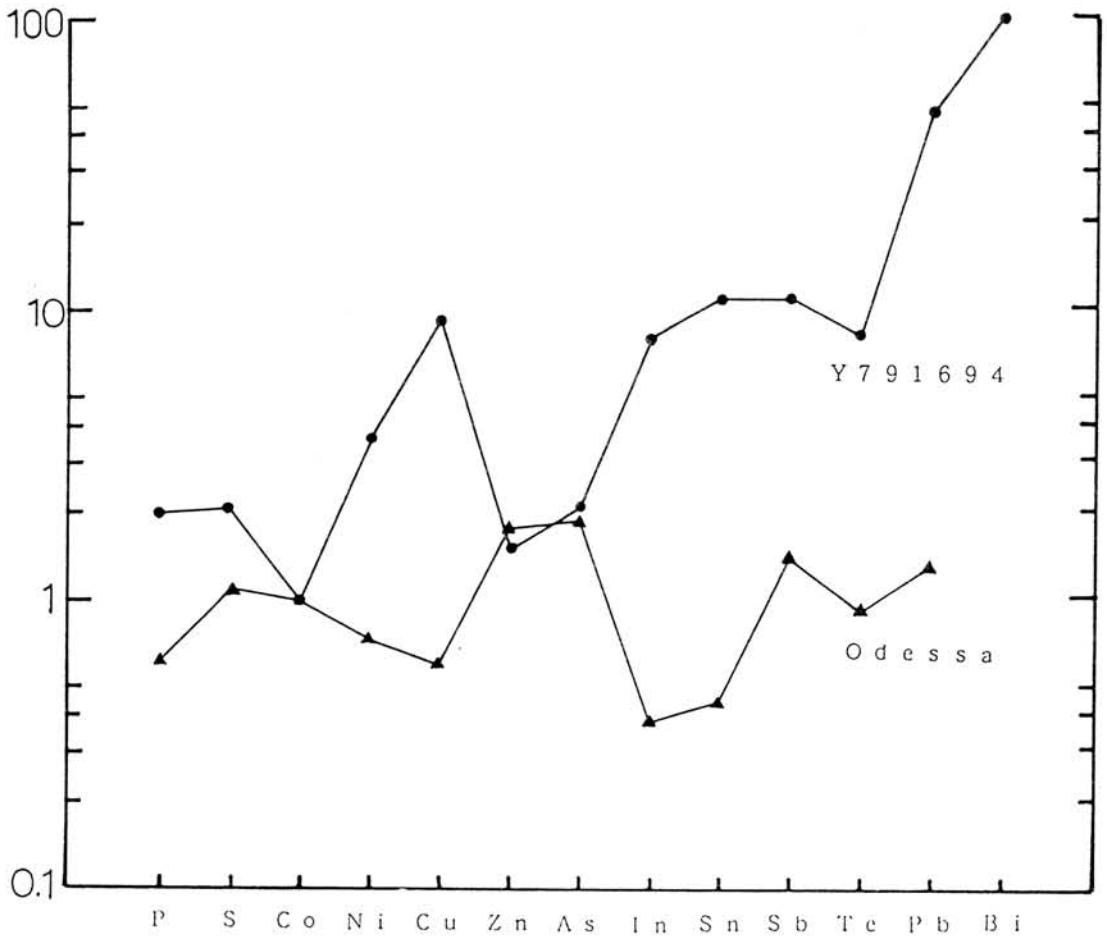
On the possibility of new subclassification of UOC's

Ebihara, M., Ozaki, H. and Hirano, K.

Department of Chemistry, Faculty of Science, Tokyo Metropolitan UNiversity,
1-1 Minami-Ohsawa, Hachioji, Tokyo 192-03

Ordinary chondrites of petrologic type 3, so-called unequilibrated ordinary chondrites (UOC's), are subclassified in two different ways: TL sensitivity (Sears et al., 1980) and volatile element content (Anders and Zadnik, 1985). Classification based on TL sensitivity reflects the difference in metamorphism in the parent body, whereas volatile element contents could be affected by metamorphism and/or nebular fractionation. In this context, no attention has been paid to the fact that these two classifications are not always correlated. Anders and Zadnik (1985) proposed a notation combining two subclassification numbers like 3.0/2, which indicates a subtype of 3.1 according to TL and 3.2 according to volatile contents.

Studying the rare earth element (REE) distribution in ordinary chondrites, Ebihara (1989) pointed out that REEs are distributed in UOC's in a different manner from those in equilibrated ordinary chondrites (EOC's). In EOC's, most REEs, especially light REEs, are in Ca-phosphates, the remaining being in acid-residual phases, which consist of pyroxene and plagioclase for the most part. A REE abundance pattern of acid residues shows a steep inclination and a prominent positive anomaly of Eu, which is attributable to the preferential migration of Eu in plagioclase. On the other hand, in UOC's, REEs were found to be allotted in acid residues to greater extent. Their abundance pattern shows a rather flat inclination, with a smaller positive anomaly of Eu (even a negative anomaly for some cases). REEs must have been largely redistributed between UOC's and EOC's, and even among UOC's. Thermal metamorphism could be a cause to make such a difference in REE distribution in acid residues.

Table 1 shows some values characterizing REE abundances in acid residues. Subclassification numbers also are listed in accordance with an Anders-Zadnik's proposal. It is notable that the degree of inclination represented by $(La/Lu)_{C1}$ and the degree of Eu anomaly represented by $Eu/Eu^*$ ($E^*$ denotes an interpolated value using contents of neighboring elements) are closely correlated with subclassification numbers according to volatile element contents. Rather poor correlation can be confirmed between these REE indexes and subclassification numbers based on TL. Although a very limited number of data are available, we come to the following speculative conclusions:
  (1) REE abundances in acid residues can yield some criteria to subclassify UOC's.
  (2) Such a subclassification must be based on metamorphism.
  (3) Subclassification based on volatile element contents seems to reflect metamorphism rather than nebular fractionation.
  (4) There is a possibility that TL sensitivity is not strictly correlated with the degree of metamorphism.

REFERENCES: Anders E. and Zadnik M.G. (1985) Geochim. Cosmochim. Acta 49, 1281. Ebihara M. (1989): Proc. NIPR Symp. Antarct. Meteorites 2, 279. Sears D.W., Grossman J.N., Melcher C.L., Ross L.M. and Mills A.A. (1980): Nature 287, 791.

Table 1  Some REE indexes for Antarctic UOC's.

| meteorites | classification[*] | $(La)_{C1}$ | $(Lu)_{C1}$ | $(La/Lu)_{C1}$ | $Eu$[**] | $Eu/Eu$[**] |
|---|---|---|---|---|---|---|
| ALH-77011[***] | L3.5/0 | 2.16 | 2.20 | 0.98 | 2.26 | 0.72 |
| ALH-78038[***] | L3.4/0 | 1.56 | 1.88 | 0.83 | 1.69 | 0.86 |
| Y-74191 | L3.6 | 1.85 | 2.69 | 0.69 | 2.23 | 1.04 |
| ALH-77299 | H3.7/4 | 1.31 | 1.63 | 0.80 | 1.35 | 1.43 |
| ALH-78084 | H3.9 | 1.10 | 1.88 | 0.59 | 1.36 | 1.67 |
| ALH-77278 | LL3.6/9 | 1.19 | 1.80 | 0.66 | 1.38 | 2.00 |
| ALH-77252[****] | L3(L4/L6) | 0.46 | 1.31 | 0.35 | 0.72 | 3.33 |

* after Anders and Zadnik (1985).
** interpolated values.
*** paired.
*****possibly EOC clast.

# Special Session

*Carbonaceous Chondrite Belgica-7904*

*Unique Meteorites*

*Lunar Meteorites*

MINERALOGICAL AND PETROLOGICAL STUDY OF ANOMALOUS BELGICA-7904 CARBONACEOUS CHONDRITE.    Makoto KIMURA and Yukio IKEDA.  Department of Earth Sciences, Ibaraki University, Mito 310.

As a part of the consortium study on antarctic anomalous carbonaceous chondrites, we have carried out the mineralogical and petrological study of the Belgica-7904 (B-7904). The B-7904 consists of many kinds of chondrules, clasts, mineral fragments, and matrix (Table 1).

Chondrules, 70-1100 microns in size, are abundant, and all the chondrules in our thin section show porphyritic textures.  Chondrules are divided into two types, forsterite-bearing (magnesian type) and ferroan olivine -bearing (ferroan type).  Magnesian type is predominant, and ferroan type is about one-third of magnesian type in abundance.  Chondrules of both types consist mainly of olivine phenocrysts and phyllosilicate groundmass, but the accessory minerals are different from each other (Table 2).  Magnesian type chondrules often have Ca-poor and Ca-rich pyroxenes, and unusual inclusions.  The inclusions, brown in color and spherical to ellipsoidal in shape, abundantly contain very fine-grained chromite, schreibersite, and troilite, in addition to phyllosilicate.  This is the first discovery of schreibersite in CM chondrites.  Anhedral chromites in magnesian type typically occur in the brown inclusions, and are almost free in $Al_2O_3$ and $TiO_2$ contents.  Kamacites abundantly occur in forsterite phenocrysts in magnesian type chondrules, rarely associating schreibersite.  Large magnesian type chondrules always show a core-mantle structure; the cores have phyllosilicates rich in $Al_2O_3$ up to 21.2 wt.%, whereas the mantle phyllosilicates are poor in $Al_2O_3$ (<6.5%).  Glassy inclusions ($Al_2O_3$ 19.6-30.1%, CaO 12.8-20.2%, $Na_2O$ 0.1-6.0%) are often encountered within forsterite phenocrysts in magnesian type.  Olivines in magnesian type have higher MnO/FeO ratios than that of CI chondrite.  Large magnesian type chondrules always have fine-grained dusty rims consisting of opaque minerals and phyllosilicates.  Ferroan type chondrules never include pyroxene.  Instead, Ca-phosphate (mostly whitlockite) occurs only in ferroan type.  Olivines in ferroan type have a MnO/FeO ratio similar to that of CI chondrites.  Unusual brown inclusions never occur in ferroan type.  Chromites in ferroan type chondrules always show euhedral forms in phyllosilicate groundmass, and contain variable amounts of $Al_2O_3$ (4.8-22.2%) and $TiO_2$ (0.7-2.3%).  Large ferroan type chondrules often have troilite-taenite rims, instead of the dust rim.  Low-$Al_2O_3$ phyllosilicates ($Al_2O_3$<6.5%) in both magnesian and ferroan type chondrules have intermediate composition between sodian talc and serpentine-chlorite [1].  Groundmasses in both types contain taenite and troilite often with pentlandite.

The B-7904 has many kinds of clasts, 30-200 microns in size.  They are classified into nine types based on their characteristic phases (Table 1).  A matrix-like clast consists of fine-grained phyllosilicates with minor amount of olivine and opaque mineral fragments. Phyllosilicate clasts are brown in color, and consist mostly of phyllosilicates.  A sulfide-rich phyllosilicate clast is black in color because of abundant very fine-grained Fe-sulfides.  A fayalite - opaque mineral clast is an aggregate of fayalite and fine-grained taenite and troilite.  A unique fayalite - phosphate - kamacite clast consists of fayalite with abundant fine-grained chlorapatite and kamacite.  Another unique schreibersite - Mn-rich forsterite clasts contain schreibersite, MnO-rich forsterite (MnO 1.2-2.7%), and MnO-rich chromite (MnO 9.0%), in addition to fine-grained phyllosilicates.  A spinel clast is an aggregate of nearly pure Mg-Al-spinel, which was also found by Tomeoka [2].  Kamacite clasts consist mainly of kamacite with variable amounts of troilite, magnetite and phyllosilicate.  Sulfide clasts consist of troilite, pentlandite and taenite, often associating Co-rich and Ni-poor kamacite (Co 11.5-16.3%, Ni 1.7-3.2%).  Co-kamacite is also found in sulfide rim around a ferroan type chondrule.  Such Co-rich kamacites were also reported

from LL3 chondrite [3].

Many kinds of mineral fragments are set in the B-7904 matrix. A unique feature of the matrix is very low-abundance of carbonate. We found only a few Ca-carbonate fragments in matrix. Tomeoka [2] also found a few carbonate vein. Instead, very fine-grained Ca-phosphates occur abundantly in the matrix, some clasts, and ferroan type chondrules, as also noticed by Matsunami *et al.* [4]. Phyllosilicates in the matrix are richer in CaO (2.1% in average) than those (0.2% in average) in chondrules, but the high CaO contents of the matrix phyllosilicates seem to be caused by the contamination of very fine-grained Ca-carbonate during analyses. Since glasses in some large magnesian type chondrules contain CaO as mentioned before, primary groundmasses in chondrules had contained CaO, and the CaO lost from chondrules formed Ca-phosphate as well as Ca-carbonate in the matrix.

Magnesian type chondrules have forsterite, schreibersite and kamacite, whereas ferroan type has ferroan olivine and Ca-phosphate. It is evident that magnesian type primarily formed under much more reducing condition than ferroan type. Kamacite clasts probably formed under a reducing condition in which the $fO_2$ was lower than that of a Fe-FeO buffer, whereas Co-kamacite-bearing sulfide clasts may have formed from Fe-Ni metals under a high $fS_2$ condition. Thus, the constituents of B-7904 probably originated in various reservoirs with contrasting $fO_2$ and $fS_2$ in the solar nebula. On the other hand, taenites occur in groundmasses of both magnesian and ferroan type chondrules. The $O_2$ partial pressure, under which phyllosilicate and taenite formed during aqueous alteration, was probably lower than a Ni-NiO buffer and higher than a Fe-FeO buffer [5]. However, the presence of kamacite clast is inconsistent with the range of $fO_2$ during aqueous alteration. The existence of schreibersites in some chondrules and clasts and phosphate in the others also excludes the possibility that all these chondrules and clasts suffered aqueous alteration under the same condition in the parent body after regolith gardening process. Alternatively, chondrules and clasts might have suffered hydrous alteration in the nebula [5].

References: [1] Ikeda Y., Mayeda T.K., Clayton R.N. and Prinz M. (1991) Abstract 16th Sym. Antarctic Meteorites (this volume). [2] Tomeoka K. (1990) Proc. NIPR Symp. Antarct. Meteorites, 3, 40-54. [3] Afiattalab F. and Wasson J.T. (1980) Geochim. Cosmochim. Acta, 44, 431-446. [4] Matsunami S., Nishimura H. and Takeshi H. (1989) Abstract 14th Sym. Antarctic Meteorites, 21. [5] Ikeda Y. and Nakamura N. (1991) Episode (in press).

Table 1. The constituents of the B-7904.

| Chondrule | Magnesian |
| --- | --- |
| | Ferroan |
| Silicate & oxide clast | Matrix-like clast |
| | Phyllosilicate clast |
| | Sulfide-rich phyllosilicate clast |
| | Fayalite - opaque mineral clast |
| | Fayalite - phosphate - kamacite clast |
| | Schreibersite - Mn-rich forsterite clast |
| | Spinel clast |
| Opaque mineral clast | Kamacite clast |
| | Sulfide clast |
| Mineral fragment | Silicate, Oxide, Phosphate, Carbonate, Metal, Sulfide |
| Matrix | |

Table 2. Mineral assemblages of the constituents of the B-7904.

| | Chondrule | | Silicate & oxide clast | | | | | | | | Opaque mineral clast | | Mineral fragment | Matrix |
|---|---|---|---|---|---|---|---|---|---|---|---|---|---|---|
| | Magnesian | Ferroan | Matrix-like | Phyllosilicate | Sulfide-rich phyllosilicate | Fayalite -opaque mineral | Fayalite -phosphate -kamacite | Fayalite -Mn-rich forsterite | Schreibersite | Spinel | Kamacite | Sulfide | | |
| Olivine | + | + | + | + | + | + | + | + | + | | | | + | |
| Ca-poor pyroxene | + | | | | | | | | | | | | | |
| Ca-rich pyroxene | + | | | | | | | | | | | | | |
| Phyllosilicate | + | + | + | + | + | + | + | + | + | + | + | | | + |
| Glass | + | | | | | | | | | | | | | |
| Phosphate | + | + | + | + | | + | + | | | | | | + | |
| Magnetite | + | | | | | | | | | | + | | | |
| Spinel | | | | | | | | | | + | | | | |
| Chromite | + | + | | + | | | | + | + | | | | + | |
| Ca-carbonate | | | | | | | | | | | | | + | |
| Kamacite | + | | + | + | | | + | | | | + | | | |
| Co-kamacite | | + | | | | | | | | | | + | | |
| Taenite | + | + | + | + | | + | | | + | + | | + | + | |
| Schreibersite | + | | | | | | | + | + | | | | | |
| Troilite | + | + | + | + | + | + | + | + | + | + | + | + | + | |
| Pentlandite | + | + | | | | | | | | | | + | + | |

PETROGRAPHY AND OXYGEN ISOTOPIC COMPOSITIONS OF CHONDRULES, CLASTS, AND MATRIX SEPARATED FROM BELGICA-7904 AND YAMATO-86720 CARBONACEOUS CHONDRITES. Y. Ikeda, Department of Earth Sciences, Ibaraki Univ., T. Mayeda, R. N. Clayton, Enrico Fermi Institute, Chicago Univ., and M. Prinz, Mineral Sciences, American Museum of Natural History.

Two partially-altered chondrules, two phyllosilicate clasts, two olivine fragments, and matrix were separated from B-7904, and two phyllosilicate clasts from Y-86720. The half of each separate was used for the measurement of oxygen isotopic compositions, and the rest for the study of petrography and mineralogy.

(1) Two chondrules (C1 and C3) from B-7904: One is a porphyritic olivine chondrule (C1) with a diameter of about 2 mm, showing a core-mantle structure. The core is an unaltered portion of the chondrule and consists mainly of forsterite ($Fo_{99}Fa_{0.5}La_{0.5}$), enstatite ($En_{82-96}Fs_1Wo_{3-17}$), diopside ($En_{60-71}Fs_1Wo_{28-39}$), anorthite ($An_{87-98}Ab_{2-13}$), and Fe-Ni metals. However, some kamacite grains in the core are altered to high-Al ferroan phyllosilicates by reactions with the surrounding anorthite and pyroxenes. The mantle is an altered portion of the chondrule, ranging from 50 to 250 microns in width. It consists mainly of dehydrated magnesian phyllosilicates and relic minerals. The $Al_2O_3$ contents of the mantle phyllosilicates range from 3 wt% up to 25 wt%, and are grouped into two types, high-Al magnesian ($Al_2O_3>6.5wt\%$) and low-Al magnesian ($Al_2O_3<6.5wt\%$). The former type is mainly replacing anorthite and pyroxenes, and the latter type mainly replacing pyroxenes. Relic olivines in the phyllosilicate mantle are similar in shape and size to those in the core and seem not to have reacted to produce the mantle phyllosilicates. The other chondrule (C3), about 2 mm across, also shows a core-mantle structure similar to chondrule C1. The core consists mainly of anorthite ($An_{91-99}Ab_{1-9}$), forsterite ($Fo_{99}Fa_{0.5}La_{0.5}$), enstatite ($En_{93-80}Fs_1Wo_{6-19}$), diopside ($En_{54-59}Fa_1Wo_{40-45}$), mesostasis, and minor Fe-Ni metals. Anorthite is predominant. The mantle consists mainly of dehydrated phyllosilicates, relic olivine and minor taenite. The mantle phyllosilicates are similar in chemical composition to those in chondrule C1.

(2) Two phyllosilicate clasts (D2 and D5) from B-7904: Clast D2, about 2 mm across, is a massive aggregate of dehydrated phyllosilicates. The phyllosilicates are homogeneous in chemical composition and a low-Al magnesian type. The other clast (D5) with a largest dimension of about 3 mm is similar in texture and mineralogy to clast D-2. The low-Al magnesian phyllosilicates in both clasts seem to be produced by complete reactions with forsteritic olivine in addition to pyroxene and plagioclase.

(3) Two olivine fragments (B1 and B2) from B-7904: Both are large pale yellow fragments of single olivine crystals, about 0.8-1 mm across. As all samples of both fragments were consumed during the measurement of oxygen isotopic composition, the mineralogy is

not known. However, they seem to be fragments of large olivine-bearing chondrules, and the oxygen isotopic compositions may represent those of unaltered chondrules.

(4) Two phyllosilicate clasts (H1 and I1) from Y-86720: Both clasts, 0.5mm x 1mm in size, are aggregates of dehydrated phyllosilicates and minor ilmenite. Clast H1 is fine-grained, but the other (I1) consists mainly of coarse-grained dehydrated phyllosilicates, up to 100 microns in width. Chemical compositions of the phyllosilicates in both clasts are heterogeneous and very similar to those in the mantle phyllosilicates of chondrules C1 and C3 from B-7904, although relic olivines are not found in clasts H1 and I1.

(5) Oxygen isotopic compositions of separates: Oxygen isotopic compositions of the components separated from B-7904 and Y-86720 are shown in Table 1 and Figure 1. Olivine fragments B1 and B2 are plotted along the chondrule mixing lines, and this is consistent with the speculation that these are unaltered broken chondrules. Two chondrules C1 and C3 and two phyllosilicate clasts D2 and D5 are plotted along the CM mixing line. Taking into consideration that volume percents of the phyllosilicate mantles are about 30-50% for chondrules C1 and C3, the oxygen isotopic compositions of the mantle phyllosilicates may be near those of clasts D2 and D5. This indicates that the phyllosilicates in chondrules and clasts from B-7904 are decidedly different in oxygen isotopic composition from the matrix phyllosilicates in B-7904. This discrepancy can be explained either by the following two ways. According to the two-stage exchange model (Clayton and Mayeda, 1984), the intermediate oxygen isotopic compositions of the phyllosilicates in chondrules and clasts may be explained by incomplete exchange in oxygen isotopes between the phyllosilicates and an aqueous solution with a water-rock ratio in their parent body. However, the phyllosilicates in clasts D2 and D5 seem to have been produced by complete reactions of anhydrous silicates including olivines. Alternative hypothsis is that the phyllosilicates in chondrules and clasts were produced by hydrous reactions of chondrules with a nebular gas prior to the accretion, whereas the oxygen isotopic compositions of the B-7904 matrix phyllosilicates had been changed by aqueous solutions in their parent body after the accretion. On the other hand, two phyllosilicate clasts H1 and I1 from Y-86720 are plotted near the oxygen isotopic composition of the Y-86720 whole rock, suggesting that the phyllosilicates in clasts are similar in oxygen isotopic composition to the matrix phyllosilicates for the case of Y-86720. There is no discrepancy in oxygen isotopic composition between them in spite of the heterogeneous chemical compositions of the phyllosilicates in Y-86720 clasts.

References:Clayton,R.N., Onuma,N., Ikeda,Y., Mayeda,T.,and Hutcheon, I.D. (1983), Chondrules and Their Origins, ed.by King,E.A., 37-52. Clayton,R.N. and Mayeda,T. (1984), E.P.S.L., 67, 151-161. Mayeda,T., Clayton,R.N., and Ikeda,Y. (1991), Lunar Planet. Sci., XXII (Abst).

Table 1. Oxygen Isotopic Compositions (in permil) of Components of B-7904 and Y-86720.

| Sample | Description | delta$^{18}$O | delta$^{17}$O |
|--------|-------------|---------------|---------------|
| B-7904 | | | |
| B1 | Olivine Fragment | 4.69 | 1.22 |
| B2 | Olivine Fragment | 3.97 | 1.70 |
| C1 | Partially-altered Chondrule | 3.56 | -1.77 |
| C3 | Partially-altered Chondrule | 3.71 | -2.71 |
| D2 | Phyllosilicate Clast | 10.34 | 4.44 |
| D5 | Phyllosilicate Clast | 13.08 | 5.71 |
| B-M | Matrix | 23.27 | 12.08 |
| Y-86720 | | | |
| H1 | Phyllosilicate Clast | 22.50 | 11.53 |
| I1 | Phyllosilicate Clast | 21.56 | 10.83 |

Fig. 1. Oxygen Isotopic Compositions of Components Separated from B-7904 and Y-86720. A chondrule denoted by cc separated from B-7904 (Mayeda et al., 1991) is also shown. For reference, terrestrial mixing line (TERRESTRIAL), chondrules-in-carbonaceous-chondrites mixing line (CHONDRULES) with a branch for barred olivine chondrules in Allende (Clayton et al., 1983), inclusion mixing line (INCLUSIONS), and CM mixing line (CM-mixing) are shown.
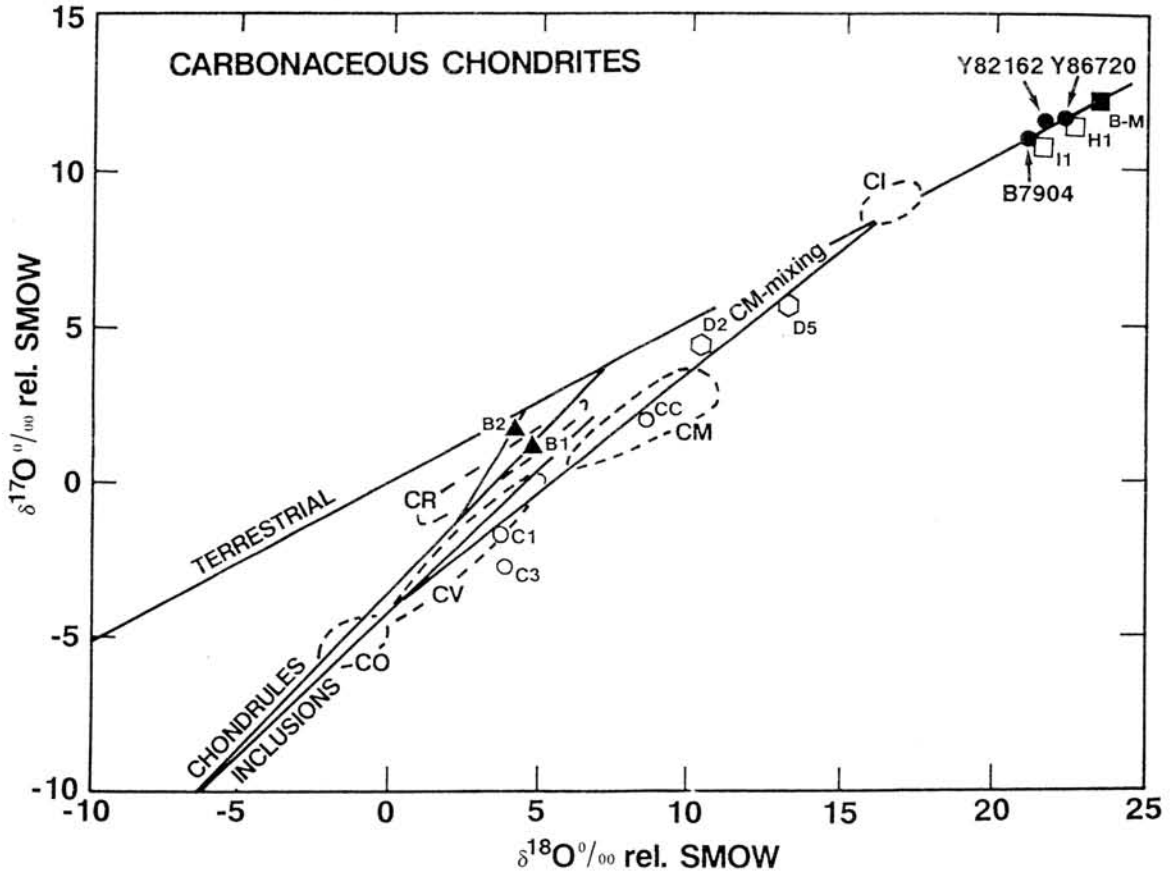
MINERALOGY AND CHEMISTRY OF ANTARCTIC WINONAITES: Y-74025, Y-75300 AND Y-75305.

M. Kimura[1], A. Tsuchiyama[2], T. Fukuoka[3] and Y. Iimura[4]
1) Ibaraki Univ., Mito 310, 2) Osaka Univ., Osaka 560, 3) Gakushuin Univ., Tokyo 171, 4) Inst. Phys. Chem. Research, Wako 351 .

As a part of the consortium study on the Antarctic unique meteorites, three winonaites, Y-74025, Y-75300 and Y-75305 were mineralogically and chemically studied, in comparison with two acapulcoites Y-74063 and ALH 77081.

The winonaites consist of anhedral to subhedral silicate and opaque minerals. The major constituent minerals are typical of equilibrated O-chondrites such as orthopyroxene, olivine, plagioclase, troilite and Fe-Ni metal. However, they do not have any relic of chondrule, and the presence of various accessory minerals characterizes these meteorites, i.e., fluorapatite, K-rich feldspar, magnesiochromite, rutile, daubreelite, schreibersite, and others. All the minerals except for taenite are almost homogeneous in chemical compositions. Y-75300 consists of coarse-grained and fine-grained parts. On the other hand, Y-74063 and ALH77081 contain abundant fine-grained euhedral to subhedral orthopyroxene and olivine. In the silicate portion of the winonaite, orthopyroxene is the most common mineral and olivine is less abundant (Table 1). The abundance of troilite and Fe-Ni metal vary widely. Y-74025 and Y-75300 have higher amount of troilite than metal, whereas metal is much more abundant than troilite in Y-75305. Chromite is more common in the acapulcoites than in the winonaites.

The average compositions of orthopyroxenes in the winonaites are $En_{96.2}$ in Y-75305, $En_{96.0}$ in Y-74025 and $En_{96.5}$ in Y-75300, respectively. On the other hand, orthopyroxenes in the acapulcoites are enriched in FeO, $En_{87.4}$ in Y-74063 and $En_{88.4}$ in ALH77081, respectively. Pyroxenes in the winonaites are lower in MnO, $Cr_2O_3$ and $Na_2O$ than those in the acapulcoites. Anhedral olivine occurs among orthopyroxene. Average Fo contents are 98.0 in Y-74025, 98.2 in Y-75305 and 98.3 in Y-75300, which is much higher than those in the acapulcoite, 88.7 in Y-74063 and 89.4 in ALH77081. Plagioclase occurs among orthopyroxene and often within orthopyroxene and diopside. Average compositions are $Ab_{76.8}Or_{2.2}$ in Y-74025, $Ab_{75.6}Or_{2.0}$ in Y-75305, $Ab_{79.4}Or_{2.5}$ in Y-75300, $Ab_{79.9}Or_{4.4}$ in Y-74063 and $Ab_{80.4}Or_{4.1}$ in ALH77081, respectively. These winonaites always have K-rich feldspar. Only one K-rich feldspar grain occurs within a diopside grain Y-75305 ($Ab_{79.1}Or_{18.7}$) . In Y-74025 a K-rich feldspar grain occurs within a troilite fragment ($Ab_{9.2}Or_{88.9}$). K-rich feldspars in Y-75300 ($Ab_{7.0-71.0}Or_{91.3-25.3}$) occur intimately with plagioclase. Some of them seem to be exsolution lamellae from plagioclase or parallel growth with plagioclase.

Magnesiochromite occurs abundantly within Fe-Ni metal in Y-75305. Only one magnesiochromite grain occurs in Y-74025. Y-75300 also contains small amount of magnesiochromite occurring with olivine or orthopyroxene. A rutile grain shows intimate intergrowth with troilite in Y-75305. It contains 3.8 wt.% $NbO_2$. Rare phosphate occurs in the winonaites. Some of them are fluorapatite. The abundance of phosphate in the acapulcoites is much higher than those in the winonaites. The acapulcoites have whitlockite as well as apatite.

The Cr contents of troilites in the winonaites (0.2-0.6 wt.%) are higher than those in the acapulcoites (0-0.3%). Troilites abundantly include daubreelite, as thin exsolution lamellae. The acapulcoites do not contain daubreelite. Y-75305 has a composite grain containing Cu, Mn and S. SEM observation, chemical analysis and X-ray microdiffraction pattern show that it probably consists of alabandite, a new Mn-bearing Cu-sulfide, and digenite or anilite. The winonaites

always contain schreibersite, whereas only one grain occurs in ALH77081.

The acapulcoites were derived from a common precursor through different degrees of partial melting (Nagahara *et al.*, 1990), which is supported by the observation of fine-grained euhedral silicate minerals. However, the winonaites do not show such a feature for melting. Fukuoka and Kimura (1988) pointed out that the abundance of REE and some trace elements of Y-74025 are basically chondritic, although they found chemical heterogeneity among different samples from Y-74025. The chemical heterogeneity may be explained by primordial heterogeneous distribution of the winonaite minerals, not by melting and fractionation.

Atomic Fe/(Fe+Mg) ratios of olivine, pyroxene and chromite increase in order of E, the winonaite, the acapulcoite and H-chondrites. Magnesiochromite as well as daubreelite occur in the winonaites, whereas in the acapulcoites only chromite occurs. The abundance of schreibersite is much higher in the winonaite than in the acapulcoite, whereas phosphate is common in the acapulcoite. Alabandite occurs only in the winonaites. On the other hand, Fe-Ni metals in the winonaite hardly contain Si, and troilites in the winonaite hardly contain Ti and Mn. Thus, the winonaite is intermediate meteorite grouplet between E-chondrite and the acapulcoite, and the redox condition of the winonaite is intermediate between them.

References: Fukuoka T. and Kimura M. (1988) Abstract 13th Sym. Antarctic Meteorites, 44. Nagahara H. *et al.* (1990) Abstract 15th Sym. Antarctic Meteorites, 92.

Table 1. Modal compositions of winonaites and acapulcoites

| | Y75305 W | Y74025 W | Y75300-c W | Y75300-f W | Y74063 A | ALH77081 A |
|---|---|---|---|---|---|---|
| Enstatite | 45.0 | 45.6 | 41.6 | 60.7 | 46.2 | 43.6 |
| Diopside | 1.2 | 7.2 | 0.0 | + | 6.2 | 3.4 |
| Olivine | 7.8 | 19.9 | 14.4 | 18.7 | 24.3 | 25.3 |
| Plagioclase | 8.3 | 8.3 | 11.2 | 9.3 | 7.2 | 13.4 |
| K-feldspar | + | + | + | + | | |
| Zircon | + | | | | | |
| Troilite | 9.2 | 13.5 | 27.5 | 10.0 | 10.6 | 5.5 |
| Daubreelite | 1.0 | 0.7 | 1.0 | 0.4 | | |
| Pentlandite | + | | | | + | |
| Pyrrhotite | + | | | | | |
| Cu-Mn-sulfide | + | | + | | | |
| Cu-sulfide | + | | | | | |
| FeNi metal | 27.0 | 3.9 | 3.8 | 0.7 | 4.6 | 6.7 |
| Schreibersite | 0.3 | 0.9 | 0.4 | 0.2 | | + |
| Chromite | 0.2 | + | + | | 1.0 | 1.0 |
| Rutile | + | | | | | |
| Fe-Ti oxide | + | | | | | |
| Apatite | + | + | | | + | 0.8 |
| Whitlockite | | | | | + | 0.3 |
| Graphite | | | | | | + |

Y-75300-c: coarse-grained part, -f: fine-grained part
W: winonaite, A: acapulcoite

## LITHOPHILE TRACE ELEMENTS AND SR ISOTOPES IN UNIQUE METEORITES, Y-74063, ALH-78230, Y-74357, Y-8002 AND Y-75300

Koshi Yamamoto[1], Noboru Nakamura[1], Keiji Misawa[2], Hideyasu Kojima[3] and Keizo Yanai[3] [1]Dept. Earth Sci., Kobe University, Nada, Kobe 657; [2]Inst. Cosmic Ray Res., University of Tokyo, Tanashi, Tokyo 188 (Present address; USGS, Br. Isotope Geol., Denver, CO 80225, USA), [3]Natl. Inst. Polar Res., Tokyo 173

As a part of a consortium study on the unique Antarctic meteorites [1], we analysed lithophile trace elements and Sr isotopes for three unique meteorites (Y-75300, Y-8002 and Y-74063) and reported preliminary results at the 15th Antarctic Meteorite Symposium [2]. Here we present additional results including new analyses of two unique meteorites, ALH-78230,56 and Y-74357,72 and compare them with previous results. Four meteorites studied here (Y-74063, ALH-78230, Y-74357 and Y-8002) are classified as Lordran-Acapulco type and one (Y-75300) as Winonite type [1].

Two meteorite samples weighing ~100mg had been transfered from Dr. T. Fukuoka, Gakushuin University, after INAA analyses [3]. The 2/3 of each specimen was broken into coarse grains (~100 mesh) and the 1/2 of aliquates were used for isotope dilution analyses of trace elements including REE and some major elements (Ca, Mg and Fe). Additional Sr isotopic analyses are also in progress.

The Rb-Sr isotopic analyses for Y-74063, Y-8002 and Y-75300 yield the ALL model ages of 4.5 $\pm$0.1, 3.3 $\pm$0.3 and 3.9 $\pm$ 0.2 Ga, respectively. It is possible that the later two meteorites were subjected to isotopic disturbances by younger events. As shown in Fig. 1, it is noted that all meteorites studied here indicate an extreme depletion of Rb relative to Sr as well as other lithophiles, even to K. It is thus suspected if this Rb depletion was caused by the weathering during the burial of meteorites in Antarctic ice sheets. The Rb-Sr isotopic feature mentioned above seem, however, inconsistent with the weathering model. We therefore suggest that the general lithophile trace element features as shown in Fig. 1 were not affected significantly by the Antarctic weathering.

As seen in Fig. 1, all the meteorites studied here indicate fractionated REE patterns with higher heavy-REE and depletion of light and/or middle-REE. The relative Sr abundances are parallel with Eu abundances and Ba is generally consistent with light-REE fractionations. Therefore, these abundance features of lithophile trace elements (REE, alkaline earths and alkali metals) are consistent with an implication that meteorites formed from similar (or same) precursor materials by the related mechanism and physical conditions. The four Lodran-Acapulco type meteorites indicate rather systematic trend with the increasing order of REE fractionation for Y-74063, ALH-78230, Y-74357 and Y-8002, although

Y-8002 indicates somewhat differenes in detailed REE features, particularly for Eu and light REE. The general fractionation trend appears to be similar to the increasing order of melting degrees suggested from the mineral chemistry [1]. The presence of Eu anomaly and light REE depletion indicate that the observed REE fractionations were produced by extraction of plagioclase and orthpyroxene for Y-74357 and extraction of orthopyroxene and addition of plagioclase for Y-8002.

As noted previously [2], Y-75300 (winonite) show V-shaped REE pattern with a large positive Eu anomaly. Qualitatively, this type of REE fractionation has been reported for a chondrule from metamorphosed ordinary chondrite, Bjurbole (L4) [4], and may thus be related to exensive thermal metamorphism.

References:
[1] Nagahara H., Fukuoka T., Kaneoka I., Kimura M. Kojima, Kushiro I., Takeda H., Tsuchiyama A. and Yanai K.(1990) Abst. 15th Symp. Antarct. Meteor. 92-94.
[2] Yamamoto K., Nakamura N., Misawa K, Yanai K and Matsumoto Y. (1990) Abst. 15th Sympos. Antarct. Meteor. 97-98.
[3] Fukuoka, T. & Kimura, M. (1990) Abst. 15th Sympos. Antarct. Meteor. 99-100.
[4] Nakamura N., Yamamoto K., Noda S., Nishikawa Y., Komi. H. Nagamoto H., Nakayama T. and Misawa K. (1989) Analyt. Chem. 61, 755-762.

Fig. 1

Orgueil (CI)-normalized lithophile patterns for unique meteorites (Data partly from ref. [2])
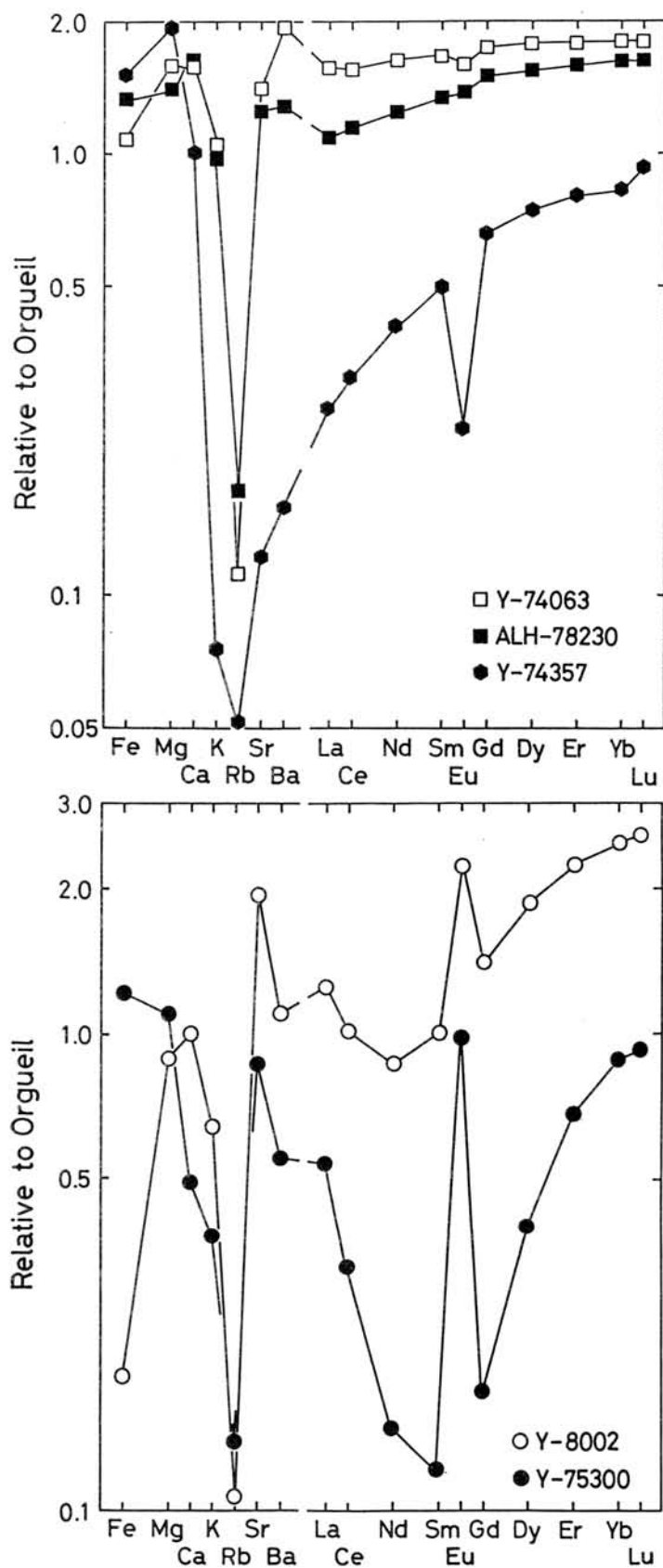
$^{40}$Ar-$^{39}$Ar ANALYSES OF ANTARCTIC METEORITES Y-74063 AND ALH-78230: CONSORTIUM STUDY ON UNIQUE CHONDRITES FROM ANTARCTICA

Kaneoka, I.[*], Takaoka, N.[**] and Yanai, K.[***]

[*]  Earthquake Research Institute, University of Tokyo, Bunkyo-ku, Tokyo 113, Japan.
[**] Department of Earth and Planetary Sciences, Faculty of Science, Kyushu University, Higashi-ku, Fukuoka 812, Japan.
[***]National Institute of Polar Research, Itabashi-ku, Tokyo 173, Japan.

As a part of a consortium study on the Antarctic unique meteorites, $^{40}$Ar-$^{39}$Ar analyses were performed for two unique meteorites Y-74063 and ALH-78230. For these meteorites, the results based on petrological and mineralogical studies(1, 2), trace element analyses(3, 4) and noble gas analyses(5) have been reported.

Both Y-74063 and ALH-78230 have been regarded to be texturally, minerallogicaly and chemically similar to Lodran and/or Acapulco(6). To identify their sources, however, more information is required based on various approaches.

Samples were wrapped in Al-foil and irradiated with neutrons in the JMTR of Tohoku University with the total fast neutron flux of about $1 \times 10^{19}$ nvt/cm$^2$. The hornblende MMhb-I (K-Ar age:519.5$\pm$2.5Ma)(7) was used as the age monitor. Ar gas was extracted and purified at the Isotope Center, University of Tokyo, and analysed on a Nier-type mass spectrometer with a resolving power of about 600 at the Yamagata University. Ten temperature fractions(600°-1600°C) were taken for each sample. Blanks and the effects of Ca- and K-derived interfering isotopes were corrected to calculate an $^{40}$Ar-$^{39}$Ar age.

The results of $^{40}$Ar-$^{39}$Ar analyses have revealed that the meteorites Y-74063 and ALH-78230 seem to have different thermal histories and also reflect different noble gas circumstances at least in the case of Ar isotopes. Although the result of $^{40}$Ar-$^{39}$Ar analyses for Y-74063 does not always show a good plateau age due to the insufficient blank corrections, it indicates an age of around 4500Ma in the intermediate temperature fractions. Furthermore, it contains large amounts of trapped $^{36}$Ar with the amount of about $1 \times 10^{-6}$ cm$^3$STP/g, which agrees well with the previously reported value(5).

On the other hand, the meteorite ALH-78230 contains the $^{36}$Ar with the amount in the order of only $10^{-8}$cm$^3$STP/g and no significant amount of trapped $^{36}$Ar was observed. Further, the $^{40}$Ar-$^{39}$Ar age spectrum indicates that the meteorite might have experienced a degassing event around 400-500Ma, which

has been identified in the lower temperature fractions (700°-800°C), whereas higher temperature fractions show $^{40}Ar$-$^{39}Ar$ ages of 4400-4500Ma.

Thus, present results suggest that the two meteorites Y-74063 and ALH-78230 seem to have experienced different thermal histories and reflect different circumstances of noble gases at least for Ar isotopes.

References

(1) Nagahara, H., Fukuoka, T., Kaneoka, I., Kimura, M., Kojima, H., Kushiro, I., Takeda, H., Tsuchiyama, A. and Yanai, K., Abstr. 15th Antarctic Meteorites Symp., 92-94, Tokyo (1990).
(2) Yanai, K. and Kojima, H., ibid., 95-96, Tokyo (1990).
(3) Yamamoto, K., Nakamura, N., Misawa, K., Yanai, K. and Matsumoto, Y., ibid., 97-98, Tokyo (1990).
(4) Fukuoka, T. and Kimura, M., ibid., 99-100, Tokyo (1990).
(5) Takaoka, N. and Yoshida, Y., ibid., 101-103, Tokyo (1990).
(6) Palme, H., Schultz, L., Spettel, B., Weber, H.W., Wanke, H., Michel-Levy, M.C. and Lorin, J.C., Geochim. Cosmochim. Acta, 45, 727-752 (1981).
(7) Alexander, E.C.,Jr., Mickelson, G.M. and Lanphere, M.A., U.S. Geol. Surv. Open-File Rep., 78-701, 6-9 (1978).

**NOBLE GAS STUDY OF UNIQUE METEORITE YAMATO-74063 BY LASER EXTRACTION.** Nobuo Takaoka [1], Keisuke Nagao [2] and Yayoi Miura [2]. 1) Dept.of Earth & Planetary Sciences, Kyushu Univ. Hakozaki, Fukuoka 812, 2) Inst. Study of the Earth's Interior, Okayama Univ., Misasa, Tottori 682-01.

Unique meteorite Y-74063 contains large amounts of trapped heavy noble gases (Takaoka and Yoshida, 1990). Enrichment of trapped $^{132}$Xe overwhelms E- and C-chondrites and even ureilites with a few exceptions. The origin and trapping sites of planetary noble gases are long-standing problems, although adsorption on C seems to be the most promising for the origin of planetary gases in C-chondrites, and diamond in ureilites is a major host phase. Y-74063 consists of olivine, pyroxene, plagioclase, chromite, Fe-Ni metal and troilite with accessory amounts of graphite and other minerals. But graphite is not a promising candidate for the planetary gas carrier because it is not the major host for the planetary gas in ureilites.

A pulsed Nd-YAG laser is used for gas extraction to investigate the noble gas carrier. A polished chip of the meteorite is mounted in an ultra-high vacuum gas purification line, and a laser beam of several tens $\mu$m in diameter is focused on a mineral grain in the polished surface. The beam energy is 0.4 J/pulse and 10 to 20 pulses are shot to release the gas enough to determine the elemental and isotopic compositions with a VG-5400 mass spectrometer(Nagao and Ogata,1991). Blanks in units of $10^{-12}$ cm$^3$ STP are: 13 for $^4$He, 9.0 for $^{20}$Ne, 2.2 for $^{36}$Ar, 0.085 for $^{84}$Kr and 0.0083 for $^{132}$Xe.

A preliminary result of noble gas analysis by the laser extraction is reported. Eight grains including silicates,troilite and Fe-Ni metal were analysed. All grains contain large amounts of Ar, Kr and Xe, suggesting the planetary gas is not enriched in special minerals, but is present in mineral grains ubiquitously, or the carrier phase disperses amongthe grains. The $^3$He / $^4$He ratio ranges from 0.0022 to 0.018, compared to 0.006 for bulk. Ne data are not available because of low concentration. The $^{38}$Ar/ $^{36}$Ar ratio agrees well with that (0.192) for the bulk sample, whereas the $^{40}$Ar/ $^{36}$Ar ratio ranges between 16 and 150, compared to 36 for bulk. The Xe isotopic ratio is AVCC-like, in agreement with that for bulk. The $^{36}$Ar / $^{132}$Xe and $^{84}$Kr / $^{132}$Xe ratios are very low, as observed in the bulk sample.

Ref. Nagao,K.and Ogata,A.(1991), Abstr. 2nd Japan-China Symp. Geochr. Cosmochr. Isot. Geol.; Takaoka,N.and Yoshida,Y.(1990) Proc.NIPR Symp. Ant. Meteor. **4** (in press)

CRYSTALLIZATION AND BRECCIATION HISTORIES OF LUNAR MARE METEORITES, YAMATO 793274 AND EET87521.

Takeda, Hiroshi, Mori, Hiroshi and Saito, Jun.
Mineralogical Institute, Faculty of Science,
University of Tokyo, Hongo, Tokyo 113.

Within last two years, four lunar meteorites EET87521, Y-793274, Y-793169 and Asuka-31 have been proposed to be derived from a mare region of the Earth's Moon (Yanai and Kojima, 1987a,b; Delaney, 1990; Warren and Kallemeyn, 1989; Yanai, 1991; Takeda et al., 1990a). We studied Y-793274 and EET87521 by mineralogical techniques, as part of two consortium studies (Lindstrom et al., 1991; Takeda et al., 1990a). Their preliminary report has been published (Takeda et al., 1990). Because Y-793274 has been proposed to contain highland materials (Warren and Kallemeyn, 1989), we searched for highland components, but we were unable to find pyroxene components from deep seated magnesian crustal rocks.

Microtextures of glassy matrices of lunar meteorites have been used to identify paired specimen and to deduce ejection histories of the lunar meteorites. However, it has been found no direct evidence of shock textures recoreded at the time of ejection of lunar meteorites, which eventurally brought them to the Earth (Takeda et al., 1990b). We investigated glassy matrices of Y-793274 by a transmission electron microscope (TEM) to deduce its brecciation, lithification and shock histories.

We investigated a polished thin section (PTS) Y-793274,91-2 supplied from NIPR and PTS EET87521,55 from the Antarctic Meteorite Working Group (AMWG). The PTS's were examined by electron probe microanalyzer (EPMA) and scanning electron microscope (SEM), JEOL 840A. Glassy matrices in small chips of Y-793274,98 from NIPR (Takeda et al., 1990a) were studied by analytical TEM, Hitachi H-600 and JEOL 100CX.

Possible highland rocks found in Y-793274 include clast(plagioclase)-laden glassy breccias and similar breccias with finely recrystallized matrix. A large granulite-like (GR1) white clast turned out to be a shock melted breccia with fragments of mare pyroxenes, olivines and plagioclase set in white glassy matrix with high FeO and MgO contents.

One gabbroic clast (GB2) 0.8 X 0.4 mm in size consists of a rounded olivine 0.2 mm across in plagioclase and pyroxene. Their modal abundances (oliv:pyx:plag) are about 1:3:3. The An contents range from 96 to 89. The pyroxene is one of the most Mg-rich ($Ca_{11}Mg_{61}Fe_{28}$) among the Y-793274 pyroxenes (Fig. 1) and its BEI shows fine exsolution lamellae of augite 1.2 μm wide with 2.3 μm interval. The olivine crystal ($Fa_{35}$) still preserves the initial zoning trend of CaO during crystal growth. Therefore, GB2 is not a plutonic rock. Fragments of GB2-like pyroxenes were found in the matrix. The most Mg-rich low-Ca pyroxene with Mg#=100XMg/(Mg+Fe)=80 was found in a small clast with lath-shaped ilmenite with high Mg#(=28) together with olivine (Fig. 1). No lithic clast with apparent plutonic pyroxenes has been recognized in the PTS up to date.

The chemical compositions of all pyroxene fragments present in Y-793274 are considered to be a combination of the zoning trends of quickly cooled lavas, and finely exsolved pyroxenes of different Mg# with limited Mg# range within one crystal. The chemical trends of all pyroxenes with fine exsolution textures have been plotted in Fig. 1. The most dominant Mg-rich trend is the exsolution trend of GB2, whereas the Fe-rich trend is similar to those of EET87521. The results suggest that the chemical variation is not

due to the presence of many pyroxene-types from different crustal rocks as
other lunar meteorites from highland exhibited (Takeda et al., 1990b).
Namely, inverted pigeonite or pyroxenes with coarse exsolution lamellae have
not been found. The presence of magnesian exsolved pyroxenes with limited
Mg# ranges indicates that they are differentiated products of fairly thick
lavas and the basaltic components represent only a differentiated part of
the entire trend.

EET87521,55 contains a large shock disturbed basaltic clast (BS1) and
their comminuted fragments in glassy matrices. Some small lithic clasts are
plagioclase rich but they are also basalts because their pyroxenes are
zoned. The BS1 clast contains strongly zoned Fe-rich pyroxenes similar to
the VLT basalt (Delaney, 1989). There is a mesostasis region in one corner
of the most Fe-Ca-rich end of a pyroxene crystal. It consists of ilmenite
and minor Cr-Ti spinel and the portion facing to the pyroxene is mantled by
fayalite. Between this portion and the pyroxene, there is a dark fine
grained portion with hedenbergite and other phases. A large silica mineral
is attached to this mesostasis.

Many Mg-rich olivines found in Y-793274 are not from pultonic or
crustal rocks as they are similar to olivines in the GB2 clast. EET87521
also contains minor olivines of such compositions. Fe-rich olivines are
similar to those of the VLT basalts and that found in the mesostasis of BS1
in EET87521.

The chemical trends of zoned pyroxenes in EET87521 and Y-793274 may
represent those of pyroxenes such as reported for rare mare-rock clasts
(Ba-2 in 60019) found in Apollo 16 breccias and Luna 16 (Takeda et al.,
1987), and lunar meteorites (Treiman and Drake, 1983). The original rock is
coarse-grained. The Apollo 16 and Y-793274 pyroxene zoning trends cover
more Mg-rich side of the pyroxene quadrilateral than EET87521. The most
Fe-rich trend of EET87521 goes to that of hedenbergite in the HPF clast in
Y-791197 (Takeda et al., 1986). Comparisons of the Fe-rich basalts in
EET87521 and the Mg-rich clast such as GB2 and exsolved pyroxene fragments
of various Mg# in Y-793274 suggest that these breccias represent thick lava
flows of differentiated materials. A clast with magnesian pyroxenes and
ilmenite which is the most magnesian among the lunar ilmenites (Papike et
al., 1976) may be the earliest crystallization product followed by GB2-like
gabbroic rocks. The VLT basalts may be final differentiated products.
These lavas may have been originated close to the lunar highland from where
many lunar meteorites were derived.

The microscopic features of matrices of EET87521 and Y-793274 are
similar. The TEM observation of Y-793274 revealed that it is characterized
by shock-produced melts of plagioclase, olivine and clinopyroxenes, etc.
The presence of shock-produced melts in the TEM scale are characteristics of
Y-793274. They are produced by melting of plagioclase, olivine,
clinopyroxene etc. by impact. An olivine crystal in it includes many
dislocations, which are not recovered. The fact suggests this stone was not
reheated after the impact. An electron photomicrograph of plagioclase in
Y-793274 shows that the crystal includes many glass lamellae produced by
shock. This texture has been observed in some maskelynites. An electron
photomicrograph of the Y-793274 olivine shows that many dislocations are
produced in the crystal. Orthopyroxene also shows stacking faults.

Microtextures in Y-793274 suggest that this sample has never been re-
heated after the shock event. This shock event can be attributed to that of
ejection from the lunar surface, but the shock event at the lunar surface
can also produce such glasses, which will be kept on a cold brecciated lava

surface until the ejection. Many other lunar meteorites from highland did not keep records of a shock event, which ejected the sample to the Earth.

In summary, (1) Main Fe-rich basaltic lavas in EET87521 and Y-793274 are differentiated products. (2) Mg-rich components are not crustal plutonic rocks, but are early crystallized components of thick lava flows. (3) A magnesian ilmenite-bearing rock found in Y-793274 may be the earliest crystallization product. (4) Shock microtextures by TEM show that Y-793274 has never been reheated after the shock event.

## References

Delaney J. S. (1989) Nature 342, 889-890.

Lindstrom M. M., Martinez R. R. and Lipschuts M. E. (1991) Lunar Planet. Sci. XXII, 817-818.

Papike J. J., Hodges F. N., Bence A. E. Cameron M. and Rhodes J. M. (1976) Rev. Geophys. Space Phys. 14, 475-540.

Takeda H., Saito J., Mori H., Yanai K., and Kojima H. (1990a) Abstr. 15th Symp. Antarctic Meteorites 110-112, Natl. Inst. Polar Res., Tokyo.

Takeda H., Miyamoto M., Mori H., Wentworth S. J. and McKay D. S. (1990b) Proc. Lunar Planet. Sci. Conf. 20th, 91-100.

Takeda H., Miyamoto M., Galindo C. and Ishii T. (1987) Proc. Lunar Planet. Sci. Conf. 7th, J.G.R. 92, E462-E470.

Takeda H., Mori H. and Tagai T. (1986) Mem. Natl Inst. Polar Res. Spec. Issue 41, 45-57.

Treiman A. H. and Drake M. J. (1983) Geophys. Res. Lett. 10, 783-786.

Warren P. H. and Kallemeyn G. W. (1989) Geochim. Cosmochim. Acta, 53, 3323-3300.

Yanai K. (1991) Proc. Lunar Planet. Sci. 21, 317-324.

Yanai K. and Kojima H. (1987a) Abstr. 12th Symp. Antarctic Meteorites, 17-18.

Yanai K. and Kojima H. (compiled) (1987b) Photographic Catalog of the Antarctic Meteorites, p. 216, NIPR, Tokyo.
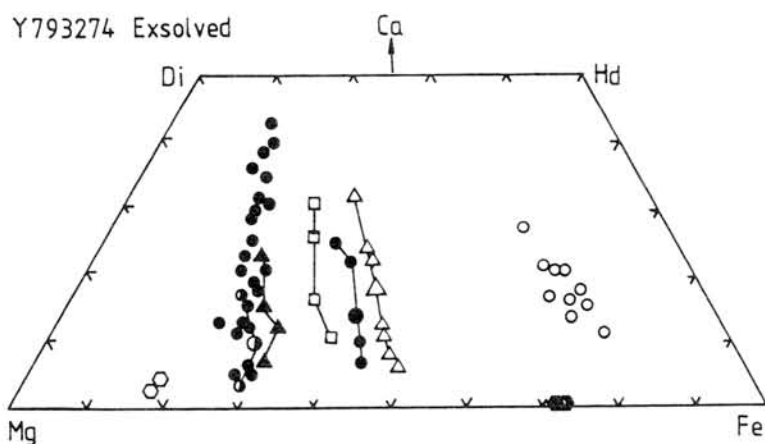
Fig. 1 Pyroxene quadrilateral of exsolved pyroxenes in Y-793274. Solid circles: Exsolution trend of GB2. Open circles: Possible zoning trend. Open hexagon: Ilmenite-opx-oliv. clast. Solid hexagon: Mg# of the coexisting ilmenite.

## LUNAR METEORITES AND LUNAR REGOLITH BRECCIAS: SOME SIMILARITIES AND DIFFERENCES.

David S. McKay, Mission Science and Technology Office/SN14, NASA Johnson Space Center, Houston TX 77058, USA.

**Maturity** As defined for lunar materials, regolith maturity is a measure of the integrated exposure time of surface materials to micrometeorites, solar wind and flares, and the attendant "weathering effects" of this surface exposure. Lunar soil samples show a wide range in maturity as indicated by the abundance of agglutinates and the measured ferromagnetic resonance normalized to FeO content , which is usually called the FMR maturity index ($I_S$/FeO). Measured values of this index for ordinary soils and cores (excluding pyroclastic material) range from 4.6 for soil 12033 to 115 for core soil 79002,49 (1, 2). Mean and standard variation of this index is given for a number of soils and regolith breccias in Table 1.

Lunar regolith breccias from the Apollo collection also show a reasonably wide range of FMR maturity values, from near zero to 112 (3, 4, 5). This range reflects the maturity of the soil from which the regolith breccias were formed. The maximum $I_S$/FeO maturity is close to the maximum for soils. A number of the 11 known lunar meteorites from Antarctica have been classified as regolith breccias (AH81005, Y791197, MAC 88104/5, and Y793274) Other Antarctic lunar breccias (Y82192/3 and Y86032) may be regolith breccias, but also appear to grade into feldspathic breccias similar in texture to those found at Apollo 16. The relationship between feldspathic fragmental breccias and regolith breccias is not entirely clear (5).

FMR maturity data exist on only one of the lunar meteorites, ALHA81005 (7). It has an $I_S$/FeO of only 5 units, which would classify it as immature. Yet, petrographic observations of this meteorite indicate that ALHA81005 is among the more mature of the lunar meteorite suite, and may be the most mature of these samples (8). For example, MAC88104/5, while having some glass (including rare spherules) has no identifiable agglutinates. Y82192 and Y82193 have very low trapped gases indicative of immature soils (9). Both ALHA-81005 and Y-86032 have low implanted nitrogen, again suggesting immature precursor soils, but ALHA-81005 is more mature than Y-86032. (10).

**Porosity** The regolith breccia lunar meteorites appear to be all compact in texture, having low intergranular porosity. Apollo regolith breccias show a wide range in intergranular porosity from 15 to 37% (4, 5). We estimate, based on petrographic observations and published descriptions (e.g. 8) that all of the lunar meteorite regolith breccias have intergranular porosity near the low end of this range; they all appear to be compact to subcompact. However this observation needs to be confirmed by direct comparison of the polished thin sections to the Apollo 16 suite of samples for which the porosity textural scale was defined (5).

For ordinary Apollo regolith breccias, porosity does not show a systematic relationship to maturity. For example, for 26 Apollo 15 regolith breccias, the 15 samples in the compact and subcompact group (low porosity) have a mean FMR maturity index of 23.1 ±17.7 while 11 samples in the porous to subporous group have a mean FMR maturity index of 25.7 ± 13.5. These differences are not considered significant. Similarly for Apollo 16 regolith breccias, the 6 measured compact and subcompact (low porosity) samples have a mean FMR index of 5.5 ± 6.5 and the 13 porous and subporous samples have a mean FMR index of 5.1 ± 13.1, again essentially identical. Furthermore, considering both Apollo 15 and 16 regolith breccias, compact and subcompact samples are about equal in abundance to porous and subporous ones, in contrast to the lunar meteorites, which as noted above, all appear to be compact to subcompact.

**Discussion**  To summarize, the lunar meteorite regolith breccias differ from the average Apollo regolith breccia in having significantly lower maturity and significantly lower intergranular porosity.  If these differences are not the result of the statistics of having only a few lunar meteorites, what is the explanation?  Several possibilities come to mind:

1. The source of the lunar regolith breccias may be generally deeper in the regolith in zones which may grade into the megaregolith material similar to the Apollo 16 feldspathic fragmental breccias (5).  This zone may have not seen much meteorite reworking over the lifetime of its regolith history.  While some of the Apollo regolith breccias are from this zone as indicated by their low maturity, even these regolith breccias have a range of porosities; they are by no means all compact low porosity varieties.

2. None of the lunar meteorites are made from compaction of ordinary surface soils having moderate to high maturity.  It may be that  regolith breccias made from the compaction of near-surface soils, and represented by the higher FMR index values (generally more than 10), common in the Apollo collection, are not represented at all in the lunar meteorite collection.

3. The low porosities are caused by the impacts which launched the meteorites.  If the compact textures were not typical of the source region (some of the low maturity Apollo 16 regolith breccias and the feldspathic fragmental breccis are porous), the relatively low porosity (highly compact texture) of lunar meteorites may result primarily from the energetic event which excavated and launched these rocks from the moon.  Relatively mild shock pressures of less than 10GPa may be enough to compact these breccias and greatly reduce their intergranular porosities (e.g. 11).  Consequently, events energetic enough to launch these samples may also modify and compact them.  Even if more porous regolith breccias are somehow launched by impact, breakup forces on entering the earth's atmosphere may be sufficient to destroy the more porous breccias.  It is interesting to note that nearly all measured chondrite porosities are less than 20%  (5), relatively low by lunar regolith breccia standards, but probably typical of the lunar meteorites.

4. The energetic event which launched the lunar meteorites may have heated them enough to destroy the fine-grained iron responsible for the FMR signature and reduced their apparent maturity.  While I have just argued that an energetic event may reduce the porosity of these samples, I also note that the FMR signature of Apollo lunar regolith breccias does not seem to be significantly modified in the more compact and obviously shocked samples in the Apollo collection.  The evidence for this is the rather close correspondence among such maturity indicators as observable agglutinates, trapped rare gases, and the FMR index over a wide range of maturity and porosity, and the lack of correlation between porosity and FMR index discussed above.  Lunar meteorite ALHA-81005, while low in FMR maturity, is also low in solar wind implanted nitrogen (10), and does not appear to contain petrographically identified agglutinates.  It therefore seems to be an intrinsically low maturity sample, regardless of any shock modification.

We conclude that while the apparent uniformly low porosities of the lunar meteorite regolith breccia suite may result from the ejection impact events, and that the lunar meteorite regolith breccia suite is intrinsically low in maturity, probably reflecting a low maturity suite of precursor soils.  Based on our experience with Apollo 15 and 16 regolith breccias, I propose that this low maturity soil zone probably exists only at some moderate depth anywhere on the moon and is not characteristic of the upper few meters of present-day regolith (although it may be present locally on the surface as ejecta from relatively fresh craters).  Consequently, the source of all of they lunar meteorite regolith breccias may be beneath the normal reworking zone represented by most of the Apollo soils and cores, and

may be transitional to a proposed fragmental megaregolith containing little or no micrometeorite reworking history (5). Again, by analogy with many of the Apollo 16 regolith breccias, material from this zone may be relatively ancient and may not at all reflect present-day surface conditions. It would be useful to date the closure time of lunar meteorites to surface exposure and reworking. This time may be different from either the compaction time or the near surface exposure time based on spallogenic species. For example, one possibility is that lack of significant KREEP in some of these lunar meteorites may result because the closure times are very old, predating much of the KREEP volcanism.

One broader implication of these observations on lunar meteorites is that ordinary chondrites and other meteorites in our possession may also have gone through a modification and selection process before we see them, and may not be representative of the regolith near the surface of their parent bodies. By analogy with the above analysis of lunar meteorites, they may come from subsurface depths below the upper regolith, they may be compacted and altered by the collisional processes which eject them, and they may undergo a selection process as they enter the earth's atmosphere. (In that regard, it is interesting to note that anhydrous interplanetary dust grains appear to be far more porous than any known meteorite, and may survive only because of the relatively gentle deceleration caused by the very small size (< 100 micrometers)). If we had only the suite of lunar regolith breccias to help us understand lunar regolith history and development, we we might have missed the entire concept of reworking, gardening, and the development of maturity over time. It may be, by analogy to the Apollo collection, that chondritic and achondritic breccias also exist which show considerable more maturity (near surface parent body reworking and modification) and considerably more porosity than those in the museum collections, but, for reasons discussed above, such samples have not been ejected intact from their parent bodies or survived the fall to earth and their investigation must await sampling missions to asteroids.

References:

1. Morris, R. M. (1978) Proc. Lunar Planet. Sci. Conf. 9th. p. 2287-2297.
2. Morris, R. M., R. L. Korotev, and H. V. Lauer, Jr. (1989) Proc. Lunar Planet. Sci. Conf. 19th, pp. 269-284.
3. Morris, R. M. (1981) Unpublished data, personal communication.
4. McKay, D. S., D. D. Bogard, R. V. Morris, R. L. Korotev, s. J. Wentworth and P. Johnson (1989). Proc. Lunar and Planet. Sci. Conf. 19th, pp. 19-41.
5. McKay, D. S., D. D. Bogard, R. V. Morris, R. L. Korotev, P. Johnson, and S. J. Wentworth. (1986) Proc. Lunar and Planet Sci. Conf. 16th, JGR Vol. 91, No. B4, pp.D277-D303.
6. Takeda, H. (1990) Proc. NIPR Symposium on Antarctic Meteorites, pp. 3-14.
7. Morris, R. V. (1983) Geophys. Res. Letters, Vol. 10, No. 9, pp.807-808.
8. Warren, P. (1990) Papers presented to NIPR 15th Symposium on Antarctic Meteorites, pp.131-133.
9. Eugster, O. (1988) Proc. NIPR Symposium on Antarctic Meteorites, pp. 135-141.
10. Grady, M. M. and C. T. Pillinger (1990) Proc. NIPR Symposium on Antarctic Meteorites, 3, pp.27-39.
11. Schaal, R. B. and F. Horz (1980) Proc. Lunar Planet. Sci. Conf. 11th, pp.1679-1695.

**Table 1.  FMR Maturity Index for various lunar samples.**

| Sample | Maturity Index ($I_S$/FeO) | |
|---|---|---|
| | Mean | Standard Deviation |
| All soils (166 samples) (Ref. 1) | 56.6 | 23.2 |
| Apollo 11 Regolith Breccias (9 samples) (Ref. 3) | 65.1 | 22.0 |
| Apollo 15 Regolith Breccias (28 samples) (Ref. 4) | 25.0 | 15.6 |
| Apollo 16 Regolith Breccias (19 samples) (Ref. 5) | 5.3 | 11.3 |
| Combined Apollo Regolith Breccias (56 samples) (Ref.3, 4, 5) | 24.0 | 24.2 |
| Lunar Meteorite ALHA 81005 (Ref. 7) | 5.0 | |
| All other lunar meteorite regolith breccias | Not measured, but maturity based petrographic and rare gas data appears to be lower than ALHA-81005. | |

# U-Th-Pb Chronology of Asuka-31 Gabbro

K. Misawa[1], M. Tatsumoto[1], and K. Yanai[2]
[1] U.S. Geological Survey, MS 963, Box 25046, Denver, CO 80225, USA.
[2] National Institute of Polar Research, Itabashi-ku, Tokyo 173, Japan.

The antarctic meteorite Asuka-31 is a coarse-grained lunar gabbro whose chemistry is similar to very-low-titanium mare basalt [1,2]. The modal mineralogy reported is roughly 59% pyroxene, 30% plagioclase (maskelynite), 6% ilmenite, and 5% other minerals including troilite and coronas of symplectite are observed around opaque minerals.

A sample weighing 1.6 gm provided to us during March, 1991 was gently crushed using a stainless steel pestle and mortar and seized into <63, 63-150, and 150-300 μm fractions with nylon sieves. Pyroxene, maskelynite and ilmenite separates were hand-picked from the 150-300 μm fraction. Minerals were further separated from the 63-150 μm fraction using a Frantz isodynamic separator equipped, with an alcohol filled chute and heavy liquids. The <63 μm fraction was analyzed as whole rock sample.

These separates (8 fractions) were washed with distilled alcohol then leached with 0.01N HBr and 0.1N HBr in order to remove any terrestrial contamination and strip the grain surface of any adsorbed Pb component. The remaining Pb in the residues should ideally represent indigenous Pb.

The Pb from pyroxene and ilmenite residues is very radiogenic (measured $^{206}Pb/^{204}Pb$ were 150 and 460, respectively). The Pb data from all residues (8 fractions) defines an isochron age of 3930 ± 52 Ma (Fig. 1) although maskelynite and whole rock fractions do not plot on the line. Excluding these maskelynite and the whole rock fractions, the remaining residues yield a Pb-Pb isochron age of 3940 ± 7.7 Ma, which is similar to those of some lunar mare basalts and lunar basin-forming events at 3.8-4.0 Ga (Imbrium 3.87-3.90 Ga; Crisium 3.90 Ga, Humorum 3.92-3.95 Ga; Nectaris 3.98 Ga; and Serenitatis 3.97 Ga [3]) The radiogenic Pb characteristics and age of Asuka-31 clearly indicate that this gabbro is the plutonic equivalent of lunar mare basalts. U and Th concentration determinations are in progress and the results of the U-Th-Pb systematics will be discussed.

References:

[1] Yanai, K., Antarctic Meteorites Symposium, 15th, 49 (1990).

[2] Yanai, K., Proc. Lunar Planet Sci., 21th, 317-324, (1991).

[3] Jessberger, E. K. et al., Proc. Lunar Conf., 5th, 1419-1449 (1974).
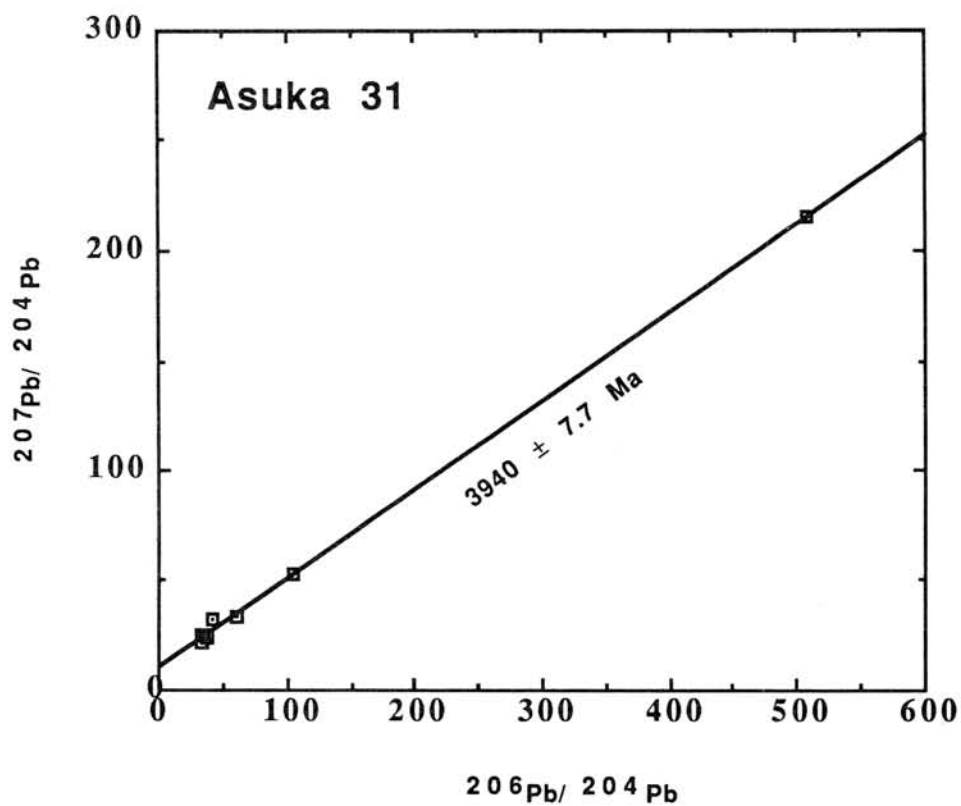
Fig. 1.   Pb-Pb diagram for Asuka 31.

# GEOCHEMISTRY OF ASUKA-31: COMPARISON TO BASALTIC LUNAR METEORITES AND MARE BASALTS.

Marilyn M. Lindstrom, David W. Mittlefehldt, and Rene R. Martinez.
SN2, NASA Johnson Space Center and Lockheed ESC, Houston TX, 77058, USA.

Lunar meteorites are unlocated samples of the lunar surface which add information on the nature of the lunar crust to that obtained from Apollo and Luna samples. There are now twelve known lunar meteorites, all but one of which are from the Japanese or US Antarctic meteorite collections. Until two years ago all identified lunar meteorites were classified as anorthositic regolith breccias. In 1989 Delaney (1) and Warren and Kallemeyn (2) identified EET87521 as a lunar basaltic breccia and not a polymict eucrite. Within a few months Yanai (3,4) identified Asuka-31 and Y793169 as coarse-grained mare gabbros and reclassified Y793274 as a basalt-rich regolith breccia. This year Hill and Boynton (pres. comm., 1991) identified Australian meteorite Calcalong Creek as a KREEP-rich lunar meteorite.

The picture of the lunar crust presented collectively by the lunar meteorites is very different today than it was two years ago. The twelve lunar meteorites include 7 anorthositic breccias, 2 basalt-rich breccias, 2 mare gabbros, and one KREEP-rich breccia. However, after considering pairing, the 7 anorthositic breccias represent just 4 distinct meteorites, while the 4 basaltic meteorites are all distinct specimens. This 50-50 proportion of anorthositic-basaltic meteorites contrasts strongly with the 83-17 proportions derived from photogeologic mapping. Furthermore, all 4 basaltic meteorites, and most basalt clasts in the anorthositic breccias, are very low Ti (VLT) basalt, a relatively rare type among returned samples. This apparent discrepancy between the proportions of lunar meteorites and the results from Apollo and Luna missions would disappear if the basaltic meteorites (and perhaps some of the anorthositic breccias) are paired ejecta and represent the same region of the moon. If, however, they were ejected by different impacts, the lunar meteorites suggest that mare basalts, particularly the VLT variety, are more common on the lunar surface than previously thought. Detailed consortium studies of all samples are required to evaluate this problem. Of particular importance is comparative studies of the mare gabbros and clasts in the basaltic breccias. Such studies have been undertaken for the anorthositic breccias and for Y793274 and EET87521. This report presents preliminary geochemical studies of Asuka-31.

Yanai (4) described Asuka-31 as a new type of lunar sample, a very coarse-grained mare gabbro. He gave a mode of 59% pyroxene, 30% plagioclase, 6% ilmenite, and 5% other minerals including troilite, olivine, ulvospinel, Fe-metal, apatite and silica. These accessory phases are concentrated in simplectic intergrowths of ferroan olivine and pyroxene with sodic plagioclase. Yanai (4) presented mineralogical and bulk compositional studies which showed that Asuka-31 is similar to both Apollo 15 pigeonite basalts and Apollo 17 and Luna 24 VLT basalts, but that it is distinct in detail from all previously studied mare basalts and represents a new type of mare gabbro.

We were allocated Asuka-31,94, a 248 mg chip for INAA, RNAA (Mike Lipschutz), and Ar-Ar dating (Don Bogard). Asuka-31,94 is a very coarse-grained gabbro with grain size of 2-4 mm. Based on inspection under a binocular microscope we estimate that our sample consists of 60% medium brown pyroxene, 25% clear plagioclase, and 15% black ilmenite. The abundance of ilmenite in our sample is much higher than the 6% reported by Yanai (4) and suggests that our sample is not representative of the bulk meteorite. Our processing and analysis scheme attempted to evaluate modal heterogeneity in this coarse-grained rock. We gently crushed the entire sample and carefully split off approximately one third for Ar-Ar dating. The remainder was ground further to a fine powder, then split into two subsamples, 94A and B, which were then each split to give a small sample for major element analysis by FB-EMP and a larger one for INAA. RNAA will be done by Lipschutz on INAA splits after completion of INAA.

Preliminary results of major and trace element analyses (INAA) are presented in Table 1 and compared to analyses of other basaltic lunar meteorites and VLT mare basalts. Variations in major element composition of Asuka-31 clearly show that heterogeneity is a major problem. Despite our careful grinding and splitting, our two subsamples analyzed for major elements are quite different from each other and, based on the Fe content, from the subsamples analyzed by INAA. The observed enrichment in ilmenite relative to Yanai's sample is seen in the TiO2 contents of 5.5% compared to 1.66%, and in the very high FeO contents (23-27% compared to 21%). An unrepresentative sample such as ours would certainly not be classified as a VLT basalt. Major element analyses of Asuka-31 are plotted in a triangular diagram of Al2O3-MgO-FeO in Figure 1.

Variations within Asuka-31 are different from those within EET87521 and Apollo 17 and Luna 24 VLT basalt suites which are dominated by variations in MgO-FeO due to magmatic differentiation. Here the mg' (molar Mg/Mg + Fe) is relatively constant. Variations in modal amounts of ilmenite, pyroxene, and plagioclase account for major element differences. Further allocations of Asuka-31 should pay particular attention to the problem of heterogeneity and representative sampling. Perhaps a large sample should be ground and split for separate studies.

This mineral and major element variation must be considered in interpreting the trace element composition of Asuka-31. Variations in the proportions of pyroxene, plagioclase, and ilmenite will have more effect on the compatible elements (Sc, Cr, Mn, Co, Ni, Sr) than on the incompatible elements (REE, Hf, Ta, Th). Variations in accessory-mineral-rich simplectite will affect the incompatible elements. Differences between our two subsamples analyzed by INAA are much less significant than between the subsamples analyzed for major elements. For the INAA splits differences in Fe, Sc, Cr, Co are generally not greater than the one sigma analytical uncertainties. Differences in La and Sm are greater than one sigma levels, while differences in other incompatible elements are not significant at the one sigma level. REE patterns for Asuka-31 are plotted in Figure 2 compared to basaltic breccias EET87521 and Y793274 and mare basalts. Asuka-31,94B has a slightly more LREE-depleted pattern than ,94A. In mare basalts REE are concentrated in pyroxene or mesostasis. Pyroxene has a LREE-depleted pattern, while plagioclase has a LREE-enriched pattern. Neither mesostasis nor ilmenite fractionate the REE significantly. Mesostasis (especially apatite) concentrates the REE, while ilmenite dilutes them. Thus the REE variations in our subsamples of Asuka-31 may be due to a slightly higher ratio of pyroxene/plagioclase in ,94B relative to ,94A. The high proportion of ilmenite in our entire specimen may have diluted REE relative to that in the bulk rock, but REE concentrations depend more on the proportion of accessory apatite in the simplectic intergrowths.

Comparing Asuka-31 to basalt breccias EET87521 and Y793274 we see that Asuka-31 is markedly enriched in Sc (112 vs 30-40 ppm) and notably depleted in Co (27 vs 40-50 ppm). Evaluation of whether this is due to selective partitioning of Sc into ilmenite or to different parental magmas requires trace element analyses of separated minerals. Cr concentrations in basaltic lunar meteorites correlate with variations in mg'. Asuka-31 has a low mg' of 31-35 and Cr concentration of 1850 ppm. These are comparable to those of ferroan samples of EET87521 (Cr 1470-1910 ppm; mg' 37-43), but lower than those of Y793274 and magnesian samples of EET87521 (Cr 1900-2400 ppm; mg' 45-56).

Incompatible element concentrations in Asuka-31 contrast sharply with those in the basaltic breccias EET87521 and Y793274 and may be evidence for a separate KREEP component in the basalt breccias as suggested by Delaney et al (5). Asuka-31 has La concentrations a factor of 2-4 lower than those of EET87521 and Y793274, but Sm contents are comparable with those of Y793274, and HREE concentrations are nearly a factor of two higher in Asuka-31 than in Y793274. The LREE-depleted pattern of Asuka-31 is typical of mare basalts, while the LREE-enriched pattern of EET87521 and Y793274 is typical of KREEP. Concentrations of other incompatible elements in Asuka-31 are not in KREEP ratios, but depend on modal proportions. Hf and Ta are concentrated in ilmenite and are enriched in our splits, while contents of Th and U are low. Determination of whether Asuka-31 represents a basaltic component in EET87521 requires detailed comparative mineralogical and geochemical studies of Asuka-31 and clasts in EET87521, as well as studies of the exposure histories of all the basaltic meteorites.

In summary, Asuka-31 is a new type of mare gabbro that is similar to both low Ti and very low Ti mare basalts. Our 248 mg split of Asuka-31 appears to be unrepresentative of the bulk meteorite. It is markedly enriched in ilmenite compared to Yanai's much larger sample. Major element analyses of Asuka-31 show extreme heterogeneity, but the somewhat larger splits analyzed by INAA are less variable in composition. Our sample of Asuka-31 shows marked enrichment in Sc and depletion in Co compared to other basaltic lunar meteorites and mare basalts. Asuka-31 has a LREE-depleted pattern typical of mare basalts, in contrast with the LREE-enriched KREEP-like patterns of EET87521 and Y793274. Evaluation of a relationship between Asuka-31 and the basaltic breccias awaits further consortium study. If these meteorites were not ejected by the same impact, and lunar meteorites are random samples of the lunar surface, it may be that mare basalts are more common than previously thought. The observation of rare mare basalt clasts in most of the anorthositic lunar meteorites, in contrast to their absence in Apollo 16 regolith breccias, suggests that mare basalts may be dispersed throughout the highlands perhaps as hypabyssal magmas such as Asuka-31.

TABLE 1. Major and trace element composition of Asuka-31 and other lunar basalts. Extreme examples of matrix analyses are given for Y793274 and EET87521; typical examples are given for Apollo 17 and Lunar 24 VLT basalts. Oxides are in Wt%, elements in ppm, except Ir and Au in ppb.

| Sample | Asuka31 | Asuka31 | Asuka31 | Asuka31 | Asuka31 | Y793274 | Y793274 | E87521 | E87521 | A17VLT | L24VLT |
|---|---|---|---|---|---|---|---|---|---|---|---|
| Ref. | (4) | 94A' | 94B' | 94A | 94B | (6) | (7) | (2) | (8) | (9,10) | (2) |
| Wt (mg) | | 3500 | 26.6 | 21.9 | 68.5 | 44.6 | 62.3 | 43 | 278 | 42.7 | 533 |
| SiO2 | 45.4 | 39.9 | 37.3 | | | 48.3 | 47.1 | 48.4 | 46 | 46.7 | 46.2 |
| TiO2 | 1.66 | 5.73 | 5.21 | | | 0.57 | 0.63 | 1.12 | 0.43 | 0.92 | 0.85 |
| Al2O3 | 11.5 | 10.9 | 17.1 | | | 13.7 | 17.4 | 12.6 | 15.1 | 10.0 | 13.1 |
| FeO | 21.2 | 24.8 | 23.4 | 27.1 | 26.8 | 15.1 | 12.5 | 19.0 | 15.9 | 18.6 | 18.6 |
| MgO | 6.41 | 6.39 | 5.95 | | | 9.0 | 9.0 | 6.34 | 10.4 | 12.2 | 6.71 |
| CaO | 12.0 | 9.61 | 8.91 | 10.1 | 10.2 | 12.0 | 12.1 | 11.6 | 11.5 | 10.0 | 13.0 |
| Na2O | 0.5 | 0.13 | 0.14 | 0.139 | 0.148 | 0.33 | 0.39 | 0.41 | 0.32 | 0.12 | 0.30 |
| K2O | 0.04 | 0.02 | 0.02 | | | 0.06 | 0.11 | 0.07 | 0.03 | 0.01 | 0.03 |
| mg' | 35 | 31 | 31 | | | 52 | 56 | 37 | 53 | 54 | 39 |
| Sc | | | | 112.6 | 111.8 | 37.8 | 28 | 44.0 | 26.8 | 51 | 48 |
| Cr | 1160 | 1810 | 2010 | 1870 | 1840 | 2200 | 1960 | 1470 | 2380 | 5070 | 1600 |
| Mn | 1940 | 2830 | 2620 | | | 1850 | 1340 | 1890 | 1700 | 2020 | 2200 |
| Co | | | | 28.0 | 27.6 | 41.1 | 43.0 | 46 | 52.6 | 45 | 43 |
| La | | | | 2.54 | 2.35 | 4.68 | 6.7 | 8.3 | 3.21 | 1.2 | 1.92 |
| Ce | | | | 7.5 | 7.4 | 12.6 | 15.0 | 20.9 | 8.0 | | 6.4 |
| Sm | | | | 2.54 | 2.43 | 2.38 | 2.79 | 3.86 | 1.67 | 1.0 | 1.54 |
| Eu | | | | 0.62 | 0.58 | 0.64 | 0.97 | 0.98 | 0.64 | | 0.68 |
| Tb | | | | 0.78 | 0.72 | 0.48 | 0.61 | 0.80 | 0.42 | | 0.33 |
| Yb | | | | 3.38 | 3.30 | 1.98 | 2.36 | 3.19 | 1.44 | 1.4 | 1.41 |
| Lu | | | | 0.54 | 0.48 | 0.27 | 0.34 | 0.48 | 0.20 | 0.23 | 0.22 |
| Hf | | | | 2.18 | 2.06 | 2.00 | 2.36 | 2.88 | 1.55 | 0.50 | 1.05 |
| Ta | | | | 0.45 | 0.42 | 0.20 | 0.32 | 0.37 | 0.14 | 0.06 | 0.16 |
| Th | | | | 0.35 | 0.31 | 0.53 | 1.07 | 0.98 | 0.35 | | 0.20 |
| U | | | | 0.11 | 0.09 | 0.19 | 0.23 | 0.23 | | | |
| Ir | | | | <2 | 3.1 | 2.5 | 6.2 | <1.2 | | | |
| Au | | | | | | 3.5 | 2.4 | <1.2 | | | |

Figure 1. Major element compositions of lunar meteorites.

* Asuka 31
• EET87521
○ other lunar meteorites
□ Apollo 17 VLT
△ Luna 24 VLT
◇ anorthosites



MgO

Al₂O₃          (weight)          FeO
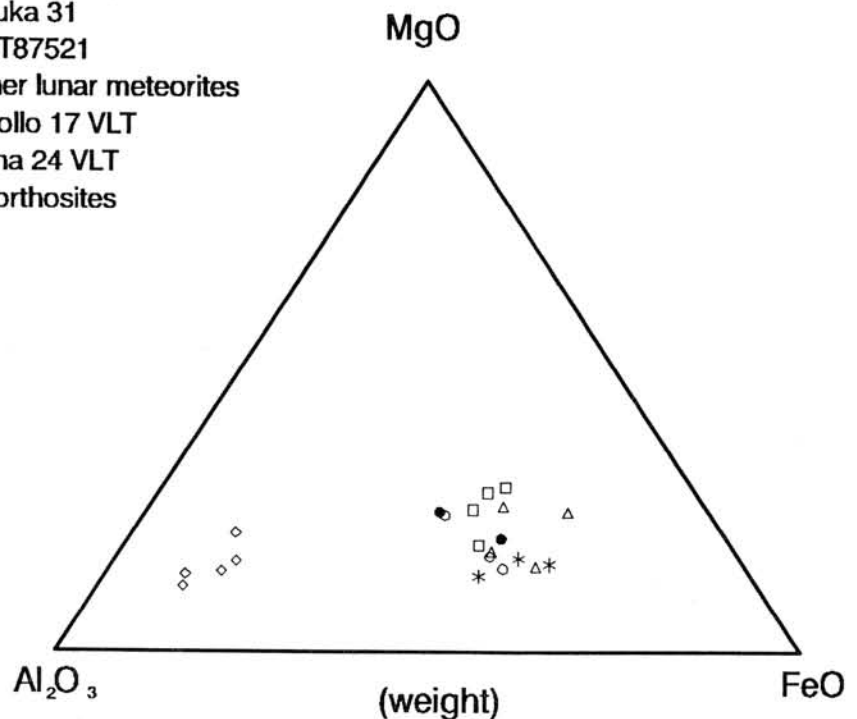
REFERENCES. (1) J. Delaney (1989) Nature 342, 889-890. (2) P. Warren and G. Kallemeyn (1989) Geochim. Cosmochim. Acta 53, 3323-3330. (3) K. Yanai and H. Kojima (1990) NIPR 15th Sym. Ant. Met., 129-130. (4) K. Yanai (1991) Proc. Lunar Planet. Sci. Conf. 21, 317-324. (5) J. Delaney et al (1990) NIPR 15th Sym. Ant. Met., 116-118. (6) M. Lindstrom et al (1991) Proc. NIPR Sym. Ant. Met. 4, in press. (7) P. Warren and G. Kallemeyn (1991) Proc. NIPR Sym. Ant. Met. 4, in press. (8) M. Lindstrom et al (1991) Lunar Planet. Sci. XXII, LPI, 817-818. (9) J.C. Laul and R. Schmitt (1975) Lunar Sci VI, LPI, 489-491. (10) G.J. Taylor et al (1977) Geophys. Res. Lett. 4, 207-210.

Figure 2. Chondrite-normalized REE patterns.
(a) Basaltic lunar meteorites          (b)Mare basalts
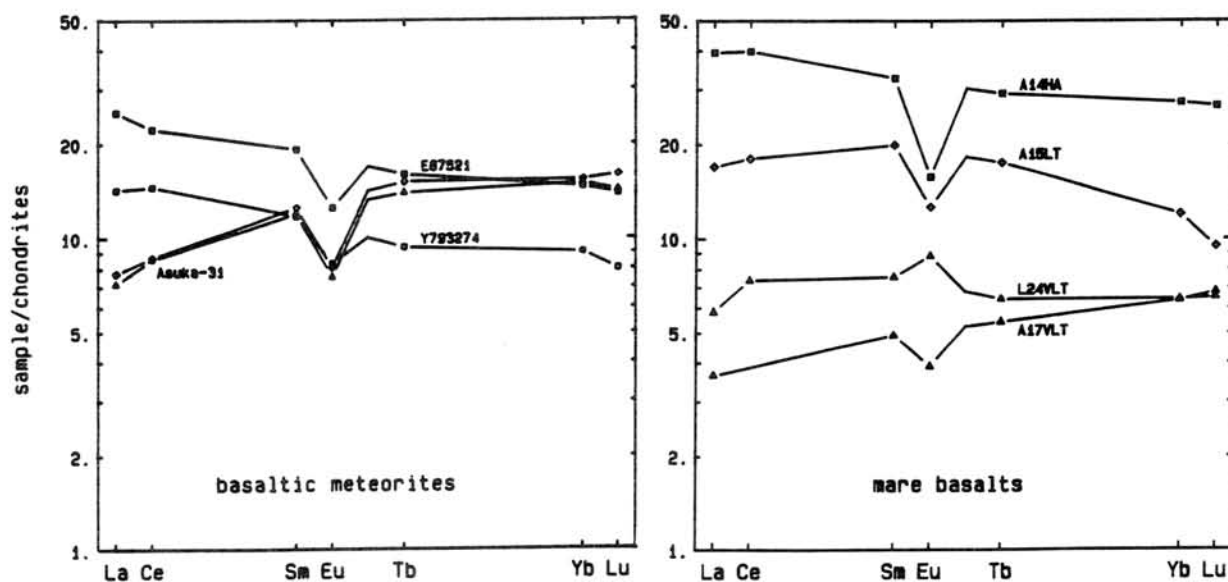
# IMPACT MARKERS IN BASALTIC REGOLITHES

Marek Żbik[1], Ewa Jackiewicz[1], Michał Kopcewicz[2], [1] Space Research Centre, Polish Academy of Sciences, 00-716 Warszawa, Bartycka Str. 18, Poland, [2] Institute of Experimental Physics, Warsaw University, 00-681 Warszawa, Hoża Str. 69, Poland.

The paper presents the results of studies on a basaltic samples various genesis, as begining to Martian surface regolith analogues were performed. This investigation is related to the planned Mössbauer experiment on Mars, as part of space program Mars 94.

Lunar soil, basaltic meteorite Stannern and Earth basalt sample were covered chemical and micromorphological analyses by JSM-T200 scaning electron microscope equipped with an energy dispersive X-ray detector, Xray difraction and Mössbauer spectroscopy.

The studied sample of Lunar soil taken by the automatic station Luna 16 (numbered 1616) from the Mare Fecunditatis basin, macroscopically represents fine-grained dark-gray powder with admixture of single coarse grains.

Morphological studies showed that major components of the regolith include: basalt and mineral grains, regolith breccias, glass, aglutinates and metallic phase (iron, troilite and magnetite). Mineral grains most common in the regolith include anortite, augite and ilmenite.

Two major types of basalt grains may be distinguished: those of fine-grained basalts with glass, and coarse crystalline, of the gabbro type. Major mineral found in these grains include plagioclases, pyroxenes, ilmenite and sometimes olivine.

Glass material is a product of rapid cooling of rocks melted as a result of impact. Grains of that type vary in shape from irregular fragments to spherical grains of various size shown in fig. 1 and 2. Thus spherules as impact markers are decorated on the surface and sometimes porous or empty inside.

Chemical composition of some soil components of the studied sample of Earth basalt, shock glass made from this basalt, Lunar regolith and Stannern eucrite as follows (table 1).

Table 1

| | basalt | glass | Lunar spher. | Lunar glass | Lunar anort | Stannern glass | Stannern cryst. |
|---|---|---|---|---|---|---|---|
| $SiO_2$ | 51.01 | 46.34 | 44.24 | 45.06 | 44.01 | 48.69 | .51.56 |
| $TiO_2$ | 1.69 | 1.89 | 1.29 | 4.33 | 0.17 | 0.74 | 0.26 |
| $Al_2O_3$ | 15.51 | 12.62 | 19.63 | 15.55 | 28.58 | 10.93 | 0.29 |
| FeO | 9.78 | 15.52 | 12.35 | 16.45 | 4.56 | 18.72 | 20.48 |
| MnO | – | – | 0 | 0.2 | 0 | 0.54 | 0.68 |
| MgO | 8.08 | 9.62 | 9.02 | 7.27 | 5.18 | 6.69 | 10.60 |
| CaO | 11.53 | 12.27 | 13.33 | 12.39 | 15.96 | 10.99 | 15.32 |
| $Na_2O$ | 2.76 | 1.79 | 0.55 | 0.24 | 0.30 | 0.56 | 0.06 |
| $K_2O$ | 0.14 | 0.06 | 0 | 0.14 | 0.03 | 0.07 | 0.001 |
| $Cr_2O_3$ | – | – | 0 | 0.11 | 0 | 0.20 | 0.25 |

The weathering process was studied for basalt samples. The oxidation effect was clearly seen as an increase of the ferric components in the Mössbauer spectroscopy. The weathering process simulated for the sample prepared from the Lunar soil collected at Mare Fecunditatis basin at Moon, by annealing the specimen at $1000^0$ C in air, was compared with the natural weathering of basalts collected in various places on the Earth. Such annealing induced complete decomposition of ilmenite. Pyroxene was partially decomposed and $\alpha$-Fe transformed completely into magnetically ordered oxide - $Fe_3O_4$.

The Mössbauer measurements of Lunar origin revealed that they consist of olivine, ortopyroxene, ilmenite and some $\alpha$-Fe, in clear distinction to basaltic meteorite - Stannern, which contains ortopyroxene, clinopyroxene and the traces of FeS only.

The presence of $\alpha$-Fe in the Lunar sample suggests that the meteorite matter influences the composition of Lunar soil, as we can see on the surface of basaltic grain in fig. 2. The chemical reduction at high temperature of iron in silicates may lead to the formation of metallic iron in impact processes. However, in fussion crust of Stannern meteorite (fig.3 ) metalic iron appears as a result of a similar reduction process of silicates, whereas the inner part of this meteorite does not contain $\alpha$-Fe, as are shown by the Mössbauer spectra.
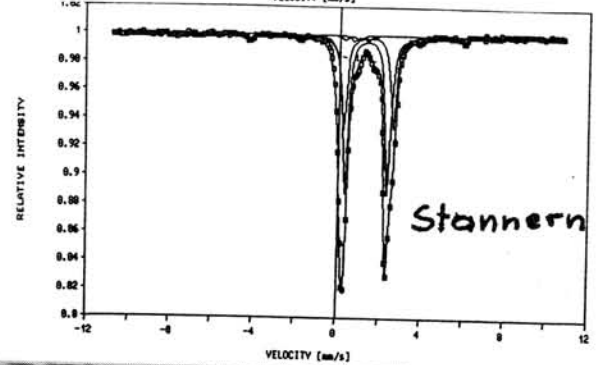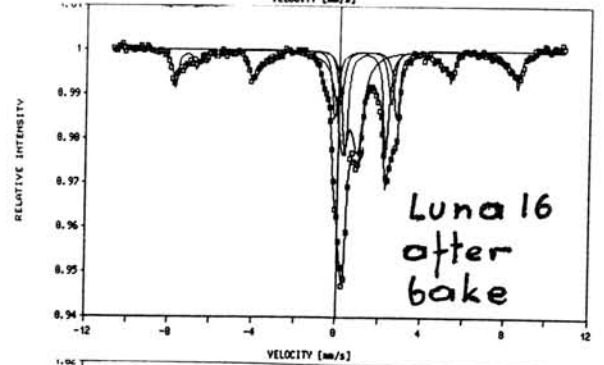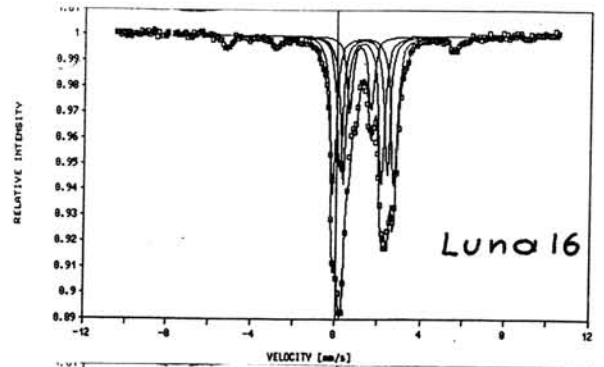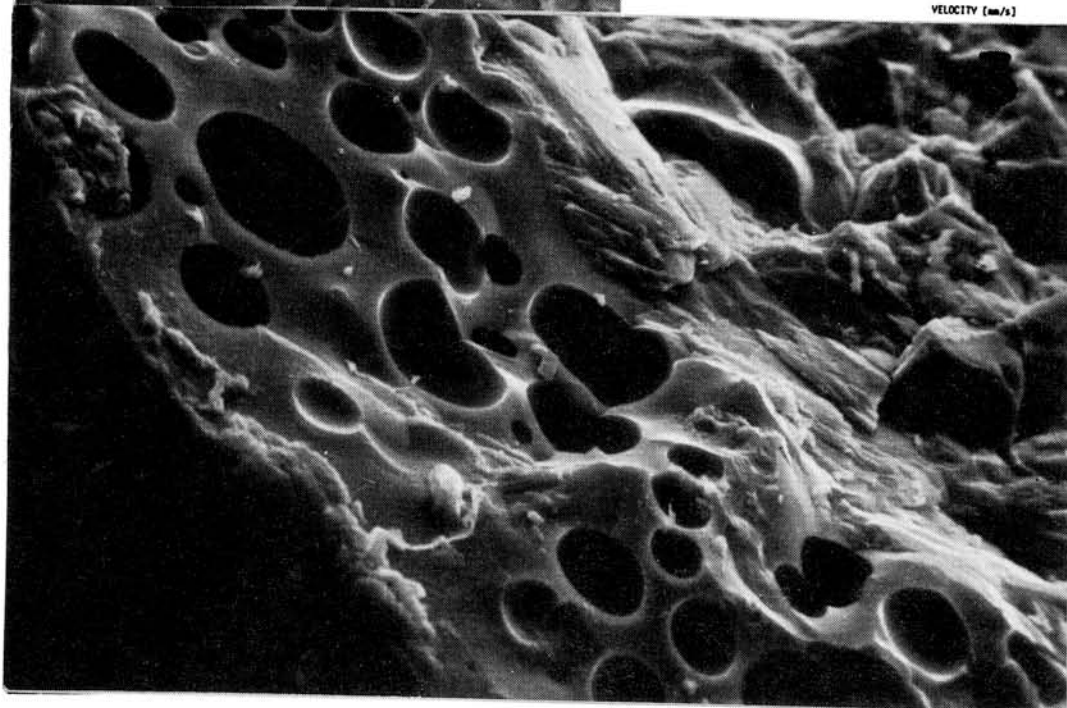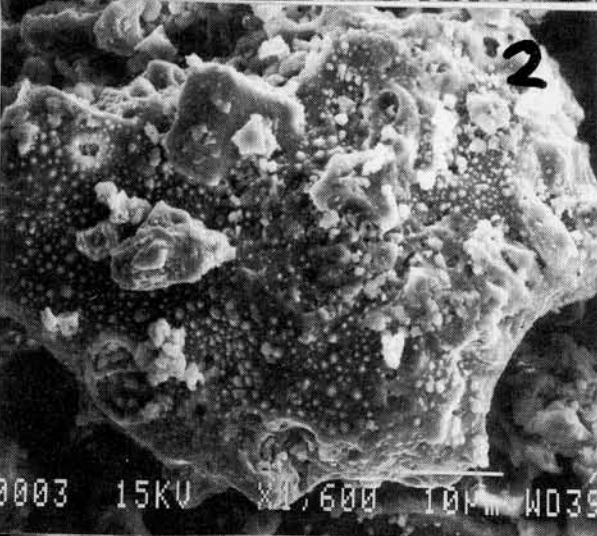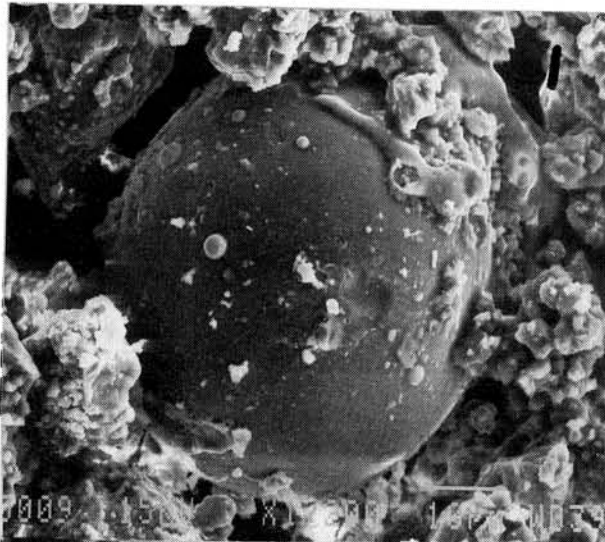
# ORIGIN OF THE MOON AND "LUNAR" METEORITES

Alexey A. Marakushev

Institute of Experimental Mineralogy, USSR Academy of Sciences,
Chernogolovka Moscow district

The planet Io, Jupiter's satellite is similar in size and density to the Moon. The similarity, however, does not concern their age. A peak in volcanic activity occurred on the Moon 3.2-4.6 Ga ago. The current volcanic activity on Io suggests that the Jupiter satellite system is relatively young, although Jupiter itself, like other solar system planets, is very ancient (4-5 Ga). Jupiter possessing an enormous energy supply in its interior had remained at a primitive stage of its development for about 3 Ga. During this period Jupiter did not experience inner differentiation into a liquid rock-iron core and fluid envelope, their separation being responsible for the development of the planet's satellite system.

The mean density of Jupiter's massive satellites increases regularly with approaching rock-iron core ($\sim$4.5 g/cm$^3$ recalculated to zero pressure), see Figure. This correlation clearly indicates thet the planet's heavy rock-iron core and its massive satellites share a common origin. This is governed by the relation between gravitational and centrifugal forces. Possibly, formation of the planet's heavy core due to fluid-silicate liquid immiscibility was accompanied by rotation acceleration and generation of centrifugal forces of higher intensity.

The rock-iron melts from the planet's interiors accumulated in the center to form a heavy core. By contrast, lighter
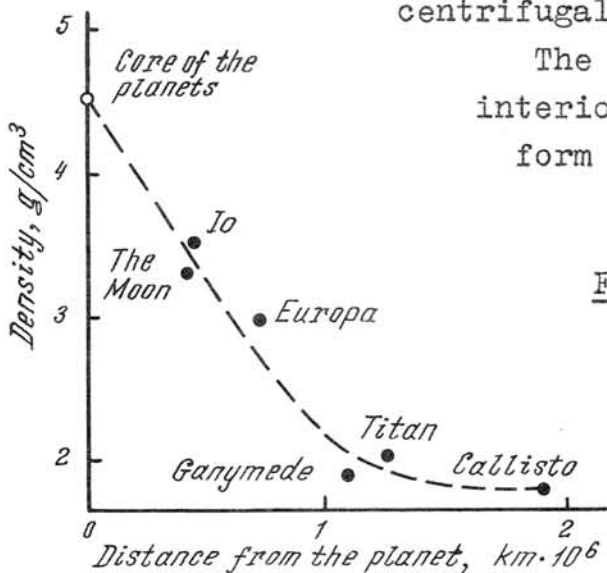


Fig. Density of massive satellites and rock-iron cores of their parent planets, such as Jupiter and Saturn, plotted against their distance from planets. The position of the Moon relative to the Earth is shown for comparison

fluid-rock melts from the planet's outer portions were subjexted to centrifugal forces. They were ejected from the planet to form a satellite system. The data on the system Moon-Earth are plotted on a graph (see Figure). They show a good fit to the above correlation. The analogy drawn between the systems Io — Jupiter's rock-iron core and Moon - Earth gives evidence that the Earth and Moon's parent planet was similar to Jupiter and formed in the same way as other fluid parent planets did. The Earth was first isolated from its parent planet as a rock-iron liquid core. Separation of the core was accompanied by isolation of the rapidly rotating envelope, in which substance inhomogeneity continued developing in the form of hydrogen-silicate immiscibility. Under centrifugal forces giant drops of fluid-silicate melts ejected from the planet for different distances to form its satellite system in which the Moon's position was similar to Io's in the Jupiter system. The satellites, on separation from their parent planet as molten fluid-silicate masses, consolidated rapidly from the surface, gaining endogenic ectivity as a result of the increase of fluid pressure in their interiors. The insufficiently consolidated satellites were therewith subjected to explosive disruption. Under tidal forces the satellites experienced natural destruction in the orbits closest to the planet (within the Roche limit), where the rings of clastic material were forming.

At the time of the Sun's maximum activity the Earth's parent planet suffered surface outgassing and lost its fluid envelope and satellites in far removed orbits. Only the Moon, disrupted satellites in the orbits closest to the Earth, and rings of clastic material have been preserved. As a result, the Earth came into being as an iron-stony planet. Because the Earth's rock-iron layering occurred under a high hydrogen envelope pressure, its iron liquid core accumulated significant hydrogen and other fluid components. This provides an explanation of the Earth's long-term endogenic activity that has already lasted about 4.6 Ga.

Disrupted satellites and rings surrounded the Earth in the past, but not the Moon itself provided a source of "lunar" meteorites collected by Japanese and American expeditions in Antarctica.

# Special Lecture (II and III)

## Professor Otto Eugster

## Dr. David S. McKay

FROM HOW MANY EJECTION SITES ON THE MOON DO THE LUNAR METEORITES ORIGINATE? Otto Eugster, Physikalisches Institut, University of Bern, CH-3012 Bern, Switzerland.

The lunar meteorite specimens discovered till now in Antarctica originate from eight individual meteorites. Four of them show the chemical composition of anorthositic lunar highland rocks, such as e.g. Apollo 15 rock 15415. These are ALHA81005, Y-791197, Y-82192, Y-82193, and Y-86032 (the latter three are paired, thus, Y-82192 subsequently stands for all three specimens) and the two paired specimens MAC88104 and MAC88105. Another four meteorites originate from lunar mare regions: EET87521 is a fragmental breccia containing diabases or gabbros of VLT (very-low Ti) bulk composition. Y-793274 is a regolith breccia of mare (probably VLT) and nonmare material in roughly 2 : 1 proportion. Asuka-31 is a VLT mare diabase or gabbro, and Y-793169 a VLT mare basalt. The latter two have not yet been allocated for consortium investigation. Numerous papers have been published on analyses of lunar meteorites. The reader may refer to the review-type articles given in the reference list.

The anorthositic lunar meteorites were dated by the K-Ar, $^{39}$Ar-$^{40}$Ar, Rb-Sr, Sm-Nd, and U/Th-Pb methods and exhibit typical lunar highland ages around 4000 Ma. The two lunar mare meteorites dated till now, EET87521 and Y-793274, yield K-Ar ages of about 3000 Ma, close to mare basalts returned by the Apollo missions, such as Apollo 12 to Mare Procellarum.

The cosmic-ray produced stable noble gas isotopes of Ne, Ar, Kr, and Xe indicate a duration of lunar regolith exposure of several hundred million years for ALHA81005, Y-791197, Y-793274, and MAC88104/5. On the other hand, Y-82192 and EET87521 contain low concentrations of stable cosmogenic species. Their lunar regolith residence time was less than 10 Ma. The duration of exposure to solar wind particles is approximately proportional to that for cosmic rays. This proves that the main fraction of the stable cosmogenic nuclei in the strongly irradiated lunar meteorites was produced before they were compacted to coherent breccia material.

In addition to the mineralogical, chemical and formation age characteristics of lunar meteorites their time of ejection from the moon allows us to distinguish between different ejection events. The concentrations of the following cosmic-ray produced radionuclides were measured in order to derive the duration of the moon-Earth transfer and the time of fall on the antarctic ice: $^{10}Be$, $^{26}Al$, $^{36}Cl$, $^{41}Ca$, $^{53}Mn$, and $^{81}Kr$. Except for Y-82192, whose moon-Earth transfer lasted $8 \pm 3$ Ma, and for Y-793274 (> 0.25 Ma) all other lunar meteorites spent less than 0.3 Ma in space. The terrestrial ages are less than 0.6 Ma (that of Y-793274 has not yet been determined). The sum of the durations for the moon-Earth transfer and for the residence in or on the antarctic ice yields the time before present when a particular lunar meteorite was ejected from the moon as a result of asteroidal or cometary impact. The ejection times are as follows: ALHA81005 - $0.2 \pm 0.1$ Ma, Y-791197 - $0.3 \pm 0.2$ Ma, MAC88104/5 - $0.4 \pm 0.3$ Ma, Y-82192 - $8 \pm 3$ Ma, EET87521 - < 0.7 Ma and Y-793274 - > 0.25 Ma.

Conclusions

At least three ejection events responsible for the lunar meteorites collected till now can be distinguished:

Event A produced Y-82192 $8 \pm 3$ Ma ago.

Event B: Anorthositic lunar highland breccias ALHA81005, Y-791197, and MAC88104/5 are mineralogically and chemically similar and the derived ejection times overlap.

Event C: In contrast to event A and B at highland sites, this impact occurred in a mare area and produced EET87521. Y-793274 contains an additional anorthositic component and high amounts of trapped solar wind and cosmic-ray produced noble gases. These differences, however, do not necessarily require an additional ejection event: mare and highland material, solar wind rich and solar wind poor material was recovered from quite restricted areas of one particular Apollo landing site. Whether the difference in mineralogical and chemical composition between the four mare meteorites is large enough to require several ejection sites is still a matter of debate.

References

Eugster O. (1989) Science 245, 1197-1202.

Koeberl Ch., Kurat G. and Brandstätter F. (1991) Geochim. Cosmochim. Acta, in press.

Nishiizumi K., Arnold J.R., Klein J., Fink D., Middleton R., Kubik P.W., Sharma P., Elmore D. and Reedy R.C. (1991) Geochim. Cosmochim. Acta, in press.

Palme H., Spettel B., Jochum K.H., Dreibus G., Weber H., Weckwerth H., Wänke H., Bischoff A. and Stöffler D. (1991) Geochim. Cosmochim. Acta, in press.

Takahashi K. and Masuda A. (1987) Proc. 11th Symp. Antarct. Meteor. 1986, 71-88.

Takaoka N. (1986) Proc. 10th Symp. Antarct. Meteor. 1985, 124-132.

Takeda H., Kojima H., Nishio F., Yanai K., Lindstrom M.M. and Yamato Lunar Meteorite Consortium Group (1989) Proc. NIPR Sym. A.M. 2, 3-14.

Vogt S., Herzog G.F., Fink D., Klein J., Middleton R., Dockhorn B., Korschinek G. and Nolte E. (1991) Geochim. Cosmochim. Acta, in press.

Warren P.H. (1990) Abstracts, 15th Sym. A.M. 131-133.

Yanai K. and Kojima H. (1990) Abstracts, 15th Sym. A.M., 129-130.

45

# Utilization of Lunar and Martian Resources

David S. McKay, Mission Science and Technology Office/SN14, Johnson Space Center, Houston, Texas 77058

To help plan the future Space Exploration Initiative (SEI), NASA is evaluating existing technology and and beginning to develop new technology which will allow utilization of local resources on the moon or on Mars. The objective of this project is to develop methods to reduce the cost of space exploration by using, where practical, local materials as a source of propellant, life support consumables, and construction materials. Some specific technical objectives are to (1) develop the technology for producing oxygen from lunar rocks and soils, (2) develop the technology for producing construction materials including ceramics and metals from lunar raw materials, (3) develop the technology for mining, ore transport, ore concentration, and spent materials handling and utilization, (4) develop the technology for extracting useful volatiles such as hydrogen from lunar soils, and (5) develop the technology for producing propellants on Mars from the martian atmosphere or from martian regolith.

We are currently evaluating the current technology status in each one of these areas and are formulating plans for additional research and development to bring these technologies to a more advanced state of readiness so that they can eventually be incorporated into detailed mission planning. Currently, many of these technologies are in a conceptual stage. A few have been investigated in the laboratory so that some basic data is available. For example, the mineral ilmenite, which is relatively common on the moon in mare areas can be reduced by hot hydrogen to provide water which can then be electrolyzed into hydrogen and oxygen. The hydrogen can be recycled through the reactor, and the oxygen can be cooled into a liquid form. The complete reaction is $FeTiO_3$ (ilmenite) $+ H_2$ = Fe (metal) $+ TiO_2 + H_2O$, $H_2O = H_2 + 1/2 O_2$. This reaction has been investigated under a variety of conditions and has been shown to work with reasonable success on simulants of lunar ilmenite. A conceptual design for a fluidized bed reactor has been developed. A variation of this approach uses other minerals or glass or even bulk regolith as feedstock. In another approach, melted lunar rock, soil, or mineral concentrates can be electrolyzed directed into metals and oxygen. Several variations of this concept have been investigated in the laboratory. In addition to direct electrolysis of molten rock, electrolysis of flux-melted rock has produced oxygen, and electrolysis of molten flux-melted aluminum oxide made by reducing the mineral anorthite plagioclase with aluminum metal has also been successful. Low temperature acid dissolution of simulated lunar minerals followed by electrolysis and recovery and recycle of the acid is also being investigated.

Metals have been produced by these and other reduction processes. Metals produced so far in the laboratory from lunar simulants include iron, silicon, aluminum, and alloys of silicon and aluminum. Other potential metal products include titanium, magnesium, and even calcium. These metals are normally available as melts which can be cast into ingots for later use or cast directly into useful products such as construction blocks, fasteners, or foundation anchors. Ceramics include fused soil, melted and cast basalt, glasses, fiberglasses, and concrete and cement formulations made mostly from local lunar materials. A number of innovative methods for producing these materials in a lunar environment have been proposed. Some innovative mining approaches have also been proposed.

*Friday, June 7, 1991*

*0900-1515    Symposium, Auditorium*

*1515-1615    Special Lecture (IV)*

    *Professor Cryil A. Ponnamperuma (Invited Speaker)*

    *Laboratory of Chemical Evolution,*

    *The University of Maryland,*

    *USA*

# MULTIELEMENT EDX MAPPING OF METEORITES

Akira Tsuchiyama[1], Masao Kitamura[2], Kenichi Ohbori[3], Hideaki Shibata[4], and Yoshinori Hosokawa[3]
1) College of General Education, Osaka University, Toyonaka 560, Japan. 2) Department of Geology and Mineralogy, Kyoto University, Kyoto 606, Japan 3) HORIBA Ltd., Kisshouin, Kyoto 601, Japan 4) MAXBRAIN Ltd., Chuhdohji Minami-cho, Kyoto 601, Japan

## Introduction

There are several digital mapping methods by a scanning electron microscope (SEM) to identify mineral phases and their distributions. These maps are obtained by using (1) back-scattered electron (BE) intensities (e.g.,[1]) or (2) X-ray intensities (e.g., Fig.2 of [2]). The first method is rapid, but sometimes difficulties arise in identifying minerals due to overlapping of BE intensities or average atomic numbers of minerals. The second method with a WDX system can give most accurate information, but it takes a long time to obtain data and needs expensive equipments. If an EDX system is used, X-ray intensities of a large number of elements can be obtained simultaneously from each point. This is suitable for study of meteorites because many kinds of phases, such as metallic alloys, sulfides, phosphides, phosphates, carbonates etc., are present as important minerals as well as silicates and oxides. This paper describes an X-ray mapping method with an EDX system [3], and this accurate and rapid method was applied to study of meteorites.

## Method

In the mapping procedure, X-ray images are obtained by measuring X-ray intensities of elements at each point with controlling a scanning electron beam (Fig.1). Phases and their distributions are determined by analyzing the X-ray images. Generally, it is difficult to identify mineral phases from a single element X-ray map because X-ray intensities are overlapping as shown in a histogram (Fig.2). If we plot X-ray intensities of two kinds of elements of each pixel, each mineral phase forms a cluster in the two-component diagram (Fig.3). In this scatter diagram, identification of phases becomes better but still imperfect. In this study, we used a new technique in a multicomponent diagram [3] to obtain a systematic method for separating mineral phases from EDS X-ray maps.

In this method, parameters for transformation of coordinate system are chosen to separate phases as much as possible by obtaining eigenvectors of variance-covariance matrix in the multicomponent space of all the measured elements. Fig.4 is an example of a scatter diagram using the parameters (P1 and P2) determined by the above method. In this diagram at least six phases can be recognized as clusters. After recognizing phases, each pixel is assigned to the recognized phase by a statistical

method of assuming normal distribution of the X-ray intensities in the multicomponent space. An example of the final result is shown in Fig.5.

*Application to meteorites*

X-ray maps were obtained by an SEM-EDX system (HITACHI X650 equipped with HORIBA EMAX-2770) with accelerating voltage of 20 kV, beam current of 1 nA, and dwell time of 40 msec at each point. Signals of an SEM image and X-ray intensities of maximum seventeen elements were obtained for 256x256 pixels.

Unique meteorites
As a part of a consortium study on the Antarctic unique meteorites, the modal compositions of winonaites (Y-74025, Y-75300 and Y-75305; *e.g.*,[4]) were determined by the present method. Because silicate minerals are almost homogeneous in these meteorites, it was easy to identify these phases on the maps. On the other hand, metals and sulfides are oxidized and become heterogeneous due to weathering. In this case, original phases were identified by using a special method described below.

Heterogeneous samples
A heterogeneous phase forming a binary solid solution is recognized as a linearly elongated cluster in scatter diagrams like Figs.2 and 3. By choosing several representative compositions in this elongated cluster, the phase and its compositional range can be assigned at each pixel by using the statistical method mentioned above. Similar methods are applicable for phases with more complex heterogeneities.

In a chondrule of Y-691, complex zoned Al-rich pyroxene crystals were reported [5]. In this sample, it is hard to recognize the zonal structures of the pyroxenes by BE images because Mg-Fe-Ca-Al-Si are changed simultaneously. The present method was applied to this sample, and a map with compositional contours was obtained. It was found that the pyroxenes change their compositions not concentrically but more complexly from a corner of a grain to another corner of the grain with lamella structures.

Classification of meteorites
Scatter diagrams obtained by the transformation of coordinate system in the present method (*e.g.*, Fig.3) have various patterns depending on the mineral compositions of samples, the chemical compositions of the minerals and their heterogeneities. These patterns might be used for classify meteorites. To check this possibility, the scatter diagrams of several types of meteorites were obtained. The samples are Allende (CV3), Julesburg (L3), Tulia (H3-4), Beaver (L5), Camel-Donga (eucrite) and Admire (pallasite). Each sample has a unique pattern in the diagram, suggesting possibility of detailed classification although the data are not still enough.

References: [1] Noro H. and Miyake A. (1986) *Ann. Meet. Mineral.*

*Soc. Japan*, 152 (abstract). [2] Nagahara H. and Ozawa K. (1986) *Mem. Natl. Inst. Polar Res.* Spec. Issue **41**, 181-205. [3] Ohbori K., Hosokawa Y., Kitamura M., Tsuchiyama A., and Shibata H. (1990) *Symp 6th Analytical TEM* (abstract). [4] Kimura M., Tsuchiyama A., Fukuoka T. and Iimura Y. (1991) *This volume.* [5] Kitamura M., Watanabe S., Isobe H., and Morimoto N. (1987) *Mem. Natl. Inst. Polar Res.* Spec. Issue **46**, 113-122.
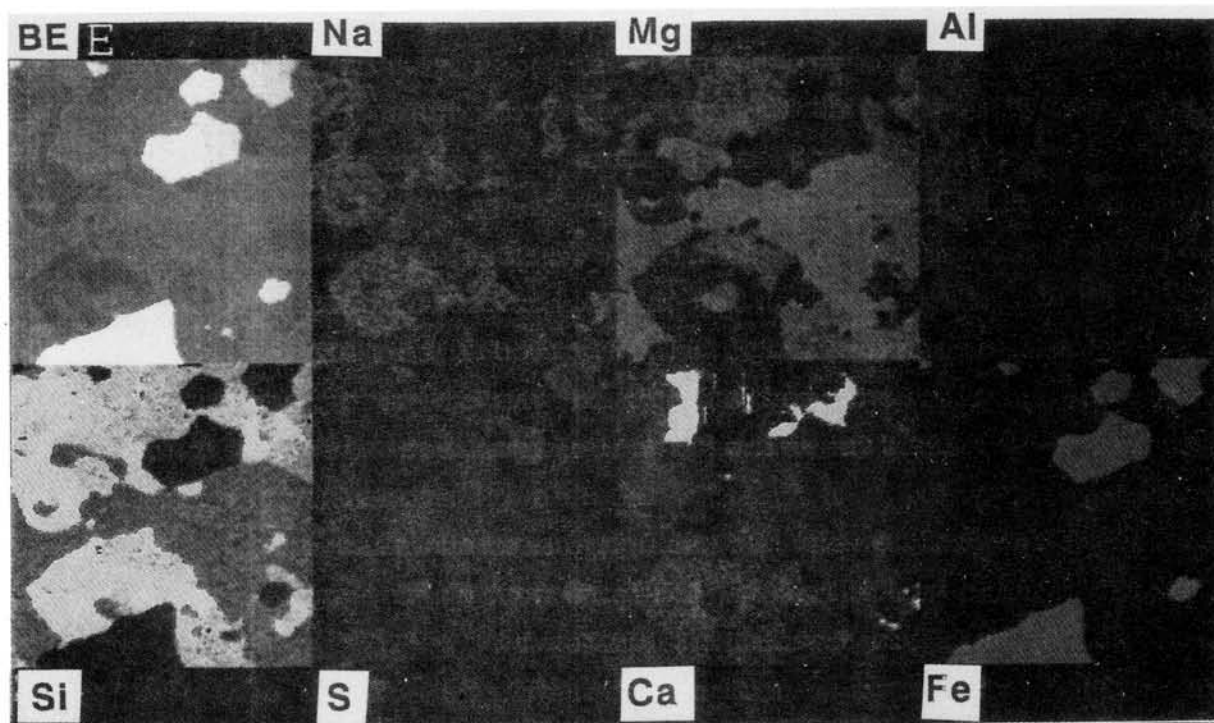
Fig.1 BE and X-ray maps of Cedar meteorite (H6).



X-ray intensity of Si
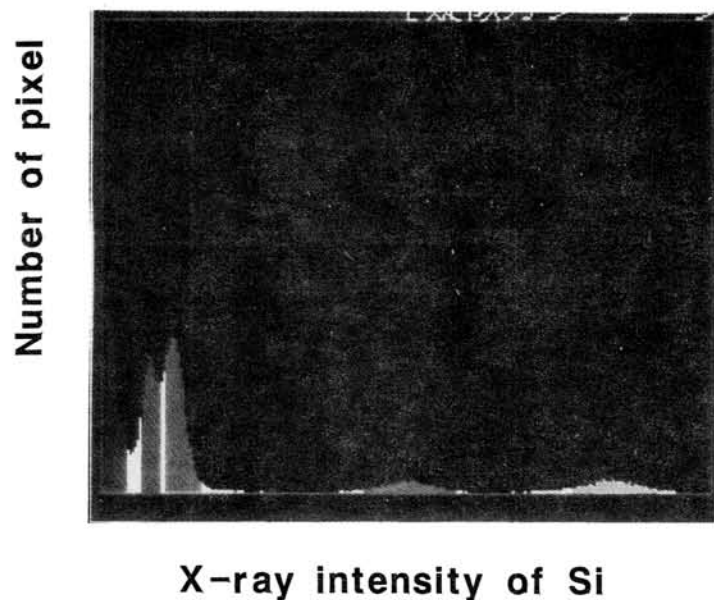
Fig.2 A histogram of X-ray intensities in the Si map of Fig.1.

Si

Fe
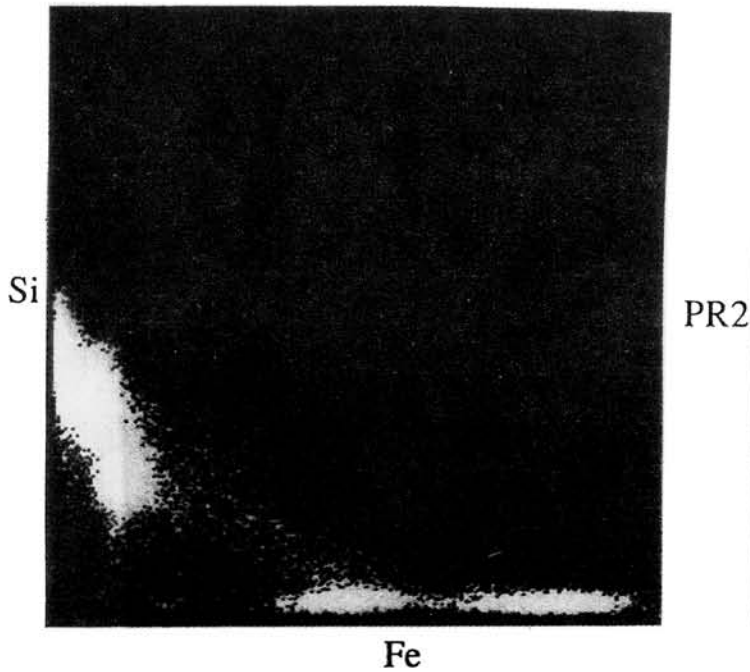
Fig.3  A scatter diagram using X-ray intensities in the Fe and Si maps of Fig.1.  Five phases can be recognized as clusters.



PR2

PR1
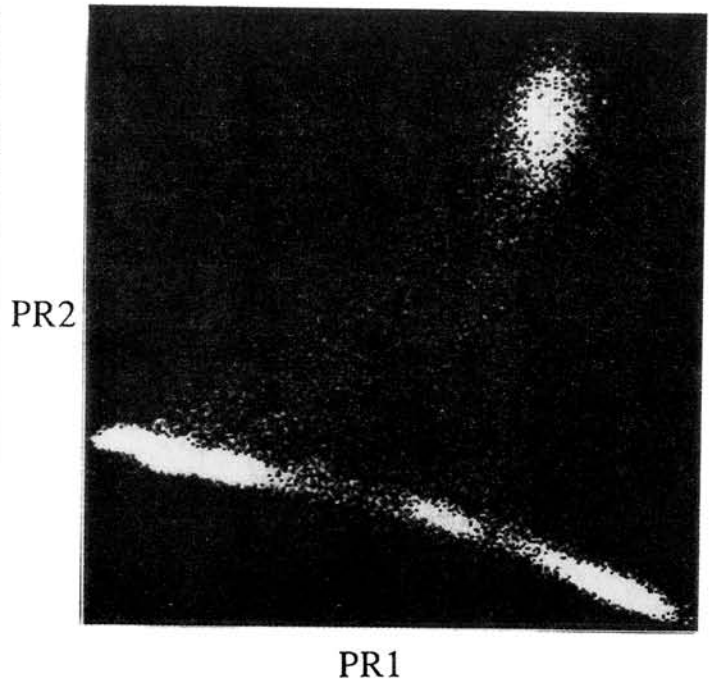
Fig.4  A scatter diagram using X-ray intensities of all the measured elements in Fig.1. PR1 and PR2 are the parameters obtained by transformation of coordinate system with variance-covariance matrix.



plagioclase (23.1%)

orthopyroxene (23.8%)

troilite (4.9%)

clinopyroxene (3.8%)

olivine (34.0%)

kamacite (8.7%)

taenite (1.4%)
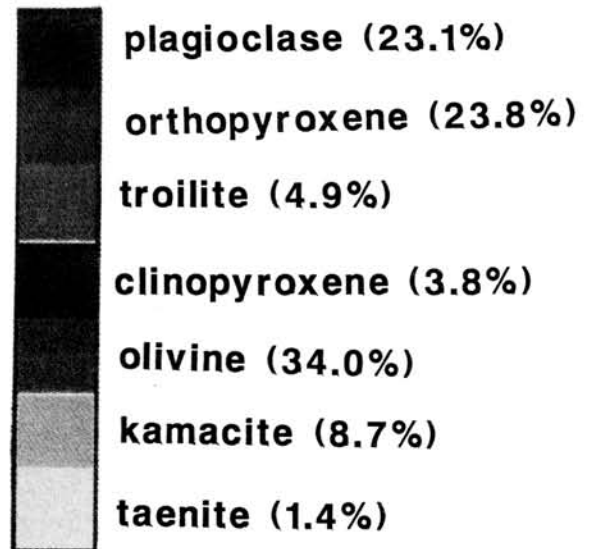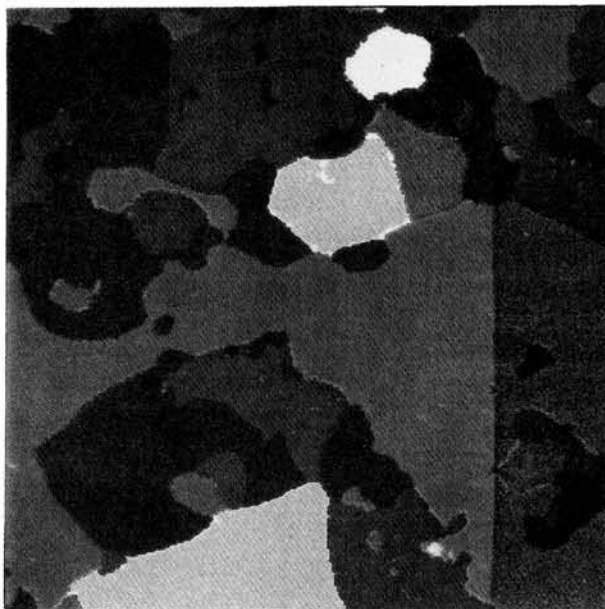
Fig.5 A result of phase separation on the BE image of Fig.1.

ISOTOPIC BEHAVIORS OF MG AND SI DURING GAS-CONDENSATION PROCESS
C.Uyeda and A.Tsuchiyama,
Institute of Earth and Planetary Science,College of General
Education,Osaka University, 560 Japan

The formation process of refractory grains in the prenormial solar nebula have been extensively studied through the isotopic fractionations found in refractory elements of primitive meteorites[1,2]. The isotopic behavior of evaporation process have been studied by Esat et al.[3] by measuring the magesium isotopic behavior of laboratory distillated pyroxene. The evaporation residues were fractionated towards the heavy isotopes, which were comparable to those of coarse grained CAI's of Allende meteorite. The condensates fractionating towards the light isotopes were comparable to those of fine grained CAI's. Further more, the residues of partially evaporated forsterite showed linear correlation between Si and Mg mass fractionation, which was comparable to that obtained for the coarse grained CAIs[4]. We have previously reported the Mg isotopic behavior of in the condensation process of a Mg-Si-H-O system[5]. The mass fractionation of Mg for condensates with respect to the initial source changed from positive to negative as the condensation temperature Tc decreased from 1300℃ to room temperature. The systematics of isotopic behavior between the silicate gas and the condensates was discussed in terms of the Rayleigh process. In the present work, the isotopic behavior of Si is studied and the correlation between Mg isotopic behavior is discussed.

The condensates were produced in a vacuum furnace under a constant hydrogen pressure of about 1.4Pa[6]. The evaporation source (synthesized $Mg_2SiO_4$) was placed at the bottom of a Mo crusible, and evaporated at about 1600℃ . A cold finger, which has a temperature gradient from 1500℃ to room temperature is inserted into the crusible from the top side of the furnace. As evaporation proceeded, Fo, Fo and Px mixtures and Mg-rich amorphous material condensed on the cold finger from 1400 to

900 ℃ , 900 to 600℃ and below 600℃ , respectively. This mineral sequence was reproducable through several truns of experiments [6]. For isotope measurements of Si and Mg, condensates of various condensation temperature $T_c$ were collected. A modified Hitachi IMA-2A microprobe analyzer was used for the isotopic measurement[7].

The obtained relation between isotopic fractionaion and Tc for Si is similar to the previously reported results of Mg[5]. $\Delta 28$, which is the amount of mass fractionation with respect to the starting material, varies from possitive to negative with the decreasing of Tc. The effective fractionation coefficient, $\alpha$ , for silicon at Tc=1300℃ is estimated to be $\alpha$ =1.014, which is considerably large compared to th calculated value for solid-gas equilibrium of 1.002-1.003[8]. The enhancement of $\alpha$ in the present experiment may be due to some kinetic effect, and further experiments are carried out to invenstigate the origin of this large $\alpha$ for both Mg and Si.

A linear correlation is seen between Mg and Si mass fractionation with respect to the initial source (Fig 1). The relation between $(\Delta 26)$ and $(\Delta 30)$ is analized based on the Rayleigh equation for Mg and Si. The temperature curve of conden- sates can be written as ,

$$(\Delta M)_s = \alpha_M f(T_c)^{\alpha-1}\{(\Delta M)_v{}^0 + 1000\} - 1000 \ ( \permil ),$$

where M=26 for Mg and 30 for Si. $\alpha_M$ is the effective fractionation factor of the condensate with respect to the gas phase, and f is the fraction of residual gas phase which can be estimated from the amount of condensates obtained on the cold finger. Thus the broken line is obtained as,

$$(\Delta 30) = a(\Delta 26) + b$$

where $a=\gamma \cdot \delta$ , $b=(\delta - 1) \times 1000$, and $\gamma = (\alpha_{30}-1)/(\alpha_{26}-1)$, $\delta = \alpha_{30}\{(\Delta 30)_v{}^0/1000 + 1\}/[\alpha_{26}\{(\Delta 26)_v{}^0/1000 + 1\}]^\gamma$ .

The numerical values for a and b are calculated as a=0.65 and b= 2‰. This gradient of Mg-Si correlation is comparable to that observed in the coarse grained CAI. Thus the existance of linear isotopic correlation in a refractory material does not necessesarily indicate that the material has been an evaporation residue.
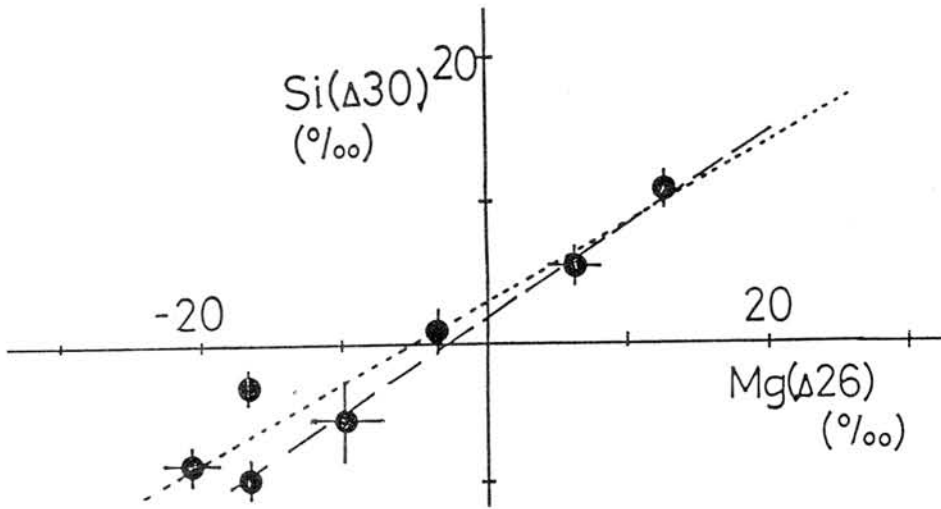


Fig.1 Relation betweenMg & Si mass fraction-nation for condensat esof various condensation temperatures.

$\triangle 26 = \{ (^{26}Mg/^{24}Mg)_{sample} / (^{26}Mg/^{24}Mg)_{initial} -1 \} \times 1000 ( ‰ )$

$\triangle 30 = \{ (^{30}Si/^{28}Si)_{sample} / (^{30}Si/^{28}Si)_{initial} -1 \} \times 1000 ( ‰ )$

References:

[1]LEE,T.,PAPANASTASSIOU,D.A. and WASSERBURG,G.J.,(1977) Geophys . Res. Lett.,3,109. [2]CLAYTON,R.N.,HINTON,R.W and Davis,A.M.(1988) Phil.Trans.R.Soc.Lond.A325,481. [3]ESAT,T.M. SPEAR,R.H. and TAYLOR,S.R.(1986)319,576. [4]DAVIS.A.M, HASHIMOTO,A.,CLAYTON.R.N.& MAYEDA,K.(1990) Nature 347,655. [5]UYEDA.C, TSUCHIYAMA,A.& OKANO,J. (1989b) Meteotitics 24 .[6]TSUCHIYAMA,A(1988)Abst.13th Symp.Antarctic ,123. [7]OKANO,J. and NISHIMURA,H.(1986) SIMS V, Benninghoven,A.etal.,254. [8]CLAYTON,R.N. et al.(1978)Proc Lunar Planet Conf.9th 1267

### ISOTOPIC AND CHEMICAL FRACTIONATIONS OF REFRACTORY ELEMENTS DURING CONDENSATION AND VAPORIZATION IN THE SOLAR NEBULA.

Akira Tsuchiyama and Chiaki Uyeda.
*College of General Education, Osaka University, Toyonaka 560, JAPAN.*

*Mass fractionation of Mg and Si isotopes during vaporization and condensation*

Recent experimental studies show that a large amount of isotopic mass fractionation of refractory elements, such as Mg and Si, takes place during vaporization and condensation [1-5] (Table 1). In these experiments, heavy isotopes are enriched in a condensed phase (solid or liquid) relative to gas irrespective of vaporization or condensation.

The isotopic mass fractionation has been applied to formation of CAI's, and it is believed that the high temperature events (vaporization and/or condensation) in the primordial solar nebula is responsible for the observed mass fractionation [1,2]. Esat and Ringwood [3] discussed fractionation of Mg isotopes during the formation of the Moon based on Mg isotopic fractionation in vaporization experiments of pyrolite, and gave constraint on the Al content of the bulk Moon. However, the isotopic mass fractionation has not been applied to the meteorite-planet system in the nebula as far as the authors know.

*Chemical composition and mass fractionation of chondrites and the Earth*

Correlation between some refractory lithophile elements has been known for bulk chondrite compositions. For example, Mg/Si ratios increase with increasing Al/Si ratios except for CO, CV and CM chondrites (*e.g.,*[6,7]). This correlation was explained in terms of Mg/Si fractionation between solid and gas at high temperatures in the solar nebula [6,7]. The primitive upper mantle (PUM) composition of the Earth was estimated from a compositional trend of lherzolites and the chondritic trend [6,7]. Because the PUM composition is different from that of CI chondrite, possibility of vaporization of Si and Mg during the formation of the Earth has been proposed [6,7].

If the Mg and Si contents of chondrites and the PUM are responsible for vaporization or condensation of Mg and Si, isotopic mass fractionation of these elements are expected. We can calculate isotope compositions of these materials based on the assumptions that (1) chondrites and the Earth were formed from a material with the solar composition, (2) solid/gas ratio was determined by equilibrium Mg/Si ratios of solid and gas, (3) fractionation of the isotopes was determined by separation between solid and gas with the effective isotopic fractionation factor in the experiments (Table 1), (4) little isotopes were fractionated by melting and crystallization, and (5) solid particles were so small that effect of diffusion in the solid to isotopic fractionation [2] was negligible during vaporization.

According to the calculations, the heavy isotopes are enriched in the Earth ( $\Delta(^{26}Mg)=+2‰$ and $\Delta(^{30}Si)=+4\sim+5‰$ for vaporization, and $\Delta(^{26}Mg)=+1‰$ and $\Delta(^{30}Si)=+2\sim+3‰$ for condensation), and the light isotopes in ordinary and enstatite chondrites ($\Delta(^{26}Mg)=-5\sim-19‰$ and $\Delta(^{30}Si)=-2-7‰$ for vaporization, and $\Delta(^{26}Mg)=-2\sim-8‰$ and $\Delta(^{30}Si)=-1\sim-4‰$ for condensation). Calculations based on the assumption that chondrites were formed from a material of the pyrolite composition [8] give similar results on the chondrites.

On the other hand, observed Mg and Si isotope compositions of chondrites and terrestrial materials show little fractionation [9-11] except for CAI's [1,9]. The isotopic fractionation was not detected either in lunar materials [3,10,11] or interplanetary dust except for a large glass spherule which experienced significant vaporization during entrance into the Earth's atmosphere [11].

*Equilibrium isotopic fractionation*

The above difference in expected fractionation from the experiments and observed fractionation can be explained by the following; (1) the variation in the Mg/Si ratios of chondrites and the Earth was not formed by vaporization and/or condensation but formed initially in heterogeneous nebula, or (2) the isotopic fractionation in the condensation experiments are kinetic as well as in the vaporization experiments, and the isotopes are distributed to solid and gas almost equally under equilibrium conditions at high temperatures. The first case seems to be unreasonable because the Mg-Si-Al systematics of the chondrites [6,7] can be hardly explained by the heterogeneous nebula. The second case is possible. In fact, the solid/gas isotopic fractionation of Si under equilibrium conditions at high temperatures was roughly calculated to be only about 2‰ [12].

In order to obtain more reliable data on solid/gas isotopic fractionation factor at equilibrium, a new experiment has been carried out. In this experiment, a fine powder of forsterite (<5 μm) are placed in a Knudsen cell of molybdenum, and heated at about $1500^{O}C$ in vacuum. Because the gas molecules (Mg and SiO) in equilibrium with the forsterite crystals are effused from the Knudsen cell according to the mass-dependent Knudsen equation with Rayleigh fractionation law, we can determine the isotope compositions of the equilibrated gas molecules by measuring the isotope compositions of a vaporization residue and fraction vaporized. Preliminary results indicate that the excess of the isotopic fractionation factor of Mg from unity is negligible although some diffusion effect in the forsterite particles is considered to be superimposed.

*Solid-gas fractionation process in the solar nebula*

If the isotopes are distributed to solid and gas almost equally at equilibrium as discussed above, the Mg/Si ratios and their isotopic compositions of chondrites and the PUM should be

determined by separation of solid and gas near equilibrium conditions in the nebula. In this case, we can constrain the fractionation process; rapid vaporization or condensation in the nebula without solid-gas equilibration should be eliminated. Probably vaporization of the elements from magma ocean on the Earth would give a large mass fractionation, and would be also eliminated. In this case, the composition of the Earth would be determined near equilibrium conditions in the nebula prior to accretion. The same discussion will be possible for S of the Earth based on the observed S isotope compositions [13] although experimental data on S isotopes has not been available at present.

References: [1] Esat T.M., Spear R.H. and Taylor S.R. (1986) *Nature*, **319**, 576-578. [2] Davis A.M., Hashimoto A., Clayton R.N. and Mayeda T.K. (1990) *Nature*, **347**, 655-958. [3] Esat T.M. and Ringwood A.E. (1990) *Lunar Planet. Sci.*, **XXI**, 329-330. [4] Uyeda C., Tsuchiyama A. and Okano J. (1990) *SIMS*, **VII**, 381-384. [5] Uyeda C. and Tsuchiyama A. (1991) this volume. [6] Jagoutz E., Palme H. Badenhaunsen H., Blum K., Cendales M., Dreibus G., Spettel G., Lorenz V. and Wanke H. (1979) *Proc. 10th Lunar Planet. Sci. Conf.*, 382-390. [7] Hart S.T. and Zendler A. (1986) *Chem. Geol.*, **57**, 247-267. [8] Ringwood A.E. (1989) *Earth Planet. Sci. Lett.*, **95**, 1-7. [9] Clayton R.N., Hinton R.W. and Davis A.M. (1988) *Phil. Trans. R. Soc. Lond.*, A **325**, 483-501. [10] Molini-Velsko C, Mayeda T.K. and Clayton R.N. (1986) *Geochim. Cosmochim. Acta*, **50**, 2719-2726. [11] Esat T.M., Brownlee D.E. Papanastassiou D.A. and Wasserburg G.J. (1979) *Science*, **206**, 190-197. [12] Clayton R.N., Mayeda T.K. and Epstein S. (1978) *Proc. 9th Lunar Planet. Sci. Conf.*, 1267-1278. [13] Chaussidon M., Albarede F. and Sheppard S.M.F. (1987) *Nature*, **330**, 242-244.

Table 1. Effective liquid/gas or solid/gas fractionation factors of Mg and Si isotopes in vaporization and condensatior experiments.

| $^{26}$Mg/$^{24}$Mg | $^{30}$Si/$^{28}$Si | Temp. [°C] | Pressure | Sample | Ref. |
|---|---|---|---|---|---|
| *Vaporization* | | | | | |
| 1.031 | 1.014 | 1900-2050 | vacuum | Fo-melt | [2] |
| 1.028 | | ≤2000 | vacuum | Pyrolite-melt | [3] |
| 1.017 | | 1500-1550 | 1 Pa H$_2$ | Fo-powder(<5μm) | [4] |
| *Condensation* | | | | | |
| 1.017 | 1.011 | RT-1400 | 1 Pa H$_2$ | Fo-En | [4,5] |

Fo: forsterite
En: enstatite
RT: room temperature

# NITROGEN ISOTOPIC COMPOSITION OF A PRIMITIVE ACHONDRITE Y-74063

Sugiura,N. and Hashizume,K.
Geophys. Institute, Faculty of Sci., Univ. of Tokyo, Tokyo, Japan

As a pilot study on the possibility of using nitrogen isotopic composition for classification of meteorites, a primitive achondrite Y-74063 was examined. Primitive achondrites are roughly subdivided into two groups; Winonaites and Lodranites (Nagahara et.al., 1990). Oxygen isotopic composition of the two groups are slightly different but intra-group difference is also quite large, making oxygen isotope classification somewhat unconvincing. Thus another measure for classification is desired. Nitrogen isotopic composition is diverse among meteorites and could be useful for classification. A previous study (Sturgeon and Marti, 1991) showed that Acapulco (a member of the Lodranite group according to the oxygen isotope classification) has a nitrogen isotopic composition (-110.5 permil) which is quite distinct from the other groups of meteorites, making nitrogen isotopic classification easy for this group.

Y-74063 is one of the primitive achondrites found in antarctica, belonging to the Lodranite subgroup. 38.66 mg of bulk sample was used for the nitrogen measurement which was done using a static mass-spectrometry system (Hashizume and Sugiura, 1990). The result of stepped combustion is shown in the figure. The lowest delta value is -122.6 permil at 1100 C, which is close to that obtained for Acapulco (-110.5 permil). At lower temperatures, the anomaly is smaller due to mixing with terrestrial nitrogen (probably organic comtamination). The abundance of isotopically light nitrogen (released at 800 C and higher temperatures) is 2.3 ppm as compared with 1.21 ppm for Acapulco (released by pyrolysis at 1080 C and higher temperatures). On the nitrogen isotopic composition vs abundance diagram (Kung and Clayton, 1978) Acapulco and Y-74063 occupy a small area, suggesting that they belong to the same group.

Although nitrogen isotopic data are not available for Winonaites at present, the present data suggest that classification of meteorites according to the nitrogen isotope is quite hopeful.

References
K.Hashizume and N.Sugiura, Mass Spectroscopy, 38 (1990) 269.
C.C.Kung and R.N.Clayton, Earth Planet. Sci. Lett., 38 (1978) 421.
N.Nagahara,T.Fukuoka, I.Kaneoka, M.Kimura, H.Kojima, I.Kushiro, H.Takeda, A.Tsuchiyama and K.Yanai, 15th Symp. Antarctic Meteorites, (1990) 92.
G.Sturgeon and K.Marti, Proc. Lunar Planet. Sci. 21(1991)523.

50
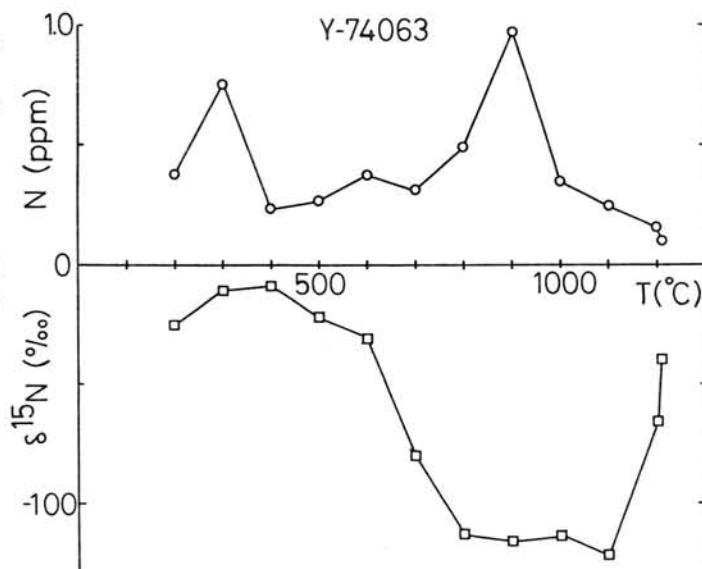
NITROGEN ISOTOPIC COMPOSITION OF A GAS RICH CHONDRITE ALH-77216

Sugiura,N. Kiyota,K. and Hashizume,K.
Geophysical Institute, Faculty of Science, Univ. of Tokyo, Tokyo, Japan.

Introduction. From the studies of nitrogen isotopes in lunar soils which is supposed to be solar wind origin, it was found that nitrogen isotopic composition has changed from -200 permil about 4 b.y. ago to the present value of about 300 permil. There are two explanations for this unexpected change in the isotopic composition. 1) The composition of the solar wind has changed due to the change in the condition of generating the wind on the surface of the sun. 2) It is due to a decreasing amount of the lunar nitrogen emanating from the interior of the moon that was implanted into the ancient soils. To solve this problem, we measured nitrogen isotopic composition of a gas rich meteorite ALH-77216 which contains a lot of solar wind nitrogen.

Results. It was found that the nitrogen in the gas rich meteorite is heavy isotopically (more than 150 permil compared with air nitrogen). This is the first direct confirmation that the nitrogen in gas rich meteorites is really heavy, although previous studies found slightly heavy ( =30 permil) nitrogen in gas rich meteorites. The abundance of the (presumably) solar nitrogen is about 1 ppm (assuming the real isotopic ratio is 300 permil). The abundance of the solar $^{22}Ne$ and solar $^{36}Ar$ are both of the order of $10^{-6}$ ccSTP/g. The abundance ratio of nitrogen to rare gases is similar to that observed for lunar soils and breccias, suggesting that the isotopically heavy nitrogen is of solar wind origin.

Discussion. Since gas rich meteorites are supposedly formed long time ago (although the exact ages are not determined), we tentatively conclude that the solar wind nitrogen has been heavy all the time. Then it seems likely that the light nitrogen observed in lunar soils is due to lunar nitrogen emanating from the interior of the moon. In other words, the indigenous lunar nitrogen seems to be isotopically light. The isotopic composition of indigenous lunar nitrogen has previously been estimated to be nearly normal (close to that of terrestrial air), conflicting with the present conclusion. We note that previous studies were made in 1970's and the quality was not good (no stepwise heating was done).

Implications. If the indigenous lunar nitrogen is really isotopically light, it has important implications on the origin of the moon. A straightforward interpretation would be that the moon and the earth originated in a different part of the solar nebular. It is not known, however, if the air nitrogen really represents the bulk terrestrial nitrogen, because hydrodynamic escape of the air could fractionate the isotopic composition of the air nitrogen. In any case, the indigenous lunar nitrogen isotopic composition should be determined by direct measurements of nitrogen in lunar igneous rocks.

# THE ORIGIN AND THE TRAPPING SITES OF THE PRIMORDIAL ARGON IN THE UOCS; THE CORRELATION WITH THE ANOMALOUS NITROGEN.

Hashizume, K. and Sugiura, N.
Geophysical Institute, University of Tokyo, Tokyo 113, JAPAN.

Primordial rare gases heavier than argon in primitive chondrites are known to be concentrated in the so called *phase "Q"* which is insoluble in HF/HCl but soluble in oxiding reagents. In case of carbonaceous chondrites, the amount of the heavy rare gases in the Q-phase accounts approximately 80% of the total amount. The Q-type rare gases are also observed in the unequilibrated ordinary chondrites (UOCs), although their amount accounts only 20-40% (in case of argon) of the total amount, which suggest the existence of some other phases where the major portion of the heavy rare gases is trapped.

We have measured isotopes of nitrogen and argon by a mass-spectrometer with a high sensitivity. The gases are extracted stepwisely from 200°C up to 1200°C in an oxygen atmosphere. We have measured more than 20 ordinary chondrites including 8 UOCs. Some of them contain nitrogen components with strikingly anomalous isotopic ratio, which suggests a possibility that their host minerals have not been equilibrated with the solar nebular gas.

In case of Y-74191 (L3.7), a nitrogen isotopic anomaly of up to nearly $\delta^{15}N \sim +750\,^0/_{00}$ has been observed in bulk sample. The release profile of the anomalous nitrogen and the primordial argon during the stepwise combustion of a bulk Y-74191 is described in fig. 1, where the "excess-$^{15}$N" is defined by, excess-$^{15}N \equiv \delta^{15}N_{AIR} \times [N] \times (^{15}N/^{14}N)_{AIR}$. The amount of the anomalous nitrogen released at each temperature fraction seems to have a good correlation with that of the primordial argon. A significant portion of the anomalous nitrogen and the primordial argon was lost by acid treatments, although they still had a good correlation. The excess-$^{15}$N and the primordial-$^{36}$Ar observed in the residues after various chemical treatments are plotted in fig. 2. Each plot represents different temperature fraction. The observed correlation suggests that the anomalous nitrogen and the primordial argon are trapped in the same sites. Consequently, a significant portion of the primordial argon in Y-74191 may be of extra-solar origin just like "planetary"-neon.
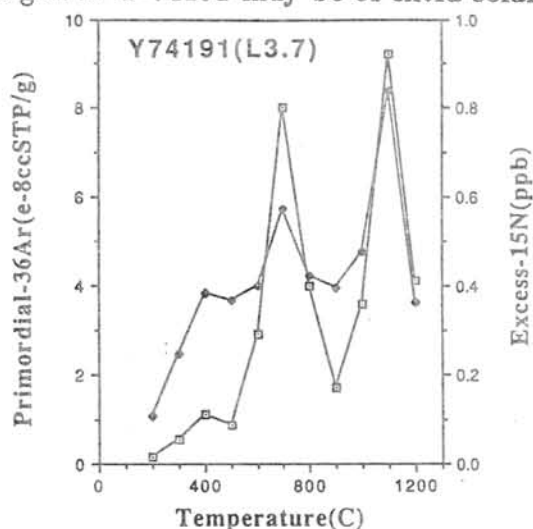


Fig 1. The release profile of the anomalous nitrogen and the primordial argon in bulk Y74191. The amount of the anomalous nitrogen is expressed by excess-$^{15}$N. The filled marks and the open marks represent nitrogen and argon, respectively.
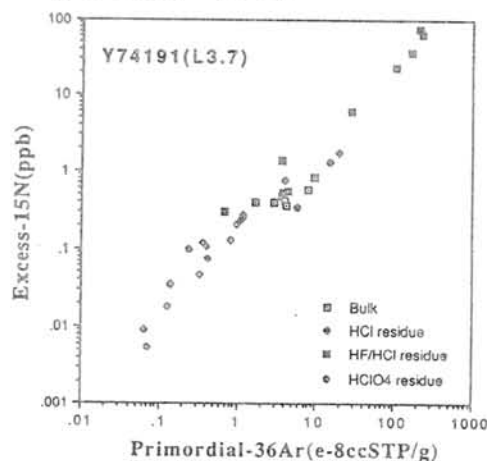


Fig 2. The correlation between the anomalous nitrogen and the primordial argon observed in Y74191 after various chemical treatments.

In case of ALH-77214 (L3.4), an anomaly whose $\delta^{15}N \sim -200\,{}^0\!/_{00}$ has been observed in bulk sample. As is shown in fig. 3, the release profile of the negative excess-$^{15}N$ (which means an isotopically light nitrogen component is released) apparently seems to correlate with that of the primordial argon. However, as shown in fig. 4, most of the primordial argon peak but only one of the two negative peaks of the excess-$^{15}N$ disappeared after HCl treatment. This suggests that the anomalous nitrogen is not always sited together with the primordial argon. At present, we cannot conclude anything about the origin of the primordial argon in this meteorite, except that the majority (more than 90%) of the primordial argon in this meteorite is *not* sited in the Q-phase, since most of the primordial argon is observed to be removed by the acid treatment.

The correlation between the release of the excess-$^{15}N$ and that of the primordial argon is also observed in other UOCs, although the trend is not clear due to their small nitrogen isotopic anomaly (relative to those of Y-74191 and ALH-77214). The detail of these data will be shown at the symposium.
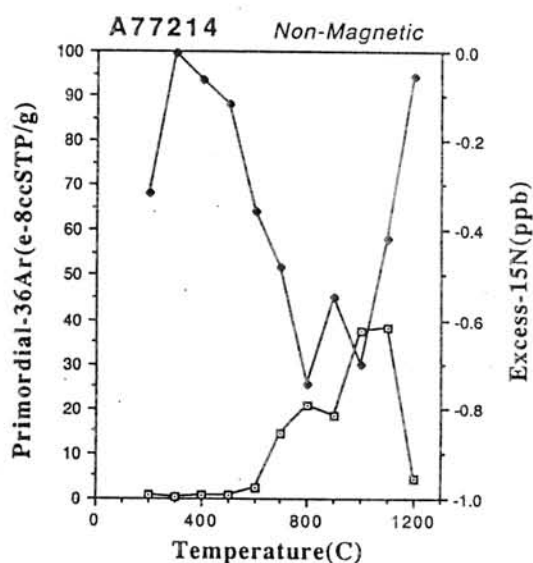


Fig 3. The release profile of the anomalous nitrogen and the primordial argon in ALH-77214 *non-magnetic* fraction (97.3 *wt*% of the bulk). Notations are identical to those of fig. 1.
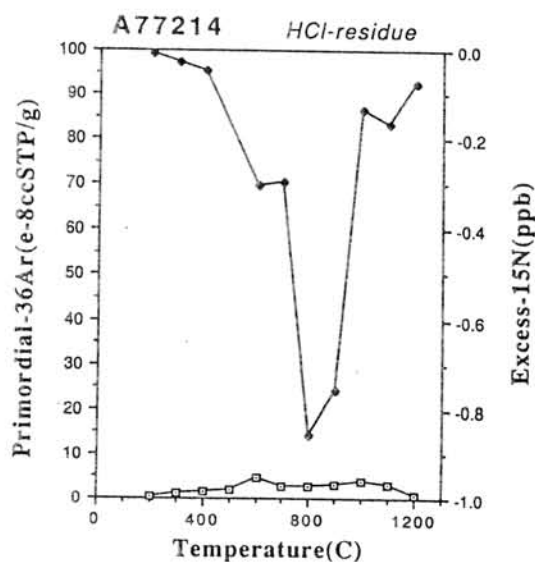
Fig 4. The release profile of the anomalous nitrogen and the primordial argon in ALH-77214 *HCl-residue* (14.8 *wt*% of the bulk). Notations are identical to those of fig. 1.

# $^{81}$KR TERRESTRIAL AGES AND GROUPING OF YAMATO EUCRITES

Yayoi MIURA[1], Keisuke NAGAO[1] and Tatsuya FUJITANI[2]
1)Institute for Study of the Earth's Interior, Okayama University,
  Misasa, Tottori 682-01, Japan
2)Marine Technical College, Nishikura-cho, Ashiya, Hyogo 659, Japan

## 1. Introduction

More than 50 eucrites have been recovered on Yamato area in Antarctica (Yanai, 1987). Among these, 12 Yamato eucrites have been divided into five groups corresponding to different falls by Nagao and Ogata (1989). In this study, the terrestrial ages, cosmic-ray exposure ages and grouping have been determined for other 14 Yamato eucrites. Xe isotopic compositions and Pu content estimated from fissiogenic Xe have been also discussed.

Generally, terrestrial age of meteorite is measured with cosmogenic radioactive nuclides such as $^{14}$C, $^{36}$Cl and $^{81}$Kr. $^{81}$Kr method used in this work is available for meteorites having terrestrial ages around the half life of $^{81}$Kr, $2.1 \times 10^5$ years. However, its concentration in equilibrium state is as low as about $10^{-13} cm^3 STP/g$, corresponding to $10^6$ atoms, even in the meteorite richest in $^{81}$Kr. Measurement of such a small amount of $^{81}$Kr needs a noble gas mass spectrometer with high sensitivity and high resolution.

The cosmic-ray exposure age using cosmogenic Kr can be calculated by,

$$T_a = (1/\lambda)(P_{81}/P_{83})(^{83}Kr/^{81}Kr)_c$$

If this equation is applied to the meteorite having long terrestrial age, the calculated age is longer than the true exposure age due to the radioactive decay of $^{81}$Kr on the earth. From this apparent exposure age ($T_a$) and true exposure age ($T_e$), the terrestrial age ($T_t$) can be calculated by,

$$T_t = (1/\lambda)\ln(T_a/T_e)$$

In this study, true exposure age was estimated from cosmogenic stable $^{38}$Ar, whose production rate was calculated using the function as chemical compositions of each meteorite proposed by Freundel et al. (1986) except for 5 eucrites. Mean production rate of Yamato eucrites reported before were used for the 5 eucrites for which chemical compositions have not been analyzed yet.

## 2. Results and discussion

Terrestrial ages of 14 Yamato eucrites measured in this work are in the range from 0 to 0.28 Ma. These eucrites can be divided into 7 groups, designated as from A to G in Table 1. Seven eucrites Y-75011, 790020, 791826, 793547, 793548, 793570 and 794002 with short terrestrial ages and long exposure ages belong to one group already reported. Y-792511, 793164 and 794043 belong to three groups. As the cosmic-ray exposure ages of Y-82049 and 82052 are similar to those of remaining group reported before, these two may belong to the group. However, their terrestrial ages slightly disagree with the age of reported group. Although the terrestrial age and exposure

age of Y-82066 are similar to those of Y-793164, disagreements in concentrations of $^4$He and $^{40}$Ar between these eucrites suggest a new group for Y-82066. Y-82082 has long exposure age similar to the age of the first group designated as group A, whereas its terrestrial age was much longer than those of the group. The concentrations of $^4$He and $^{40}$Ar were also largely different from those of the first group. These results imply the seventh group for Yamato eucrites. Therefore, it seems that there are two new groups corresponding to different falls in addition to the five groups already reported for Yamato eucrites. Major elements and rare earth elements of nine eucrites were analyzed and the results support the grouping based on noble gases, the terrestrial and the cosmic-ray exposure ages (Miura et al., 1991).

High concentrations of extinct radioactive $^{244}$Pu in eucrites were implied from the fissiogenic Xe in these eucrites. Heavy Xe isotopes were plotted on a mixing line between U-Xe (Takaoka, 1972) and $^{244}$Pu-fission-Xe. Estimated $^{244}$Pu content in Y-793164, which has larger amount of fissiogenic Xe than the other eucrites, is $1 \times 10^{-9}$g/g. On the other hand, $^{244}$Pu contents could be estimated to be $(0.8-1.3) \times 10^{-9}$g/g using the measured uranium content of 190ppb (Miura et al., 1991) and the $^{244}$Pu/$^{238}$U ratio of 0.004-0.007 for early solar system (Podosek and Swindle, 1988). The $^{244}$Pu content estimated above is in good agreement with the content from fission-Xe.

Reference: Yanai,K. (1987), in *Science in Antarctica, Series 6.* eds. K.Yanai, H.Takeda and A.Shimoyama (Natl. Inst. Polar Res., Tokyo) 45-57; Nagao,K. and Ogata,A. (1989), *Mass Spec.,* 37, 313-324; Freundel,M., Schultz,L. and Reedy,C. (1986), *Geochim. Cosmochim. Acta,* 50, 1-11; Takaoka,N. (1972) *Mass Spec.,* 20, 287-302; Podosek,F.A. and Swindle,T.D. (1988), in *Meteorites and the Early Solar System.* eds. J.F. Kerridge and M.S.Mattews (Tucson:Univ. of Arizona Press), 1093-1113; Miura,Y., Nagao,K. and Fujitani,T. (1991) Submitted to Geochim. Cosmochim. Acta.

Table 1. Concentrations and isotopic ratios of He, Ne and Ar in Yamato eucrites. Cosmic-ray exposure ages(T38), apparent ages(Ta) and terrestrial ages(Tt) are also given.

| Eucrite | $^3$He | $^4$He | 3/4 | $^{20}$Ne | $^{21}$Ne | $^{22}$Ne | 20/22 | 21/22 | $^{36}$Ar | $^{38}$Ar | $^{40}$Ar | 38/36 | 40/36 | (38Ar)c | T38 | Ta | Tt | Group |
|---|---|---|---|---|---|---|---|---|---|---|---|---|---|---|---|---|---|---|
| Y-75011 | 654 | 101000 | 0.00638 ±.00026 | 133 | 135 | 168 | 0.7908 ±.0010 | 0.8055 ±.0029 | 63.2 | 89.8 | 28800 | 1.421 ±.003 | 455.5 ±.5 | 88 | 70 ±8 | 64 ±7 | -0.03 ±.05 | A |
| Y-790020 | 724 | 67100 | 0.01079 ±.00010 | 128 | 121 | 144 | 0.8902 ±.0012 | 0.8415 ±.0098 | 62.6 | 92.7 | 24900 | 1.482 ±.008 | 397.9 ±1.4 | 92 | 70 ±7 | 66 ±10 | -0.02 ±.05 | A |
| Y-791826 | 635 | 64700 | 0.00982 ±.00040 | 134 | 138 | 170 | 0.7880 ±.0006 | 0.8095 ±.0029 | 57.0 | 80.3 | 28300 | 1.406 ±.003 | 496.5 ±.9 | 79 | 61 ±7 | 67 ±4 | 0.03 ±.04 | A |
| Y-792511 | 220 | 36200 | 0.00608 ±.00025 | 43.9 | 42.5 | 53.2 | 0.8247 ±.0008 | 0.7984 ±.0003 | 16.8 | 22.9 | 14200 | 1.366 ±.007 | 846.4 ±7.1 | 22 | 17 ±2 | 27 ±2 | 0.14 ±.04 | B |
| Y-793164 | 90.0 | 38900 | 0.00231 ±.00009 | 14.7 | 14.0 | 17.4 | 0.8460 ±.0009 | 0.8081 ±.0029 | 9.19 | 12.0 | 27500 | 1.303 ±.008 | 2993.0 ±20.2 | 12 | 8.5 ±1.1 | 12 ±1 | 0.11 ±.05 | C |
| Y-793547 | 741 | 72600 | 0.01021 ±.00041 | 164 | 169 | 207 | 0.7909 ±.0007 | 0.8141 ±.0029 | 63.0 | 88.8 | 30100 | 1.410 ±.003 | 477.8 ±.6 | 87 | 68 ±8 | 72 ±5 | 0.02 ±.04 | A |
| Y-793548 | 677 | 77200 | 0.00877 ±.00036 | 136 | 139 | 171 | 0.7936 ±.0008 | 0.8106 ±.0029 | 55.6 | 79.0 | 29300 | 1.420 ±.003 | 526.6 ±.7 | 78 | 58 ±7 | 73 ±5 | 0.07 ±.04 | A |
| Y-793570 | 691 | 71000 | 0.00974 ±.00040 | 151 | 155 | 190 | 0.7947 ±.0006 | 0.8167 ±.0029 | 60.7 | 85.7 | 28800 | 1.412 ±.003 | 474.3 ±.6 | 88 | 66 ±8 | 60 ±3 | 0.03 ±.04 | A |
| Y-794002 | 686 | 61800 | 0.01110 ±.00045 | 163 | 168 | 204 | 0.8003 ±.0006 | 0.8269 ±.0029 | 62.5 | 88.2 | 25600 | 1.411 ±.003 | 409.4 ±.6 | 87 | 68 ±8 | 60 ±4 | 0.04 ±.04 | A |
| Y-794043 | 317 | 24000 | 0.01319 ±.00054 | 57.5 | 56.5 | 71.3 | 0.8064 ±.0011 | 0.7917 ±.0032 | 16.6 | 22.8 | 15600 | 1.374 ±.006 | 940.9 ±4.3 | 22 | 17 ±2 | 42 ±9 | 0.28 ±.08 | D |
| Y-82049 | 161 | 4640 | 0.03461 ±.00033 | 30.1 | 27.4 | 33.7 | 0.8924 ±.0013 | 0.8119 ±.0094 | 7.99 | 9.99 | 12000 | 1.250 ±.014 | 1501.9 ±20.5 | 9.7 | 7.4 ±.7 | 13 ±2 | 0.19 ±.05 | E |
| Y-82052 | 170 | 3910 | 0.04360 ±.00041 | 35.7 | 26.2 | 32.0 | 1.1166 ±.0012 | 0.8203 ±.0095 | 8.25 | 9.96 | 11400 | 1.208 ±.006 | 1382.0 ±6.6 | 9.6 | 7.3 ±.7 | 12 ±1 | 0.14 ±.05 | E |
| Y-82066 | 14.0 | 7160 | 0.00196 ±.00002 | 16.2 | 16.2 | 20.1 | 0.8055 ±.0041 | 0.8065 ±.0094 | 8.70 | 12.3 | 16500 | 1.415 ±.025 | 1896.1 ±31.7 | 12 | 9.3 ±.9 | 14 ±2 | 0.13 ±.05 | F |
| Y-82082 | 670 | 16300 | 0.04112 ±.00039 | 91.8 | 95.5 | 111 | 0.8237 ±.0011 | 0.8567 ±.0100 | 51.5 | 77.2 | 11000 | 1.498 ±.007 | 213.5 ±.6 | 77 | 59 ±6 | 98 ±13 | 0.16 ±.05 | G |

Concentrations of He, Ne and Ar are given in unit of $10^{-9}$cm$^3$STP/g. Ages T38, Ta and Tt are in unit of Ma.

# $^{10}$Be IN METEORITIC CARBONS

H.Nagai[1],M.Honda[1],M.Asano[1],M.Imamura[2] and K.Kobayashi[3]
1)College of Human.and Sci.,Nihon Univ.,Setagaya,Tokyo156
2)Institute for Nuclear Study,Univ.of Tokyo,Tanashi,Tokyo188
3)Res.Center for Nucl.Sci.and Tech.,Univ.of Tokyo,Bunkyo,Tokyo113

We have been investigated distributions of long-lived cosmogenic nuclides, $^{10}$Be and $^{26}$Al, in different target materials in meteorites, i.e. in metals (Fe,Ni) and in silicates (O, Mg, Si$\cdots$). The contents of cosmogenic nuclides are variable with targets and also depend on size of meteorite and irradiated position(shielding). The last factor is correlated to the type of nuclear reactions, such as high energy production (large $\Delta A$) or low energy production (small $\Delta A$). $^{10}$Be and $^{26}$Al in metal, $^{10}$Be in silicate and $^{26}$Al in silicate were examples for high, medium and low energy products, respectively. Last year we found extremely higher $^{10}$Be contents in carbon fraction of Landes(IA)[1] and Campo del Cielo(IA, El Taco )[2]. The observed $^{10}$Be contents in carbon were 6 to 7 times higher than those in silicates. We report here similar high $^{10}$Be contents in carbon fractions separated from Odessa (IA) and Zagora (IAB).

The meteorites were crushed and sieved first, then the stone fractions finer than 200 mesh were separated magnetically. Before separation of silicate and carbon fraction, Zagora was treated with HF + HCl till the sample weight was reduced to about 6% of the initial weight. Silicate and carbon fractions were separated by using a heavy liquid (d=2.5). The carbon content in lighter fraction was determined by weight loss after an ignition in air at 700°C. To each sample was added 0.3-0.5 mg Be carrier and only to metal sample was added 1mg Al carrier. After purification by anion and cation exchange techniques, each sample was converted to the oxide for AMS (Accelerator Mass Spectrometry)[3,4]. AMS measurements of $^{10}$Be and $^{26}$Al were performed at the tandem accelerator facility at the Research Center for Nuclear Science and Technology, University of Tokyo[3,4].

The results are shown in Table 1. To estimate the contents (or production rates) of $^{10}$Be and $^{26}$Al in each "pure" fraction, small corrections of silicate contamination were made for metal samples, 0.014% for Odessa and 0.02% for Zagora, and for carbon samples. Relatively large correction was made for Zagora silicate fraction considering the chemical composition. The estimated $^{10}$Be and $^{26}$Al contents in metal, silicate and carbon in five iron meteorites are shown in Table 2. The dif-

ferences of shielding conditions among five samples were clearly shown in the ratios of $^{10}$Be(silicate/metal) and $^{26}$Al(silicate/metal). On the contrary, $^{10}$Be(silicate/carbon) was almost constant.

Table 1    $^{10}$Be and $^{26}$Al contents found in iron meteorites

| Sample, Class | | Weight (mg) | Carbon Content (%) | $^{10}$Be found (dpm/kg) | $^{26}$Al found (dpm/kg) |
|---|---|---|---|---|---|
| Odessa, I A | [M] | 1378 | – | 0.667±0.061 | |
| | [S] | 74.8 | (0) | 7.48 ±0.78 | |
| | [C] | 19.5 | 90 | 45.4 ±3.9 | – |
| Zagora, I AB | [M] | 383.2 | – | 2.98 ±0.32 | |
| | [S] | 312 | (0) | 13.2 ±0.5 | 64.1±2.7 |
| | [C] | 4.9 | 75 | 91.5 ±8.5 | – |
| | [C] | 18.6 | 74 | 91.3 ±8.2 | – |

[M]:metal, [S]:silicates, [C]:carbon

Table 2    Estimated $^{10}$Be and $^{26}$Al contents in metal, silicate and carbon fraction of meteorites.

| Sample | Estimated contents (dpm/kg) | | | | |
|---|---|---|---|---|---|
| | Metal | | Silicates | | Carbon |
| | $^{10}$Be | $^{26}$Al | $^{10}$Be | $^{26}$Al | $^{10}$Be |
| Landes*, I A | 5.4 | 3.8 | 23 | 86 | 141 |
| Zagora | 3.0 | | (17) | 64 | 117 |
| Odessa | 0.67 | | 7.5 | | 50 |
| Campo del Cielo**, I A(El Taco) | 0.014 | 0.0084 | 0.13 | 0.64 | 0.77 |
| Y790981,Ureilite* | – | – | 18 | (30) | 84 |

* ref.[1], ** ref.[2]

REFERENCES
[1] H.Nagai,M.Imamura,K.Kobayashi,K.Yoshida,H.Ohashi and M.Honda, (1990)Nucl.Instr.Meth.,B52,568-571
[2] H.Nagai,I.Kobayashi,M.Honda,M.Imamura and K.Kobayashi,(1990) Meteoritics,25,390
[3] M.Imamura,Y.Hashimoto,K.Yoshida,I.Yamane,H.Yamashita,T.Inoue, S.Tanaka,H.Nagai,M.Honda,K.Kobayashi,N.Takaoka and Y.Ohba, (1984)Nucl.Instr.Meth.,B5,211-216
[4] H.Nagai,T.Kobayashi,M.Honda,M.Imamura,K.Kobayashi,K.Yoshida and H.Yamashita,(1987)Nucl.Instr.Meth.,B29,266-270

STUDY ON NOBLE GAS DISTRIBUTION IN CARBONACEOUS CHONDRITES
USING LASER MICROPROBE

Keisuke NAGAO, Atsumi OGATA and Yayoi MIURA
Institute for Study of the Earth's Interior, Okayama University, Misasa, Tottori
682-01, Japan.

## Introduction

Noble gases play an important and unique role in study of the history of our solar system. In this study, primitive meteorites such as carbonaceous chondrites have special importance because of the primordial noble gas components and radiogenic noble gas isotopes from extinct nuclides trapped in the meteorites. It is well known that the primordial noble gases are distributed heterogeneously in these meteorites. Their carriers are mainly carbon, diamond and silicon carbide etc. (e.g. Anders, 1988; Amari $et$ $al$., 1990). Although various investigations have been carried out to find out the relationship between noble gas components and their carrier phases, it has not been known well until now.

## Experimental method

This study attempts to investigate noble gas components and their carrier phases by melting a small portion of meteorite using laser microprobe and by measuring all noble gas isotopic compositions. The laser unit employed in this work was pulse YAG laser. The wave length of the YAG laser is 1.064 $\mu$m. The maximum output energy of a single pulse is 470 mJ. Plates of about 0.8 mm thick cut out from a meteorite block were used for noble gas analysis. Noble gases evolved from laser pit were purified and admitted to a noble gas mass spectrometer. Sensitivities and mass discrimination correction factors of the mass spectrometer were determined by measuring known amounts of atmospheric noble gases. Blank levels were $8 \times 10^{-11}$, $5 \times 10^{-12}$, $3 \times 10^{-12}$, $8 \times 10^{-10}$, $8 \times 10^{-14}$ and $1 \times 10^{-14}$ cm$^3$STP for $^4$He, $^{20}$Ne, $^{36}$Ar, $^{40}$Ar, $^{84}$Kr and $^{132}$Xe, respectively. The estimated weights of a laser pit was 40 and 200 $\mu$g for aperture-in and -out mode, respectively.

## Results and discussion

More than 40 points of Allende and Murchison carbonaceous chondrites have been analyzed. Some of the interesting results obtained until now are followings;

1) Anomalously high concentrations of $^4$He, $^{40}$Ar and $^{129}$Xe in CAIs of Allende imply high concentrations of volatile elements K and I as well as high U content in the CAIs. The high concentrations of K and I estimated from $^{40}$Ar and $^{129}$Xe concentrations in the CAIs were 0.7 wt.% and 2 ppm, respectively. High concentrations of Na and Br in the CAIs were also suggested by low $^{20}$Ne/$^{22}$Ne, and high $^{80}$Kr/$^{84}$Kr and $^{82}$Kr/$^{84}$Kr ratios, respectively. As CAIs are thought to be high temperature condensates, the high concentrations of volatiles in CAIs are difficult to be explained by the condensation model.

2) Isotopic ratios of trapped Ne in chondrules are different between Allende and Murchison. The $^{20}$Ne/$^{22}$Ne ratios were 10.3 and 12.5 for Allende and Murchison, respectively. The former ratio is similar to that of Ne-C, and

the latter is of Ne-B. The differences may suggest different circumstances for chondrule formation of these chondrites.

3) Ne isotopic ratios of CAI of Allende show another trend implying low $^{20}Ne/^{22}Ne$ ratio of 5.9 for trapped component. However, the ratios might be lowered by Na spallation in the CAI.

4) Noble gas concentrations and isotopic ratios show wide variations even in a single chondrule or in a CAI.
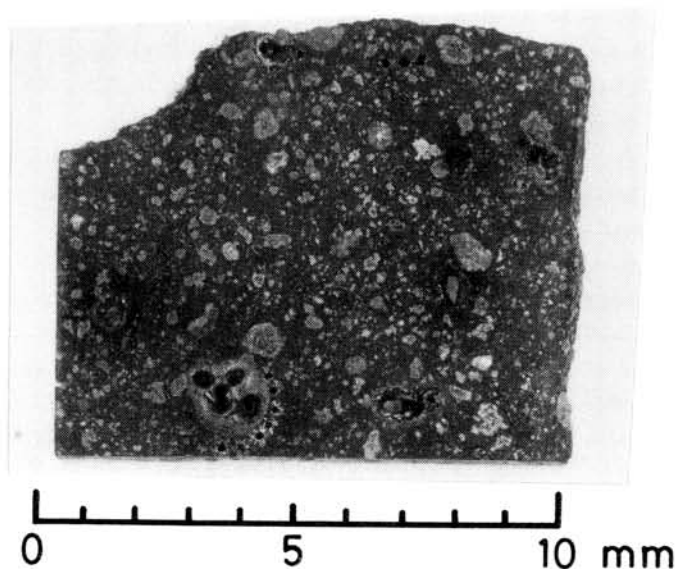


Photograph showing laser pits produced in a plate of Murchison.
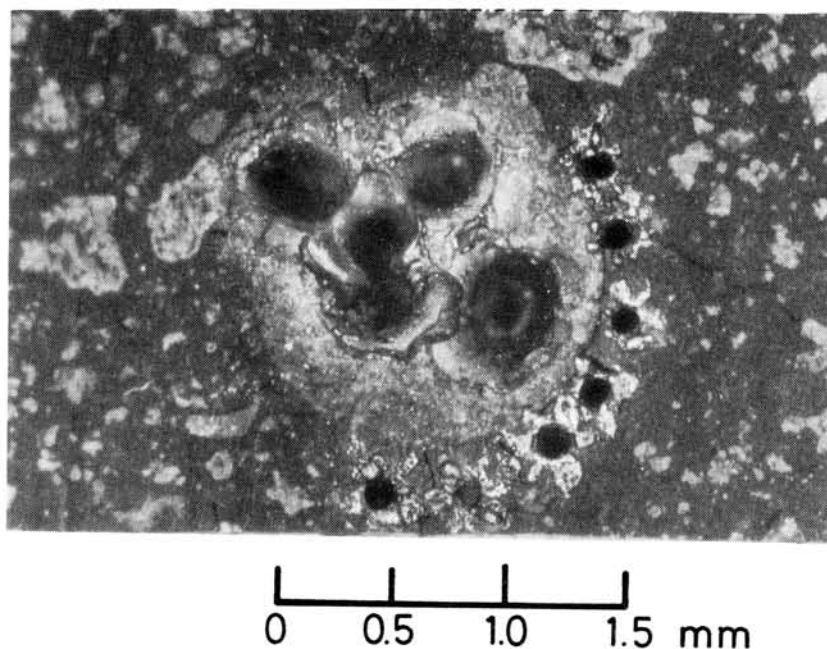


Close-up of a chondrule. The large laser pits in the chondule and the small laser pits around the chondrule were produced by aperture-out and -in mode, respectively.

Noble gases in amorphous carbon and the origin of carbon material in ureilites

Kazuya FUKUNAGA[1] and Jun-ichi MATSUDA[2]

1.Department of Earth Sciences, Faculty of Science, Yamagata University, Yamagata 990.
2.Department of Planetary and Earth Sciences, Faculty of Science, Oosaka University, Toyonaka 560.

In previous works, we synthesized diamond by CVD (Chemical Vapor Deposition) using microwave in the atmosphere containing noble gases. As for Ar, Kr and Xe, the diamonds trapped large amounts of noble gases which showed the fractionation enriched in heavier noble gases (Matsuda et al.,1991). This result consists with the fact that diamonds in ureilites contain large amount of 'planetary' noble gases which are enriched in heavy noble gases (Göbel et al., 1978). The fractionation patterns of heavy noble gases also match the pattern of which the calculation abundances of ions. This result suggests that ion implantation plays an important role for trapping of noble gases. On the other hand, as for the light noble gases, CVD diamonds were more enriched in He and Ne than were those in ureilites (Matsuda et al.,1991). We thought that light noble gas enrichment might be caused by neutral species. If we want to decrease the neutral species, we must decrease the total pressure. But we could not succeed the experiment at law pressure. On the other hand CVD diamonds using a hot filament were also synthesized. But these diamonds contained little noble gases.

In this study, we used a modified hot filament method. Fig.1 shows the experimental apparatus. Ambient gas was composed of 99% of methane and 1% of noble gas mixture. Noble gas mixture was composed of 1% of He, Ne ,Kr and Xe and 96% of Ar. Gases were introduced in quartz tube and evacuated by turbo molecular pump. Total pressure was about $2 \times 10^{-2}$ torr. Total pressure was controlled by the valve between the flow controller and the quartz tube. Gases were decomposed and ionized by thermal electron from the W filament. Ions were accelerated by electric potential between electrode and substrate holder. Electric potentials of electrode were 0V, 10V, 50V, 100V and 200V. To check the reproducibility two samples were synthesized at 100V. Carbon products were deposited on scratched silicon wafer substrate. The temperature of the substrate was monitored by thermocouple attached to the substrate holder and maintained at 800°C by an outside furnace.

The carbon deposit on the silicon wafer was isolated by dissolving the silicon wafer in acid. All samples were analyzed by X-ray diffraction analysis. No line could be detected by this analysis. This fact means that these samples are amorphous.

Noble gases in these samples were analyzed by mass spectrometry employing stepwise heating. Temperature steps were 800, 1400 and 2000°C. At each step elemental abundances of all noble gases and Xe isotopic composition were measured.

Fig.2 shows the release patterns from the sample at the potential of 200V. The abundances of He at all temperature steps and Ne at 2000°C are blank level. For the most part of noble gases released at 1400°C step. The abundance of Ne at 800°C may be air contamination between synthesizing and studying of mass spectrometry.

Fig. 3 shows the relationship between the electric potential difference and the concentration of $^{132}$Xe released at 1400°C. There is a trend of increasing the concentration of noble gases with increasing electric potential difference.

The "trapping efficiency" is defined as concentration of noble gases per ambient gas pressure when material was formed. The highest value of trapping efficiency of Ar in this study is about $4\times10^3$ cm$^3$ g$^{-1}$ atm$^{-1}$. This value is significantly higher than the values which were given by other trapping mechanism and were similar to that of carbon material in ureilites.

Xenon isotope compositions of amorphous carbon don't show fractionation at 200V. At low voltage Xe isotope compositions show small fractionation in favoring the heavy Xe. On the other hand, elemental abundance patterns show strong fractionation favoring the heavy gases (Fig.4). Although all data of He and some data of Ne are given by upper limits, we did not observe the enrichment in light noble gas which were often reported in our previous works. This difference is considered to be caused by variation of total pressures of the ambient gas. The elemental abundance patterns obtained in this study are considerably similar to that of ureilites. This fact suggests that carbon material in ureilites directly formed from primitive solar nebula. This pattern is also similar to the that of Q phase detected in carbonaceous chondrite. It is conceivable that noble gases in Q phase may be trapped by ion implantation.

References
Göbel R., Ott U. and Begemann F. (1978) On trapped noble gases in ureilites. J. Geophys. Res. 83, 855-867
Matsuda J., Ito K. and Fukunaga K. (1991) Noble gas studies in vapor-growth diamonds: Comparison with shock-produced diamonds and the origin of diamonds in ureilites. Geochim. Cosmochim. Acta (in press).
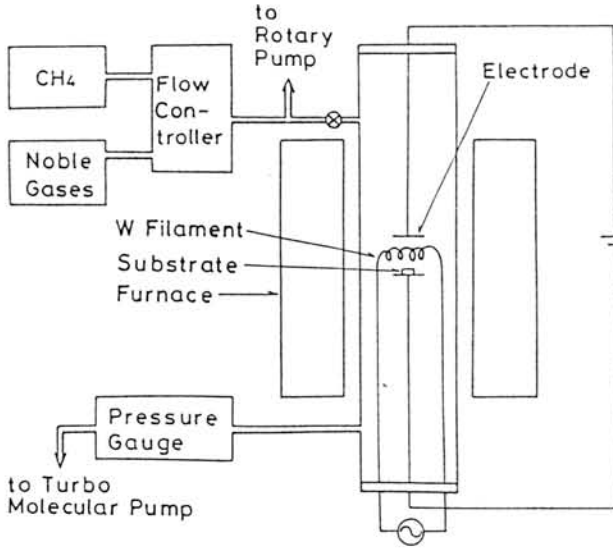
Figure 1
Experimental apparatus
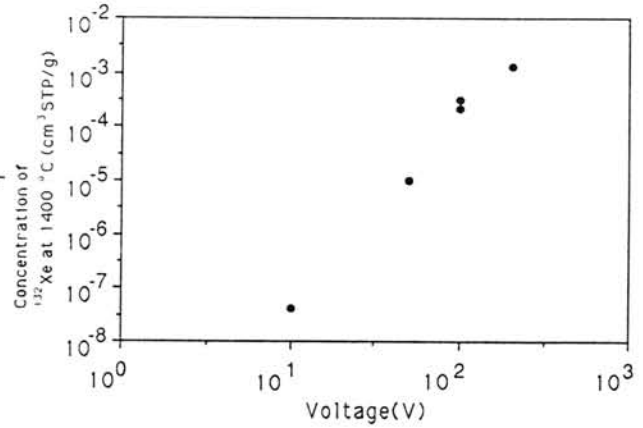


Figure 3
Relationship between voltage and
the concentration of $^{132}$Xe
released at 1400°C
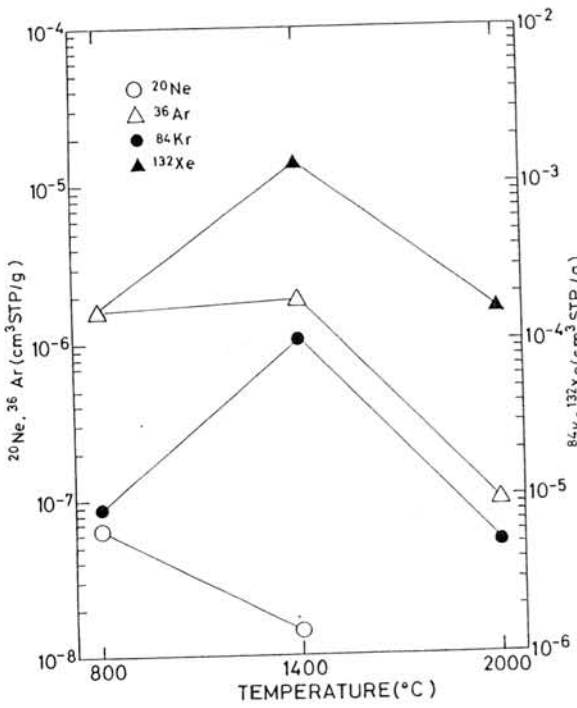


Figure 2
Release patterns of noble gases
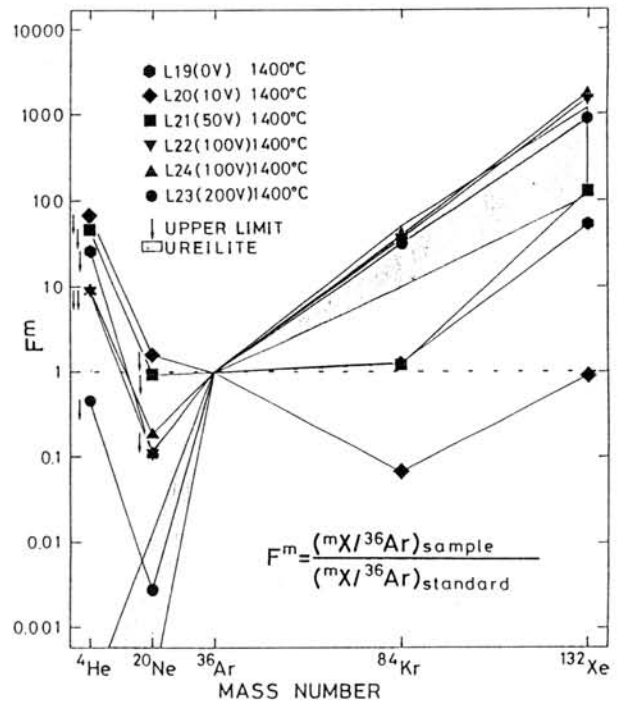


Figure 4
Elemental abundance patterns of
noble gases in carbon products
and ureilites.

TRAPPING MECHANISM OF NOBLE GASES IN VAPOR-GROWTH
DIAMONDS. Jun-ichi Matsuda[1] and Tatsuo Maekawa[2]. 1. Department
of Earth and Space Science, Faculty of Science, Osaka
University, Toyonaka, Osaka 560, Japan.  2. Department of Earth
Sciences, Faculty of Science, Kobe University, Nada, Kobe 657,
Japan.

Introduction  We previously showed that large amounts of
noble gases were trapped in the CVD diamonds produced by using
microwave (MWCVD diamonds) but not in the CVD diamonds produced
by hot filament (HFCVD diamonds) [1].  The elemental abundance
pattern of noble gases in MWCVD diamonds was similar to that in
the amorphous carbon synthesized by glow discharge experiment
[2], and is also in good agreement with the calculated
fractionation patterns of noble gases in plasma.  These results
suggest that "ion implantation" during the diamond growth is
the main mechanism of trapping noble gases in the MWCVD
diamonds, and that ureilite diamonds are of nebular origin [1].
In this study we examined implantation efficiencies of noble
gases for diamond and graphite in the glow discharge state.
These studies would give us further information for the noble
gas feature in ureilite that ureilite diamond is a host phase
of noble gases while graphite is gas-free [3].

Experimental  The diamond used in this study is HFCVD
diamonds synthesized in our laboratory from $H_2$ (99%) and $CH_4$
(1%) mixture [1].  The HFCVD diamond is less than 1mg with the
surface area of about $8mm^2$.  The graphite (99.9% purity) was
pressed into a small pellet by applying a load of 0.125GPa.
The graphite pellet is about 98mg in weight with a diameter of
5mm.  The calculated porosity is 18%.  The discharge equipment
is shown in Fig. 1.  The pressure of the ambient gas (He 1%, Ne
1%, Ar 96%, Kr 1% and Xe 1%) is about 0.8Torr.  The diamond and
the graphite were patched on the electrode.  We used an
induction coil as an electric power source.  The output voltage
was 3.5kV when the input voltage was 100V.  We made the
implantation experiments at the input voltages of 30, 60, and
90V, respectively.  The duration time of the discharge was
30min.
    The elemental abundances of noble gases were measured by
mass spectrometry using stepwise heating technique.  The
details of the experimental procedure are essentially the same
as in our previous studies [1,2,4].

Results and Discussion  We have obtained several
interesting results from this study.

1. The heavier noble gases are more enriched in both diamonds
and graphite compared to the elemental abundances in the
ambient gas.  It is conceivable that this related with the
ionization effect of individual noble gases.

2. There is a beautiful correlation between the amounts of noble gases and the applied discharge voltage for the diamonds, but not for the graphite.

3. The heavy noble gases in the graphite were released below 800°C, and the relative patterns have no relationship with the applied discharge voltage. Meanwhile, considerable amounts of heavy noble gases in the diamond were released at the higher temperature steps for the higher applied discharge voltage.

These results suggest that the implanted noble gases in diamond are much stable in comparison with those in graphite, which should be related with that the MWCVD diamonds are noble gas carrier but the MWCVD graphite is gas free [5], and also to the noble gas feature in ureilite [3].

References 1.Matsuda J., Fukunaga K. and Ito K. (1991) GCA 55 (in press). 2.Suzuki K. and Matsuda J. (1990) Lunar Planet. Sci. 21, 1227-1228. 3. Göbel R. Ott U. and Begemann F. (1978) JGR 83, 855-867. 4.Matsuda J. Matsubara K., Yajima H. and Yamamoto K. (1989) GCA 53, 3025-3033. 5.Fukunaga K., Matsuda J., Nagao K., Miyamoto M. and Ito K. (1987) Nature 328, 141-143.
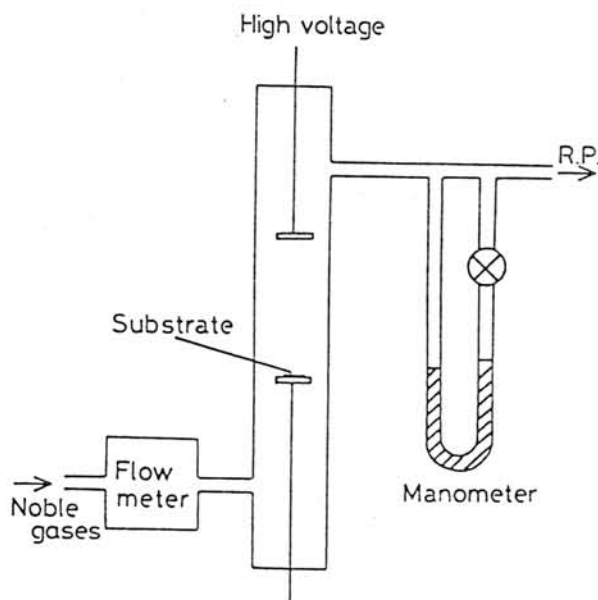


Fig. 1

# NOBLE GASES IN IMPACT GLASSES

Kayo Matsubara[1], Jun-ichi Matsuda[2] and Christian Koeberl[3]

1. Division of Science of Materials, The Graduate School of
   Science and Technology, Kobe University, Nada, Kobe 657,
   Japan.
2. Department of Earth and Space Science, Faculty of Science,
   Osaka University, Toyonaka, Osaka 560, Japan.
3. Institute of Geochemistry, University of Vienna, Dr.-Karl-
   Lueger-Ring, A-1010 Vienna, Austria.

Impact glasses are a kind of natural glass which are produced by melting of terrestrial rocks during the impact of meteorite on Earth. We measured noble gases in impact glasses in comparison with those in tektites.

Impact glass samples used in this study are shown in Table 1. We measured elemental abundances of all noble gases and isotopic compositions of Ne and Ar in seven Aouelloul and four Zhamanshin impact glasses (The sample Zh62/3b is silica-poor zhamanshinite. The other samples are silica-rich zhamanshinites) and in one Libyan Desert Glass sample. We also measured noble gases in a sample of Zli sandstone which is the local target rock from which the Aouelloul impact glasses have been derived.

About 1g of chipped samples were used for noble gas analysis. The noble gases in the samples were extracted at 1600 °C. Blank corrections were applied to the data. If the blank correction exceeded 20%, we listed only the measured amount as an upper limit without blank correction. The uncertainty in the elemental abundances was less than 5%. For the isotopic compositions of Ne and Ar, we made a correction for mass discrimination by measuring standard atmospheric Ne and Ar. The errors in isotopic compositions include both blank correction and mass discrimination errors. The results are listed in Table 2 and 3.

The high Ne/Ar ratios were observed in these impact glasses. Although the Ne concentrations in these impact glasses are of the same order of magnitude as those in tektites [1,2], the Ar, Kr and Xe concentrations in impact glasses are significantly higher than those in the tektites. Therfore, the Ne/Ar ratios in the impact glasses are lower than in tektites. The Ne isotopic compositions agreed well with that of air, suggesting that the Ne diffused in from air.

From the K content and radiogenic $^{40}$Ar content in the impact glasses, we determined K-Ar ages of them. The K-Ar ages of the impact glasses are shown in Table 4. For Aouelloul impact glasses, the ages of 10-15 Ma were obtained. The K-Ar ages agree with older K-Ar ages reported by Gentner et al. [3], but not with the younger fission track ages [4,5]. The ages of 0.7-1.0 Ma were obtained for Zhamanshin impact glasses. These ages are in good agreement with fission track age reported by Storzer and Wagner [6]. The K-Ar age of the Libyan Desert Glass was not detetrmined because of its low K content (0.017%).

REFERENCES   1. Hennecke E.W., Manuel O.K. and Sabu D.D. (1975) J. Geophys. Res. 80, 2931-2934.  2. Matsubara K. and Matsuda J. (1991) Meteoritics, (submitted).  3. Gentner W., Kleinmann B., Storzer D. and Wagner G.A. (1968) Max-Plank-Inst. Kernphysik, Jahresbericht. 211-212.  4. Fleischer R.L., and Price P.B. (1967) Geochim. Cosmochim. Acta 31, 2451-2452.  5. Storzer D. and Wagner G.A. (1977) Meteoritics 12, 368-369.  6. Storzer D. and Wagner G.A. (1979) Meteoritics 14, 541-542.

Table 1. Sampling locations of impact glasses.

| Sample name | Sampling location |
|---|---|
| Aouelloul impact glasses | Adrar Desert, Mauritania West Africa |
| Zhamanshin impact glasses | Aralsk, Khazakhstan, USSR U.S.S.R. |
| Libyan Desert glass | Libyan Desert, Egypt |

Table 2. Noble gases in impact glasses.

| Sample Name | Sample Weight (g) | $^4$He | $^{20}$Ne | $^{36}$Ar | $^{84}$Kr | $^{132}$Xe |
|---|---|---|---|---|---|---|
| | | ( x$10^{-8}$cm$^3$STP/g) | | | (x$10^{-10}$cm$^3$STP/g) | |
| **Aouelloul impact glasses** | | | | | | |
| 9001 | 1.0323 | 42.3 | 47.0 | 4.11 | 9.17 | 0.428 |
| 9002 | 0.9806 | 44.9 | 36.8 | 4.31 | 8.96 | 0.387 |
| 9003 | 0.8344 | 81.4 | 31.3 | 4.05 | 8.64 | 0.418 |
| 9004 | 0.9802 | 5.18 | 29.5 | 3.68 | 7.28 | 0.441 |
| 9005 | 0.9996 | 3.89 | 40.4 | 8.08 | 14.5 | 0.657 |
| 9006 | 1.0030 | 6.95 | 30.2 | 3.45 | 7.12 | 0.406 |
| 9007 | 0.9167 | 12.8 | 40.4 | 3.65 | 7.65 | 0.467 |
| Z1i | 0.9717 | 1670 | 0.403 | 0.345 | 1.30 | 0.460 |
| **Zhamanshin impact glasses** | | | | | | |
| Zh57/2b | 0.8938 | 32.7 | 24.4 | 1.83 | 3.71 | 0.461 |
| Zh36/2 | 0.9627 | 1.81 | 11.3 | 0.788 | 1.54 | 0.0378 |
| Zh30a | 0.8156 | 4.84 | 14.3 | 0.143 | 0.426 | <0.0312 |
| Zh62/3b | 0.9259 | 17.0 | 1.58 | 0.224 | 0.495 | <0.0368 |
| **Libyan Desert Glass** | | | | | | |
| LYD8504 | 0.5505 | 2.51 | 21.6 | 10.1 | 19.8 | 1.27 |

Table 3. Ne and Ar isotopic ratios in impact glasses.

| Sample Name | $\dfrac{^{20}Ne}{^{22}Ne}$ | $\dfrac{^{21}Ne}{^{22}Ne}$ | $\dfrac{^{38}Ar}{^{36}Ar}$ | $\dfrac{^{40}Ar}{^{36}Ar}$ |
|---|---|---|---|---|
| **Aouelloul impact glasses** | | | | |
| 9001 | 9.80 ± .08 | 0.0270 ± .0004 | 0.189 ± .003 | 346 ± 5 |
| 9002 | 9.88 ± .08 | 0.0278 ± .0004 | 0.190 ± .003 | 320 ± 5 |
| 9003 | 9.75 ± .08 | 0.0276 ± .0004 | 0.190 ± .003 | 323 ± 5 |
| 9004 | 9.85 ± .09 | 0.0279 ± .0004 | 0.189 ± .003 | 318 ± 5 |
| 9005 | 9.88 ± .09 | 0.0275 ± .0004 | 0.189 ± .003 | 306 ± 4 |
| 9006 | 9.81 ± .08 | 0.0281 ± .0005 | 0.190 ± .003 | 325 ± 5 |
| 9007 | 9.89 ± .08 | 0.0275 ± .0004 | 0.189 ± .003 | 316 ± 5 |
| Zli | 9.71 ± .12 | 0.0339 ± .0021 | 0.192 ± .005 | 7590 ± 273 |
| **Zhamanshin impact glasses** | | | | |
| Zh57/2b | 9.91 ± .10 | 0.0282 ± .0004 | 0.186 ± .003 | 328 ± 5 |
| Zh36/2 | 9.94 ± .09 | 0.0293 ± .0005 | 0.189 ± .003 | 306 ± 4 |
| Zh30a | 9.89 ± .08 | 0.0287 ± .0004 | 0.190 ± .003 | 352 ± 5 |
| Zh62/3b | 9.77 ± .11 | 0.0300 ± .0007 | 0.190 ± .003 | 342 ± 5 |
| **Libyan Desert Glass** | | | | |
| LYD8504 | 9.82 ± .08 | 0.0286 ± .0004 | 0.187 ± .003 | 289 ± 4 |
| Air | 9.80 | 0.0290 | 0.188 | 296 |

Table 4. K-Ar ages of impact glasses.

| Sample Name | $^{40}Ar_{radi.}$ $(\times 10^{-8} cm^3 STP/g)$ | Age (Ma) | References |
|---|---|---|---|
| **Aouelloul impact glasses** | | | |
| 9001 | 204 ± 23 | 26.3 ± 3.0 | Fleischer and Price (1967) |
| 9002 | 102 ± 20 | 14.8 ± 3.0 | 0.16-0.61 Ma (F.T.age) |
| 9003 | 109 ± 20 | 14.5 ± 2.6 | |
| 9004 | 80 ± 17 | 12.1 ± 2.7 | Storzer and Wagner (1977) |
| 9005 | 79 ± 35 | 11.8 ± 5.3 | 3.25 Ma (F.T.age) |
| 9006 | 101 ± 16 | 14.0 ± 2.3 | |
| 9007 | 72 ± 17 | 9.6 ± 2.3 | Gentner et al. (1968) |
| Zli | 2500 ± 110 | 418 ± 23 | 18.6 Ma (K-Ar age) |
| **Zhamanshin impact glasses** | | | |
| Zh57/2b | 58.5 ± 9.3 | 5.20 ± 0.84 | Storzer ans Wagner (1979) |
| Zh36/2 | 8.2 ± 3.5 | 1.00 ± 0.43 | 1.07 Ma (F.T.age) |
| Zh30a | 8.06 ± 0.81 | 0.69 ± 0.07 | |
| Zh62/3b | 10.2 ± 1.1 | (0.99 ± 0.12) | |

BEHAVIOR OF NOBLE GASES IMPLANTED INTO MINERALS

Futagami, T.[1], Ozima, M.[2], Nagai, S.[3], and Aoki, Y.[3]
1)Geophysical Institute, University of Tokyo, Tokyo 113, Japan.
2)Physical Institute, University of Osaka, Osaka, Japan.
3)Japan Atomic Energy Research Institute, Takasaki, Japan.

Introduction    Elemental and isotopic ratios in the solar wind are important for understanding the origin and evolution of the solar system. Solar wind particles in space are trapped in extraterrestrial materials such as interplanetary dust particles and meteorites. The solar wind implantation is also relevant to the hypotheses for the origin of Venusian atmosphere[1,2]. In this work, noble gas ions were implanted into minerals, and their thermal retention was investigated.

Experimental    Specimens of olivine ($Mg_2SiO_4$) and ilmenite ($FeTiO_3$) were prepared as plates of several mm in length and 50-150 $\mu$m in width. The specimens were irradiated with noble gas ions (helium, neon, and argon) at room temperature, with different ion energies (20, 40, and 200keV) at a constant dose of $10^{14}$/cm$^2$, and with different ion doses ($10^{14}$, $10^{15}$, $10^{16}$/cm$^2$) at a constant energy of 5keV/n. Implanted noble gases were extracted by stepwise heatings in a ultrahigh vacuum, and their amounts were measured by a mass spectrometer.

Results and Discussion    Dependence of the retention for noble gases on ion energy is shown in Fig. 1. The results showed that the retention for noble gases increases with the higher irradiation energy. This means that the retention increases with the depth of implanted ions, because the ions implanted at the higher energy penetrate deeper into target. This can be reasonably explained by considering that the gas release is controlled by the thermal diffusion.
    Dependence of the retention for noble gases on ion dose is shown in Fig. 2. The retention for noble gases changes with ion dose. The retention for helium increases with the ion dose ($10^{14}$-$10^{16}$/cm$^2$). The observation by scanning electron microscopy showed that micron-sized helium bubble is formed when olivine implanted with helium at the dose of $10^{16}$/cm$^2$ is heated. Then such bubble is thermally stable. In contrast, the retention for neon and argon is highest at the dose of $10^{15}$/cm$^2$. Since neon and argon can produce damage more efficiently than helium, we speculate that less retention of neon and argon at the dose of $10^{16}$/cm$^2$ is relevant to damage efficiently created in the target.

References    1. Wetherill, G.W.(1981) Icarus 46, 70-80.
2. Sasaki, S.(1989) Proc. NIPR Symp. Antarct. Meteorites, 2, 328-336.
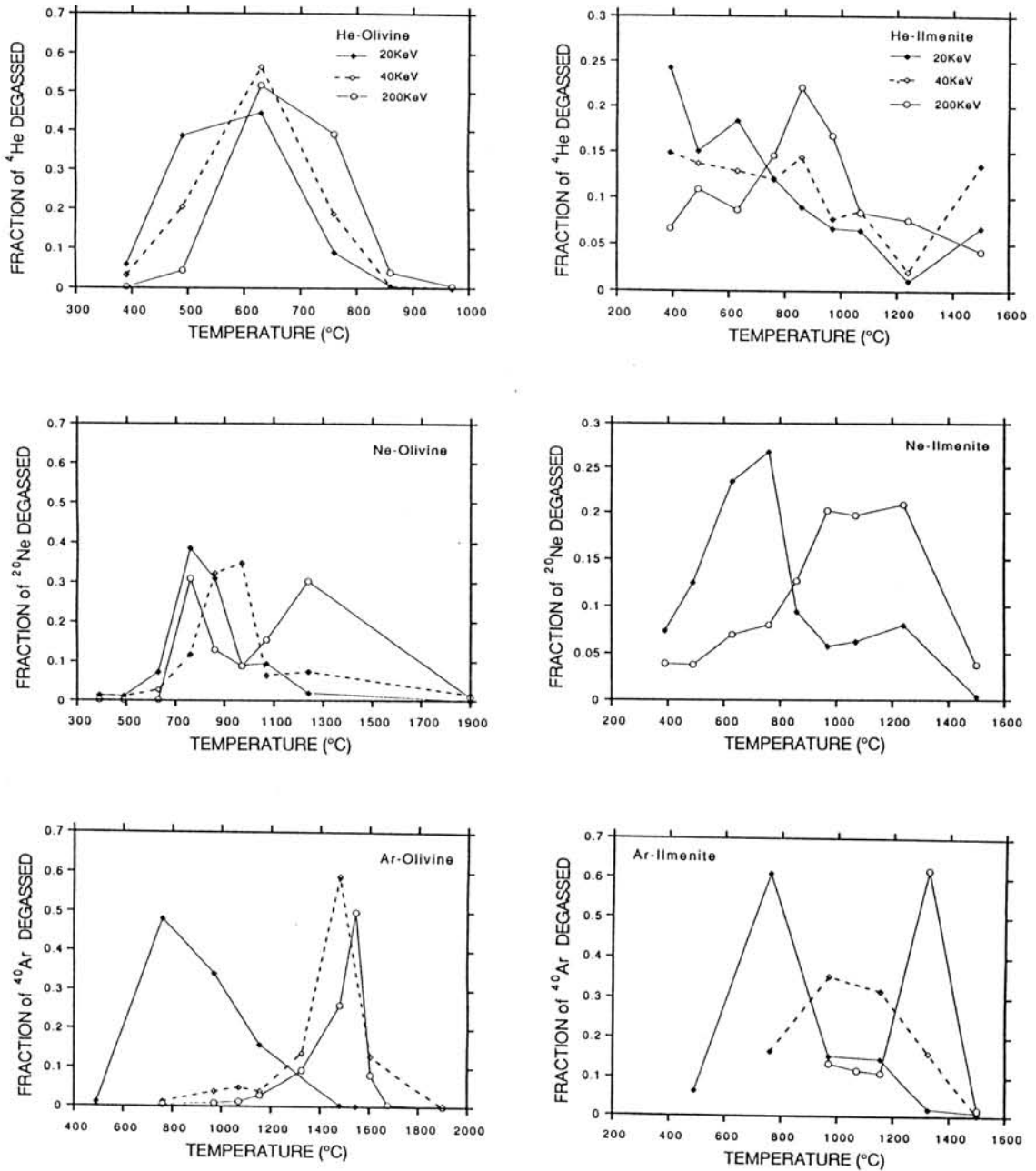
Fig. 1. Dependence of the retention of noble gases on ion energy. Ion doses are $7\times10^{14}/cm^2$ and $1\times10^{14}/cm^2$ for helium and neon, argon, respectively. Solid lines (filled diamonds), dotted lines, and solid lines (open circles) represent the ion energy of 20, 40, and 200keV, respectively.
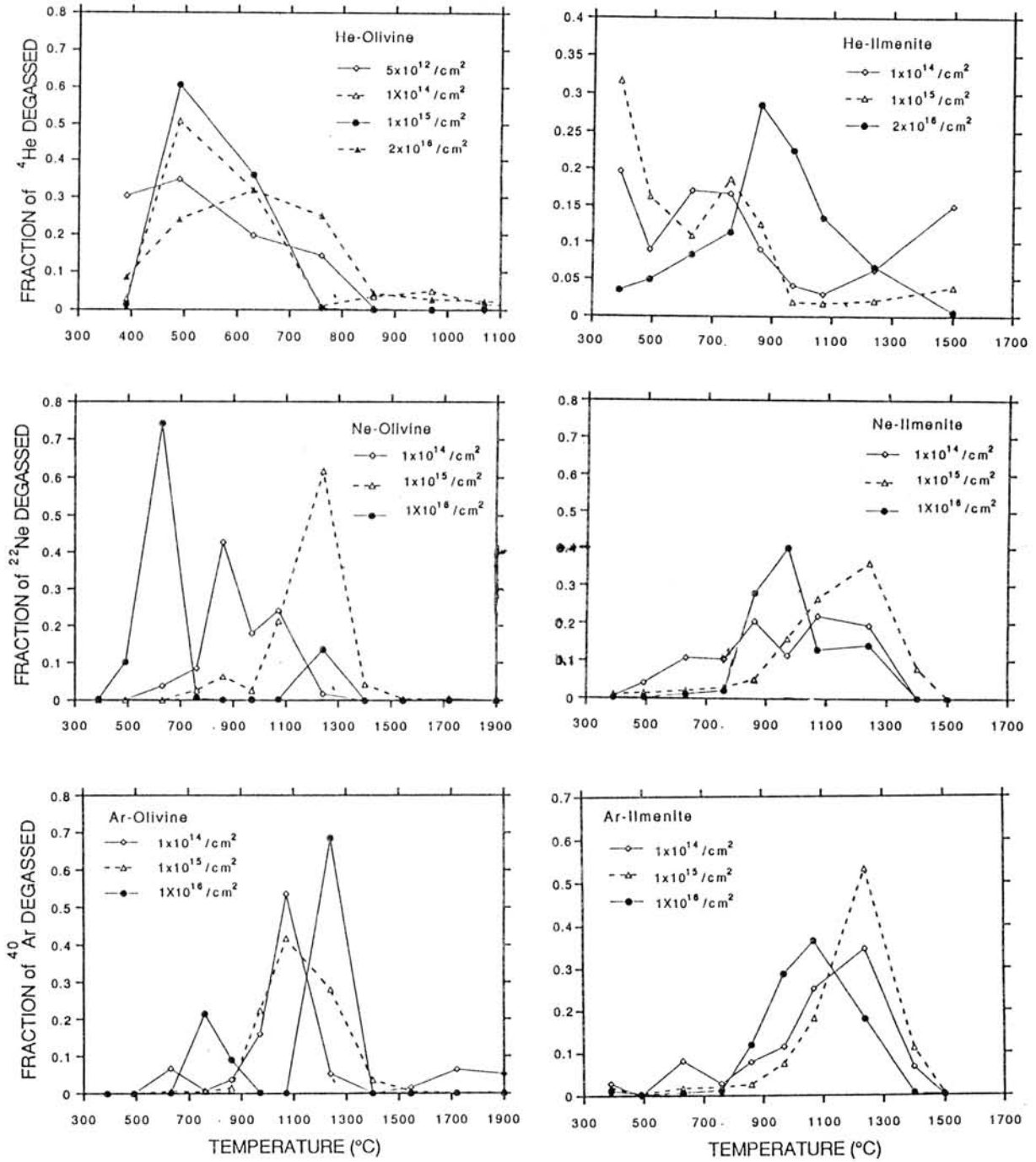
Fig. 2. Dependence of the retention of noble gases on ion dose. Ion energy is 5KeV/n.

# ORGANIC COMPOUNDS IN ASUKA CARBONACEOUS CHONDRITES - II.

Naraoka,H., Shimoyama,A. and Harada,K.

Department of Chemistry, University of Tsukuba, Tsukuba, Ibaraki 305.

In the previous study [1], three Asuka CM2 chondrites, which were collected from Antarctica by the 29th JARE during 1988-89 field season, were examined for amino acids. It was revealed that one specimen (A-14; tentative name) contained at least 14 amino acids including proteineous and non-proteineous structures, and that the amino acids with a chiral carbon were present as recemic mixtures. Based on the results, it was concluded that the amino acids were abiotic in origin, not from terrestrial biological contamination. The others (A-2 and A-6; tentative names), however, contained no detectable amounts in spite of their reasonable carbon and nitrogen contents.

In this study, the same three specimens were analyzed for carboxylic acids. Analytical procedures were similar to those as reported previously [2]. Figure 1 shows gas chromatograms of the carboxylic acids from A-14, together with a procedural blank. Thirty peaks were identified by GC-MS (EI and CI methods) and the retention times of standard samples. Of these, 26 peaks are attributed to 27 monocarboxylic acids including aliphatic and aromatic ones, and the others are dimethylsulfone and phenolic compounds.

Aliphatic ones contained straight-chain structures having two to twelve carbon atoms ($C_2$-$C_{12}$), and branched-chain ($C_4$-$C_7$) structures. At the same carbon number, straight-chain isomer was predominant. As to $C_4$, $C_5$ and $C_6$, all the isomer were observed. Of the expected 17 isomers at $C_7$, 13 isomer were suggested to be present. At $C_8$ or above, peaks of branched-chain isomers become obscure because the number of isomers are very large and the amounts are very small. Aromatic ones (toluic acids) also contained o-, m- and p- isomers.

Total amount of carboxylic acids was about 2μmol/g. The quantities of straight-chain ones decrease logarithmically with increasing carbon number (Fig. 2). The figure also indicates that carboxylic acids detected show no predominance of either odd or even carbon number.

Both A-2 and A-6 samples did not yield carboxylic acids except for small amounts of acetic acid and dimethylsulfone. This result is consistent with the result of amino acid analysis [1].

The depletion of these extractable organic compounds appears to be due to thermal alteration on parent body. However, the relationship between the amounts of these compounds and the degree of alteration has not been clear yet. Sor far, analyses for extractable organic compounds of Antarctic CM2 chondrites have been carried out with eight specimens including the present ones. In half of these, the contents of extractable organic compounds are appropriate for CM2, while in the others they are devoid (Table 1). These results indicate that all CM2 chondrites do not necessarily contain extractable organic compounds.

Table 1. Solvent extractable organic compounds found in Antarctic CM2 chondrites.

| Appropriate amount | Extraordinary small amount |
| --- | --- |
| Yamato-74662 | Yamato-793321 |
| Yamato-791198 | Belgica-7904 |
| Allan Hills-77306 | Asuka-2* |
| Asuka-14* | Asuka-6* |

*tentative names

REFERENCES: [1]Naraoka *et al.*(1990) *Abstr. 15th Symp. Antarct. Meteor.*, p.3-4, [2]Shimoyama *et al.* (1989) *Geochem. J.*, **23**, 181-193.
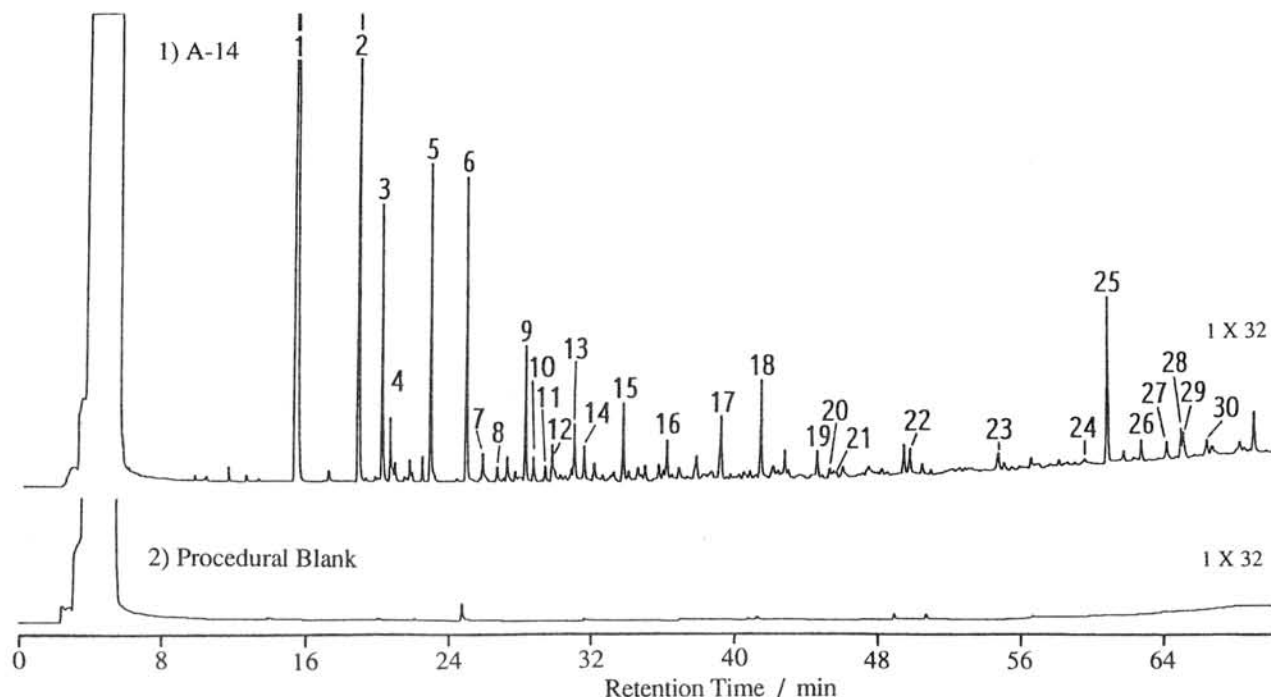
Fig. 1. Gas chromatograms of carboxylic acids from 1) A-14 and 2) procedural blank

1. Acetic acid, 2. Propanoic acid, 3. 2-Methylpropanoic acid, 4. 2,2-Dimethylpropanoic acid, 5. Butanoic acid, 6. 2- and 3-Methylbutanoic acid, 7. 3,3-Dimethylbutanoic acid, 8. 2,2- Dimethylbutanoic acid, 9. Pentanoic acid, 10. 2,3-Dimethylbutanoic acid, 11. 2-Ethylbutanoic acid, 12. 2-Methylpentanoic acid, 13. 3-Methylpentanoic acid, 14. 4-Methylpentanoic acid, 15. Hexanoic acid, 16. Dimethylsulfone, 17. Heptanoic acid, 18. Phenol and o-Cresol, 19. Octanoic acid, 20. p-Cresol, 21. m-Cresol, 22. Nonanoic acid, 23. Decanoic acid, 24. Undecanoic acid, 25. Benzoic acid, 26. o-Toluic acid, 27. Dodecanoic acid, 28. m-Toluic acid, 29. p-Toluic acid, 30. Phenylacetic acid.
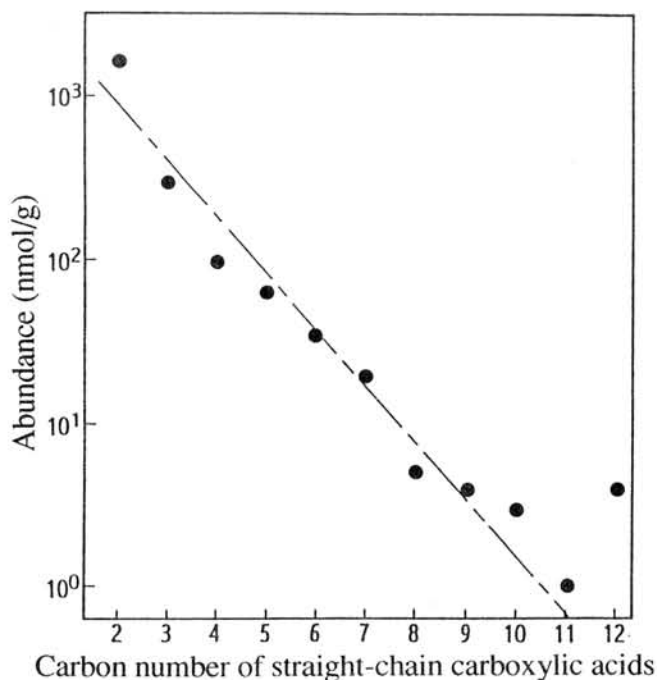


Fig. 2. Amounts of straight-chain carboxylic acids against the carbon number.

IRON-SULFIDE GRAINS IN CARBONACEOUS CHONDRITE AND EXPERIMENTAL DEMONSTRATION OF FORMATION OF IRON-SULFIDE GRAINS WITH Fe-S COALESCENCE TECHNIQUE

C.Kaito and T.Nagata*
Kyoto Institute of Technology, kyoto 606.
*National Institute of Polar Research, Tokyo 173

Since carbonaceous chondrites(C-chondrites) are the most primordial undifferentiated meteorites, it is belived that their natural remanent magnetization(NRM) was acquired in the early stage of the primordial solar system formation. One of the distinct difference of meteorite NRM from terrestrial one is the difference of magnetic minerals carring their NRM. The most common NRM carriers in meteorites are the ferromagnetic tetrataenite ($Fe_{50}Ni_{50}$ ordered structure) and ferrimagnetic pyrrhotite. In the present study, magnetic mineralogy,magnetic properties and NRM of four c-condrites,i.e. Y-74602(CM2), and Y81020(CO3),Allende (CV3) and Leoville(CV3) have been summarized,and the existence of the phyrrhotite phase have been shown. On the other hand, a new preparation method of iron-sulfide grains by the coalescence between Fe and S smokes have been shown.

Iron-sulfide in carbonaceous condrites

From the bulk chemical composition analysis data of Atrantic carbonaceous chondrites, the averrage bulk content of FeS is estimsted as( $6.82\pm2.00$) wt % for 8 samples. These results indicate that all groups of chondrite contain 5-10 wt% of FeS. The stoichiometric FeS (troilite) is antiferromagnetic, but $FeS_{1+x}$ (pyrrlotite for $0<X<1/7$) is ferrimagnetic depending on the various values of X. Figure 1 shows the histograms of atomic ratio of S to Fe (S/Fe) in individual iron-sulfide grains in four C-chondrites i.e. the Allende (CV3), Y-74662(CM2), Y-81020(CO3) and Y-791717(CO3), where N denote the number of samples analyzed in each group by the EPMA analyses. The madian values of S/Fe historograms of both the Y-74662 and allende are close to the stoichiometric composition of ferrimagnetic monoclinic pyrrhotite, $Fe_7S_8$ . The S/Fe histogram of Y-81020 also shifted to the ferrimagnetic structure composition. The S/Fe histogram of Y-791717 is also shown as a standered troilite grain assemblage for the shake of a comparison. Presence of tetrataenite grains in Y-791717 c-chondrite was confirmed and suggested that the tetrataenite grains were directly formed by a coalescence process of Fe and Ni fine smoke on the soler nebula[1]. Another ferrimagnetic mineral in C-chondrites is magnetite ($Fe_3O_4$),whose bulk content in C-chondrites ranges from 0 to about 35 wt%. Some C-chondrites contain taenite and even tetrataenite as ferromagnetic minerals in addition to ferrimagnetic pyrrhotite and magnetite.

In table 1. the main and auxiliary magnetic minerals, NRM intensity and its allotment over its blocking temperatute(t) range, and the paleomagnetic field intensity($F_p$)derived separately from the low and high temperature components of NRM of four c-chondrites are summarized. The classification of magnetic minerals in the table is based on the total results of wet chemical analysis of bulk composition,EPMA analysis of individal
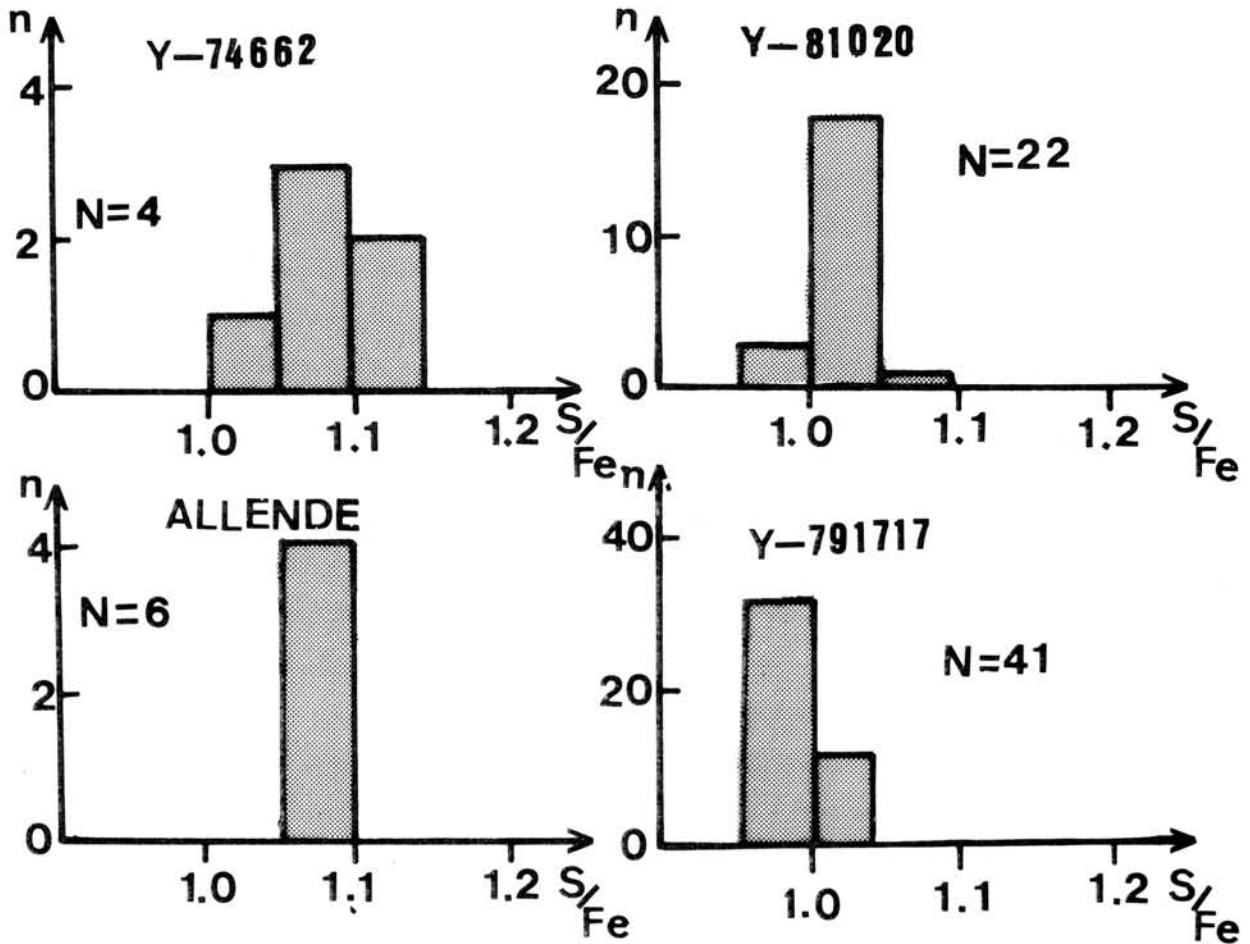
Fig.1

Table 1. Magnetic mineralogy and NMR characteristics

| Item | Y-74662 (CM2) | Y-8102 (CO3) | Allende (CV3) | Leoville (CV3) |
|---|---|---|---|---|
| Main mag. mineral | $FeS_{1+x}$ | $Fe_3O_4$ | $Fe_3O_4$ | $Fe_3O_4$ |
| Auxiliary mag. mineral | Fe-Ni$\gamma$ Fe-Ni$\alpha$ | $FeS_{1+x}$ Fe-Ni$\alpha$ | $FeS_{1+x}$ Fe-Ni$\gamma$ | $FeS_{1+x}$ |
| NMR intensity | $5.9 \times 10^{-4}$ | $8.6 \times 10^{-4}$ | $(0.8 \sim 2.5) \times 10^{-4}$ | $2.1 \times 10^{-4}$ |
| Low tem. comp. | $T \leqq 300$°C (86%) | $T \leqq 320$°C (60%) | $T \leqq 320$°C ($\geqq$95%) | $T \leqq 300$°C (66%) |
| High temp. comp. | $300 < T < 700$°C (13%) | $320 < T < 640$°C (36%) | $320 < T < 700$°C ($<$5%) | $300 < T < 560$°C (19%) |
| Low tem. Fp (Oe) | 0.82 | 1.2 | 0.8~3.0 | 0.97 |
| High tem. Fp (Oe) | 0.011 | 0.09 | $<$0.06 | 0.05 |

opaque minerals, and magnetic analysis of both thermomagnetic curves and NRM thermal demagnetization curve. The NRM of the four C-chondrites consists of the high temperature component which is ferromagnetic at temperatures higher than 300$^{\circ}$C and the low temperature one possessed by ferrimagnetic pyrrhotite.

## Experimental formation of pyrrhotite , troilite and marcasite grains by coalescence of Fe and S smoke streams

The instrumentation system for producing iron-sulfide grains is schematically shown in Fig.2. The whole system is operated in a glass cylindrical jar filled with Ar gas at 13 kPa in pressure.Two tungsten v-boats A and B were placed 40 mm apart and parallel to each other. Boat A was the evaporation source of iron metal. The quartz boat C which was set above boat B was the evaporation source of sulfur.The boats A and B were heated at 1700$^{\circ}$C and 1400$^{\circ}$C. Since the temperature at the boat C became at about 320$^{\circ}$C due to the heating of boat B at 1400 $^{\circ}$C, the gas pressure of sulfur at boat C became $4 \times 10^{-1}$ torr, then sulfur smoke was produced. The upward stream of Fe smoke and that of S smoke emerge near the top of a guiding system composed of 2 glass plate roofs, further flowing upword through a heater system to the grain collector. The collected metallic grains are analyzed with the aid of electron microscopic images, X-ray spectra and electron diffraction.

The temperature of the smoke at the point where the two streams of smokes joined was of about 50$^{\circ}$C. Fe and S grains produced by this method were $\alpha$-iron and amorphouse sulfur. If the temperature at the heater is higher than 100 $^{\circ}$C, grains of iron sulfides have been produced. Troilite, marcasite and pyrrhotite grains were predominately produced by the coalescence between solid iron grain and liquid sulfur grain. Troilite and marcasite grains are grown as a single crystal of complicated polyhedron. The pyrrhotite grains can be seen as the typical DDSS (diffusion dependence shell structure) shape[2] which was produced by the diffusion of iron atoms to the sulfer layer as shown in Fig 3. Figure 3 shows the high resolution electron microscopic image and EDX spectrum of a DDSS grain. The grain was collected after the passed through the heater at 300$^{\circ}$C. The image shows the production of pyrrhotite with 4c structure. The outer layer was composed of an aggregation of crystallites 20-30 nm in size. Different super structure grains of pyrrhotite have been produced by the heater temperature. It can be said that a highly super structure was produced at low temperature.Since the grain size can be controlled by the evaporation temperature and gas pressure, the iron grains of a reratively large size were produced by an elevated evaporation temperature. By the coalescence of large size iron grains with S grains in the present experimental system, the DDSS structure was predominately produced.

[1] T. Nagata and B.J.Carleton: Proc.Japan Acad.,66B. 183-188 1990
[2] C.Kaito and Y.Saito: J.Geomag.Geoelectr.,43,1991 in press.
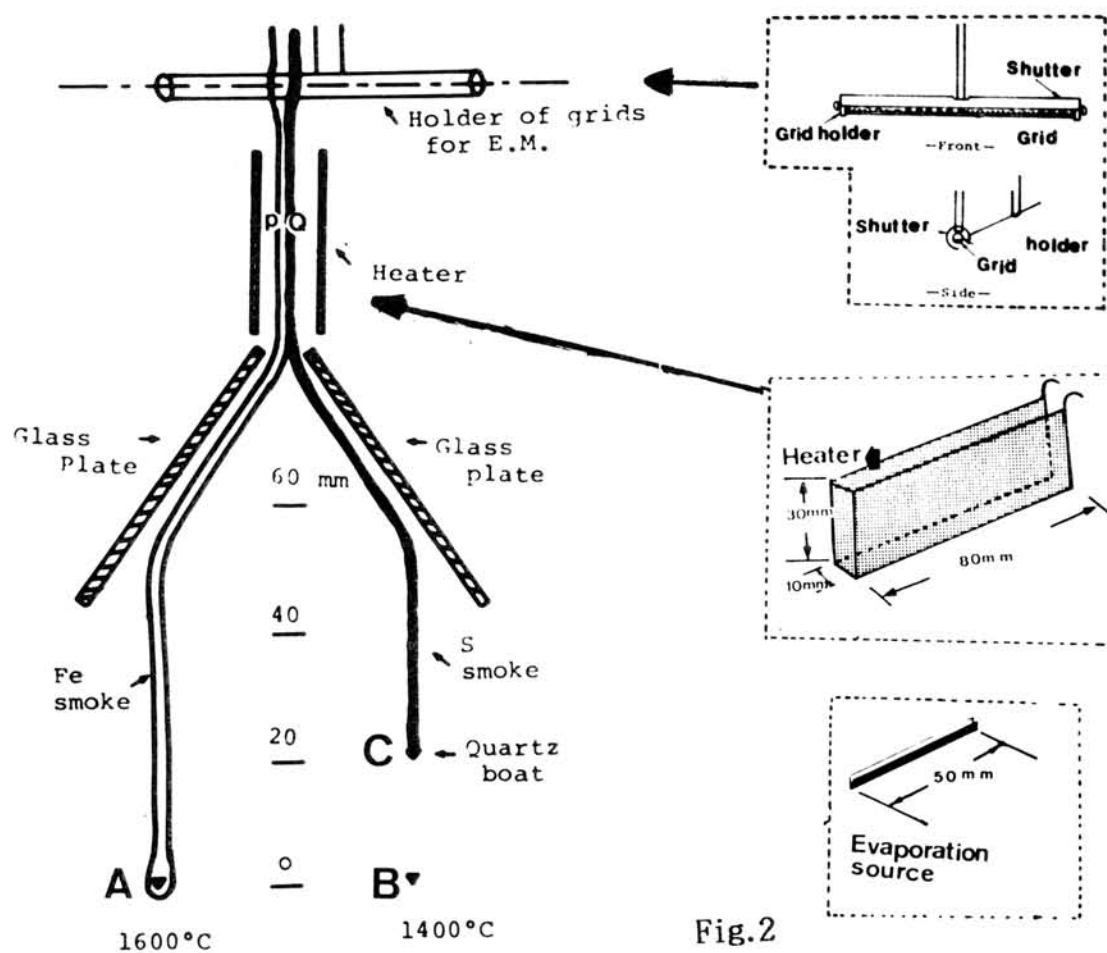
Fig.2
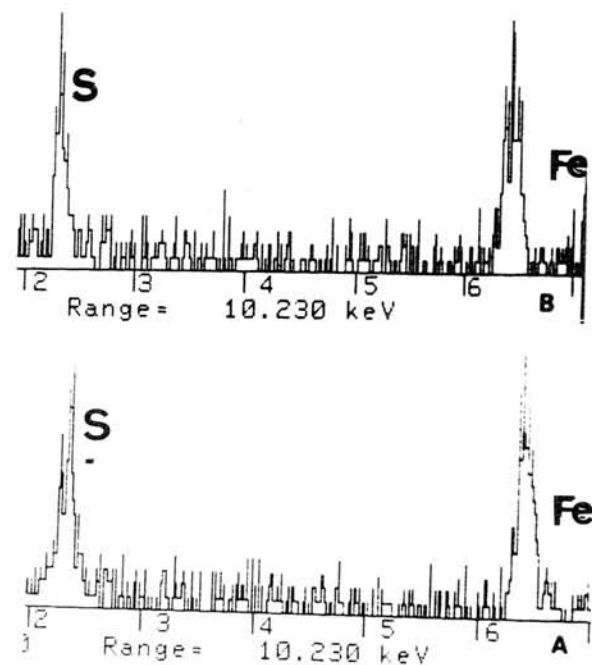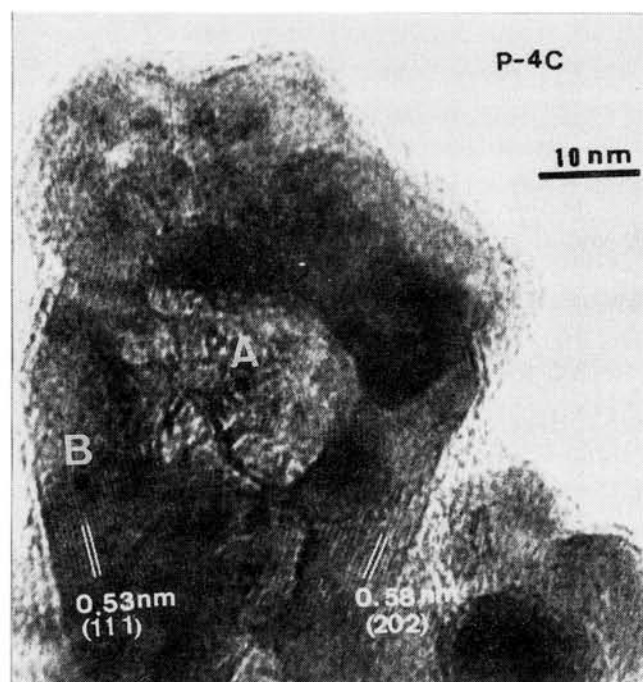


Fig.3

THERMOLUMINESCENCE CHARACTERISTICS AND CHEMICAL COMPOSITIONS OF MESOSTASES
IN PRIMITIVE ORDINARY CHONDRITES - I

NINAGAWA,K., NISHIMURA,S., KUBONO,N., YAMAMOTO,I., KOHATA,M., WADA,T.[1]
YAMASHITA,Y.[1], Jie,L.[2], Sears,D.[2], MATSUNAMI,S.[3] and NISHIMURA,H.[3]

Okayama University of Science, 1-1, Ridai-cho, Okayama 700, Japan
[1]Okayama University, 1-1, Tsushimanaka 3-chome, Okayama 700, Japan
[2]University of Arkansas, Fayetteville, Arkansas 72701, USA
[3]Naruto University of Education, Takashima, Naruto, Tokushima 772, Japan

Sears et al. have made great progress in quantitative classification
of ordinary and CO chondrites, using the TL sensitivity due to crystal-
lization of mesostases [1,2,3]. Semarkona(LL3.0) and Bishunpur (LL3.1),
which are primitive ordinary chondrites, have the lowest TL sensitivity.
The low TL sensitivity is usually due to the localized TL emission of
materials. What kinds of minerals or chondrules are responsible for the TL
in the primitive chondrites ? The development of TL spatial distribution
readout systems [4,5,6,7] has made TL petrography possible [8]. In this
paper, we report the induced TL images of primitive ordinary chondrites,
Semarkona(LL3.0) and Bishunpur(LL3.1), and local glow curves of chondrules.
The TL was measured immediately after $\gamma$ -rays irradiation of 1320 krad at
the heating rate 0.25 ℃/sec with a Corning band pass filter 4-96. The
chemical compositions of mesostases responsible for the TL were also
analyzed by an electron probe X-ray microanalyzer [EPMA].
    Fig.1 shows a BEI, a TL image and a TL glow curve of a slice sample of
Semarkona. A certain chondrule showed intense TL with a 300 ℃ peak. This
was the first time that the above type of glow curve had been measured in
ordinary chondrites. It is revealed by the EPMA that this chondrule is
classified to the type IA [9,10] and mesostasis with high normative anor-
thite is responsible for the TL. The TL image shows that the TL intensity
of the marginal portion is stronger than that of the central one.
    Fig.2 shows a BEI, a TL image and glow curves of another slice sample
of Semarkona. The glow curve of the square region I in Fig.2 (b) has two
peaks of 140°C and 260°C, and the mesostasis of this chondrule is charac-
terized by high anorthite composition. This glow curve is also a new type.
The glow curve of the square region II in Fig.2 (b) has a peak of 160°C.
This chondrule was revealed to be classified to the type II [9] and a high
albite mesostasis was responsible for the TL. In the case of type II
chondrule the marginal portion showed the relatively intense TL.
    Fig.3 shows a BEI, a TL image and glow curves of a slice sample of
Bishunpur. The other new type of glow curve was found. The glow curve of
the square region I in Fig.3 (b) has a 110°C peak and the TL becomes
stronger at higher temperature region. The texture of this chondrule was
barred olivine chondrule and this chondrule had a high anorthite mesostasis.

Fig.1 (a)



Fig.2 (a)



Fig.1 (b)



Fig.2 (b)



Fig.1 (c)



Fig.2 (c)

Fig.3 (a)



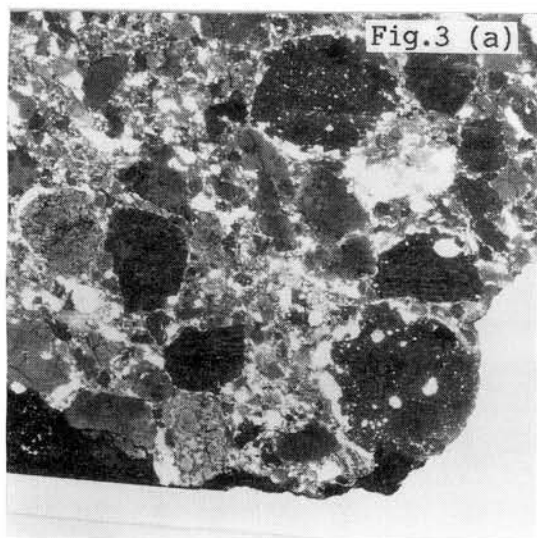Fig.3 (b)

II

I



Fig.3 (c)
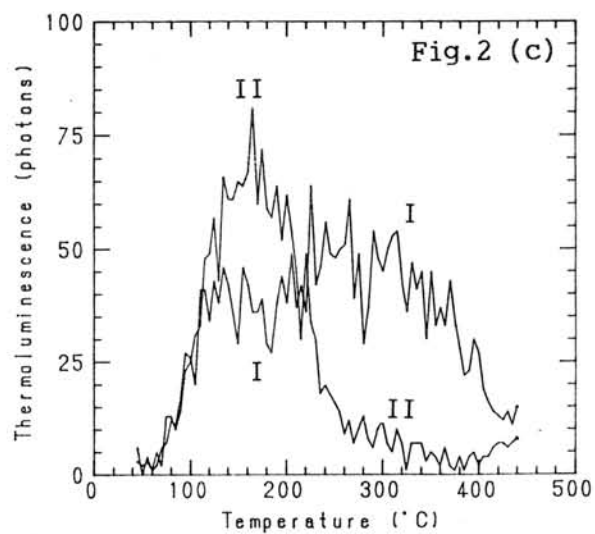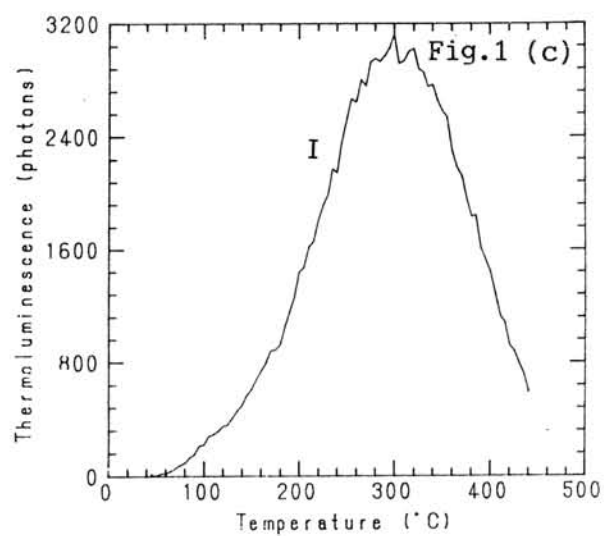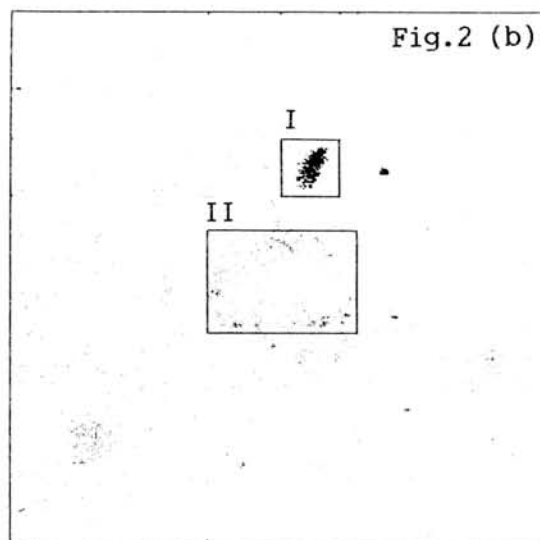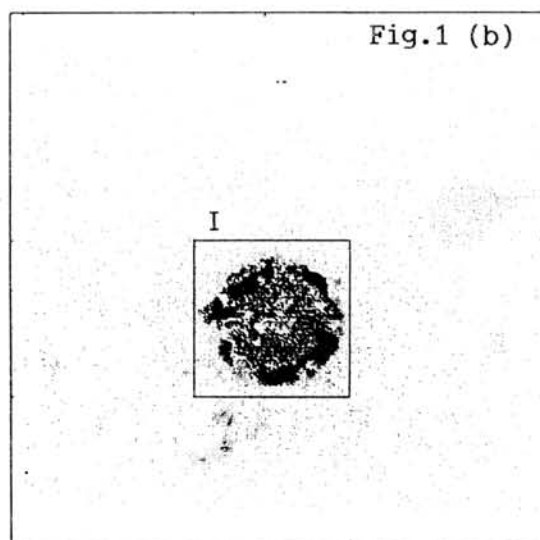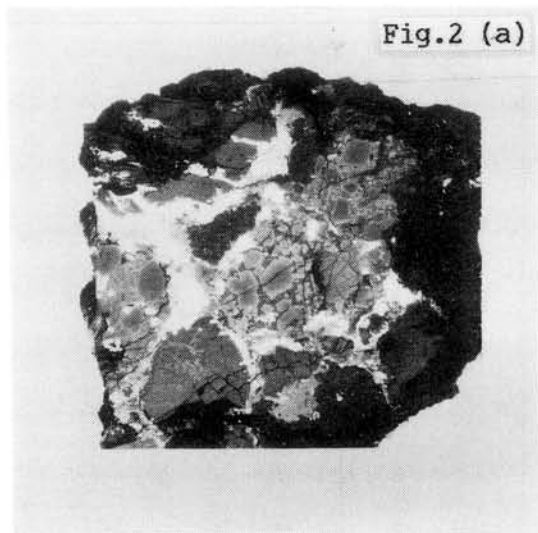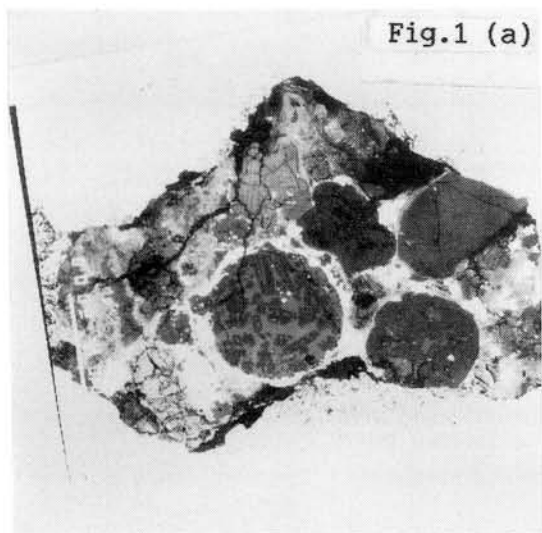
Fig.1  BEI, TL image and Glow curve of Semarkona(LL3.0).

Long dimension is 2.9 mm.  The position of high TL intensity is put by deep black points.  The square shows the region, where local TL glow curve was analyzed.
(a) BEI,
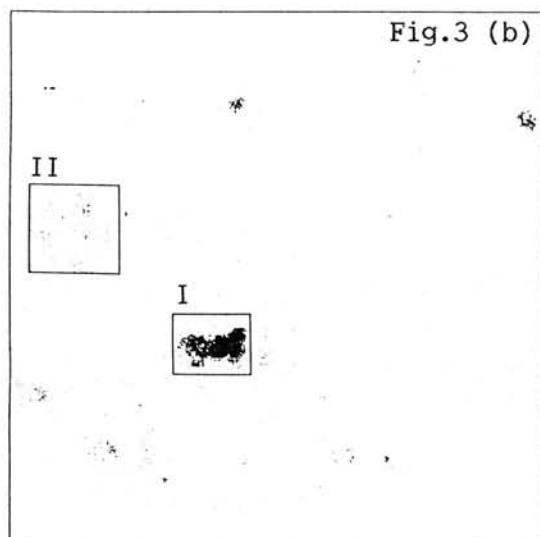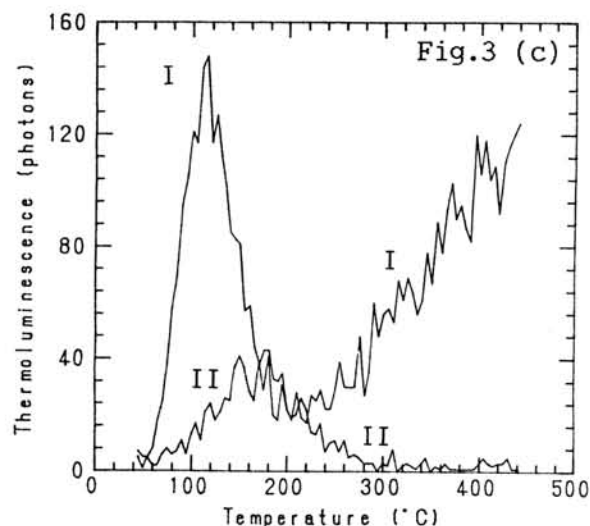(b) TL image at the temperature interval 40-440°C,
(c) Local glow curve.

Fig.2  BEI, TL image and Glow curves of Semarkona(LL3.0).

Long dimension is 2.9 mm.  The position of high TL intensity is put by deep black points.  The squares show the regions, where local TL glow curves were analyzed.
(a) BEI,
(b) TL image at the temperature interval 40-440°C,
(c) Local glow curves.

Fig.3  BEI, TL image and Glow curves of Bishunpur(LL3.1).

Long dimension is 2.9 mm.  The position of high TL intensity is put by deep black points.  The squares show the regions, where local TL glow curves were analyzed.
(a) BEI,
(b) TL image at the temperature interval 40-440°C,
(c) Local glow curves.

The glow curve of the square region II in Fig.3 (b) has a 170°C peak. This chondrule was also revealed to be classified to the type II and a high albite mesostasis was responsible for the TL.

We found three new types of glow curves from high anorthite mesostases in the primitive ordinary chondrites. These varieties were produced by the conditions of chondrule formation and the content of minor element like manganese because their textures are various (type IA chondrule, porphyritic olivine pyroxene chondrule and barred olivine chondrule) and $Mn^{2+}$ would act as an emission center (See part II). These TL glow curves have the possibility to classify the primitive chondrites more precisely.

### References

1. Sears, D.W., Grossman, J.N., Melcher, C.L., Ross, L.M. and Mills, A.A. (1980) Nature, **287**, 791-795.

2. Sears, D. W., Hasan, F. A., Batchelor, J. D. and Jie L. (1990a) Proc. 21th Lunar Planet. Sci. Conf., preprint.

3. Sears, D. W., Batchelor, J. D., Jie L. and Keck B. D. (1990b) Papers presented to the 15th symposium on Antarctic meteorite, 67-69.

4. Walton, A.J. and Debenham, N.C. (1980) Nature, **284**, 42-44.

5. Imaeda, K., Kitajima, T., Kuga, K., Miono, S., Misaki, A., Nakamura, M., Ninagawa, K., Okamoto, Y., Saavedra, O., Saito, T., Takahashi, N., Takano, Y., Tomiyama, T., Wada, T., Yamamoto, I. and Yamashita, Y. (1985) Nucl. Instrum. & Methods, **A241**, 567-571.

6. Yamamoto, I., Imaeda, K., Takahashi, N., Ninagawa, K., Tomiyama, T., Wada,T. and Yamashita, Y. (1987) Nucl. Instrum. & Methods , **A256**, 567-575.

7. Ninagawa, K., Yamamoto, I., Wada T., Matsunami S. and Nishimura H. (1990) Proc. NIPR Symp. Antarct. Meteorites, 3, 244-253.

8. Kohata, M. (1986) Proc. 19th Ann. Hawaii Int. Conf. System Sci., 111-116.

9. Scott, E.R.D. and Taylor, G.J. (1983) Proc. 14th Lunar Planet. Sci. Conf., B275-B286.

10. Jones, R.H. and Scott, E.R.D. (1989) Proc. 19th Lunar Planet. Sci. Conf., B523-B536.

THERMOLUMINESCENCE CHARACTERISTICS AND CHEMICAL COMPOSITIONS OF MESOSTASES
IN PRIMITIVE ORDINARY CHONDRITES - II: A TYPE IA CHONDRULE WITH HIGH TL IN
SEMARKONA (LL3.0) CHONDRITE

MATSUNAMI,S., NINAGAWA,K.[1], NISHIMURA,S.[1], KUBONO,N.[1], YAMAMOTO,I.[1],
KOHATA,M.[1], WADA,T.[2], YAMASHITA,Y.[2] and NISHIMURA,H.

Naruto University of Education, Takashima, Naruto, Tokushima 772
[1]Okayama University of Science, 1-1, Ridai-cho, Okayama 700
[2]Okayama University, 1-1, Tsushimanaka 3-chome, Okayama 700

**Introduction**  Sears et al. (1980) studied thermoluminescence (TL) of a
series of type 3 ordinary chondrites and proposed petrologic subtypes rang-
ing from subtype 3.0 to 3.9, based on the TL sensitivities.  In the present
work, we report a petrograhical study of a type IA chondrule with high TL in
Semarkona (LL3.0) chondrite, using EPMA.  We discuss the implication for TL
phosphors of Semarkona chondrite and the formation of the type IA chondrule.
**Results**  [1] Zonal structure: As already presented in Part I, we dis-
covered a type IA chondrule with high TL.  It is revealed that the high TL
portion is corresponding to the mesostasis with high normative anorthite of
the chondrule and that this chondrule has a zonal structure of TL.
Generally the marginal portion of the chondrule shows TL intensity higher
than the central one.
[2] Petrographic classification: BEI of the chondrule shows that this
is one of typical porphyritic olivine chondrules.  Fig. 1 is a sketch of the
chondrule, showing that olivine phenocrysts are embedded in glassy or partly
micrcrystalline mesostasis.  Olivine phenocrysts have highly magnesian com-
position (core), ranging from $Fa_{0.3}$ to $Fa_{0.5}$.  Average composition of
olivine is as follows: $SiO_2$ 43.2 wt%, $Al_2O_3$ 0.21 wt%, $Cr_2O_3$ 0.12 wt%, FeO
0.38 wt%, MgO 55.6 wt%, CaO 0.36 wt%, NiO 0.04 wt%, and $Fa_{0.4}$.  These
petrographical features show that this chondrule is classified into type IA
chondrules of Scott and Taylor (1983) and Jones and Scott (1989).
[3] Compositional zoning within mesostasis: A step scan analysis using
WDA shows that the mesostasis of the chondrule is compositionally zoned from
core to rim of the chondrule.  The 12 positions for step scan analysis from
core (No.1) to rim (No.12) are also plotted in Fig. 1, which were selected
to traverse the marginal portion with TL intensity higher than the central
one.  EPMA analyses are also tabulated in Table 1.  Fig. 2 shows zonal
structures in terms of the contents of 7 oxides ($SiO_2$, $Al_2O_3$, FeO, MnO, MgO,
CaO and $Na_2O$).  Local intensities of TL along step scan positions from No.1
to No.12 are also plotted in this figure.  The $SiO_2$ contents increase from
50 to 56 wt%, and the $Al_2O_3$ contents decrease from 22 to 18 wt% from core to
rim.  The contents of CaO, MgO and FeO show no systematic variations.
However, the contents of $Na_2O$ and MnO show remarkable increase from core to
rim.  The local intensity of TL shows a similar tendency to the variations

of Na$_2$O and MnO contents. This indicates that the zonal structure of TL is genetically related to the formation of compositional zoning of Na$_2$O and MnO contents within the mesostasis of the chondrule.

**Discussion** [1] Implications for TL phosphors in Semarkona: There is a positive correlation of TL intensity with the contents of Na$_2$O and MnO. Fig. 3 shows the TL emission spectra of the chondrule. The spectra show a wide band with the maximum at about 570 nm in the temperature interval between 200 and 350°C. Strain et al. (1985) have suggested that Mn$^{2+}$ ions act as luminescence sites in oligoclase feldspar of type 5 ordinary chondrites. It is possible that the luminescence site producing the above feature of TL emission is arising from Mn$^{2+}$ ions in plagioclase, which crystallized within mesostasis of the chondrule. A positive correlation of TL intensity with the MnO content of mesostasis can be explained by a hypothesis that the increase of the MnO content in mesostasis causes the increase of the amount of luminescence sites (or Mn$^{2+}$ ions as impurity) in Ca-rich plagioclase within mesostasis. It is suggested that Ca-rich plagioclase which crystallized within Mn-rich, Ca,Al-rich mesostasis of the type IA chondrule is one of high TL phosphors in Semarkona.

[2] Zonation of Na$_2$O and MnO contents within mesostasis of a type IA chondrule with high TL: Finally, we discuss the formation of compositional zoning within mesostasis of the type IA chondrule. There are four possible explanations: (1) difference of the degree of crystallization of forsterite during cooling of the chondrule; (2) diffusional transport of ions due to steep temperature gradient within chondrule melt (Soret effect); (3) infiltration of Na and Mn during cooling of the chondrule; (4) zonal heterogeneity of chemical composition in precursor materials of the chondrule. In particular, the possibility of (4) will be discussed in detail.

**References** Jones, R.H. and Scott, E.R.D. (1989): Proc. Lunar Planet. Sci. Conf. 19th, 523-536, Lunar and Planetary Institute, Houston; Scott, E.R.D. and Taylor, G.J. (1983): Proc. Lunar Planet. Sci. Conf. 14th, Jour. Geophys. Res., **88**, B275-B286; Sears, D.W., Grossman, J.N., Melcher, C.L., Ross, L.M. and Mills, A.A. (1980): Nature, **287**, 791-795; Strain, J.A., Townsend, P.D., Jassemnejad, B. and McKeever, S.W.S. (1985): Earth Planet. Sci. Lett., **77**, 14-19.
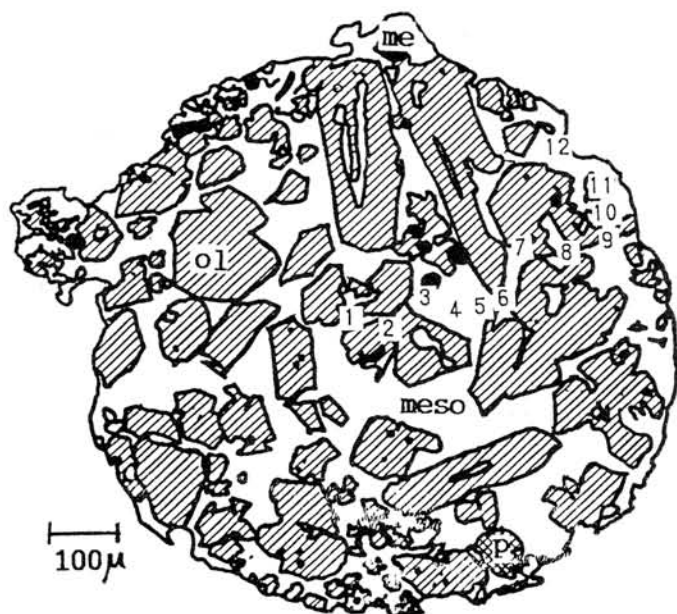
Figure 1.
Sketch of a porphyritic olivine chondrule (type IA) with high TL in Semarkona (LL3.0) chondrite. Forsteritic olivine phenocrysts ($Fa_{0.3-0.5}$) are embedded in Ca,Al-rich mesostasis. The 12 positions for step scan analysis from core (No.1) to rim (No.12) within the mesostasis of the chondrule are also shown in this figure. ol: olivine; meso: mesostasis; me: metallic FeNi; p: pore.
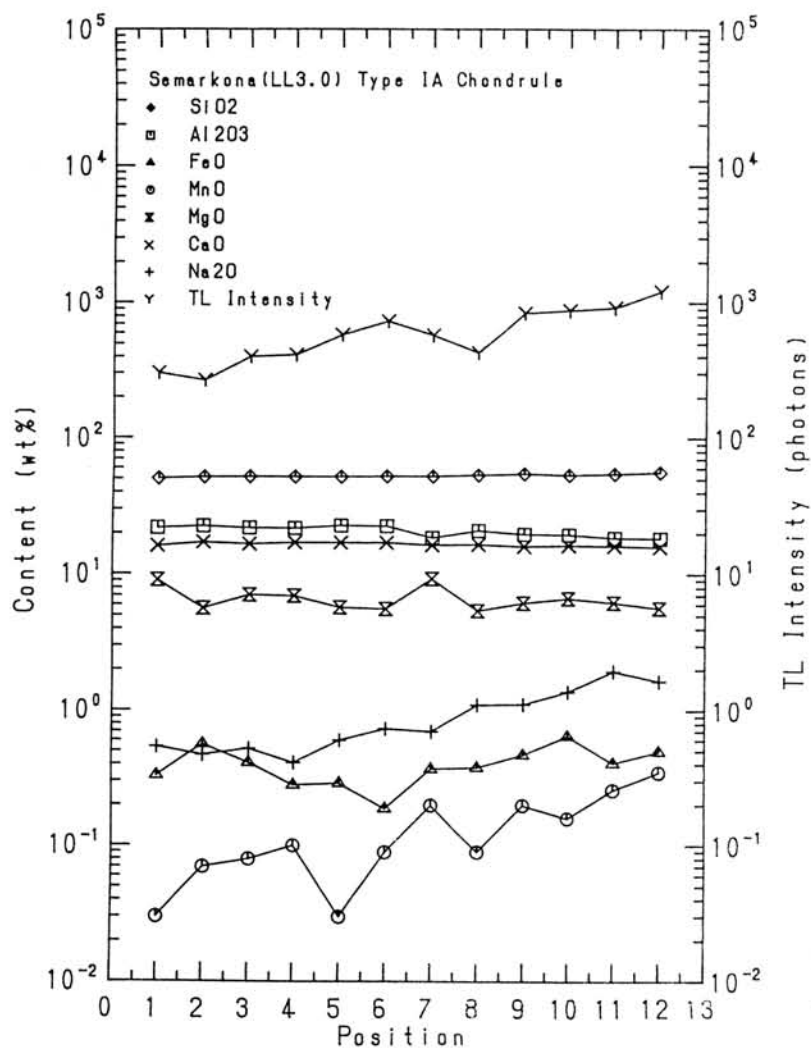


Figure 2.
Zoning of compositions and TL intensity within the mesostasis from core to rim of the chondrule. From core to rim, both $Na_2O$ and $MnO$ contents and TL intensity increase remarkably.

Table 1. Compositional zoning of mesostasis of a type IA chondrule with high TL in Semarkona (LL3.0) chondrite. Step scan analyses of the mesostasis from core (No.1) to rim (No.12) of the chondrule were obtained by WDA (recalculated to total 100%).

| | core 1 | 2 | 3 | 4 | 5 | 6 | 7 | 8 | 9 | 10 | 11 | rim 12 |
|---|---|---|---|---|---|---|---|---|---|---|---|---|
| $SiO_2$ | 50.5 | 51.7 | 51.8 | 51.8 | 52.0 | 52.3 | 52.3 | 53.6 | 54.6 | 53.4 | 54.9 | 56.3 |
| $TiO_2$ | .67 | 1.11 | 1.03 | .88 | .94 | .92 | 1.28 | .92 | .86 | .94 | .86 | .64 |
| $Al_2O_3$ | 22.0 | 22.6 | 22.0 | 21.8 | 22.8 | 22.6 | 18.5 | 21.0 | 19.7 | 19.5 | 18.6 | 18.4 |
| $Cr_2O_3$ | .36 | .38 | .34 | .44 | .38 | .29 | .67 | .48 | .38 | .40 | .40 | .27 |
| $FeO^{\#1}$ | .33 | .56 | .41 | .28 | .29 | .19 | .37 | .38 | .47 | .65 | .41 | .50 |
| $MnO$ | .03 | .07 | .08 | .10 | .03 | .09 | .20 | .09 | .20 | .16 | .26 | .35 |
| $MgO$ | 9.11 | 5.66 | 7.07 | 6.93 | 5.75 | 5.60 | 9.33 | 5.42 | 6.21 | 6.70 | 6.23 | 5.71 |
| $CaO$ | 16.2 | 17.2 | 16.7 | 17.1 | 17.0 | 17.1 | 16.4 | 16.6 | 16.1 | 16.3 | 16.2 | 15.9 |
| $Na_2O$ | .54 | .47 | .52 | .41 | .60 | .73 | .70 | 1.11 | 1.12 | 1.39 | 1.96 | 1.66 |
| $K_2O$ | .04 | .04 | -- | -- | .05 | -- | .04 | .03 | .12 | .04 | -- | .05 |
| $NiO$ | --$^{\#2}$ | .06 | -- | .06 | -- | -- | -- | .24 | .09 | .37 | -- | .05 |
| $S_2O$ | .03 | .09 | .05 | .06 | .05 | .06 | .05 | .06 | .05 | .03 | -- | -- |
| $P_2O_5$ | .09 | .06 | .05 | .04 | .06 | .05 | .03 | .08 | .12 | .09 | .17 | .23 |
| $V_2O_3$ | .08 | -- | -- | .06 | -- | -- | .07 | -- | -- | -- | -- | -- |

#1: total Fe as FeO; #2: not detected.
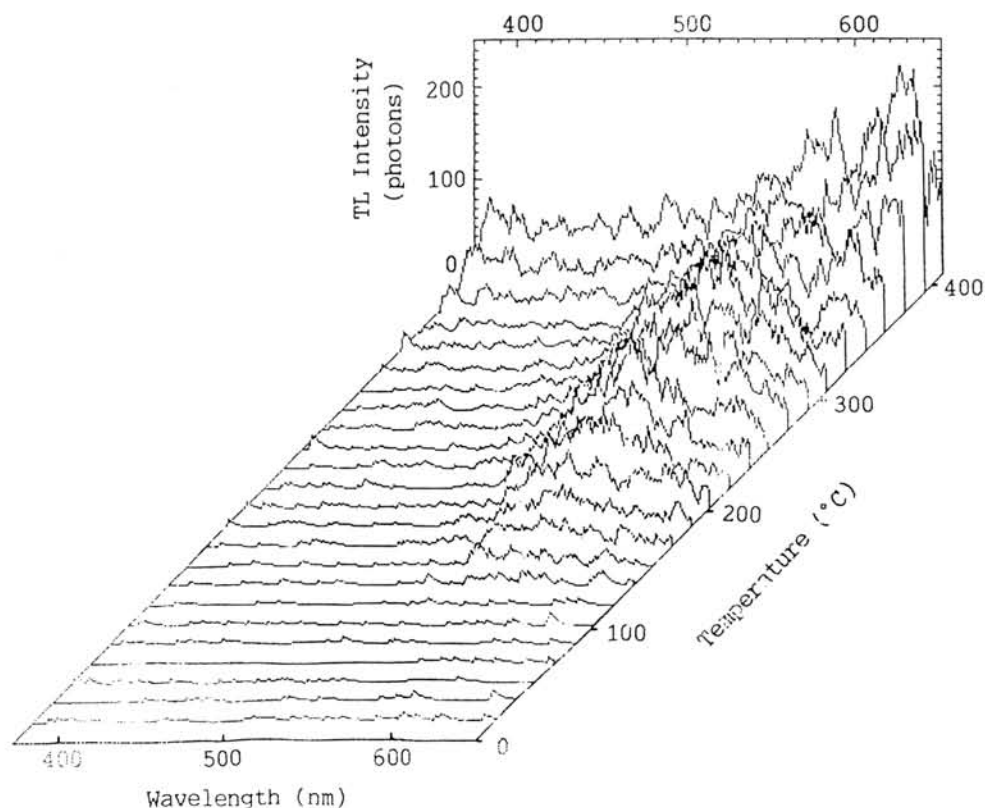


Figure 3. The TL emission spectra of a type IA chondrule in Semarkona (LL3.0) chondrite.

The Magnetic Properties of Antarctic Iron Meteorites

Nagai,H.[1], Moriyama,A.[1], Funaki,M.[2] and Momose,K.[1]

1) Faculty of Science, Shinshu University, Matsumoto 390, Japan.

2) National Institute of Polar Research, Tokyo 173, Japan.

In order to study the magnetic properties of meteorites, we have investigated the thermo-magnetic behaviours of Fe-Ni alloys [1], because the main magnetic substance in the meteorite is Fe-Ni alloy. The present work aims to study the magnetic properties of antarctic iron meteorites (ALH77250, DRP78008, Y790724).

In the case of ALH77250, the saturation magnetization ($I_S$) is obtained to be 194[emu/g] and the Ni content is about 6.5% from the thermo-magnetic measurements. The coercive force ($H_C$) and the remanent magnetization ($I_R$) are nearly zero.

For DRP78008, the $I_S$ is 180[emu/g] and the magnetization after AC demagnetizing is constant in intensity and direction. The Ni content is estimated to be 7% from the thermo-magnetic measurement.

For Y790724, the $I_S$ is 200[emu/g] and $I_R$ and $H_C$ are 0.2[emu/g] and 4.2[Oe], respectively. The thermo-magnetic measurements indicate the typical curves of the kamacite as shown in Fig.1. The Ni content is estinated to be about 8%. This meteorite may contain the small part of the terataenite phase according to the thermo-magnetic measurement.

The Mossbauer spectra are obtained by using the powder samples of these meteorites and are also shown in Fig.2 where they suggest each other to be similar in magnetic property. The thermo-magnetic curves of the meteorites resemble each other in shape. The measured results indicate that these meteorites contain nearly equal contents of Fe-Ni alloys.
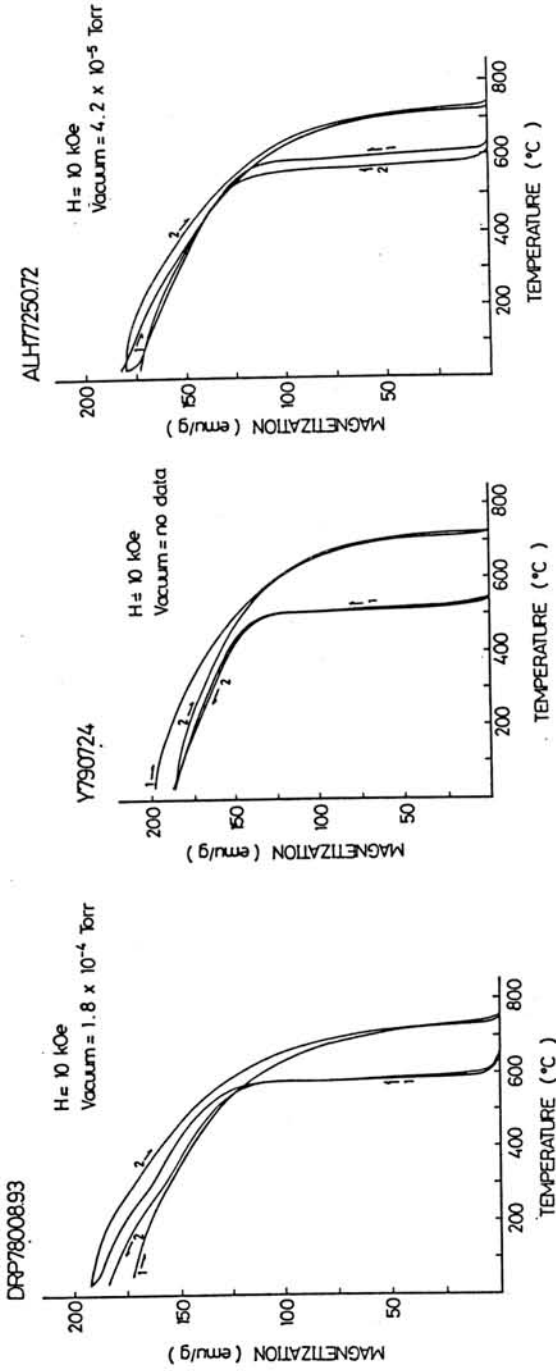
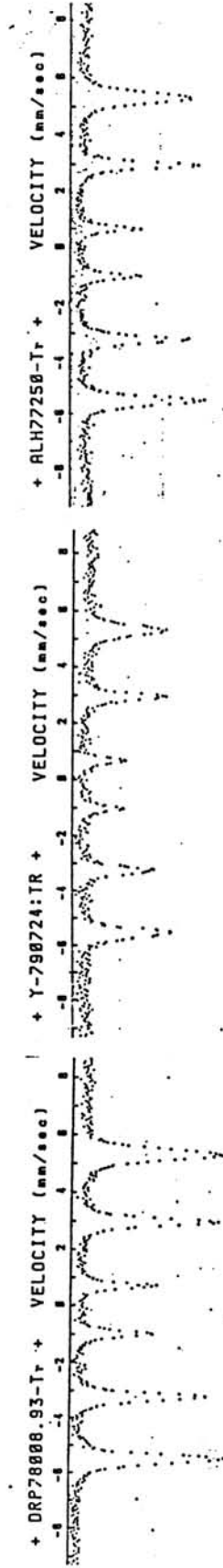Fig.1. The themo-magnetic curves of DRP78008, Y790724 and ALH77250.



Fig.2. The Mossbauer spectra at 290K of DRP78008, Y790724 and ALH77250

References;

[1] Momose,K. and Nagai,H.(1983) Mem.Natl.Inst.Polar Res.,Spec.Issue
30 447

Momose,K.,Nagai,H. and Muraoka,Y.(1984) Mem.Natl.Inst.Polar Res.,
Spec.Issue 35 298

Momose,K. and Nagai,H.(1985) J. Geomag. Geoelectr., 37 817

Momose,K. and Nagai,H.(1986) J. Geomag. Geoelectr., 38 721

Nagai,H., Momose,K. and Funaki,M.(1987) J.Geomag.Geoelectr.39 431

# IDENTIFICATION OF THE FINE MAGNETIC STRUCTURES IN SOME ORDINARY CHONDRITES USING MAGNETIC FLUID AND MAGNETOTACTIC BACTERIA

M. FUNAKI[1] and H. SAKAI[2]

1: National Institute of Polar Research, 9-10 Kaga 1-chome Itabashi-ku Tokyo 173
2: Faculty of Sciences, Toyama University, 3190 Gofuku Toyama 930

## 1. Introduction

Natural remanent magnetization (NRM) of ordinary chondrites measured by common magnetometer is an average value of numerous fine FeNi grains in the chondrites. Usually the magnetization is decomposed into extremely soft and hard components. The hard one may result from tetrataenite which consists of Fe 50% Ni 50% of ordering phase. If we are able to know the dipole configuration of the hard one in individual tetrataenite grains, paleomagnetic meaning of the chondrites is established.

The Bitter pattern configuration, using magnetite suspension fluid, shows strong magnetization area without information of the N or S poles on the FeNi grains. Configuration of magnetotactic bacteria indicates not only strong magnetization area but also the polarity information, although the technic has not been established completely. North seeking bacteria (NSB) of coccus of 1 μm in diameter living in Japan were cultivated. Migrate property of the NSB was switched to the south seeking bacteria (SSB) by pulsic field at 200 mT toward the opposite direction with the bacterial magnetization. The N and S poles were identified by these bacteria and also by a combined method of the NSB and the Bitter pattern.

The samples of St. Sèverin (LL6), ALH-769 (L6) and Y-75097 (L4) were prepared in this study. The domain structures determined by these technic may be disturbed due to mechanical polish.

## 2. Experimental results

The Bitter pattern configuration indicates the strong NRM around limbs of the taenite phase. Probably these limbs are formed by tetrataenite phase. Any strong configuration did not appear in interior taenite. Network of the weak configuration, resulting domain structures, appeared on the kamacite phase. The NSB and SSB made dense clusters on the taenite limbs. The respective clusters located independently,

but a part of them were overlapped each other.  These characteristics consisted with the chondrites.

The N  and S poles  may be estimated  by a  combination of the  Bitter pattern  and NSB  methods; the area  where magnetic fluid accumulates  without the NSB is  estimated to the N pole. The distribution  of NRM direction of  each FeNi  grains in the St. Severin seemed to be scattered.

## 3. Discussion

The  configuration of  the  Bitter pattern  consisted with the one of main  part bacteria pattern is essentially, but  the latter covered wide  area of the taenite limb.  The reason may be  explained due to  higher sensitivity of the latter compared with the former.  The overlapped area of  the cluster for  the NSB and SSB  may appear  by following reasons:  (1) The  domain structures of  the area are  very fine,  indicating mixture  of the  N  and  S  poles.  (2)  The  area  radiated  strong  field gradient, consequently both bacteria were drawn to the area.

The  random  configuration  of  the  N  and  S  poles  may indicate that  these chondrites  acquired local  magnetic field rather than the dipole field of their parent body.

COOLING HISTORY OF ANTARCTIC PRIMITIVE ACHONDRITE YAMATO-74357.

Miyamoto, M.[1] and Takeda, H.[2]

[1]Department of Pure and Applied Sciences, University of Tokyo, Komaba,
 Tokyo 153
[2]Mineralogical Instituite, Faculty of Science, University of Tokyo,
 Hongo, Tokyo 113, Japan.

Introduction This study was performed as part of unique meteorite
consortium study headed by Prof. I. Kushiro [1,2]. Antarctic primitive
achondrite Yamato-74357 has many chemical and mineralogical characteristics
which suggest it is closely related to lodranite [1-3]. An apparent
overall feature of this meteorite is similar to that of ureilites, except
for the absence of carbonaceous veins and presence of nickel-iron and
troilite [3]. Y-74357 consists of 83 % olivine, 6% orthopyroxene (opx), 3%
augite, 8% metal, and traces of chromite and troilite [3]. Although the mg
number (=100xMg/(Mg+Fe)) of olivine is almost constant, orthopyroxenes show
reduced rims like olivine rims in ureilites [4], suggesting cooling of this
sample was slow enough to homogenize olivines, but too fast to homogenize
entire orthopyroxenes. This zoning information enables us to quantify the
cooling rate of this meteorite [4].

Chemical Zoning We measured chemical zoning profiles (Fe-Mg, CaO,
MnO) of orthopyroxenes and olivines in Y-74357 with an electron microprobe
analyzer. Opx shows a reverse chemical zoning at the rim of a few tens
microns in width (Fig. 1). CaO contents in opx rapidly decrease at the
rim. MnO contents in opx slightly increase at the rim probably due to
effects of the reduction (Fig. 1)[5]. The normal zoning profile of MnO
contents in opx is in line with our hypothesis that the Fe-Mg zoning pro-
file of opx is produced by reduction. Reduction rims were not detected in
augites with the microprobe. CaO contents in olivine gradually decrease
from core to rim. Olivine is uniform in the mg number of about 92 which is
similar to the mg number of opx at the edge of the reduced rim (Figs. 1,2).

Calculations We assume that these compositional gradients of the mg
number of opx and CaO contents in olivine are controlled by atomic
diffusion and fit diffusional calculation profiles to the observed zonings
to obtain cooling rates. The Fe diffusion coefficient in pyroxene has not
been accurately determined, although an upper limit of $4 \times 10^{-14}$ cm$^2$/s at
1200 $^\circ$C has been reported [6]. In olivine it is known that
the Fe diffusion coefficient is greater than that of Ca [7,8]; that is,
the Fe diffusion coefficient is about $2.4 \times 10^{-11}$ cm$^2$/s at 1200 $^\circ$C and
the Ca diffusion coefficient is about $1.3 \times 10^{-13}$ cm$^2$/s. We assume that
the Fe diffusion coefficient is greater than that of Ca even in pyroxene.
The Ca diffusion coefficient in pyroxene is experimentally determined by
[9,10]. This is about $6 \times 10^{-15}$ cm$^2$/s at 1200 $^\circ$C. Therefore, we used $1 \times$
$10^{-15}$ cm$^2$/s at 1200 $^\circ$C for the Fe diffusion coefficient in opx. The
activation energy for Fe diffusion in pyroxene is assumed to be 100 kcal/
mol (>1100 $^\circ$C) and 25 kcal/mol (<1100 $^\circ$C) which are estimated from the data
by [10]. Although the activation energy of Ca diffusion in olivine is 99.3
kcal/mol [8], the activation energy below 1100 $^\circ$C is assumed to be 25

kcal/mol which is estimated from the data of the Ca diffusion in pyroxene [10]. We started diffusional calculations by assuming uniform initial profiles of the mg number of opx and CaO content in olivine. Constant boundary conditions during calculations are assumed to be the mg number of 92 in opx and CaO content of 0.015 wt% in olivine. Details of calculations are given in [11,12].

Results and Discussion    We estimate an initial temperature of 1000 °C based on the coexisting opx and augite compositions in Y-74357 [13]. A cooling rate of 1.5 °C/year from 1000 to 600 °C gives the best fit for the observed Fe-Mg profile at the rim of opx (Fig. 1). This cooling rate corresponds to a burial depth of about 70m under solid rock (thermal diffusivity = 0.004 cm²/s). For CaO zoning profile in olivine, a cooling rate of 1.5 °C/year also gives the best fit for the observed profile. The cooling rate obtained by Fe-Mg zoning of opx agrees well with that by CaO profile. At this cooling rate, any primary Fe-Mg zoning in olivine will be homogenized because of diffusion coefficient of Fe greater than that of Ca, in agreement with observation. The observation that the absence of the reduction rim of augite in Y-74357 gives a constraint for the upper limit of Fe diffusion coefficient in augite; that is, Fe diffusion coefficient in augite is 2 or 3 orders of magnitude smaller than that in opx. In fact, Ca diffusion coefficient in augite is about 1.5 orders of magnitude smaller than that in pigeonite [10]. In conclusion, the calculated cooling rate of Y-74357 is about 4 orders of magnitude slower than that of ureilites [4]. This information will be useful in deducing their formation conditions.

We thank the Natl. Inst. Polar Res. for the meteorite sample and Dr. H. Nagahara for allowing us to use the PTS of Y-74357.

References: 1. Yanai K., Kojima H., Prinz M., Nehru C. E., Weisberg M. K. and Delaney J. S. (1984) 9th Symp. Antarct. Meteorites, 24-28. 2. Nagahara H., Fukuoka T., Kaneoka I., Kimura M., Kojima H., Kushiro I., Takeda H., Tsuchiyama A. and Yanai K. (1990) 15th Symp. Antarct. Meteorites, 92-94. 3. Hiroi T. and Takeda H. (1991) Proc. NIPR Symp. Antarct. Meteorites. 4, 163-177. 4. Miyamoto M., Toyoda H. and Takeda H. (1985) Proc. 16th Lunar Planet. Sci. Conf., J. Geophys. Res., 90, D116-D122. 5. Miyamoto M., Furuta T. and Fujii N. (1990) Meteoritics 25, 388. 6. Freer M., Carpenter M. A., Long J. V. P. and Reed S. J. B. (1982) Earth Planet. Sci. Lett. 58, 285-292. 7. Buening D. K. and Buseck P. R. (1973) J. Geophys. Res. 78, 6852-6862. 8. Morioka M. (1981) Geochim. Cosmochim. Acta 45, 1573-1580. 9. Brady J. B. and McCallister R. H. (1983) Am. Mineral. 68, 95-105. 10. Fujino K., Naohara H. and Momoi H. (1990) EOS 71, 943. 11. Miyamoto M., McKay D. S., McKay G. A. and M. B. Duke (1986) J. Geophys. Res. 91, 12804-12816. 12. Miyamoto M., Duke M. B. and McKay D. S. (1985) Proc. Lunar Planet. Sci. Conf. 15th, J. Geophys. Res. 90, C629-C635. 13. Lindsley D. H. (1983) Am. Mineral. 68, 477-493.
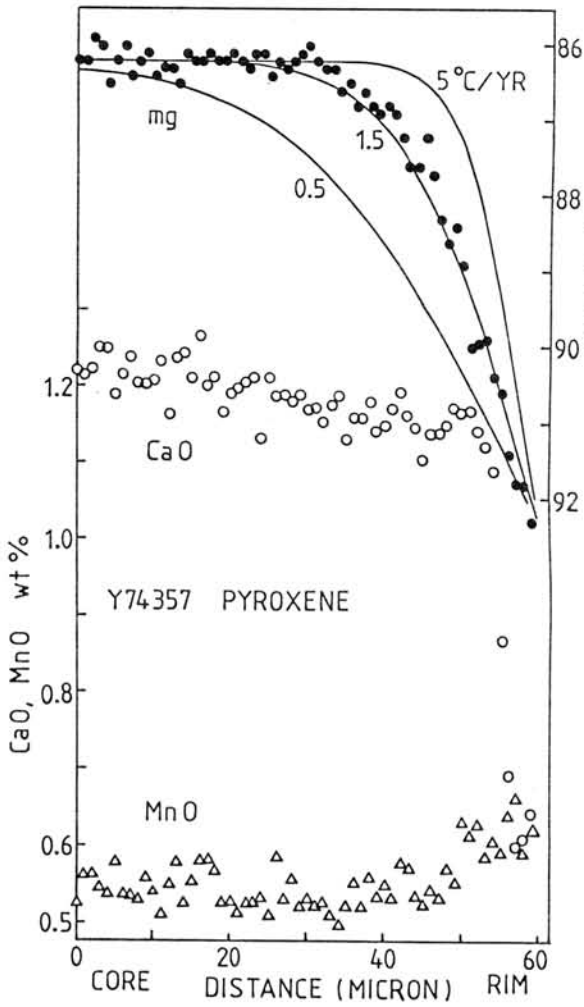
Fig. 1. Chemical zoning profiles of an orthopyroxene in Yamato-74357. Solid circles indicate mg number (=100xMg/(Mg+Fe); right-hand scale). Open circles and triangles indicate CaO and MnO contents, respectively (wt%; left-hand scale). Curves show calculated diffusion profiles. Numbers on curves show cooling rates in °C/year. Data are at 1-micron intervals.



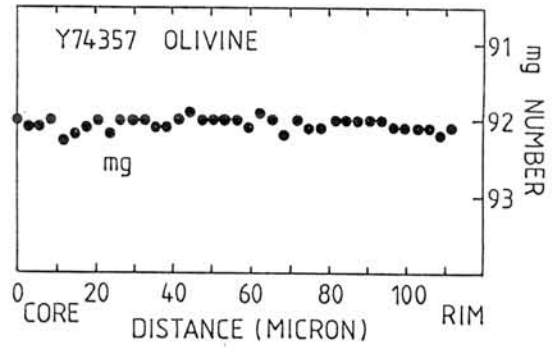Fig. 2. Fe-Mg profile of an olivine in Yamato-74357. Solid circles indicate mg number. Data are at 3-micron intervals.

**MÖSSBAUER SPECTROSCOPY STUDIES IN ANTARCTIC CARBONACEOUS CHONDRITES Y-86720 AND Y-82162; R. B. Scorzelli and I. Souza Azevedo,** Centro Brasileiro de Pesquisas Fisicas - R. Dr. Xavier Sigaud, 150-22290, Rio de Janeiro, RJ, Brazil

The Antarctic carbonaceous chondrites Y-86720 and Y-82162 have been investigated by Mössbauer Spectroscopy through the temperature range $4.2K \leq T \leq 300K$. The preliminary results showed differences in the hyperfine parameters of Y-86720 and Y-82162, probably due to their different thermal history (1, 2). Both exhibit Mössbauer spectra at 300K that indicate the presence of: a) a magnetic spectrum that can be attributed to Fe-sulfides; b) an $Fe^{3+}$ doublet, probably ferrihydrite; c) an $Fe^{2+}$ doublet relative to olivine. These spectra apparently differ from other non Antarctic carbonaceous chondrite, e.g., the Niger meteorite, where the presence of magnetite was reported (3).

Lowering the temperature, important changes have been observed. The analysis of these low temperature spectra is necessary and is in progress in order to well characterize all the phases.

The existence of superparamagnetism in these meteorites in also under investigation.

**References:**

(1) Kazushige Tomeoka, Hideyasu Kojima and Keizo Yanai: Proc. NIPR Symp. Antarct. Meteorites, 2, 36, 1989.

(2) Kazushige Tomeoka, Hideyasu Kojima and Keizo Yanai: Proc. NIPR Symp. Antarct. Meteorites, 2, 55, 1989.

(3) R. B. Scorzelli, I. Souza Azevedo and J. Danon, Meteoritics 25(3), 300, 1988.

# Special Lecture (IV)

*Professor Cryil A. Ponnamperuma*

# THE ORIGIN OF LIFE

**Cyril A. Ponnamperuma**; Laboratory of Chemical Evolution, Dept. of Chemistry, The University of Maryland, College Park, MD 20742, U.S.A.

According to the hypothesis of chemical evolution the molecules necessary for life were formed before the emergence of life. In our studies we have followed two major approaches: synthesis and analysis. The synthetic approach is an attempt to trace the path by which the components of the nucleic acids and the proteins were made by the action of different energy sources on the primordial atmosphere. In the analytical studies the story of the origin of life is unravelled from the molecular fossils present in the earliest rocks and sediments. Of special interest are the carbonaceous chondrites which contain organic compounds synthesized during the early stage of planetary formation. Here we have in our hands the only prebiotic organic matter available for laboratory study. Radio astronomers have extended these searches to the interstellar medium. They have found a host of molecules which may be considered to be intermediaries in Chemical Evolution. The laboratory synthesis, the analysis of carbonaceous chondrites, and the detection of interstellar organic molecules lead one to the conclusion that the process of chemical evolution is commonplace in the universe.

*Poster Session*

*and*

*Abstract Only*

EXPERIMENTAL DEMONSTRATION  OF FORMATION OF MAGNETITE AND WUSTITE
FINE GRAINS

C.Kaito and Y.Saito
Kyoto Institute of Technology, Kyoto 606

The most advanced method for producing grains of metal or
oxide from gas phase is the so-called "GAS EVAPORATION METHOD",
in which  a material is heated in inert gas atmosphere[1].  The
evaporated vapor is subsequently cooled and condensed in the gas
atmosphere,resulting in a smoke which looks like that  of a
candle. The direct evaporation of the oxide or sulfide in the gas
was not always given  the same components of the evaporant,i.e.
decomposition took place.  We proposed various methods for pro-
ducing compounds[2-4],by using  the convection  flow of inert
gas.  The coalescence growth is regarded as an important process
in the gas evaporation tecqnique.  The growth late of the grains
can be presented as follows,

$$dr/dt = mk/4\pi\rho$$

where r, $\rho$, m and k are grain radius,  mass density and the
factor of  the coalescence probability.The coalescence in smoke
takes place in a very short time of $10^{-2\sim-3}$ s.  Since the mass
density m increases with gas pressure and the source temperature,
the gas pressure was one of the important factor to controll the
grain size.  In this paper , it is shown  iron oxides can be
controlled by gas pressure.

The sample preparation  chamber is a glass cylinder of 17 cm
in inner diameter and 33 cm in height . A tantalum v-boat charged
with powder  of FeO was heated at $1800^\circ C$ in Ar gas at 10-100
Torr.Grains in the produced smoke were collected  on thin carbon
film supported  by electron microscopic grids and observed  with
a Hitachi H-800 electron microscope.

Typical smokes which formed by evaporating  FeO in Ar gas at
10 and 100 Torr are shown in Fig.1.  The evaporation source was
almost perpendicular to the photographic  plane. Fig.2 (a) and
(b) shows electron microscopic (EM) image and electron diffrac-
tion (ED) pattern from the grain collected in  smoke of 100 Torr.
ED pattern shows formation of magnetite. External shape of the
well-grown  grains was cubic octahedron.  Fig.3(a) and (b) also
shows EM image and ED pattern  of the grains  produced Ar gas
pressure of 20 Torr.  ED pattern shows the growth of FeO (wustite
) grain.  Produced grains were  changed by the gas pressure of
inert gas.   A summary  of the produced grains due to the gas
pressure is shown in table 1.  The magnetite grains were predomi-
nantly produced  above 25 Torr.  At 10 Torr gas pressure , iron
grains were produced. At 15 Torr gas pressure, wustite  oxide was
produced on the surface of iron grains.  the grain of wustite
predominatly  appeared in gas pressure 17-20 Torr.  These results
show that the evaporated  FeO powder was decomposed  and oxida-
tion took place in the atmosphere. Since the temperature of the
grains  became  a few hundered degrees at a point about 10 mm
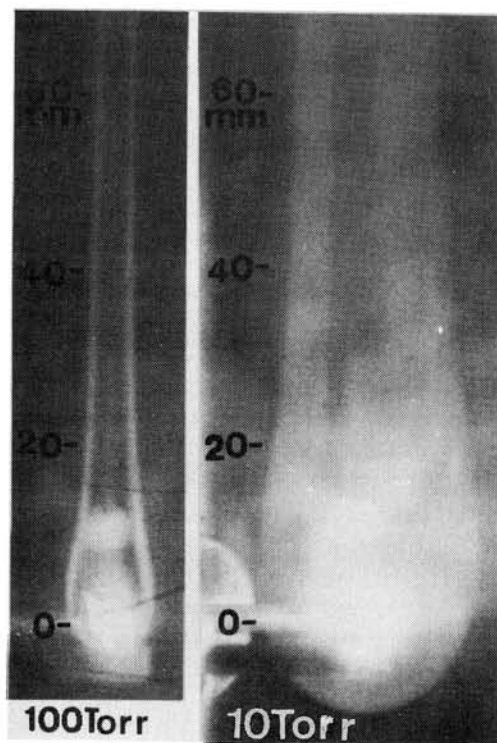above  the evaporation source, the oxidation of iron grain took
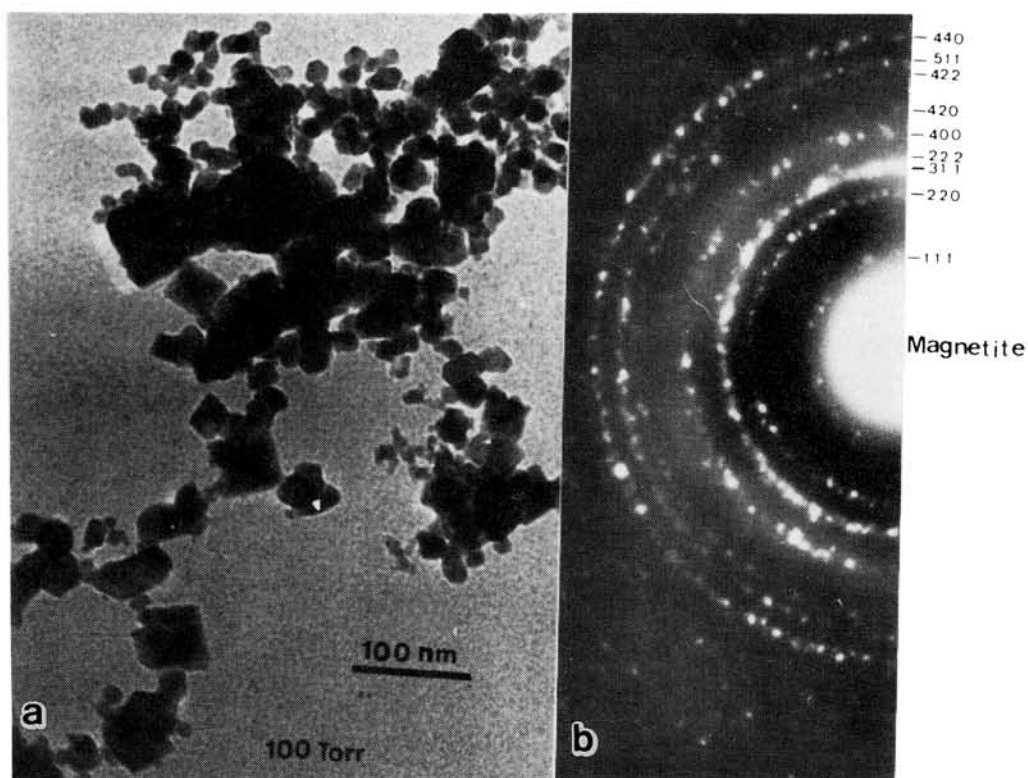
Fig.1



Fig.2

place near the heat dsource. Therefore the formation of various oxides by the gas pressure is due to variation of the oxygen gas density per unit volume in the smoke. The shape of the smoke changes drastic below the gas pressure of 25 Torr. The width of the smoke at 100 Torr at 10 mm from the evaporation sourve is about 7 mm as seen in Fig.1, but the values becomes about 1.7 and 3 times greater at gas pressure of 20 Torr and 10 Torr. Since the shape of the smoke is due to the convection of inert gas, decmposed oxygen gas also flows along to the convection. Therefore the density of the decomposed oxygen vapors per unit volume becomes smaller with decrease of gas pressure. Since the melting point of iron is $1536^\circ$ C , the decomposed iron gas was condensed as the iron grain near the evaporation source. Therefore oxidation of iron took place and oxide grains can be produced in a high gas pressure. Since the gas pressure at the evaporation source is the order of 1 torr which is the critical condition to produce the smoke grains, number of the decomposed oxygen gas atoms is about $10^{15}$.

[1] Kimoto etal., Jpn.J.Appl.Phys.,2(1963)702
[2] Kaito , J. Cryst. Growth 55 (1981) 273
[3] Kaito, Jpn.J.Appl.Phys.,23 (1984) 525
[4] Kaito etal., J.Cryst Growth 94(1987) 967
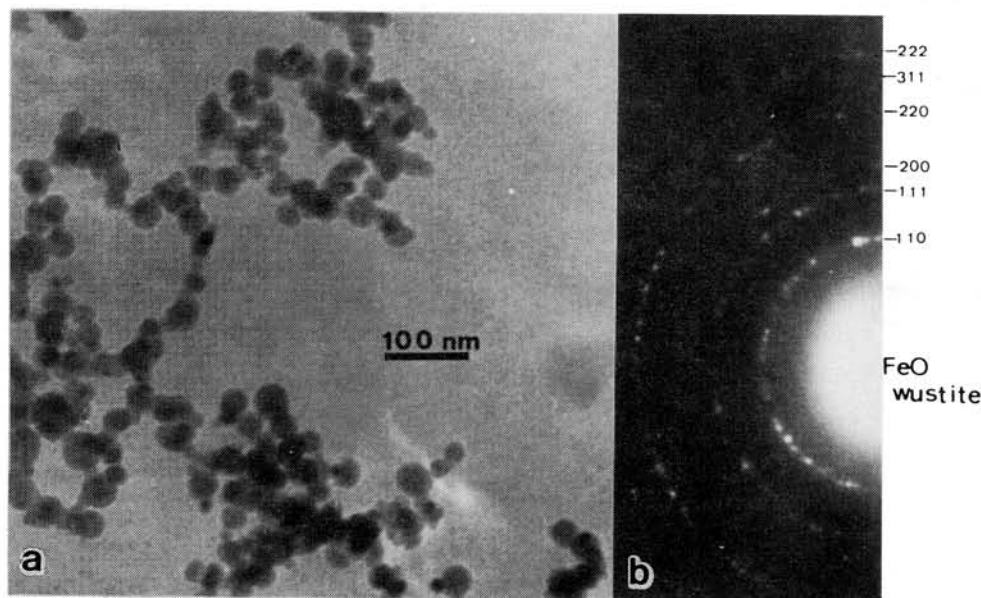
Fig.3

TABLE 1. Results of analyses of iron oxide grains

| Ar Gas Pressure (Torr) | 10 | 15 | 17-20 | 25-100 |
|---|---|---|---|---|
| Produced Grain | $\alpha$-Fe | $\alpha$-Fe (FeO) | FeO | $Fe_3O_4$ |

( ) means the oxide produced on the surface of $\alpha$-Fe

# A NEW FALLEN YANZHUANG CHONDRITE FROM CHINA.

Wang Daode, Xie Xiande, Li Zhaohui and Chen Yongheng, Insitute of Geochemistry, Academia Sinica, Guangzhou Branch, Guangzhou 510640, Guangdong Province, The People's Republic of China

The Yanzhuang chondrite fell in a field of Yanzhuang Country(24° 34'N,114° 10'E), Wengyuan County, Guangdong Province, on October 31, 1990, 0945 hrs (Beijing time). After appearance of a luminous meteor and detonations several fragments totalling 3.5kg were recovered by farmers. The largest recovered fragments has a mass of 823g. Yanzhuang chondrite is recognized as distinct from previously collected chinese ordinary chondrites. Yanzhuang chondrite shows the strong shocked effect with localized shock-melting and the black vein-like mass on the surface of these samples. All these samplesare located at the Institute of Geochemistry, Academia Sinica, Guangzhou Branch, Guangdong Province, China.

The mean bulk composition(determined by wet chemical analysis) is (in wt.%): $SiO_2$, 36.76; MgO, 23.25; FeO, 10.25; $Al_2O_3$, 2.44; CaO, 1.70; $Na_2O$, 0.93; $K_2O$, 0.13; $Cr_2O_3$, 0.45; MnO, 0.39; $TiO_2$, 0.10; $P_2O_5$, 0.18; Cu, 0.029; Ni, 1.81; Co, 0.086; Fe, 17.16; FeS, 4.73; $H2O^-$, 0.08; $H2O^+$, 0.09; total, 100.475. Total Fe is 28.11.According to the bulk chemical composition and content of total Fe Yanzhuang chondrite belongs to H group. The meteorite has a very recrystallized texture; relict chondrules are poorly-defined. Silicate grains are fractures and exhibit undulose extinction. The electron microprobe analyses indicatee the chemical composition of olvine and low-calcium pyroxene are homogeneous, Fa 18.1 in average, Fs 16.0 Wo 1. 2. We classify Yanzhuang as an H6 chondrite.

Preliminary results of noble gases ( O. Eugaster, personal communication, 1991) are shown as follows (concentration in $10^{-8}$ $cm^3$ STP/g): $^4He$, 95; $^{20}Ne$, 0.71; $^{40}Ar$, 220; $^4He/^3He$, 28; $^{20}Ne/^{22}Ne$, 0. 88; $^{22}Ne/^{21}Ne$, 1.05; $^{40}Ar/^{36}Ar$, 444 and $^{36}Ar/^{38}Ar$, 2. 6. Cosmic ray exposure ages derived from $^3He$, $^{21}Ne$ and $^{38}Ar$ are ca. 2.1, 1.6 and 2.4 Ma, respectively. The average cosmic ray exposure age of Yanzhuang chondrite is about 2 Ma. We will study Yanzhuang chondrite in detail.

We thank Prof. Otto Eugster for the noble gas analyses.

FEATURES OF CHROMITE CHEMISM OF THE UPPER MANTLE AND METEORITES: OXYGEN FUGASITY AND COMPOSITION OF CHROMITE-BEARING ASOCIATIONS.N.S.Gorbatchev,A.A Krot.Institute of experimental mineralogy USSR Academy of sciences 142432 Chernogolovka, Moscow district, USSR.

Introduction The features of chromite composition from kimberlites (ultramafic modules, megacryst, intergrowths) of Yakutiya and different type meteorites are investigated. Two main tendencies of a change of chromite composition are observed: (Fig.1)1. With the replacement of the type $FMAl_2O_4$ $FMCr_2O_4$ at wide variations of the contents of $Al_2O_3$ and $Cr_2O_3$ in chromites of the upper mantle and narrow ones - in meteorite chromites. Maximum concentrations $Cr_2O_3$ are typical for chromites of the high-baric assosiations of the diamond facies of the depth of the upper mantle, as well as for the iron meteorites and pallasites are typical. In meteorite chromites the content of $Cr_2O_3$ decreases in the following sequence: iron meteorites-pallasites, where $Cr_2O_3$ and $Al_2O_3$ content is similar to those of the diamond facies of the depth-mesosiderites. 2. With the replacement of the type $FMCr_3O_3$ $TiFe_2O_4 + FeFe_2O_4$ under wide variations $Cr_2O_3$, $Fe_2O_3$ and $TiO_2$ in chromites of the upper mantle and narrow - in meteorite chromites. The content in the latter $Cr_2O_3$ decreases, $TiO_2$ and $Fe_2O_3$ increase from ordinary hondrites of the H-type to the ordinary hondrites of the LL type.

The first direction of the evolution of the chromite composition is related to the pressure increase, and possible to the decrease of oxygen fugacity, the second is related to the increase of oxygen fugacity and possibly - to the pressure decrease. However, it is difficult to estimate the influence of each factor upon chromite composition.

Results Taking into account an important role of chromite-bearing associations to estimate physico-chemical conditions of magmatic petrogenesis, the influence of oxygen fugacity upon the composition of chromite-bearing associations, forming under melting of sulphide-bearing peridotite in the range $T = 1250 - 1300^{o}C$, $P = 5 - 10$ kbar, at oxygen fugacity, corresponding to the NNO buffer and stability field of wustite is experimentally studied.

Under oxidation conditions under NNO oxygen buffer moderately alumina chromite coexits with magnesian olivine, orthopyroxene, sulphide and silicate melts. Olivine, glass, sulphide coexisting with the phase chromite are characterized by low contents of chromium, not exceeding 0,1-0,2 wt.% (Tabl.1)

Under reduction conditions, corresponding to wustite stability, the coexisting phases-chromite, olivine, sulphide melt are sharply enriched with chromium The pressure does not effect markedly upon the composition of the coexisting chromite and phases coexisting with it.

Discussion The enrichement of chromite, olivine and sulphide melt with chromium can be explained by the existence of chromium at a low fugacity not only in the form of $Cr^{+3}$, but as $Cr^{+2}$. Two- valency chromium is similar to two-valency iron by crystalochemical properties what contributes to its isomorphic entering into the olivines and sulphide melt.

Thus, the increase of chromium content in the chromite and coexisting olivine and sulphides is a feature of formation of chromite-bearing associations under reduction conditions.

Table 1. The composition of chromite bearing association (wt.%).

| number | 1 | | | 2 | | | 3 | | |
|---|---|---|---|---|---|---|---|---|---|
| $T^oC$ | 1300 | | | 1300 | | | 1300 | | |
| P kbar | 5 | | | 10 | | | 5 | | |
| $lgf_{O_2}$ | -6,65 | | | -6,80 | | | -9,70 | | |
| oxide | Chr | Ol | Gl | Chr | Ol | Gl | Chr | Ol | Gl* |
| $SiO_2$ | - | 42.79 | 53,85 | - | 42,43 | 52,71 | - | 40,92 | 50,91 |
| $TiO_2$ | 0,48 | - | 1,25 | 0,47 | - | 0,91 | 0,68 | - | 0,79 |
| $Al_2O_3$ | 17,97 | - | 14,75 | 16,48 | - | 12,13 | 9,34 | - | 12,55 |
| $Cr_2O_3$ | 51,51 | 0,30 | 0,22 | 50,46 | 0,22 | 0,31 | 63,16 | 0,88 | 0,28 |
| FeO | 13,29 | 8,51 | 7,55 | 13,60 | 8,19 | 8,19 | 7,31 | 7,15 | 7,56 |
| MgO | 18,11 | 48,67 | 12,72 | 17,64 | 48,10 | 13,89 | 19,35 | 52,19 | 18,41 |
| CaO | 0,13 | 0,17 | 6,22 | 0,21 | 0,14 | 6,81 | 0,22 | 0,20 | 5,59 |
| $Na_2O$ | - | - | 2,98 | - | - | 3,11 | - | - | 2,15 |
| $K_2O$ | - | - | 0,51 | - | - | 0,57 | - | - | 0,46 |
| total | 101,5 | 100,4 | 100,1 | 98,9 | 99,1 | 98,6 | 100,1 | 101,2 | 98,7 |

sulfide

| | | | |
|---|---|---|---|
| Fe | 47,72 | 50,30 | 51,63 |
| Cr | 0,30 | 0,21 | 4,67 |
| Ni | 14,96 | 10,93 | 13,46 |
| Cu | 0,80 | 0,70 | 0,91 |
| S | 36,50 | 39,54 | 38,77 |
| total | 100,28 | 101,14 | 98,94 |

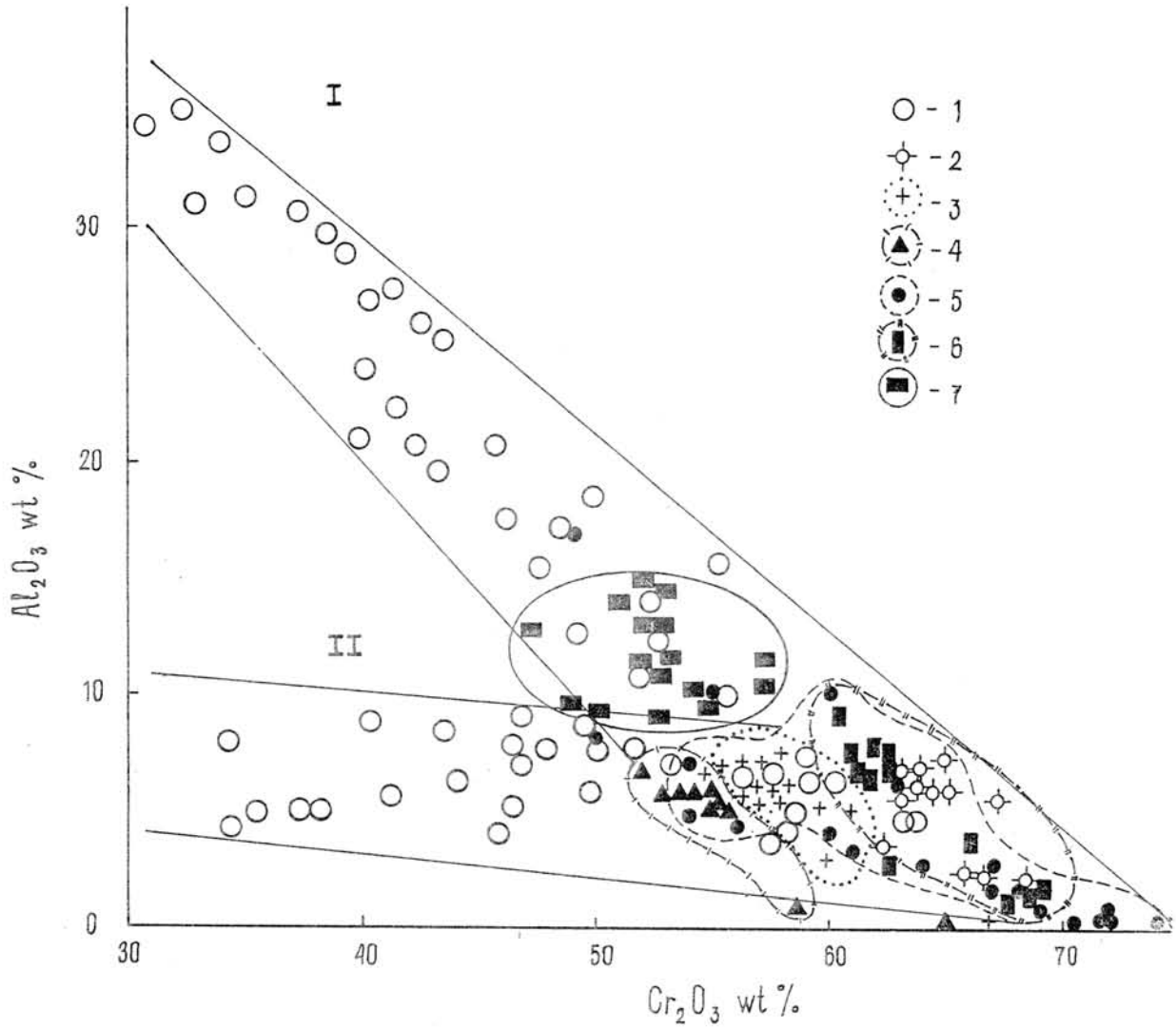* Chr - chromite, Ol - olivine, Gl - glass.

Fig.1.The composition of meteorites;
1 - 2 - from upper mantle; 1 - averedge,
2 - diamond bearing. 3 - 7-from meteo-
rites: 3 - 4 - ordinary chondrite,
3 - H type,4 - LL type,5 - iron meteo-
rite, 6 - pallasite, 7 - mesosiderite.

Rb-Sr AND Sm-Nd SYSTEMATICS IN POMOZDINO METEORITE

S.F.Karpenko, M.I.Smoliar*. M.I.Petaev, Yu.A.Shukolykov, Vernadsky Institute of Geochemistry and Analitical Chemistry, USSR Academy of Sciences, Moscow 117975, USSR; * Moscow State University, Geological Department, Moscow 119899, USSR

Pomozdino that was classified as an eucrite in its first description [1] has some anomalies in mineralogy and chemistry as compared with other eucrites. New isotopic [2], petrological and geochemical [3] studies confirmed its initial classification as an anomalous, high magnezia and REE-rich monomictic eucrite. It follows from geochemical data that Pomozdino is a partial cummulate with unusually high content of trapped melt, which distinguishes it from other eucrites. Thus it seems very important to study the geochronolgy of this meteorite using Sm-Nd and Rb-Sr systems and compare these results with published data on other eucrites.

Mineralogy of Pomozdino is common for eucrites: it consists of pyroxene (53.3%), plagioclase(32.8%), quartz(4.6%), ilmenite(0.93%), chromite(0.56%) and slightly increased content of metal and troilite(2.4%). Rare grains of phosphate occur sometimes in the plagioclase, and their composition corresponds to low-chlorine apatite.

Three whole rock samples of the meteorite and monomineral fractions of pyroxene (Cpx), plagioclase (Plag), and cromite-ilmenite (Quint) were used for isotopic dating, as well as HCl leachate of total rock sample(WR3 leach) and the corresponding residue (WR3 res).

All the chemical operations with these samples and separation of Sm, Nd, Rb and Sr for mass-spectrometric measurements were done in the Vernadsky Inst. of Geochemistry and Moscow State University using standart procedures [4,5]. Isotopic measurements were done on MAT-261 mass-spectrometer at the Inst.of Precambrian Geology and Geochronology in Leningrad (Sm,Nd) and on MI 1201T mass-spectrometer at Moscow State University (Rb, Sr). The results are shown in the table and on Fig.1 and 2.

These data show that the crystallization age of Pomozdino meteorite determined from Sm-Nd internal isochrone is 4.54 ±.15b.y. with $(^{143}Nd/^{144}Nd)_o=$ 0.50600. These results are completely comparable with the data of J.Hammet et al.[6] for cumulative eucrite Moama (it should be mentioned that Caltech people obtained somewhat different results for the same meteorite[7]). Rb-Sr systems in these samples were badly disturbed as a result of Rb pollution(?) at one of the stages of analysis. For the least disturbed samples, however, (WR2, Cpx, WR3-leach and WR3-residue) an internal isochrone can be build which corresponds to 4.21 ± .18 b.y. and $(^{87}Sr/^{86}Sr)_o = 0.69898 ± 7$. It follows from these data that the Rb-Sr system of Pomozdino was rather strongly disturbed ≈300 m.y. after its formation, so that the results of Sr isotopic studies of such meteorites can not be used as a strong evidence pro (or contra) the unique source for their formation. Similar conclusions were made by Birck and Allegre [8] in their study of Rb-Sr systematics in several basaltic achondrites.

So we conclude that better understanding of the eucrite formation processes requires further studies of Sm-Nd systems in eucrites.

Rb-Sr AND Sm-Nd SYSTEMATICS IN **P**OMOZDINO **MET**EORITE  S.F.Karpenko et al.

TABLE OF RESULTS

| SAMPLE | sample weight | [$^{86}$Sr] | $\frac{^{87}Rb}{^{86}Sr}$ | $\frac{^{87}Sr}{^{86}Sr}$ | [$^{144}$Nd] | $\frac{^{147}Sm}{^{144}Nd}$ | $\frac{^{143}Nd}{^{144}Nd}$ |
|---|---|---|---|---|---|---|---|
| | mg | nmol/g | | | nmol/g | | |
| Cpx | 110.4 | 16.74 | .0078 ±1 | .69948 ± 3 | 3.338 | .2536 ±2 | .51359 ±2 |
| Quint | 20.6 | 51.72 | .0193 ±3 | .69960 ± 7 | 8.357 | .1954 ±2 | .51189 ±2 |
| WR1 | 94.7 | 93.60 | .0664 ±4 | .69926 ± 7 | 17.56 | .1885 ±2 | .51170 ±2 |
| WR2 | 46.2 | 94.42 | .0070 ±3 | .69940 ±10 | | | |
| WR3 leach | 19.2 | 472.1 | .0052 ±1 | .69928 ± 3 | 35.15 | .1752 ±2 | .51124 ±2 |
| WR3 res | 94.9 | 8.978 | .0569 ±3 | .70248 ± 5 | 2.321 | .3108 ±3 | .51539 ±2 |
| Plag | 63.4 | 165.9 | .0345 ±4 | .69949 ± 6 | 2.889 | .1868 ±2 | .51168 ±2 |
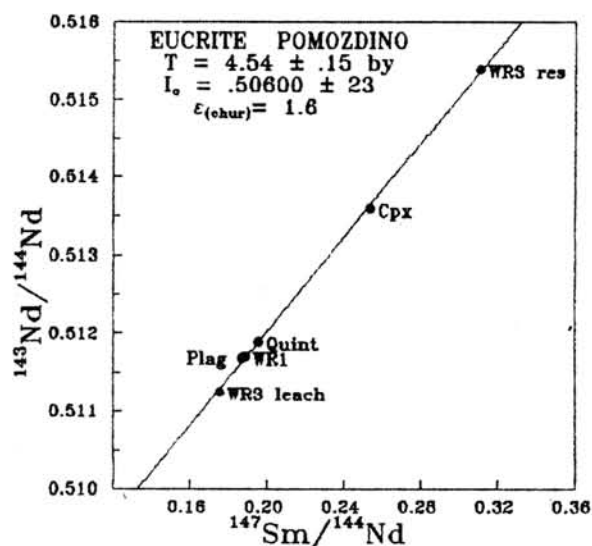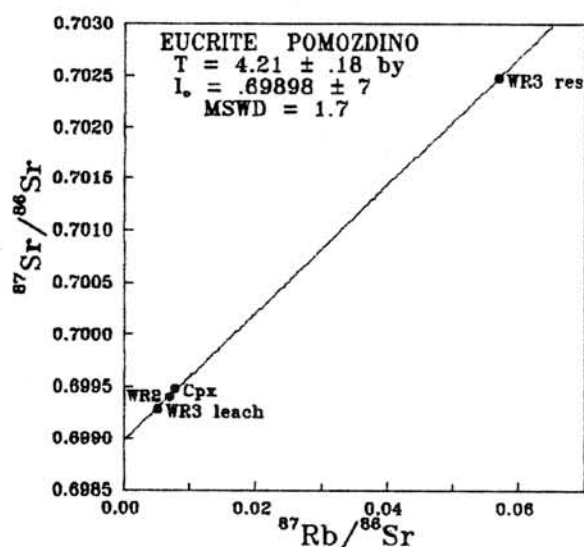


REFERENCES
[1] Kvasha L.G., Dyakonova M.I., Meteoritics, 1976, v.36(in Russian)
[2] Petaev M.I. et. al., Abstr. XIX LPSC, 1988, Pt 2
[3] Warren P.I. et. al., Proc.20th LPSC, 1990
[4] Karpenko S.F. et. al., Geochemia, 1984, n7(in Russian)
[5] Smoliar M.I. et. al., this volume
[6] Hammet J. et. al., Proc.9th LPSC, 1978, p.1115
[7] Jacobsen S.B. and Wasserburg G.J., EPSL, 1984, v.67, p.137
[8] Birck J.L. and Allegre C.J., EPSL, 1978, v.39, p.37

# CHROMITE-RICH INCLUSIONS IN ORDINARY CHONDRITES

Krot A.N.[*], Mitrejkina O.B.[**], Zinov'eva N.G.[**], Stroganov I.A.[*], Ivanova M.A.[*], Petaev M.I.[*] (Vernadsky Inst. Geochem. Anal. Chem., USSR Acad. Sci.[*], Moscow States University[**], Moscow, USSR)

Unusual inclusions in H-chondrites Raguly (3-4), Gorlovka (3-4), Krasny Klyuch (4), Ivanovka (5) were investigated by SEM and EPMA. These inlusions varying in size from 50 to 300 um are composed of chromite (Chr), whitlockite (Wh), plagioclase (Pl)-, potassium-feldspar (K-Fsp)- and Q-normative glasses, Ca - rich (Cpx), Ca-poor pyroxene (Opx), ilmenite (Ilm), olivine (Ol), Fe-Ni, usually converted to Fe-oxides (Ox). Similar objects were described in ordinary chondrites by Ramdohr [1]. Based on morphology, mineralogy and chemistry the incusions may be divided into 5 groups.

I. Rounded or ellipsoidal aggregates of fine (<5 um) Chr grains, forming sometimes massive cores, embeded in and/or surrounded by Pl - K-Fsp-glass rims and occurring within Ox. The outer parts of the rims are usually framed by euhedral grains (< 10 um) of Cpx, rarely Opx and Ol (Fig. 1a). Chrs are similar in composition (Fig. 2) with those from H-chondrites [2]. CIPW normative compositions of glasses correspond to Pl- and K-Fsp varieties (Fig. 3). Pxs are high-Ca- (Fs 5-12 En 47-50 Wo 41-46), sub-Ca- (Fs 13 En 68 Wo 19) and low-Ca- (Fs 16-17 En 82-83 Wo 1) types.

II. Isometrical inclusions occurring in silicate matrix and composed of massive and fine-grained Chrs, Wh, Pl - K-Fsp-glasses (Fig. 1b). Rary Fe,Ni-inclusions (< 1 um) have been found in some Chr grains. Chrs have chemical compositions similar with ones from the I group inclusions (Fig. 2). Glass compositions vary from Pl- to K-Fsp-normative (Fig. 3).

III. Zonal irregular inclusions occurring in silicate matrix or partly surronded by Ox are composed of Chr-silicate core --> intermediate Chr rim --> external silicate rim (Fig. 1c,d). Silicate constituent of the cores containes Cpx (Fs 6 En 48 Wo 45), sometimes overgrowing Opx (Fs 16 En 83 Wo 1), Pl-normative glass, ±Ol. Chrs are homogeneous in composition within individual inclusions and vary between them (Fig. 2). The core of inclusion #4/07 having Chrs richest in $Al_2O_3$ (18 wt.%) contains Px-Q - normative glass (Ab 3.8% Ns 23.6% Di 25.5% Q 43.9%). The external silicate rims consist of Pl-normative glasses, sometimes with inclusions of Al-rich Cpx (up to 9 wt.% $Al_2O_3$) and Cpx (2-7 wt.% $Al_2O_3$, 1-1.3 wt.% $Cr_2O_3$) forming the outer part of the silicate rims.

IV. Zonal irregular inclusions occurring in silicate matrix are composed of Chr-silicate core --> massive Chr rim --> silicate rim --> continuous or
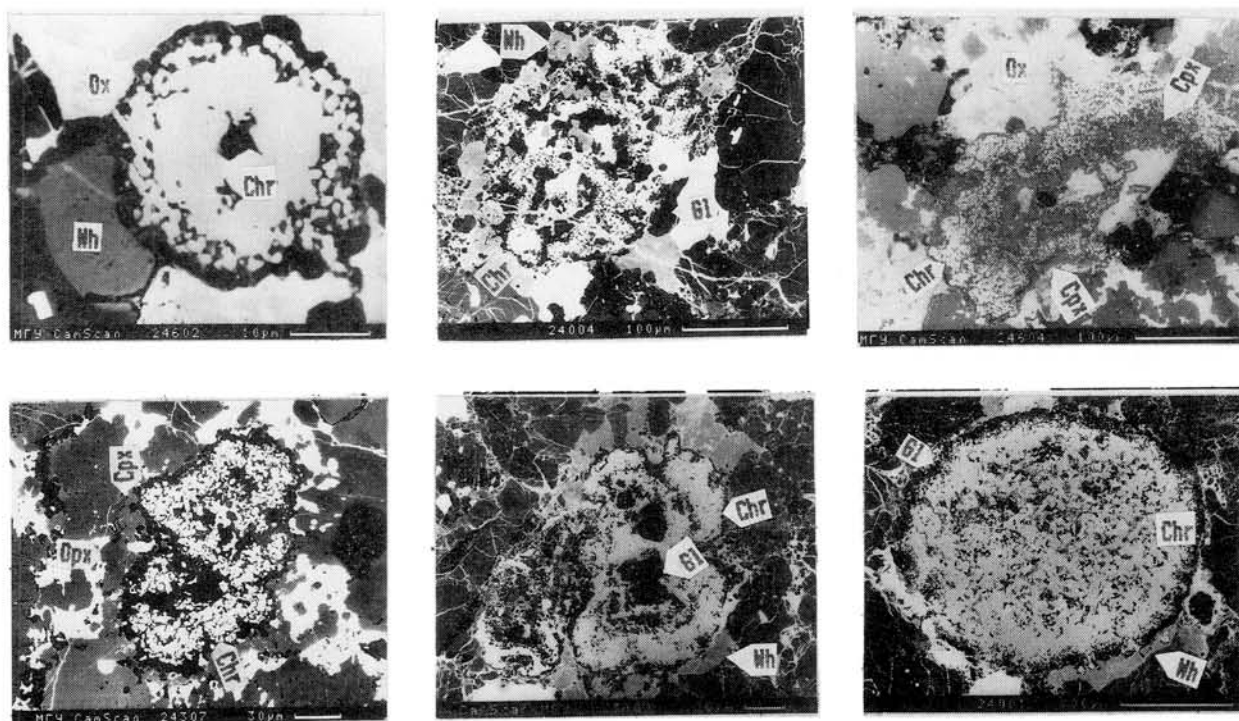
Fig. 1. Chromite - rich inclusions:a - type I, b - type II, c, d - type III, e - type IV, f - type V.
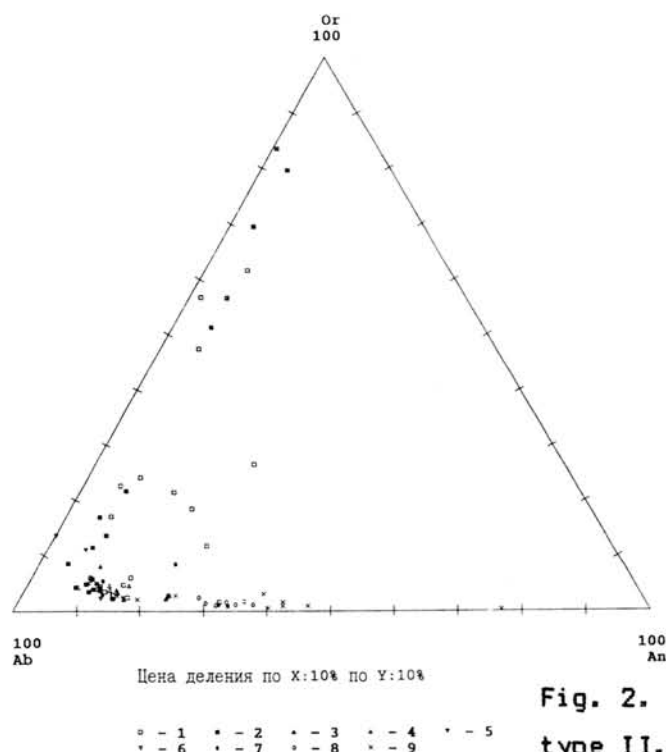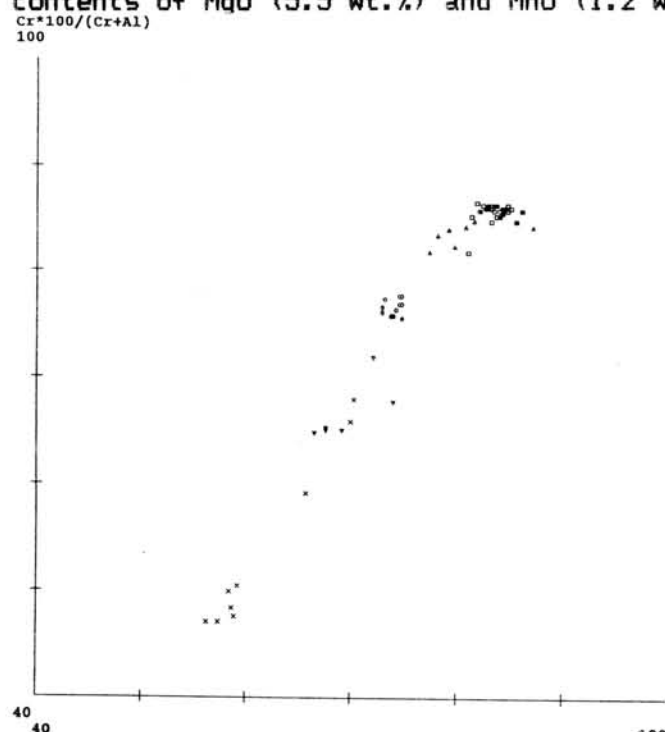


Цена деления по X:10% по Y:10%

Fig. 2. Glass chemistry: 1 - type I, 2 - type II, 3 - 5 - type III, 6 - 7 - type IV, 8 - 9 - type V.

interrupted Wh rim. Silicate core and rim are consisted of Pl-glass (Fig. 1 e, 3). Chrs being constant in composition within separate grains have high $Al_2O_3$ contents decreasing from core to rim or constant within inclusion (Fig.2).

V. Chondrule-like inclusions occurring in silicate matrix and having zonal structure: Chr±Ilm-silicate core --> intermediate Chr rim --> silicate

rim --> continuous or interrupted Wh rim sometimes with Chr inclusions (Fig. 1 f). Silicate costituent of the core and rim is Pl-normative glass (Fig. 3). Cpx grains (Fs 9.3 En 48.2 Wo 42.3, 5.1 wt.% $Al_2O_3$) occur in an external part of silicate rim. Chrs are variable in composition from core to Wh rim (29.1-28.3 wt $Al_2O_3$ - core; 27.9-26.8 wt.% $Al_2O_3$ - intermediate Chr rim; 21.2 wt.% $Al_2O_3$ - silicate rim; 17.1-16.0 wt.% $Al_2O_3$ - Wh rim) or constant within inclusion. Ilm occurring as intergrowths with Chrs is characterized by high contents of MgO (5.5 wt.%) and MnO (1.2 wt.%).



Цена деления по X:10% по Y:10%

□ - 1   · - 2   · - 3   · - 4   · - 5
· - 6   · - 7   · - 8   × - 9

Fig. 3. Chromite chemistry: 1 - type I, 2 - type II, 3 - 5 - type III, 6 - 7 - type IV, 8 - 9 - type V.

Early K-rich-phases were found in ordinary chondrites but in a different assemblage [3]. Similar mineralogical assemblage containing K-Fsp, Q, Al-Chr, Wh, Cpx, Ilm was described in silicate inclusions in IIE irons [4] and are supposed to be related with H - chondrites [5]. Perhaps in a similar object in the Simmern chondrite (H5) [6] zircon was found. Presence of such assemblage in unequilibrated H-chondrites (Raguly) suggests their primitive nature. Data obtained suggest complicated history of their formation in a fractionated system.

References: [1] Ramdohr P. (1973) The opaque minerals in stony meteoriotes [2] Bunch T.E. et al. (1967) GCA, v.31, p.1569-1582; [3] Wlotzka F. et al. (1983) GCA, 47, 743-757 [4] Bunch T.E. et al. (1970) Contr. Miner. Petrol., v.25, p.297-340; [5] Olsen E., Jarosewich E. (1970) EPSL, 8, 261-266 [6] Wlotzka F. (1990) Abstr. 53 Ann. Meteor. Soc. p.186

THE GENETIC TYPES OF METEORITES

Marakushev A.A.

Institute of Experimental Mineralogy, USSR Acad. Sci.
Chernogolovka Moscow district, USSR

In a general evolution of cosmic substance at least five
stages are distinguished: 1. High temperature condensation of
gases and formation of solid dust particles in protostellar
clouds; 2. Low temperature condensation (and congelation) of
gases and formation of ice bodies of comets and comet-like
planetesimals; 3. Origin of fluid planets by accretion of the
comet-like planetesimals and their complete melting; 4. Layer-
ing of the fluid planets and formation of their chondritic co-
res and achondritic satellites; 5. Appearance of the Earth and
other iron-stone planets as the result of surface degasing of
their parent fluid planets. Explosive destruction some of them
produced asteroids and meteorites.

Dust particles in protostellar dense molecular clouds con-
sist of aggregates of silicates, quartz, metals, sulfides, gra-
phite, covered with thin layers of organic compounds and water
ice. Dust particles are also included into ice core of comets
and introduced into the Solar system by them. They fall periodi-
cally to the Earth, giving rise to meteoric rains. Their behavi-
or in atmosphere proves, that dust particles are composed of a
very porous material, being quite different from dense meteori-
tic substance. The same conclusion has been obtained from the
study of dust particles, collected in the upper stratosphere.

In contrast to dust particles, which have never experien-
ced melting, meteorites of all types are magmatic, closely con-
nected with the formation of planets by their origin.

The planets in the Solar system were originated by accretion
of primitive comet-like bodies (ice-planetesimals). The mass of
the material accumulating in planets was big enough to attain
their complete melting. The next step of the evolution was in-
ner layering of planets with separation by liquid immiscibility
of iron-stone melts (chondritic) in their cores from fluid mate-
rial in their shells. In the same way in the external parts of

fluid shells big drops of silicate melts (achondritic) were formed and thrown out by centrifugal forces to create satellite systems of planets. Suchlike was created the state of planets, which is traced now in the planets of the Jupiter group. In contrast to them the planets of the Earth group under the influence of the Sun have lost their fluid shells and almost all satellites. As a result they passed into strain condition produced by pressure of fluids confined in their cores. It is realized in explosive volcanism and destruction some of the planets with the formation asteroids and heliocentric meteorites. The similar destruction of satellites of the Earth and other planets has produced meteorites of planetcentric type, such as so-called lunar meteorites collected from Antarctida (Yamato 763274, 86032 et al.). The explosions of planets and their satellites produced shock metamorphism which is very typical for meteorites.

The planets were mainly exploded at the early stages of their development in the conclusion of a very explosive chondritic volcanism. The main row of chondrites LL-L-H-HH-C3 reflects the increase of the reducing conditions of their formation according to $(H_2+CH_4)/(H_2O+CO_2)$ ratio in the fluid shells of their parent planets. At the end of the row elements pass into extremely low degree of oxidation ($Al_2O$, $SiO$ instead of $Al_2O_3$, $SiO_2$ et al.) and have got an anomalous high chemical affinity with light oxygen isotope ($^{16}O$). So oxygen isotope composition of minerals (Figure) is an indicator of the reducing conditions of chondrite formation.

Development of all-type chondrites is accompanied by the increase of oxidation conditions and results in a typical shifting of their oxygen isotopic characteristics: C3 → HH, H → L, L → LL (due to migration of hydrogen from their parent planets).

Oxidation processes are not limited by magmatic stages and continue in postmagmatic period especially in highly reduced types of chondrites C3, which are replaced by carbonaceous types C2 and C1. The reaction of fluid components ($H_2$ + CO = C + $H_2O$, $CH_4$ + $CO_2$ = 2 C + 2 $H_2O$ and others) stimulates hydratation of magmatic minerals (olivine, pyroxene) and volcanic glasses of carbonaceous chondrites.
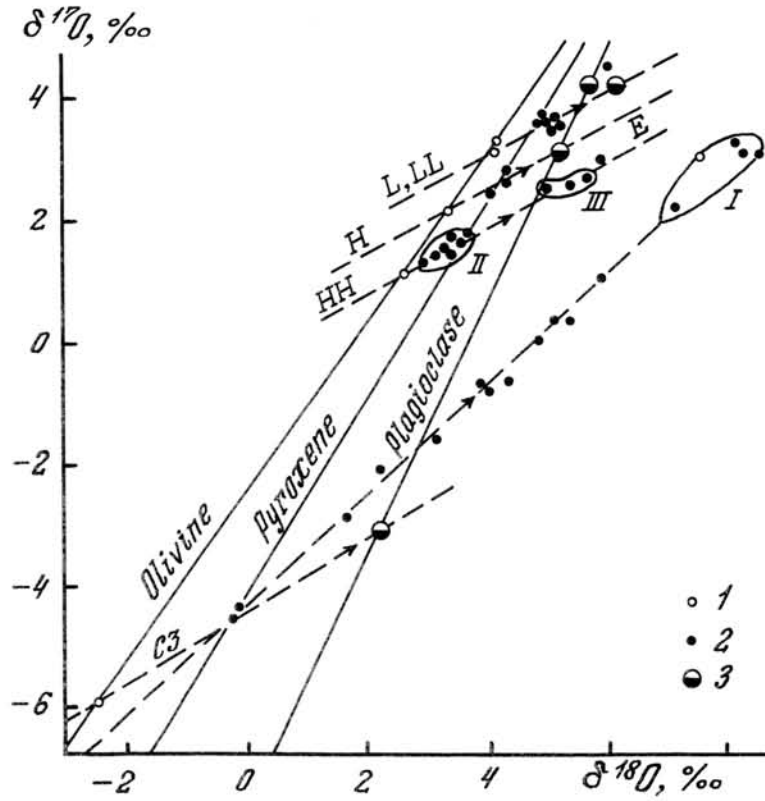
Figure. Mineral oxygen isotope composition plot
1- olivine, 2- pyroxene, 3- plagioclase in
chondrites (LL, L, H, HH, C3 and E); in
achondrites (I - in ureilites, II- in howar-
dites, eucrites); in terrestrial and lunar
rocks (III). After R.N.Clayton, T.K.Mayeda et
al. Solid lines show oxygen composition
change in the minerals of the chondrites of
main row LL-L-H-HH-C3; stroke arrors show
trends of oxygen isotopes fractionation -
normal (coincide with olivine-pyroxene-pla-
gioclase rows) and anomal (C3 - I)

LL-L-H-HH-C3 are primal chondrites. In relation to them all
other meteorites, including E-chondrites, are the result of the
magma differentiation within the corresponding parent planets.
Oxygen isotope correlations testify to the genetic relations of
meteorites marked by stroke arrors in Figure.

Ureilites (I) are originated in C3-chondritic system due to separation of fassaite ($\delta^{17}O = -36$, $\delta^{18}O = -35$ $^o/oo$), spinel ($\delta^{17}O = -39$, $\delta^{18}O = -38$) or melts enriched by the normative minerals (anomal trend of oxygen isotope fractionation in Figure).

E-chondrites are the result of layering of a very iron-rich planets (HH type) into pallasite core ($\delta^{17}O = 1,1$; $\delta^{18}O = 2,9$) and E-chondrite mantle. In this case the separation of olivine or corresponding melts has created the trend of normal mass--fractionation of oxygen isotopes in residual melts and minerals of late crystallization.

This HH-trend embraces howardites and eucrites (low degree of oxygen isotope fractionation), earth and lunar rocks (high degree of the fractionation).

AEOLIAN TRANSPORT OF ANTARCTIC METEORITES IMMEDIATELY AFTER IMPACT: IMPLICATIONS FOR CURRENT TRANSPORTATION MODELS; A. A. Mardon, EDCI, Texas A & M University, College Station, Texas, USA. 77844.

The current transportation models for Antarctic meteorite movement to placer zones is postulated as a simple under surface transportation of the meteorites within the surface layer of the ice to locales that have extensive ongoing abalation, liquification, and sublimation of the exposed blue ice. The author postulates that extensive aeolian movement of meteorites can occur at the stage immediately after impact of the meteorite. This transport mechanism might affect the ice on which the meteorite eventually surfaces in a placer zone. This would bring additional questions into the ability to date meteorites using radiometric oxygen isotope dating systems of the ice that the meteorite is either found within or on.

Current research would indicate that impact velocities of incoming meteorites and the pedistal cratering that occurs on other non-terrestrial surfaces that the meteorites lie on the surface of the ice mass rather than being conveniently buried. The mechanism for burial of the meteorite is though drifting of snow. Characteristics of windscoping of surface obstructiuons in the Antarctic are such that drifting can expose rather than bury objects. (Scheps,1986) If all samples are exposed and are blown around at the begining of the transport process and then this could be a constant process and not affect exposure rates at placers.

With 200 kilometer force winds relatively common on the Antarctic plateau in winter and the average percipitation on the plateau of approximately 4.5 centimeters per year the immediate deposition of meteorites can be brought into some question. The fall rates being even over the entire plateau falls on portions of the polar plateau are up ice of any bedrock that might inject material into the surface layer of the slowly moving ice mass. Any material would not be in the surface layer of the ice. In the case of smaller meteorite samples complete wind transport might occur. Similiar micro-topographical environments depositional characteristics might result in wind-borne meteorite deposit zones in the katabatic wind regions that meteorites have been recovered from in the Antarctic. The physical barrier of mountain ranges and a decrease in altitude and the folowing decrease in speed would result in meteorites being deposited in locales that result in an upwelling in the ice and then exposure through sublimation. Extensive windborne transport of meteorites after fall could transport extensive amounts of meteorites thereby selecting falls by density and size. This figure might in turn affect the ability to project past flux rates based on Antarctic samples. If the depositional rates are not constant or through one mechanism then dating regime models must be revised.

Scheps, Bernard. Perdsonal Communication, 1989.

COSMIC RAY EXPOSURE HISTORY OF LUNAR METEORITE YAMATO 793274 ;
K. Nishiizumi[1], J. R. Arnold[1], J. Klein[2], D. Fink[2], R. Middleton[2], P. Sharma[3], and P. W. Kubik[3] ; (1) Dept. of Chemistry, Univ. of California, San Diego, CA 92093-0317, (2) Dept. of Physics, Univ. of Pennsylvania, Philadelphia, PA 19104, (3) Nuclear Structure Research Lab., Univ. of Rochester, Rochester, NY 14627

Lunar meteorites are expected to have complex cosmic ray exposure histories. They have been exposed both at some depth on the moon ($2\pi$ irradiation) before their ejection and as small bodies in space ($4\pi$ irradiation) during transportation from the moon to the earth. Their terrestrial age can also be long, similar to other Antarctic meteorites. Measurement of cosmogenic nuclides can provide essential constraints for these ages and help to unravel the complex history of these objects. This complexity requires measurement of three or more cosmogenic nuclides in the same sample.

We report here cosmogenic $^{41}Ca$ ($t_{1/2} = 1.0 \times 10^5$ years), $^{36}Cl$ ($t_{1/2} = 3.0 \times 10^5$ years), and $^{26}Al$ ($t_{1/2} = 7.1 \times 10^5$ years) results in lunar meteorite Yamato 793274,65 (Y-793274,65). The $^{41}Ca$ and $^{26}Al$ results were determined using the University of Pennsylvania tandem accelerator [1, 2] and the $^{36}Cl$ result was determined using the University of Rochester tandem accelerator [3]. The results are shown in Table 1 along with cosmogenic nuclide concentrations in other lunar meteorites [4, 5, 6]. Table 1 contains our results along with some reported by others. The $^{10}Be$ and $^{53}Mn$ measurements in Y-793274,65 are in progress. Although three nuclides do not provide enough information to fully explain the complex history of this meteorite, our results do constrain the system.

The depth profiles of $^{10}Be$, $^{26}Al$, $^{36}Cl$, $^{41}Ca$, and $^{53}Mn$ have been measured in the Apollo 15 deep drill core [7, 8, 9, 10]. These observed profiles can be used to derive the exposure histories of lunar meteorites. Since the target chemical composition of Y-793274 is slightly different from that of the Apollo 15 drill core, the observed cosmogenic radionuclide concentrations in the meteorite have to be normalized to those in the core using the Reedy-Arnold model [11]. The activities of Y-793274 normalized to the Apollo 15 drill core are 61±2 dpm $^{41}Ca$/kg, 8.3±0.4 dpm $^{10}Be$/kg, and 32.1±1.6 dpm $^{26}Al$/kg respectively. The observed activities for the five lunar meteorites (normalized to the Apollo 15 drill core chemical composition) are plotted along with the Apollo 15 depth profiles in Fig 1. $^{41}Ca$ is not plotted for MAC88104/88105 and Y-791197. The height of each box represents experimental error and the width indicates corresponding possible depth on the moon for zero terrestrial age. The results for Y-82192, 82193, and 86032 are not plotted in the figure since these paired meteorites were clearly exposed to cosmic rays in $4\pi$ geometry for a significant period of time [4]. The normalized activities in Y-793274 are similar to those in ALHA81005. The noble gas concentrations of both meteorites are also similar [12]. For a given lunar meteorite, the observed activities of the five nuclides (after normalizing to the Apollo 15 drill core chemical composition) do not always fall at the same depth. This can be ascribed to the shorter half-lives of $^{41}Ca$ and $^{36}Cl$ compared to the longer half-lived nuclides. The existence of terrestrial age gives

anomalously low depths especially for short half-lived nuclides, without an independent measurement of terrestrial age.

In general, cosmogenic nuclide production rates by $4\pi$ irradiation are higher than those by $2\pi$ irradiation except for $^{41}Ca$ which is produced by thermal neutron capture instead of by spallation reactions. Unless these lunar meteorites were as large as Jilin or Allende in space, the $4\pi$ saturation value of $^{41}Ca$ could be no more than about 10 dpm/kg in an object with the chemical composition of Y-793274. The high $^{41}Ca$ concentration in Y-793274 eliminates the possibility of a long transition time from the moon to the earth. The maximum transition time is $0.04\pm0.01$ million years based on the measured $^{41}Ca$ value. On the other hand, the slightly lower activity of $^{41}Ca$ compared to the expected value at the depth on the moon estimated from activities of $^{36}Cl$ and $^{26}Al$ in Y-793274 is due to the decay of $^{41}Ca$ during the meteorite transition to the earth and residence in Antarctica.

The most probable scenario is that all significant cosmic ray exposure of Y-793274 took place at a depth of 150-190 g/cm$^2$ in the lunar surface. The $^{41}Ca$ and $^{36}Cl$ concentrations compared to the $^{26}Al$ concentration indicate that the sum of the transition time to the earth ($4\pi$ exposure) and the terrestrial age for Y-793274 is less than $(4\pm1)\times10^4$ years. Although some other combinations of $2\pi$ and $4\pi$ exposures are possible, useful discussions must wait until other cosmogenic nuclides such as $^{10}Be$ and $^{53}Mn$ have been determined.

The exposure histories of 9 lunar meteorites (6 independent cases) have been studied based on cosmogenic nuclide measurements. Five out of six lunar meteorites were ejected from relatively shallow depths (a few cm to about 3 m) and their transition times from the moon to the earth were all short (much shorter than $1\times10^5$ years). The impact events seem to have occurred within the last $10^5$ years for four lunar meteorites and $3\times10^5$ years ago for one. A comparison of these events and impact models have been discussed elsewhere [6, and in preparation].

**References**

[1] Fink D. *et al.*(1990) *Nucl. Inst. Meth. B47*, 79-96. [2] Middleton R. *et al.*(1983) *Nucl. Inst. Meth. 218*, 430-438. [3] Elmore D. *et al.*(1979) *Nature 277*, 22-25. [4] Nishiizumi K. *et al.*(1988) *Meteoritics 23*, 294-295. [5] Nishiizumi K. *et al.*(1991) *Geochim. Cosmochim. Acta* (in press) [6] Nishiizumi K. *et al.* (1991) *Lunar Planet Sci XXII*, 977-978 (Lunar Planet. Inst., Houston). [7] Imamura M. *et al.*(1973) *Earth Planet. Sci. Lett. 20*, 107-112. [8] Nishiizumi K. *et al.*(1984) *Earth Planet. Sci. Lett. 70*, 157-163. [9] Nishiizumi K. *et al.*(1984) *Earth Planet. Sci. Lett. 70*, 164-168. [10] Nishiizumi K. *et al.* (1990) *Lunar Planet Sci XXI*, 893-894 (Lunar Planet. Inst., Houston). [11] Reedy R.C. and Arnold J.R.(1972) *J. Geophys. Res. 77*, 537-555. [12] Eugster O. (1990) *15th Symp. on Antarctic Meteorites*, 188-190 (Natl Inst. Polar Res., Tokyo). [13] Tuniz C. *et al.*(1983) *Geophys. Res. Lett. 10*, 804-806. [14] Vogt S. *et al.*(1991) *Geochim. Cosmochim. Acta* (in press). [15] Wacker J.(1989) *Antarctic Meteorite Newsletter 12, No. 3*, 21.

Table 1. Concentrations of Cosmogenic Radionuclides in Lunar Meteorites

| Meteorite | $^{41}Ca$ | $^{36}Cl$ | $^{26}Al$ | $^{10}Be$ | $^{53}Mn$ |
|---|---|---|---|---|---|
| | | | (dpm/kg meteorite*) | | (dpm/kg Fe) |
| ALHA81005,16 | 168 ± 11 | 8.82 ± 0.44 | 41.3 ± 4.1 | 6.33 ± 0.25 | 176 ± 12 |
| ALHA81005 | | | 46 ± 3[a] | 4.1 ± 0.5[a] | |
| EET 87521,48 | | 0.875± 0.052 | 3.21± 0.13 | 0.666± 0.034 | |
| MAC 88104,9 | 15.9 ± 0.9 | 3.29 ± 0.17 | 16.1 ± 1.0 | 2.33 ± 0.11 | |
| MAC 88104,10 | | | 14.4 ± 1.2[b] | 2.1 ± 0.1[b] | |
| MAC 88105,19 | 16.5 ± 0.7 | 3.57 ± 0.22 | 20.3 ± 1.2 | 2.45 ± 0.10 | |
| MAC 88105,25 | 17.7 ± 1.0 | 3.41 ± 0.27 | 16.0 ± 1.0 | 2.01 ± 0.08 | |
| MAC 88105,41 | | | 15.7 ± 1.3[b] | 2.1 ± 0.1[b] | |
| MAC 88105 | | | 19.5 ± 2.6[c] | | |
| Y-791197,75 | 17.6 ± 1.4 | 12.34 ± 0.86 | 85.1 ± 8.5 | 11.61 ± 0.46 | 249 ± 18 |
| Y-793274,65 | 91.2 ± 2.3 | 8.95 ± 0.42 | 34.1 ± 1.7 | | |
| Y-82192,73 | 2.68 ± 0.21 | 18.03 ± 1.07 | 106.6±7.5 | 23.96 ± 1.20 | 327 ± 24 |
| Y-82193,101 | 3.02 ± 0.20 | 18.86 ± 0.66 | 138.9±9.7 | 20.10 ± 1.00 | 320 ± 22 |
| Y-86032,55 | 3.55 ± 0.28 | 17.64 ± 0.53 | 107.1±3.7 | 21.47 ± 0.86 | |

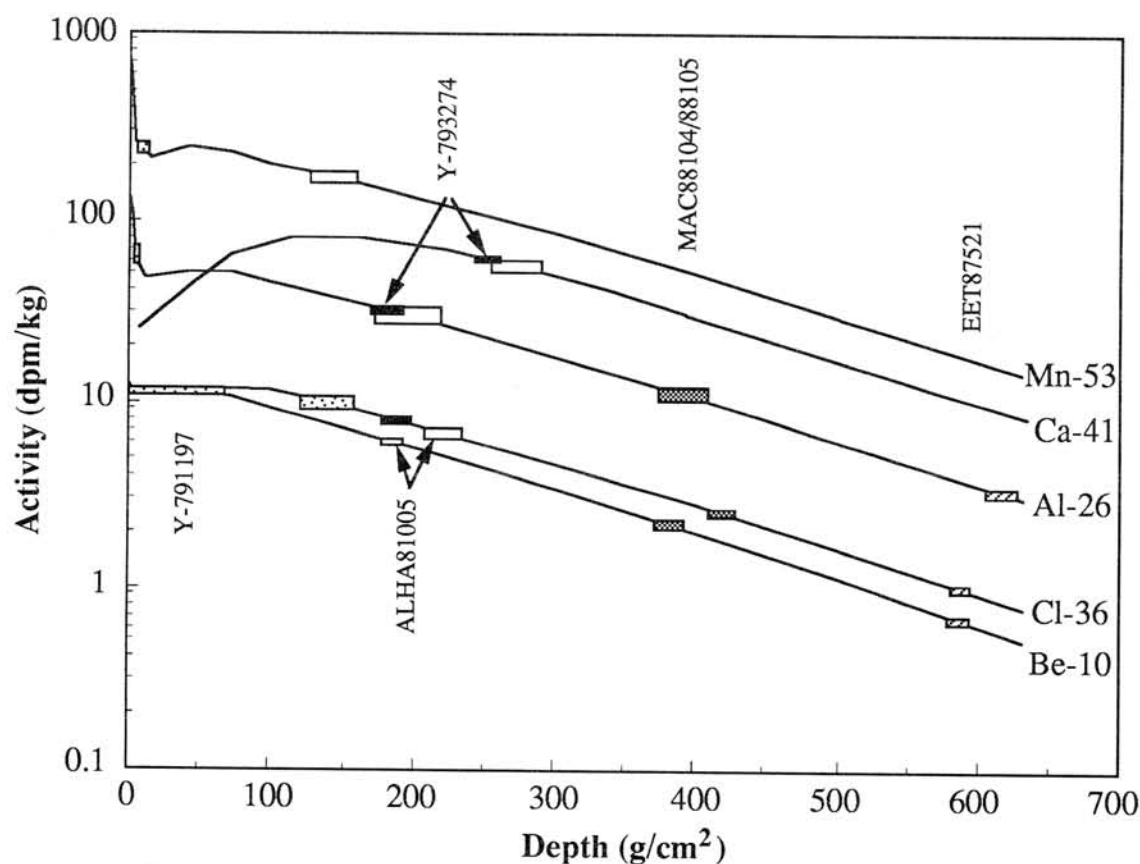* dpm/kg meteorite for $^{41}Ca$, $^{36}Cl$, $^{26}Al$, and $^{10}Be$;  a) [13], b) [14], c) [15]



Figure 1. Observed activities for the five lunar meteorites and Apollo 15 core depth profiles

INFRARED STUDIES ON SHOCK-LOADING JILIN METEORITE

Lin Wenzhu. Institute of Geochemistry, Academia Sinica, Guiyang, Guizhou Provence, 550002, China.

Most of the chondrites have been observed brecciation and shock metamorphism from mechanica fracture to impact-melting in varying degrees. As Stöffler et al (1) suggests that a full understanding of shook metamorphism and brecia fromation in meteorites is necessary in order to resolve more clearly not only the early processes of accretion, differentiation and regolith evolution of the parent bodies, but also the primordial composition of the accreted material itself. The infrared of shock minerals is an important indicator of mineral structural state. The olivine and pyroxene are both an important minerals in ordinary chondrites and important constitution of the earth's upper mantle (2). Consequently, determination infrared of the meteorites under shock can explore evolutional process of the earth's internal construction.

Sample cut up disc shape into 10 mm diameter and 2 mm in thickness. Shock wave were produced by planar impact of a projectile on the sample. The acceleration of the projectile was carried out by two-stage light gun. Shock pressure were calculated using the impedance-match method. In this experimental we have been got in five the shock recovery specimen, the corresponding pressure (Gpa):

| Shot 1 | Shot 2 | Shot 3 | Shot 4 | Shot 5 |
|--------|--------|--------|--------|--------|
| 12.4 | 27.3 | 39.0 | 53.0 | 77.5 |

The infrared spectral specimen was measured using a model Perkin-Klmer 621 infrared spectrometer, over the range from 300 to 4000 cm$^{-1}$. Spectrometer samples were prepard using a mixture of 1mg meteorite and 60 mg KBr. Pellets were obtained by grinding this mixture and pressing the mixture.

Fig. 1 shows the infrared spectra pattern of recovery specimen of meteorite after shock compression. The infrared spectra of severly minerals. We can diagnose bands of olivine and pyroxene. Infrared spectra divided into three region whether initial specimen or recovery. At 800-1000 cm$^{-1}$ were bands of both pyroxene and olivine, 600-800 cm$^{-1}$ were bands of pyroxene, lower 500 cm$^{-1}$ were bands of superposition of olivine and pyroxene. Generally speaking, unshock framework silicates display some common group freqencies which can be assigned to Si-O stretcking mode (1200-1000 cm$^{-1}$), Si-O-Si bending modes (600-390 cm$^{-1}$) and low frequency lattice vibration mode. If the minerals have existed isomorphous replacement or phase transformation, spectral band can appears shifting or splitting. When the order state of the mineral structre became disorder, fine structure of infrared spectra disapper maximal value of peak will approach smooth or clear up and bands will approximate to smooth envelope in some wavenumber region. It appear that several typical bands of olivine and pyroxene disappears difference except for 980 cm$^{-1}$, as compared with unshock sample, shot1-4. To our surprise, we can't find out high-pressure polymorphs of both olivine and pyroxene from the spectral pattern. However, considerable shock wave and static high-pressure research bear out that a set of transformations and a decomposition both olivine and pyroxene at pressure of above 12 Gpa. Appearantly, these high-pressure phase minerals don't were freezed during pressure release, but return to reversible unquenching phase of initial mineral. However, when release from final shock state along $53<P\leqslant77.5$ Gpa occur diapiectic glass, a short-range-order phase and keeping crystal initial outlin. Diaplectic glasses constructionally don't exist long-range-order. At 1300-900 cm$^{-1}$ wavenumber region Si-O band widen and approach smooth. At 1050 cm$^{-1}$ marked

disappeared also. A new band is designated mark to occur a diaplectic at 1740 cm$^{-1}$. From harmonic oscillator mode decision 1740 wavenumber can be assigned to stretching mode wavenumber for C=O band. The major results of this paper are as follows:

1 The vitreous materials in unshock Jilin meteorite isn't impact product lately, but it is the residuum of the meteoritic parent.

2 Incipient pressure of occurrence diaplectic glass of the meteorite is $53 < P \leqslant 77.5$ Gpa. The wavenumber near by 1740 cm$^{-1}$ may be as a mark of diaplectic glass.

3 Polymorphous and high pressure phase of olivine and pyroxene were locked on only under quenching condition. According this result we can understand information about temperature history of meteorites containing $\gamma$-spinel structute.
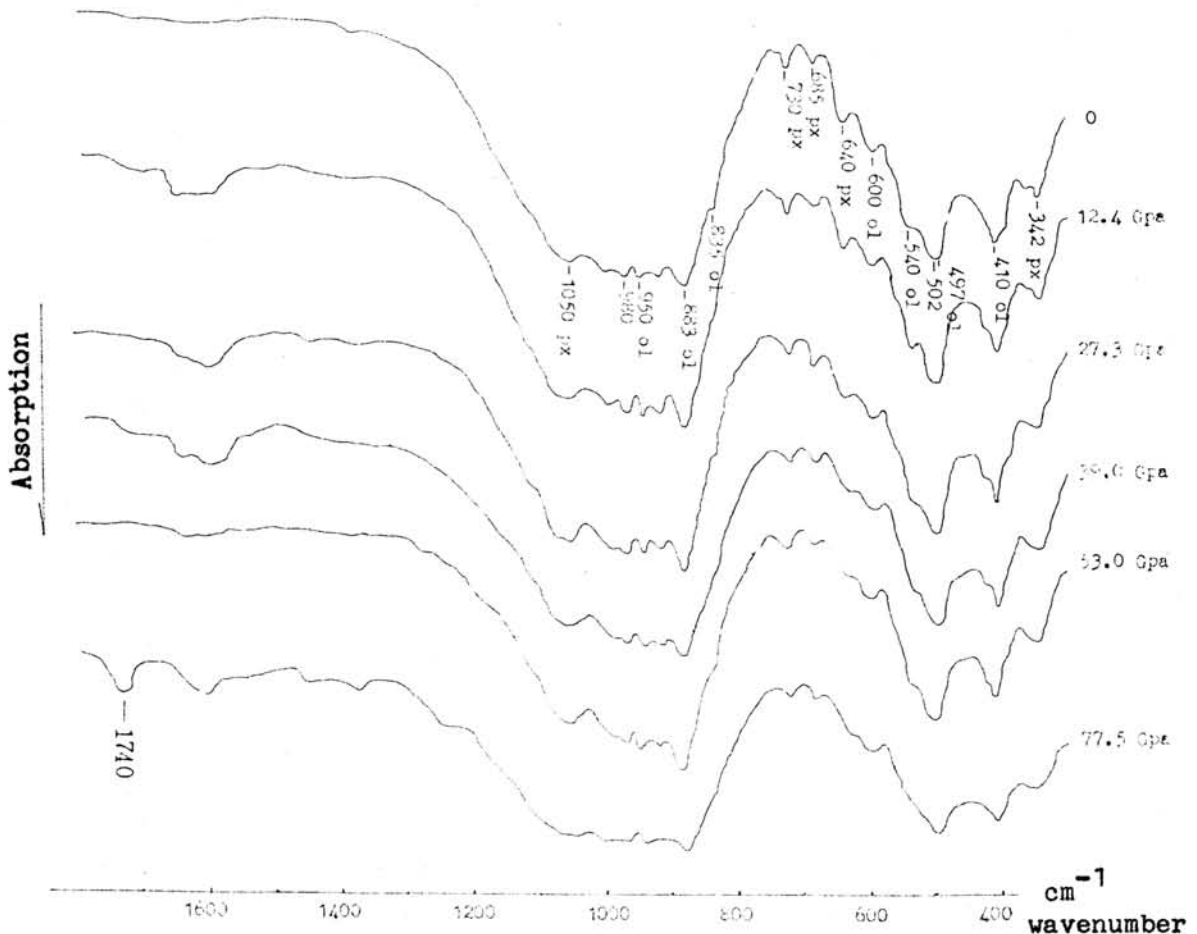


Fig. 1, Infrared spectra of shock Jilin meteorite

REPERENCES:(1) D. Stöffler et al. In " Meteorites and the Early solar system " Eds: J. F. Kerridge and M. S. Mathews, University of Arizona press. 1988. (2) M. D. Furnish and J. M. Brown 1986, J. G. R. 92, 4723-4729. (3) A. E. Ringwood and T. Iritune 1988 Nature 331, 131-136.

DOES VENUS EXPAND ?

Marek Żbik[1] and Leszek Czechowski[2]

1)Centre of Space Research Polish Academy of Sciene 2)Warsaw University.

Most of hypotheses of the expansion of the Earth are based on the proportion of continental area to oceanic area - Fig.1. This assumption leads to conclusion that present Earth's radius is about 1.4 of initial radius. There are two disadvantages of similar hypotheses: - the first is a lack of physical mechanism of the expansion, the second one is a lack of simple correlation between planet size and increase of its radius- see Fig. 1.

The new data from orbiters of Venera 15 and 16 and Magellan suggest rather moderate increase of Venus. Its surface is charecterized by bands of highlands and lowlands distributed along parallels of latitude. There are also fragments of crust separated by ridge belts - i.e. regions of apparent extension of the planet's surface.- Fig.2 . They are major tectonical features on the planet. We used them in our calculations. We assume that the ridge belts are a result of planet's expansion. This means that area of the surface of ridge belts is a measure of the increase of the planet's radius. We calculate the total area of the ridge belts on that part of Venus that are mapped by orbiters. We obtain $10ml \ km^2$ .The mapped area is 20 percent of the planet's surface. Assuming that this part is a good statistical sample we conclude that total area of the Venus increased on 11.3 % and planet's radius increased on 353 km - Fig.1 .

We suggest that Vallis Marineris on Mars and continental rifts on Earth may be of similar origin. In the case of Earth the effects of expansion may be not evident because of plate tectonics and volcanic activity. The common features of compressional origin found on Mercury indicate that radius of Mercury is decreasing. It may be a result of cooling.

1. Barsukov /ed/ 1989 - Planet Venus, Nauka.

2. Sukhanov et al 1989 - maps of N. hem. of Venus. US Geolog. Survey.

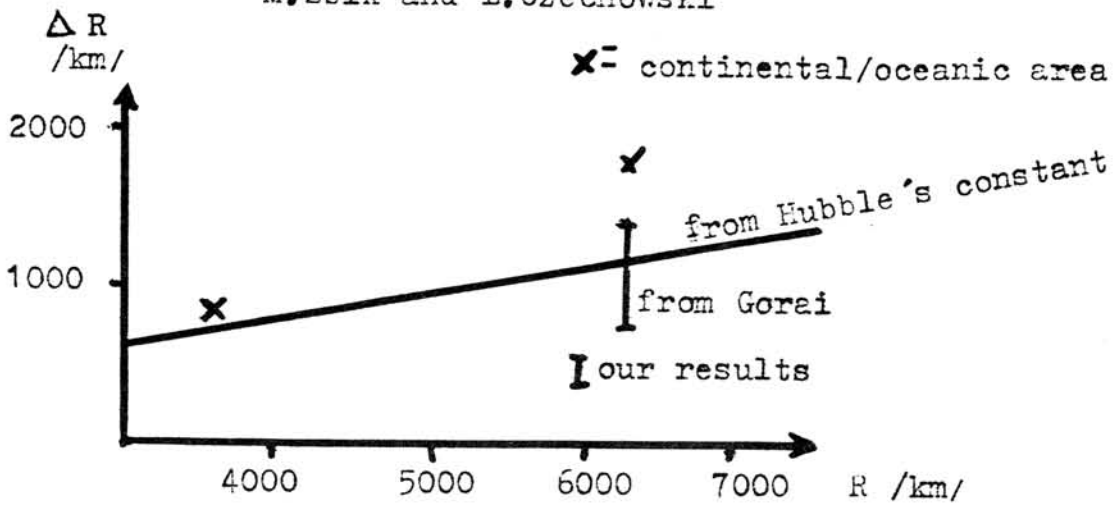3. Gorai 1983 Proc. The Expanding Earth a Symposium.

M.Żbik and L.Czechowski



**x** continental/oceanic area

Fig. 1 Comparison of the results of △R calculation

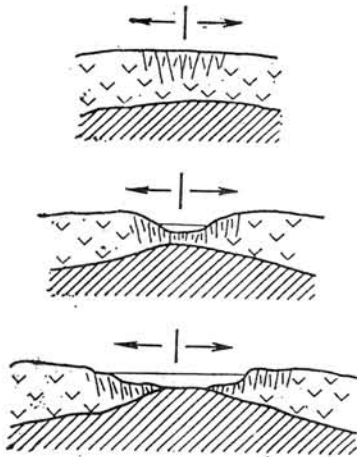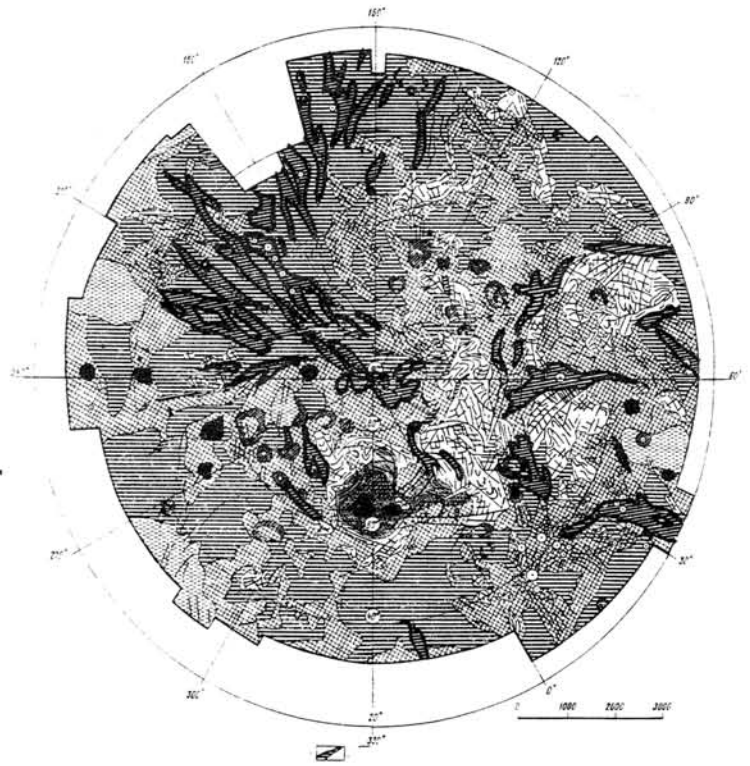

Fig. 2 General scheme of
ridge belts formation



Fig. 3 Schematic geomorphological map
of part of the northen hemisphere of
Venus with ridge belts sites.

# MINERALOGY AND THERMAL HISTORY OF Y-82162, Y-86720 AND B-7904

Michael Zolensky[1], Martin Prinz[2] and Michael Lipschutz[3], [1]SN2, NASA Johnson Space Center, Houston, TX 77058, [2]Dept. Mineral Sciences, American Museum of Natural History, New York, NY 10024, [3]Dept. of Chemistry, Purdue University, West Lafayette, IN 47907.

**INTRODUCTION:** We and others have previously described the coarse-grained mineralogy and petrology of Yamato (herein "Y-") 82162 and 86720 and Belgica ("B-") 7904 [1-5]. While once thought to represent unusual CI chondrites, these meteorites may all be CM chondrites [6]. All three meteorites have experienced late stage heating events on their respective parent bodies [1-5]. We report here the results of an investigation of the fine-grained matrix from each of these meteorites. We also report results of an experiment designed to simulate some aspects of the parent-body heating of CM material, in order to shed additional light on the histories of these three interesting meteorites.

**PROCEDURE:** All matrix samples described here were embedded in a low-viscosity epoxy, ultramicrotomed into 800-1000 A thick serial sections, and observed in a JEOL 2000FX STEM with an attached Link EDX system.

**MATRIX MINERALOGY OF Y-82162:** As previously described [1&3], Y-82162 matrix consists largely of olivine (Fo65-83) and, to a lesser extent, pyroxene (enstatite and sub-calcic pigeonite). These materials are pseudomorphous after flaky serpentine and saponite, both of which can still be observed among the anhydrous material. Saponite is well-crystalline in places, exhibits Mg:Fe ratios of 0.66 to 2, and is commonly enriched in Na. These compositions are Fe-rich compared with the bulk compositions of coarse-grained Y-82162 saponite determined previously by microprobe [1]. Serpentine in Y-82162 is poorly crystalline, exhibiting few good 7 A basal fringes. It has a Mg:Fe ratio of 1.4 to 2, which is in good agreement with microprobe analyses of coarser-grained Y-82162 serpentine [1]. Common matrix phases include awaruite (commonly on the periphery of sulfide grains), pyrrhotite, pentlandite, chromite, and, probably, ferrihydrite.

**MATRIX MINERALOGY OF Y-86720:** The matrix of Y-86720 also consists largely of olivine (~Fo70) and pyroxene (enstatite) pseudomorphous after phyllosilicate [2&4]. Compared to Y-82162, Y-86720 phyllosilicates are less crystalline. Saponite in Y-86720 exhibits few characteristic 10-14 A basal fringes, and serpentine has none. This saponite is notably enriched in Na, and has an Mg:Fe ratio of 2 to 3. Serpentine in Y-86720 has a Mg:Fe ratio of approximately 3, in good agreement with probe analyses of coarser-grained serpentine from the same meteorite [2]. Clinochlore, tentatively identified in a previous microprobe study [2], was not observed among the matrix. Rectangular, euhedral, 100 nm wide grains of probable ferrihydrite are abundant in the matrix, as reported earlier [4]. Because such forms are uncharacteristic of ferrihydrite, we suggest that these are also pseudomorphs after some other Fe-Ni bearing mineral. Fine-grained sulfides are not as abundant as the coarse-grained mineralogy would suggest.

**MATRIX MINERALOGY OF B-7904:** The matrix of B-7904 consists largely of olivine (Fo50-100), with lesser amounts of poorly crystalline saponite, and a phase apparently intermediate between serpentine and enstatite (i.e., a composition near that of serpentine, but a structure similar to that of enstatite) [7]. The Mg:Fe ratio of the saponite is approximately 1.3, while that of the intermediate phase is ~15. Both saponite and the intermediate phase are rich in Na. Grains of Fe-Ni metal (up to ~100 nm) are abundant. Fine-grained sulfides are not abundant.

**COMPARISON OF Y-82162 TO Y-86720**: The saponite of both meteorites is enriched in alkalies, indicating anoxic conditions [1]. The compositional range of saponites extends to greater Fe-contents than the serpentines in both meteorites, perhaps also a function of $fO_2$. The Mg-content of serpentine in Y-86720 is greater than for Y-82162. This fact, together with the report of CI1 levels of moderately labile trace elements [9], suggests more extensive preterrestrial aqueous alteration [8] for the latter. Matrix phyllosilicates are less crystalline in Y-86720, indicating that it was heated to the higher temperature. The heating event experienced by Y-82162 must have been under continued anoxic conditions, as evidenced by the common occurrence of metal on the periphery of pyrrhotite grains. This is in contrast to CIs, which experienced a late-stage oxidizing event.

**COMPARISON TO B-7904**: In contrast to Y-86720 and Y-82162, where serpentines are at worst poorly crystalline, in B-7904 serpentine has been replaced by a phase structurally similar to enstatite. Previous work [7] has established that this indicates heating to still higher temperatures. Accordingly, B-7904 has experienced temperatures higher than that for any known CIs or other CMs. All three meteorites contained at one stage both saponite and serpentine. Unpublished work by Zolensky has shown that among carbonaceous chondrites only Essebi, Renazzo and similar carbonaceous chondrites (e.g. EET 87770 and MAC 87300) contain both phyllosilicates in discreet crystals (permitting compositional analyses to be made). CI1 meteorites contain both saponite and serpentine also, but in complexly intergrown crystals. We also note that in general it appears that the coarse- and fine-grained phyllosilicates in each meteorite are not compositionally identical. Matrix serpentine in B-7904 is far more Mg-rich than the fine-grained fraction from the same meteorite. Coarse-grained saponite (from large aggregates) in Y-82162 is significantly more Mg-rich than the fine-grained saponite in the matrix of the same meteorite. However, analyses of coarse-grained phyllosilicates were performed by an electron microprobe, and it is accordingly possible that these compositional differences are an analytical artifact.

**HEATING EXPERIMENTS**: Akai reported results of heating experiments on Murchison, to quantify the degree of preterrestrial heating experienced by Y-86720, Y-82162 and B-7904 [7]. To test these results we obtained samples of Murchison, heated, in an anoxic ($10^{-4}$ bars $H_2$) environment, at 400, 500, 600, 700 and 800°C for 1 week each. These samples did not contain saponite, but did contain serpentine, which persisted to 400°C. The serpentine-anhydrous silicate intermediate phase was present in the range 500-600°C. At 800°C only well-crystalline pyroxene and olivine grains were present. Due to the conditions of this heating experiment, metal was present at all temperatures (having been produced by reduction of sulfides and tochilinite). From the preservational state of phyllosilicates, the three meteorites discussed here did not locally experience temperatures higher than 600°C, and more probably 400 to 500°C. These temperatures are lower by several hundred degrees than those suggested by Akai [7], from experiments carried out in a vacuum. Our temperatures are also below those estimated by Paul and Lipschutz, from labile trace element measurements on these samples and on Murchison heated in the same runs that provided our petrologic samples [9].

**REFERENCES**: [1] Zolensky, M.E. et al. (1989) Lunar and Planetary Science XX, 1253-1254; [2] Zolensky, M.E. et al. (1989) Fourteenth Symposium on Antarctic Meteorites, 24-26; [3] Tomeoka, K. et al. (1989) Proceedings of the NIPR Symposium on Antarctic Meteorites, 2, 36-54; [4] Tomeoka, K. et al. (1989) Proceedings of the NIPR Symposium on Antarctic Meteorites, 2, 55-74; [5] Tomeoka, K (1990) Proceedings of the Symposium on Antarctic Meteorites, 3, 40-54; [6] Mayeda, T.K. et al. (1991) Lunar and Planetary Science XXII, 865-866; [7] Akai, J. (1990) Proceedings of the NIPR Symposium on Antarctic Meteorites, 3, 55-68; [8] Browning, L. et al. (1991) Lunar and Planetary Science XXII, 145-146; [9] Paul, R.L. and M.E. Lipschutz (1989) Zeitschrift fur Naturforschung, 44A, 979-987.